PALACKÝ UNIVERSITY OLOMOUC

Faculty of Science

Department of Biochemistry

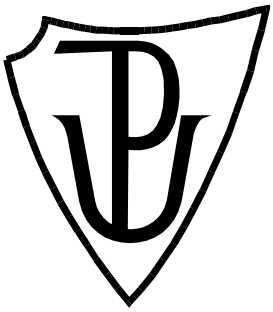

New microscopic methods for studies of plant cytoskeleton

Ph.D. Thesis

Author: **Mgr. Petra Illésová**

Study program: P1406 Biochemistry

Supervisor: Prof. RNDr. Jozef Šamaj, DrSc.

Form of study: Full-time study

Submitted: June 29th 2018

I hereby declare that this PhD thesis has been written solely by me. All the sources cited in this thesis are listed in the Reference list. All published results included in this work are approved by co-authors.

Olomouc …… ……

Petra Illésová

Poděkování

Tímto bych chtěla poděkovat zejména svému školiteli, prof. Jozefu Šamajovi, za jeho odborné vedení během celého mého Ph.D. studia, za jeho rady, cenné připomínky, ochotu a pomoc nejen v průběhu sepisování této práce. Také děkuji všem svým kolegům z Oddělení buněčné biologie, kteří mi svým přátelským přístupem zpříjemnili čas strávený v laboratoři a vždy mi byli ochotni ve všem poradit a pomoct.

Ráda bych také poděkovala Doc. Miroslavu Ovečkovi a Dr. Georgovi Komisovi za jejich pomoc s úpravami anglického textu této práce.

Mé díky patří také prof. Karstenu Niehausovi, Dr. Hanně Bednarz a celému jejich kolektivu z ústavu Centre for Biotechnology v Bielefeldu za možnost spolupracovat s nimi v rámci mé zahraniční stáže.

V neposlední řadě bych chtěla srdečně poděkovat svému manželovi, rodičům, celé rodině a všem přátelům, kteří mě podporovali v průběhu celého mého studia a kteří mi celou dobu věřili, že to dotáhnu do konce.

Tato práce vznikla za podpory projektu uděleného Grantovou agenturou České republiky (GAČR) č. 16-24313S a také za podpory studentských projektů IGA PřF UP (IGA_PrF_2014_033, IGA_PrF_2015_015, IGA_PrF_2016_012).

Acknowledgements

I would like to sincerely thank my supervisor, Prof. Jozef Šamaj, for his professional leadership during my Ph.D. studies, for his advices, valuable suggestions and kind help, beyond the writing the present thesis. I would like to also thank all my colleagues from the Department of Cell Biology for providing me a friendly environment during the time spent in the laboratory and for their willingness to help me at any time.

I would like to thank also Doc. Miroslav Ovečka and Dr. George Komis for their careful revisions of English text of this Ph.D. thesis.

My thanks are also extended to Prof. Karsten Niehaus, Dr. Hanna Bednarz and their research team at the Center for Biotechnology in Bielefeld for the opportunity to collaborate with them during my foreign internship.

Last but not least, I would like to thank my husband, parents, family and friends for their support throughout all my studies and for their encouraging attitude which greatly contributed to successful accomplishment of my Ph.D. study.

This work was supported by Czech Science Foundation (GAČR), grant no. 16-24313S and by student grants IGA PrF UP (IGA_PrF_2014_033, IGA_PrF_2015_015, IGA_PrF_2016_012).

Bibliografická identifikace

Jméno a příjmení autora	Mgr. Petra Illésová
Název práce	Nové mikroskopické metody pro studium rostlinného cytoskeletu
Typ práce	Disertační
Pracoviště	Centrum regionu Haná pro biotechnologický a zemědělský výzkum, Oddělení buněčné biologie, PřF UP
Vedoucí práce	Prof. RNDr. Jozef Šamaj, DrSc.
Rok obhajoby práce	2018

Abstrakt

Předkládaná disertační práce je zaměřena na možnosti studia rostlinného cytoskeletu pomocí moderních mikroskopických metod jako jsou „light-sheet“ fluorescenční mikroskopie (LSFM), konfokální mikroskopie s rotujícím diskem (SDCM) a Airyscan konfokální laserová skenovací mikroskopie (CLSM). Mikroskopické analýzy byly provedeny na mikrotubulech v průběhu buněčného dělení v kořenech modelové rostliny *Arabidopsis thaliana* a v kořenech hospodářsky významné luštěniny *Medicago sativa*. Práce je rozdělena na tři části, z nichž první část shrnuje ověřené poznatky o rostlinném cytoskeletu, jeho složení a funkci. Tato část také obsahuje kapitoly pojednávající o uspořádání a úloze mikrotubulů (MT) v průběhu mitózy. Dále jsou zde charakterizovány jednotlivé modelové rostliny a základní principy použitých mikroskopických metod.

Druhá část práce je zaměřena zejména na přípravu rostlinného materiálu pro následnou mikroskopickou analýzu mitotických MT. Mitóza je velmi dynamický proces, který je citlivý na jakékoliv vnější stresové faktory. Z tohoto důvodu je výběr mikroskopické metody velice důležitý. Využitím fluorescenčně značených MT a moderních mikroskopických metod (LSFM, SDCM a Airyscan CLSM), které jsou dostatečně rychlé, mají vysoké rozlišení a zároveň jsou v průběhu snímání šetrnější k rostlinnému preparátu díky nižší fototoxicitě, jsme schopni studovat tyto dynamické procesy v reálném čase.

Třetí část této práce se zaměřuje na využití LSFM při studiu mitotických MT v rostoucích kořenech *M. sativa* exprimujících *35S::GFP:MBD* konstrukt. Zejména díky vysokému optickému rozlišení, možnosti vytváření efektivních optických řezů, vysoké rychlosti snímání, nízké fototoxicitě a možnosti snímání preparátu umístěného ve vertikální poloze je tato mikroskopická metoda vhodná pro dlouhodobé 4D snímání živých rostlinných preparátů při téměř fyziologických podmínkách růstu. Celkem devět snímaných kořenů *M. sativa* bylo rozděleno do tří skupin podle rychlosti jejich růstu. V každé skupině kořenů jsme zaznamenali a kvantitativně vyhodnotili trvání mitotického buněčného dělení, zejména trvání přítomnosti jednotlivých mitotických mikrotubulárních struktur jako je preprofázní svazek, mitotické vřeténko a fragmoplast a to jak v epidermis, tak v první vrstvě kortexu. Získaná data ukázala průkaznou korelaci mezi rychlostí růstu kořenů a trváním buněčného dělení v kořenech *M. sativa*.

Klíčová slova	mikrotubuly, *Medicago sativa*, „light-sheet“ mikroskopie, konfokální mikroskopie s rotujícím diskem, Airyscan, *Arabidopsis thaliana*, preprofázní svazek, dělicí vřeténko, fragmoplast, mitóza
Počet stran	165
Počet příloh	3
Jazyk	Anglický

Bibliographical identification

Autor's first name and surname	Mgr. Petra Illésová
Title	New microscopic methods for studies of plant cytoskeleton
Type of thesis	Ph.D.
Department	Department of Cell Biology, Centre of the Region Haná for Biotechnological and Agricultural Research, Faculty of Science, Palacký University Olomouc
Supervisor	Prof. RNDr. Jozef Šamaj, DrSc.
The year of presentation	2018

Abstract

This Ph.D. thesis is focused on the possibilities of studying the plant cytoskeleton using modern microscopic methods such as light-sheet fluorescence microscopy (LSFM), spinning disk confocal microscopy (SDCM) and Airyscan confocal laser scanning microscopy (CLSM). Microscopic analyses were performed on microtubules (MTs) during cell divisions in the roots of the model species *Arabidopsis thaliana* and in the roots of the important legume crop *Medicago sativa*. The thesis is divided into three parts. The first part summarizes the current knowledge about plant cytoskeleton, its structure and function. This part contains chapters focused on the organization and the roles of MTs during the mitosis. In the same section, the chosen model plants are described while an account of the used microscopic methods is also given.

The second part is mainly focused on the preparation of plant material for subsequent microscopic analysis of mitotic MT arrays. Mitosis is a highly dynamic process, sensitive to many stress factors. For this reason, the selection of the suitable microscopic method is very important. Using genetically encoded fluorescent MT markers and modern microscopic methods (LSFM, SDCM and Airyscan CLSM) with high spatio-temporal capabilities, it was possible to track and document dynamic processes, such as mitosis, in real time.

The third part of thesis is more specified on the use of LSFM to study mitotic MTs in growing *M. sativa* roots expressing *35S::GFP:MBD* construct. Owing to the high optical resolution, efficient optical sectioning, high speed image acquisition, low phototoxicity and ability to scan the sample oriented in a vertical position, this microscopic method is suitable for the 4D long-term live-cell imaging of plant under nearly physiological conditions. In total, nine imaged *M. sativa* roots were divided into three groups according to their growth rates. In each group we recorded and quantitatively evaluated the duration of the mitotic cell division and specific mitotic MT arrays such as the preprophase band, the mitotic spindle and the phragmoplast in both, the epidermis and the first outer layer of cortex, respectively. Obtained data showed strong correlation between the root growth rate and the duration of cell division in the *M. sativa* roots.

Keywords	microtubule, *Medicago sativa*, light-sheet microscopy, spinning disk confocal microscopy, Airyscan, *Arabidopsis thaliana*, preprophase band, spindle, phragmoplast, mitosis
Number of pages	165
Number of appendices	3
Language	English

Content

1. OBJECTIVES

1. Summary of knowledge about the plant cytoskeleton and advanced microscopic methods suitable for its study
2. Optimizing the preparation of plant material for the study of the *M. sativa* root using light-sheet microscopy
3. Study of mitotic microtubules during cell division in *M. sativa* using light-sheet microscopy
4. Measurement and statistical analysis of the duration of the individual mitotic stages
5. Preparation of plant material for the study of mitotic microtubules in dividing cells using spinning disk microscopy and Airyscan microscopy

2. GENERAL INTRODUCTION

2.1 Cytoskeleton

The cytoskeleton is a dynamic subcellular system that forms a three-dimensional network similar to a scaffolding. It has mainly the structural, transporting, signaling and motional functions. It determines the shape and orientation of cell growth and participates in the cellular movement and positioning of organelles and macromolecules. It also plays a key role in cell division, vesicle trafficking and programmed cell death (Goode *et al*., 2000; Smith, 2003; Smertenko and Franklin-Tong, 2011; Zhang and Dawe, 2011).

Generally, the cytoskeletal components of the actin and microtubule cytoskeleton are highly conserved. The origin of the cytoskeleton is most likely prokaryotic. Although the prokaryotic "ancestors" of actin and tubulin, such as MreB and FtsZ proteins respectively do not show a high homology with eukaryotic actin and tubulin (Erickson, 2007), these proteins have similar three dimentional structures and functions. For example, MreB in *Bacillus subtilis* has been shown to act as a cortical actin for the formation of lipid rafts and for the distribution of lipids and proteins in the plasma membrane (Chichili and Rodgers, 2009; Strahl *et al*., 2014). FtsZ, a bacterial homologue of tubulin, has the same tubulin GTPase activity and is indispensable for cell division (Bi and Lutkenhaus, 1991; Hong *et al*., 2013).

The cytoskeleton of green plants consists of microtubules and actin filaments (Wasteneys, 2002). Intermediate filaments have not been described, except some exceptions, in plants. Historically, actin filaments and microtubule arrays have been considered as separate cytoskeletal systems with different functions. However, the structural and functional cooperation of these two cytoskeletal components during cellular processes such as phragmoplast formation and cytokinesis was shown (Gavin, 1997; Bezanilla *et al*., 2015).

2.1.1 Microtubules (MTs)

2.1.1.1 Structure of MTs

MTs are rigid cylindrical structures with internal hollow which have an inner diameter of 14 nm and an outer diameter of 25 nm. They consist of 13 protofilaments arranged in a B-type lattice. Individual protofilaments are polymers of globular α- and β-tubulin heterodimers which are longitudinally stacked together by lateral interactions, giving rise to the polar MT structure with

rapidly polymerizing/depolymerizing plus and minus ends (Ledbetter and Porter, 1964; Tilney *et al*., 1973; Desai and Mitchison, 1997; Wade and Hyman, 1997; Wade, 2009). Rapid depolymerization of MTs is called "catastrophe" and return to growth is "rescue". MTs often associate together and occur in the cell in the form of MT bundles and arrays. MT dynamics have been described within such bundles (Shaw *et al*., 2003; Komis *et al*., 2014).

2.1.1.2 MT dynamics

During MT treadmilling, the MT plus end is able to grow via via αβ-tubulin dimer incorporation, while subunit dissociation occurs on the minus end. A third member of the tubulin family, γ-tubulin, plays a role in nucleation and assembly of MTs (Wade, 2009). When MTs break up from the plus end, stable rings of individual protofilaments are often observed (Mandelkow *et al*., 1991). It indicates that longitudinal interactions between the tubulin heterodimers inside a protofilament are stronger than mutual interactions between the protofilaments. Therefore, the protofilaments are considered as basic units of MT structure (Tilney *et al*., 1973). Both α- and β-tubulins have a guanosine triphosphate (GTP) binding site. Whereas α-tubulin binds GTP tightly, β-tubulin exhibits GTPase activity promoting GTP/GDP hydrolysis. Growing MTs have a GTP cap on their plus end because GTP/GDP hydrolysis occurs with a slight delay. The energy released by cleavage of this binding is used to bind the heterodimer to the second heterodimer, and to form longitudinal protofilaments. When GTP binds to β-tubulin, the heterodimer acquires direct conformation that facilitates lateral protofilament linkages. During GTP/GDP hydrolysis, the conformation is changed to curve and thus the protofilaments are sensitive to break up (Hyman *et al*., 1998; Rice *et al*., 2008). If GTP hydrolysis is faster than the addition of new tubulin heterodimers, the GTP cap is lost and MTs begin to shorten.

In eukaryotic cells, the minus ends of MTs are usually anchored to the MT organizing center (MTOC), in which they are nucleated. The main protein involved in MT nucleation is γ-tubulin (Oakley *et al*., 1990; Binarová *et al*., 2006), since γ-tubulin complexes consist of two molecules of γ-tubulin and one molecule of γ-TUBULIN COMPLEX PROTEINS 2 and 3 (GCP2 and GCP3; Gunawardane *et al*., 2000; Dryková *et al*., 2003; Raynaud-Messina and Merdes, 2007). Although plant MTs are nucleated from γ-tubulin complexes, they have no strictly defined MTOCs comparable to animal or yeast cells (Dryková *et al*., 2003). Nevertheless, nucleation of MTs in plants occurs on the nuclear envelope (Stoppin *et al*., 1994), on the plasma membrane (Schmit,

2002), on the Golgi membranes (Dryková *et al*., 2003) or on the kinetochore (Binarová *et al*., 2000). Last but not least, MTs are nucleated on other pre-existing MTs and this occurs predominantly in the cellular cortex close to the plasma membrane (Murata *et al*., 2005; 2007; 2013).

2.1.1.3 MT functions

The MT cytoskeleton plays a key role in plant cell morphogenesis and multicellular development. MTs are involved in various processes such as cell division and growth, polarity determination, cell shape control, vesicular transport, as well as programmed cell death (Smertenko and Franklin-Tong, 2011; Hashimoto, 2015).

2.1.2 Cortical MTs

Plant cells have different MT systems in comparison to animal cells. During interphase, cortical MTs are oriented predominantly in parallel arrays underneath the plasma membrane. The function of cortical MTs is closely related to cell wall formation and relate to the directional movement of cellulose synthases, responsible for the deposition of cellulose microfibrils. (Paredez *et al*., 2006).

Plant cortical MT arrays are reorganized in response to various environmental and stress conditions (Cyr, 1994; Hush *et al*., 1994). MTs together with motor proteins (kinesins in plants) contribute to the movement of the cellular components in the cytoplasm. Plant kinesins can move cargo either to the plus to the minus ends of MTs (McDonald *et al*., 1990; Sablin *et al*., 1998; Yamagishi *et al*., 2016). Kinesins create enzymatic complexes moving along the MT surface based on energy provided by ATP/ADP hydrolysis (Asada *et al*., 1997; Paluh *et al*., 2000; Vaughan, 2005; Kikkawa, 2013). MT dynamics and bundling are regulated by microtubule-associated proteins (MAPs) such as KATANIN, END-BINDING PROTEIN 1 (EB1), MAP65, MAP70, CLIP-ASSOCIATED PROTEIN (CLASP), MICROTUBULE ORGANIZATION 1 (MOR1). Also, both the C-terminal motor and N-terminal tail domains of KINESIN-LIKE CALMODULIN-BINDING PROTEIN (KCBP) are involved in MTs bundling (Kao *et al*., 2000). The important role of MAPs in MT organization and bundling can be demonstrated by studies of mutant plants defective in expression of particular genes encoding MAPs. As an example, *A. thaliana* mutants *mor1*, *ton1*, *ton2* and *katanin P60* show distinct disorganization of MT arrays

(McClinton *et al*., 1997; Burk *et al*., 2001; McClinton *et al*., 2001; Whittington *et al*., 2001; Camilleri *et al*., 2002).

2.1.3 Mitotic MTs

In somatic cells, chromosomes and cytoplasm containing individual cell organelles and subcellular compartments are divided into two daughter cells during mitotic (M) phase of cell cycle. This M phase can be subdivided into two tightly interconnected parts – mitosis and cytokinesis. Chromosomes are segregated in mitosis, while the cytoplasm is partitioned during cytokinesis. The mitotic part itself is divided into five basic steps, namely prophase, prometaphase, metaphase, anaphase and telophase (Fig. 1).

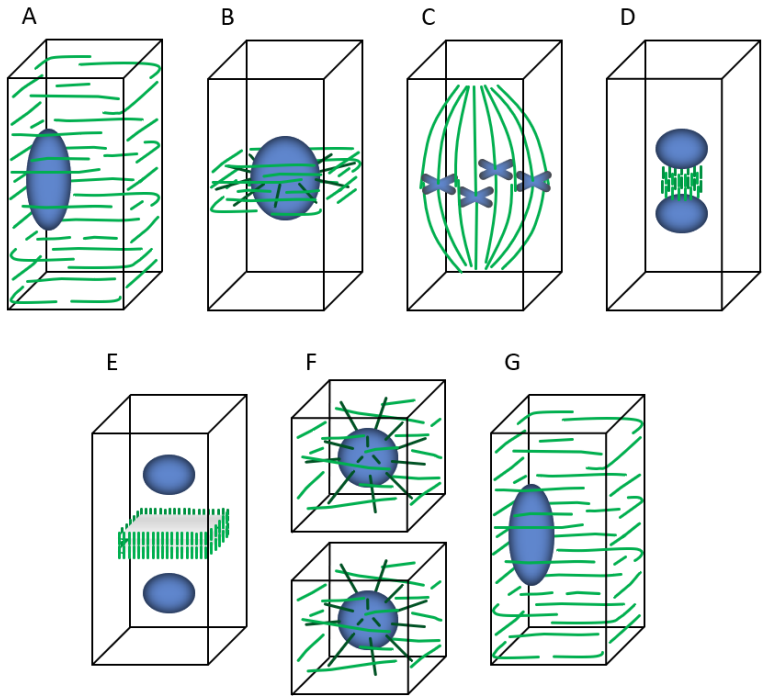

Figure 1. Scheme of MTs arrangement during the plant cell division. (A) Parallel arrangement of cortical MTs during interphase in mature plant cell. (B) Temporary rearrangement of MTs into PPB, which marks the future cell division plane. (C) MTs are formed into mitotic spindle during prometaphase. The chromosomes are localized in equatorial region. (D) The early phragmoplast is formed in place of the future cell plate. (E) The late phragmoplast is formed as temporary MTs ring between two daughter nuclei. (F) The cytokinesis is complete and two daughter cells are created. MTs extend from the nucleus toward the cell cortex and plasma membrane-associated MTs appear. (G) The cortical MTs are again formed in post-mitotic plant cell. Adapted from Wasteneys, 2002.

Preparation of cells for mitotic entry in plants is characterized by a dramatic reorganization of cortical MTs. These progressively coalesce to the so-called preprophase band (PPB). After maturation and disassembly, the PPB is rearranged to the mitotic spindle and eventually the cytokinetic phragmoplast during progression of mitosis and cytokinesis (Fig. 1; Yuan *et al*., 1994; Wasteneys, 2002; Hashimoto, 2015).

During prophase, the microtubular PPB disappears and the mitotic spindle begins to develop (Fig. 1B, C). In plants, however, minus ends of mitotic spindle MTs do not originate from centrosomes as in animals and yeasts but they are likely associated with MTOCs located close to the nuclear envelope (Dibbayawan *et al*., 2001; Binarova *et al*., 2006; Wiese and Zheng, 2006).

The prometaphase is determined by nuclear envelope breakdown. Chromosomes become attached to MTs of the mitotic spindle at kinetochores and progressively align to the equatorial plane of the dividing cell (Fig. 1C). Spindle is completed and three groups of spindle MTs are apparent. Kinetochore MTs attach the chromosomes to the spindle pole, interpolar MTs which extend in a pole-to-pole fashion and astral MTs which project from the spindle pole towards the cell membrane in a radial fashion.

During anaphase, each chromosome separates to sister chromatids which move to opposite poles of the cell. Meanwhile, changes in MT length provide the mechanism for chromatid movements. Upon separation, chromatids mature to independent chromosomes.

During telophase, equivalent sister chromatid groups converge to the cell poles, and MTs gradually form the phragmoplast (Fig. 1D, E). Progressively a new nuclear envelope is formed around each group of chromosomes.

At the same time, the centrifugally expanding phragmoplast directs the deposition of the daughter cell wall – the cell plate – which physically partitions the two nuclei into two daughter cells (Fig. 1F; Alberts *et al*., 2008).

2.1.3.1 PPB

The PPB is a transient MT structure that forms before mitosis (Fig 1B). PPB formation is not essential for the future onset and progress of mitosis and cytokinesis, as some plant cell types such as starchy endosperm, nuclear endosperm or *Arabidopsis thaliana* suspension cells are devoid of PPBs (Otegui and Staehelin, 2000; Chan *et al*., 2005; Sabelli and Larkins, 2009). However, pharmacological or genetic disruption (e.g. of *TONNEAU2* gene) of PPBs can cause aberrant

orientations of divisions in plant cells (Camilleri *et al*., 2002; Vanstraelen *et al*., 2006). These observations confirm that the PPB plays a key role in the determination of the cell division plane (CDP) orientation.

During the G2 phase of cell cycle, the cortical network of MTs becomes reorganized to a temporal ring around the nucleus called PPB which defines the future CDP (Fig. 1A, B; Pickett-Heaps and Northcote, 1966; Nogami and Mineyuki, 1999). The PPB narrows during prophase and subsequently disappears along with the nuclear envelope breakdown and the mitotic spindle formation (Fig. 1C; Dixit and Cyr, 2002; Smertenko *et al*., 2017). Several MAPs have been identified to participate in PPB formation. In *A. thaliana*, MOR1 can accelerate both, the growth and shrinkage of MTs *in vitro* and *in vivo* (Kawamura *et al*., 2006; Kawamura and Wasteneys, 2008). MOR1 is localized along the entire length of MTs in interphase arrays, PPB, mitotic spindle and phragmoplast (Kawamura *et al*., 2006). Study of *A. thaliana* temperature-sensitive mutants *mor1-1* revealed that mutation in the N-terminal HEAT repeat of *MOR1* gene does not affect the ability of MOR1 to bind MTs, but it results in the loss of the function. Mutant *mor1-1* plants display distinct defects in PPB formation and PPB is absent from almost 50% of dividing cells prior to mitotic spindle formation (Kawamura *et al*., 2006). The tobacco MOR1 ortholog MICROTUBULE-BINDING PROTEIN 200 (TMBP200), is also localized to the PPB (Hamada *et al*., 2004). In addition, CLASP is connected with PPB formation in *A. thaliana* (Mimori-Kiyosue *et al*., 2005). Next, the SABRE protein, which has unknown function in eukaryotes, plays an important role in the orientation of cell division and planar polarity. Moreover, SABRE stabilizes the orientation of CLASP-labelled MTs in the PPB, which is crucial for CDP orientation in *A. thaliana* (Pietra *et al*., 2013). Some members of MAP65 family are also involved in PPB formation. MAP65s bundle MTs by forming cross bridges between adjacent, antiparallel MTs, and potentially promote the formation and the stability of PPB via their bundling activity (Smertenko *et al*., 2004). KATANIN, a protein responsible for severing of MTs, is involved in the organization of cortical MTs and PPB and thus plays a role in CDP orientation (Komis *et al*., 2017, Luptovčiak *et al*., 2017). KATANIN mutants such as *lue1*, *fra2* and *ktn1-2* (Panteris *et al*., 2011; Komis *et al*., 2017) exhibit PPB disorganization at variable extend and drastically delayed narrowing.

Despite of the fact that plant cells lack centrosomes, proteins similar to the human centrosomal proteins are required for the PPB formation in plants. An example of such protein is *A. thaliana* TONNEAU 1 (TON1), which colocalizes with the PPB. The *ton1* mutants are not able to form

PPB (Azimzadeh *et al*., 2008). It has been reported that the activity of regulatory TTP complex consisting of TON1, TON1 RECRUITNG MOTIF PROTEINS (TRMs), phosphatase 2A (PPA2) heterotrimeric holoenzyme with FASS as regulatory subunit is required for PPB formation and spatial control of cell division. All members of the TTP complex are similar to animal centrosomal proteins, suggesting an evolutionary linkage between the MT organizing mechanisms in plants and other eukaryotes (Spinner *et al*., 2013).The PPB underlies a plasma membrane region known as the cortical division zone (CDZ), which persists during all stages of M phase. Mutants *tan, sab* and *clasp* show aberrant orientation of CDZ (Kirik *et al*., 2007; Walker *et al*., 2007; Pietra *et al*., 2013). Moreover, regulatory proteins such as AURORA 1/2, RanGAP1, YODA, MPK6 and FASS/TONNEAU2 are involved in the orientation of CDZ in *A. thaliana* cells (Camilleri *et al*., 2002; Lukowitz *et al*., 2004; Xu *et al*., 2008; Müller *et al*., 2010; Van Damme *et al*., 2011; Kirik *et al*., 2012; Spinner *et al*., 2013; Smékalová *et al*., 2014; Boruc *et al*., 2017).

2.1.3.2 Mitotic spindle

Segregation of duplicated genetic material between two daughter cells in the process of mitosis is a conserved feature among eukaryotes and requires the assembly of the mitotic spindle (Prosser and Pelletier, 2017). In plants, it is starting to form at some later stage of PPB formation, around the still intact nuclear envelope. The mitotic spindle is bipolar and its longitudinal axis is always perpendicular to the plane of the PPB (Fig. 1C; van Damme, 2009). After the conclusion of anaphase, kinetochore MTs are replaced by antiparallel, interzonal MT systems spanning the space between the progressively reconstituting daughter nuclei. During prophase/ prometaphase the mitotic spindle drives the alignment of chromosomal kinetochores at the so-called equatorial plane, while during the stages of anaphase, the spindle actively segregates two equivalent sister chromatid groups which eventually occupy positions at the opposite spindle poles (Hashimoto, 2015). Spindle bipolarity and most importantly orientation is actively assisted by the position of the PPB (Ambrose and Cyr, 2008; Schaefer et al., 2017; Komis et al., 2017).

In animals and fungi, the assembly of mitotic spindle is dominated by the occurrence of structurally defined MTOCs such as the centrosome and the spindle pole body respectively (Vertii *et al*., 2016; Kilmartin, 2014). In higher plants, however, mitotic spindle assembly is acentrosomal while spindle itself undergoes significant changes during mitotic progression (Yamada and

Goshima, 2017). The plant mitotic spindle largely comprises of kinetochore MT bundles but it lacks astral MTs, possibly due to the absence of MTOCs at the spindle poles.

Several MAPs are involved in MT nucleation and bundling, regulation of MT plus end dynamics, and MT-dependent motor activities during spindle dynamic rearrangements. Other proteins with regulatory functions such as protein kinases, were found to be enriched in the mitotic spindle (Yamada and Goshima, 2017).

Thus, MOR1, TMBP200, CLASP, SABRE and members of MAP65 family participate on spindle formation (Kawamura *et al*., 2006; Ambrose *et al*., 2007; Fache *et al*., 2010; Yasuhara and Oe, 2011; Pietra *et al*., 2013). Bundling of MTs is an important feature of structural organization of all MT arrays (Hamada, 2007) and in plants it is mostly related to the crosslinking activity of proteins belonging to the MAP65 family. It has been shown that MAP65-4 controls the dynamics of individual MTs within a bundle. It decreases the frequency of catastrophes and simultaneously increases the frequency of rescue events, thereby promoting elongation of MT bundles over the time (Fache *et al*., 2010). On the other hand, MAP65-1 is responsible for integrity of the anaphase spindle and for binding and bundling of MTs by creating bridges in the interphase, anaphase and telophase mitotic stages (Smertenko *et al.*, 2006). Other proteins essential for mitotic spindle assembly are γ-tubulins (TUBG1 and TUBG2) that are involved in MT nucleation. They act together with NEURAL PRECURSOR CELL EXPRESSED, DEVELOPMENTALLY DOWN-REGULATED 1 (NEDD1) protein, which serves as an anchor for γ-tubulin complex (Binarová *et al*., 2006; Pastuglia *et al*., 2006; Zeng *et al*., 2009). Another important component of γ-tubulin complex is γ-TUBULIN COMPLEX PROTEIN 4 (GCP4). Downregulation of *GCP4* expression leads to abnormal MTs organization in the mitotic spindle (Kong *et al*., 2010). Localization analyses revealed, that also GCP3 INTERACTION PROTEINS 1 and 2 (GIP1 and GIP2) colocalize with γ-tubulin while *gip1* and *gip2* mutants are characterized by disorganized MTs and abnormal mitotic spindle polarity (Janski *et al*., 2012).

The bipolar symmetry of the mitotic spindle requires opposite forces, which are generated by motor proteins, mainly MT plus end directed kinesins. It has been shown in *A. thaliana* that KINESIN-RELATED PROTEIN 125c, which belongs to the kinesin-5 group, plays a crucial role in stabilizing the mitotic spindle by cross-linking antiparallel MTs at the midzone (Bannigan *et al*., 2007). Another kinesins ATK1 and ATK5, belonging to kinesin-14 group, are atypical MT minus end directed proteins that are required for bipolar spindle assembly (Marcus *et al*., 2003; Ambrose

et al., 2005). While ATK5 is localized to the mitotic spindle midzone, ATK1 accumulates at the spindle poles. Mutant *atk5* is characterized by prolonged period of mitotic spindle elongation and the formation of mitotic spindle with extended poles (Ambrose and Cyr, 2007). In addition, an extensive spindle rotation was observed in the mutant *ktn1-2*. It indicates that KATANIN 1 contributes to the positioning of mitotic spindle (Komis *et al*., 2017). Study of Komaki *et al.* (2010) shows that EB1c, localized to growing plus ends of MTs, plays an important role in the regulation of spindle organization while it is required for positioning of spindle poles and chromosome segregation. During the interphase, TARGETING PROTEIN for Xenopus KINESIN-LIKE PROTEIN 2 (Xklp2; TPX2) is localized to the nucleus. Throughout prophase, TPX2 is localized to the perinuclear region and after nuclear envelope breakdown it is relocated to the mitotic spindle (Wittmann *et al*., 2000; Vos *et al*., 2008). TPX2 binds and activates Ran, a small GTPase which is responsible for induction of spindle formation (Gruss *et al*., 2001). In addition, TPX2 activates Aurora A kinases. Demidov *et al*. (2005) found that Arabidopsis AURORA 1 and AURORA 2 are associated with spindle MTs, thus their activation via TPX2 can play a role in the organization of mitotic spindle.

2.1.3.3 Phragmoplast

The phragmoplast is a dynamic structure formed from the spindle MTs at telophase stage of mitosis (Fig. 1D, E; Hashimoto, 2015). Typical phragmoplast is a barrel-shaped structure and it serves as a scaffold for cell plate assembly and subsequent formation of a new cell wall separating the two daughter cells (Fig. 1D, E). This cytokinetic apparatus mainly consists of antiparallel MT arrays and cytokinetic vesicles participating on the cell plate formation (Fig. 1F; Goddard *et al*., 1994; Ho *et al*., 2011a; Liu *et al*., 2011). Phragmoplast MTs are perpendicular to the CDP; their plus ends are located close to the midzone and the minus ends are pointed towards the daughter nuclei (distal zone; Smertenko *et al*., 2017). New dynamic MTs in the phragmoplast are nucleated by γ-tubulin and are branching-off preexisting stable MTs (Murata *et al*., 2013).

A large number of MAPs and other MT-interacting components participate on the formation and the functionality of the phragmoplast (Hamada, 2007). Besides previously mentioned proteins, which are involved also in the formation of mitotic spindle (TUBG1, TUBG2, GCP4) and in the formation of both PPB and spindle MT arrays (MOR1, TMBP200, CLASP, SABRE,

KATANIN 1, MAP65-1, MAP65-4), proteins that are exclusively required for the phragmoplast formation have been identified. Thus, PHRAGMOPLAST KINESIN RELATED PROTEINS 1 and 1L (PAKRP1 and PAKRP1L), which belong to kinesin-12 family, are localized to the MT plus ends in the phragmoplast midzone (Lee *et al*., 2007). Both, PAKRP1 and PAKRP1L, act as MT motors and play an essential role in dynamic organization of phragmoplast during the cytokinesis. In addition, they create connections between MT plus ends of antiparallel MTs leading to better stability of the phragmoplast structure (Lee *et al*., 2007). Another protein, MAP65-3, is required for the engagement of antiparallel MTs in the phragmoplast. It interacts with MTs before kinesins (Ho *et al*., 2011a). The role of TWO-IN-ONE kinase (TIO) in the formation of phragmoplast during the cytokinesis was confirmed by Oh *et al*. (2005). TIO is localized to the phragmoplast midzone and remains associated with the expanding phragmoplast ring. Genetic disruption of this kinase in *tio* mutants leads to the formation of aberrant phragmoplasts and consequent defects in the cytokinesis. Moreover, augmin complex plays an important role in γ-tubulin-dependent nucleation of MTs during phragmoplast formation (Hotta *et al*., 2012). AUGMIN COMPLEX in Arabidopsis consists of eight subunits (AUG1 – AUG8) and its main function is to anchor the γ-tubulin nucleation complex to existing phragmoplast MTs. A critical role of AUGMIN 7 (AUG7) has been shown in the mutant *aug7-1*, showing relocalization of γ-tubulin in the phragmoplast and disorganization of MT bundles (Hotta *et al*., 2012).

2.1.4 Actin filaments (AFs)

2.1.4.1 Structure of AFs

The plant actin cytoskeleton is characterized by a high diversity concerning gene families of actins and actin binding proteins (ABPs), high number of isoforms and degree of polymerization. AFs are thin and flexible microfilaments with a diameter of 7 nm. When compared to MTs, AFs are much more flexible. The basic unit of AF is the monomeric globular actin (G-actin), polymerizing into two helically arranged and interconnected fibers. Such polymerized actin is called filamentous actin or F-actin. Actin is a highly conserved globular protein of 43 kDa containing the ATP/ADP nucleotide binding site located in the center of the protein. The energy released by the hydrolysis of ATP to ADP allows the interconnection of individual subunits in actin fiber (polymerization). The actin fiber is then formed by the helical association of two F-actin filaments. AFs show

structural polarity at their ends. This inherent polarity is very important for all polymeric cytoskeletal proteins and plays a key role in the function of the polymer chain (Li and Gundersen, 2008). The individual ends of the actin fiber have different properties. The end marked as the plus (+) end is dynamic, fast growing, but at the same time it can be quickly shortened. At the other end of the fiber is the minus (-) end that is much less dynamic (Li and Gundersen, 2008). F-actin can be bundled, while G-actin can be assembled into actin oligomers composed of a few actin molecules which can be cross-linked into complex dynamic networks (Volkmann and Baluška, 1999).

2.1.4.2 Functions of AFs

The actin cytoskeleton plays important roles in the formation of cell polarity, control over CDP and progress of cell division, delivery of cell wall components, subcellular transport and positioning of organelles and subcellular compartments. In addition, it provides highly dynamic tracks for cytoplasmic streaming and participates in endocytosis and plant signaling (Meagher and Williamson, 1994; Fowler and Quatrano, 1997; Kropf *et al*., 1998; Nick, 1999; Volkmann and Baluška, 1999; Baluška *et al*., 2000; Hepler *et al*., 2001; Šamaj *et al*., 2004).). The actin cytoskeleton comprises of actin microfilaments and a number of ABPs. These significantly contribute to the properties and functions of the actin cytoskeleton. ABPs can be grouped into several categories according of their biochemical activities. Profilins represent group of actin monomer-binding proteins regulating polymerization rates of AFs by binding to G-actin. Actin depolymerizing factors (ADFs)/cofillins belong to severing and dynamizing proteins and are supposed to be involved in several aspects of plant morphogenesis. Such dynamizing proteins can change conformation of AFs, cut and facilitate the loss of subunits from the slowly growing end. Fimbrins and villins belong to side-binding proteins which allow formation of higher-order AF structures. They can be classified as crosslinking or bundling proteins (Volkmann and Baluška, 1999; McCurdy *et al*., 2001). The ACTIN-RELATED PROTEINS 2/3 (ARP2/3) and formins belong to the group of nucleation factors which form or stabilize the actin subunits that catalyze polymerization (McCurdy *et al*., 2001; Ketelaar, 2013).

Several studies confirmed that ABPs participate on cell division polarity determination in plants and on the tip growth of pollen tubes (Vidali and Hepler, 2001; Ren and Xiang, 2007; Rasmussen *et al*., 2013; Zhu *et al*., 2013) and root hairs (Baluška *et al*., 2000; Hepler *et al*. 2001). Cooperation

between mitogen-activated protein kinases (MAPKs) and actin cytoskeleton during root hair growth of *Medicago sativa* was also described (Šamaj *et al*., 2002; 2003).

2.1.4.3 Role of AFs in interphase and during cell division

Possibility that actin cytoskeleton could be involved in the positioning CDP was shown on cell suspension cultures of carrot (*Daucus carota* L.) (Traas *et al*., 1987) and on the presence of microfilaments which are associated with the spindle and the phragmoplast (Seagull *et al*., 1987). AFs were also observed in the mitotic spindle during metaphase and anaphase stages. Moreover, a net of actin-bundles linked the spindle to the cortex (Traas *et al*., 1987). Later on, Katsuta *et al*. (1990) confirmed the role of premitotic array of MTs which serves as a scaffold for building up the array of AFs that keeps position of mitotic and cytokinetic apparatuses in tobacco BY-2 cells (Katsuta *et al*., 1990). Studies using fluorescent molecular markers showed presence of F-actin in the early stages of PPB development, and their disappearance in the later stages (Takeuchi *et al*., 2016). The actin cytoskeleton during cell division of *Daucus carota* L. cell suspension cultures was studied using microscopic methods. AFs are also abundant in the phragmoplast during cytokinesis. Disorientations of CDPs in tobacco BY-2 cells were induced by application of actin-depolymerizing or actin-stabilizing drugs (Sano *et al*., 2005; Kojo *et al*., 2013; 2014). Localization analysis showed that MTs intersect AFs between the leading edge of the phragmoplast and the cell cortex (Wu and Bezanilla, 2014). It was also found that *A. thaliana* FORMIN 14 (AFH14) and new kinesin with a calponin homology domain (KCH) isolated from tobacco BY-2 cells promote interactions and crosslinking between MTs and AFs. Both of them play roles in the cell division. KCH is accumulated in PPB and phragmoplast and AFH14 localized to PPB, spindle and phragmoplast (Li *et al*., 2010; Klotz and Nick; 2012). Moreover, a cotton kinesin KCH2 is also able to bind and cross-link MTs and AFs (Xu *et al*., 2009). These facts suggest that AFs and MTs cooperate during mitosis on the establishment of the CDP and the correct deposition of the cell plate.

2.1.5 Cell division plane orientation

Localization studies have shown that TPLATE protein, which is associated with CDZ at the end of cytokinesis, has a function in vesicle-trafficking events required for site-specific cell wall modifications and for anchoring cell plate to the mother cell wall at the correct cortical position

(Van Damme *et al*., 2006; 2011). Syntaxin-like protein KNOLLE mediates vesicle fusion in the CDP (Lauber *et al*., 1997) while it is interacting with SNAP33 (Heese *et al*., 2001). Thus, SNAP33 represents a membrane-associated protein, which accumulates at the plasma membrane and together with KNOLLE plays an important role in the formation of the cell plate during mitosis. Another protein localized to the CDZ is ROOT-SHOOT-HYPOCOTYL-DEFECTIVE (RSH) protein. It is hydroxyproline-rich cell wall glycoprotein that has an essential function in the correct positioning of the cell plate during cytokinesis (Hall and Cannon, 2002). AUXIN-INDUCED IN ROOT cultures 9 (AIR9) is a MAP localizing to PPB and disappearing from the cell cortex after PPB disassembly. Later on, AIR9 reappears at the CDZ, in the place of cell plate insertion (Buschmann *et al*., 2006). Thus, TPLATE, AIR9 and RSH are all implicated in the cell plate attachment to the CDZ and are involved in the cell plate maturation (Hall and Cannon, 2002). Buschmann *et al*. (2006) reported about interaction of AIR9 with KCBP. KCBP is localized to the cortical division plane and remains in the CDZ throughout mitosis linked to the cell cortex via its MyTH4-FERM domain. The MT minus end directed KCBP helps to guide the centrifugally expanding phragmoplast to the CDZ. It was also described that the actin motor protein myosin VIII which is localized at MT ends and moves along actin filaments, plays a role in guiding the growing phragmoplast to the cell wall. This myosin can guide the expansion of the phragmoplast by pulling MTs along the AFs (Wu and Bezanilla, 2014). The plant-specific protein TANGLED (TAN) was characterized as molecular marker remaining at the division site from preprophase to the cytokinesis (Walker *et al*., 2007). Similarly to TAN, also Ran GTPase ACTIVATING PROTEIN 1 (RanGAP1) is a positive protein marker of CDZ, which remains associated with the future site of cell division throughout cell cycle and plays a role in spatial signalling during plant cell division (Xu *et al*., 2008). Finally, findings of Lipka *et al*. (2014) suggest that PHRAGMOPLAST ORIENTING KINESIN 1 and 2 (POK1 and POK2) are key players in division plane maintenance. POKs represent fundamental early anchoring components of the cortical division zone, translating and preserving the positional information of the PPB.

2.2 Plant models for studies of cytoskeleton during mitosis

Medicago sativa as a legume species represents a new and attractive plant organism in cell biology due to its biotechnology potencial. Our research is focused on the study of cytoskeleton during developmental processes. *M. sativa* is challenging organism for long-term live-cell imaging due

to its robust size. *Arabidopsis thaliana* as an established model plant species is routinely used for microscopic analyses. It represents a crucial model in the studies devoted to dynamic cytoskeletal rearrangements in living plant cells.

In the first case, we prepared and regenerated *M. sativa* plants carrying cytoskeletal markers from transgenic somatic embryos while in the second case transgenic *A. thaliana* plants carrying MT marker were germinated from available seeds. Since process of somatic embryogenesis and transformation of *M. sativa* is crucial for regeneration of plants carrying cytoskeletal markers it is described in more detail below.

2.2.1 Basic characteristics of *Medicago sativa*

Medicago sativa Linn., routinly known as alfalfa, belongs to the family Fabaceae. It grows naturaly in the Caucasian region, Iran and Afghanistan, especially in mountains and neighboring regions. The cultivated form probably originated in western Persia. Later it was introduced to many landscapes including the United States of America. Nowadays it is ranking at the fourth place after corn, soybeans and wheat in terms of acreage and economic value (Rashmi *et al*., 1997; Samac and Temple, 2004).

The genus Medicago includes both perennial and annual species. Alfalfa is a very important deep-rooted forage legume, especially due to the widespread production and significance in feeding of livestock, soil protection and enrichment in soil nitrogen (Radović *et al*., 2009). In addition, it is also used by pharmaceutical industry for production of homeopatic medicaments. Last but not least, some annual Medicago species are used in grasslands as cover crops and for weed control. Alfalfa has high contents of proteins, minerals, enzymes (amylase, coagulase, peroxidase, erepsin, lipase, invertase and pectinase) and vitamins A and E. Fresh plants contain a large amount of vitamin C, but about 80% is lost by drying. Thus, *Medicago sativa* represents one of the most valuable crops.

An important feature of legumes is the ability to fix atmospheric nitrogen through symbiotic soil bacteria such as *Sinorhizobium* (Gage *et al*., 1996). The invasion of rhizobial bacteria into host plant is initiated at the tip of root hair. Root hair is able to recognize symbiotic bacteria producing nodulation factor (Nod factor). This Nod factor induces initial host plant responses including root hair deformation and curling (Suzaki *et al*., 2015). It is recognized by the plant Nod factor receptor (NF receptor), which is located in the plasma membrane of plant cells (Limpens *et al*., 2003).

Rhizobia enter root hairs and dividing cortical cells of the host plant throught infection threads (ITs) (Suzaki *et al*., 2015). Expansion of this structure and subsequent branching in root cortex cells provides of bacterial colonization in the primordial nodule formation (Tian *et al*., 2012). The IT contains dividing and growing bacteria which can move through the root hair and transport themselves through several cell layers to the place of the nodule creating (Gage *et al*., 1996). Eventually, rhizobia leave the IT and form structures called symbiosomes, where atmospheric nitrogen (N_2) is fixed. This process consists of 3 steps. First, N_2 is reduced to diimine (N_2H_2), then by another reduction it is converted to hydrazine (N_2H_4). Finally, two molecules of ammonia (2 NH_3) or ammonium ions (2 NH_4 +) are created (Udvardi and Poole, 2013). Ammonia is toxic for the plant at higher concentrations, and is therefore incorporated into newly formed amino acids, most commonly glutamine (Setién *et al*., 2014). Whole process of atmospheric nitrogen requires consumption of large amounts of ATP. In this manner Medicago is involved in the nitrogen cycle in nature.

2.2.2 Somatic embryogenesis of *M. sativa*

Effective plant regeneration from one or more cells in tissue culture is necessary for successful improvement of crops by transformation and genetic modifications (Rashmi *et al*., 1997; Samac and Temple, 2004). Somatic embryogenesis is a developmental process by which diploid somatic cells produce differentiated plants via embryonal phases without fusion of gametes. From a morphological point of view, somatic embryos look like zygotic ones. Somatic embryogenesis was first described by Steward *et al*. (1958) on *Daucus carota* suspension cells and it can likely occur in all plant species under suitable conditions (von Arnold, 2002). Cultivation of explants from diverse organs (e.g. cotyledons, petioles, hypocotyls, stems, leaves) on media supplemented with plant growth regulators can lead either to the production of embryos directly from explant (direct somatic embryogenesis) or to the formation of embryogenic callus (indirect somatic embryogenesis).

Limited initial cell divisions and subsequent plant development were related to direct somatic embryogenesis, which was accompanied by random but frequent cell death in cell aggregates. Embryos grew only from living cells within these cell aggregates (Dijak and Brown, 1987). Overall, somatic embryogenesis depends on the balance between pro-life and pro-death processes. Understanding and compliance of this balance is important for induction of somatic embryos,

especially in poorly regenerable species (Smertenko and Bozhkov, 2014). Somatic embryogenesis is also useful for propagation of sterile or high-value plants due to the low probability of chimera appearance and large numbers of regenerants (Suprasanna and Rao, 1997; Rai *et al*., 2007).

2.2.2.1 Indirect somatic embryogenesis

Inditrect somatic embryogenesis as regeneration procedure consists of several steps. It starts with callus induction, which is followed by formation of somatic embryos, embryo maturation, desiccation and subsequent plant regeneration and development. It has been demonstrated, that alfalfa and other Medicago cultivars can be simply regenerated through somatic embryogenesis (Saunders and Bingham 1972; Mitten *et al*., 1983). Shoot regeneration from callus tissue of *Medicago sativa* L. was described by Saunders and Bingham (1972; 1975) and whole alfalfa plants were produced from callus cultivated on several semisolid media (Saunders and Bingham, 1972). Regeneration was performed in two steps: callus initiation and propagation was carried out using Blaydes medium supplemented with auxin and cytokinin (Blaydes, 1966) while plant regeneration continues with transfer of this callus on Blaydes medium supplemented with yeast extract and myoinositol (possessing no auxin and cytokinin).

Each somatic embryo was created from single callus tissue, but also secondary embryos can be observed. This suggests that it is important to follow development of somatic embryos as independent events (Saunders and Bingham, 1972). In *Medicago sativa*, similarly to *Daucus carota*, somatic embryogenesis is independent on explant type and it can be induced from any part of the plant. In contrast, juvenile tissues are used in other plant species (Litz and Gray, 1995).

The major problems of somatic embryogenesis in many Medicago cultivars are connected with lack of mature embryos and subsequent difficult conversion of embryos to plantlets. Unfortunately, endosperm, as a main source of plant regulators and nutrients, is not developed in somatic embryos of Medicago. Endosperm contains storage carbohydrates (starch) and provides embryo with natural plant regulators (Lai and McKersie, 1994a; Vahdati *et al*., 2008). Hence, appropriate composition of culture media plays a key role in the process of somatic embryogenesis (Amini *et al*., 2016). In general, slower growth and plantlet regeneration is linked to the lower levels of storage proteins in somatic embryos (Lai and McKersie, 1994b). Nevertheless, culture medium can be enhanced with necessary amino acids, vitamins and growth regulators to increase effectivity of somatic embryogenesis.

Optimized procedure published by Samac and Austin-Phillips (2006) contains several media, namely callus induction medium B5H with Gamborg´s vitamins, amino acids, auxin (2,4-D) and cytokinin (kinetin), B50 medium supporting embryo formation with only Gamborg´s vitamins and amino acids, MMS medium for root initiation enriched with Nitsch & Nitsch vitamins, and finally Murashige and Skoog (MS) medium without growth regulators, vitamins and amino acids, which is suitable for maintenance of *in vitro* plants. Many papers describe optimization of culture media composition. Several physical and chemical treatments can be performed to achieve more successful convertion of embryos to plants (von Arnold *et al*., 2002).

2.2.2.2 Direct somatic embryogenesis

Direct somatic embryogenesis leads to plant regeneration without intermediate callus formation. Kao and Michayluk (1980) described direct somatic embryogenesis from leaf mesophyll protoplasts and Lu *et al*. (1983) from leaf and root protoplasts of *M. sativa*. Other approach of direct somatic embryogenesis in Medicago was reported by Denchev *et al*. (1991). Callus stage was omitted by adding polyethylene glycol to the culture medium, thus the whole process of somatic embryogensis was shortened. Leaves of *M. sativa* and *M. falcata* directly produced somatic embryos which were later converted to plants on MS medium. These regenerated plants showed normal morphology.

2.2.3 Growth regulators

Auxins belong to the most important plant growth regulators. They play a key role in cell division and growth but are also involved in the development of plant organs (Hoori *et al*., 2007). In alfalfa, auxins such as 2,4-D (2,4-dichlorophenoxyacetid acid) and 2,4,5-T (2,4,5-trichlorophenoxyacetid acid) induce formation of callus and somatic embryos. CPA (4-chlorophenoxyacetic acid) and NAA (a-naphthaleneacetic acid) support only callus formation. IAA (indole-3-acetic acid) is effectless in both cases. Efficiency of somatic embryos production depends on auxin dose and exposure time (Dudits *et al*., 1991) while high levels of auxins might have also negative effects. Alfalfa suspension culture treated with high concentration of 2,4-D (50 μM) produces many somatic embryos, but they have a low content of storage protein resulting in lower number of converted plants in comparison to embryos exposed to lower concentration of 2,4-D (10 μM)

(Stuart *et al*., 1988). Long term culture under high 2,4-D concentrations can also cause higher somaclonal variability (Larkin, 1987).

In most cases, auxins are added into culture media in combination with cytokinins. Cytokinins are phytohormones playing role in cell division, growth and differentiation. In general, callus is formed when levels of auxin and cytokinin are equal. Roots are induces when auxin concentration is higher, while shoots are induced when cytokinin concentration is higher.

2.2.4 Overview and limitations of *M. sativa* somatic embryogenesis

Propagation and regeneration of plant via somatic embryogenesis is not suitable for all species (Bingham *et al*., 1975; Ammirato, 1983; Vasil, 1988). It is dependent on genotype and is different between cultivars (Bingham *et al*., 1975; Atanassov and Brown, 1984) as well as between genotypes of a cultivar (Kao and Michayluk, 1981). When highly regenerable plants of *M. sativa* were freely intercrossed, offspring regeneration ability decreased. It suggests that genetic background has influence on regeneration capacity (Reisch and Bingham, 1980; Hernández-Fernández and Christie, 1989; Kielly and Bowley, 1992; Crea, 1995). This fact causes serious problem for biotechnology. Moreover, genotype can be influenced both genetically and epigenetically (e.g. by pattern of chromatin condensation). It is likely that somatic embryogenesis is affected by DNA methylation, histone post-translational modifications and micro RNA (miRNA) pathways. DNA methylation is heritable and can be conserved during mitosis (Henderson and Jacobsen, 2007).

Kao and Michayluk (1980) studied embryo-like structures iniciated from mesophyll protoplasts of alfalfa leaves. Protoplasts isolated from young leaves divided faster than protoplasts isolated from older ones. Division frequency of protoplasts and capability to form embryos and plantlets varied significantly from plant to plant within the same cultivar. They also described genotypic variation of alfalfa embryogenic callus derived from cell suspension culture established from shoot tips. Only seven from total nine different alfalfa cultivars succesfully converted their somatic embryos to plantlets (Kao and Michayluk, 1981). Atanassov and Brown (1984) clarified that highly regenerable cultivars of alfalfa produce more somatic embryos irrespective of media protocol and type of explant (Brown and Atanassov, 1985). Similar results were obtained by Chen and colleagues (1987). Moreover, they observed that the same genotypes produced large amounts of embryos from calli, derived from cotyledons or leaves. Hindson *et al*. (1998) studied various

pretreatments such as addition of abscisic acid (ABA), glutamine and sucrose into culture media following by dessication of four different genotypes of alfalfa somatic embryos and their effect on conversion to plants. Results showed some positive effect mainly after supplementation of 1 μM ABA, 50 mM glutamine and 5 % sucrose into media, but it was not uniform for all genotypes.

Barbulova *et al*. (2014) tested regeneration ability of five Bulgarian alfalfa cultivars via indirect somatic embryogenesis. Explants from *in vitro* grown leaves and petioles were incubated on different media with various growth regulators. Only three cultivars were able to convert to plantlets.

Novák and Konečná (1982) showed influence of explant source on *in vitro* alfalfa regeneration. Type of primary explant correlated with cell growth rate in following order: cotyledon > petiole > hypocotyl > stem> leaf.

Medium enriched with auxin and ethinyl estradiol supported development of somatic embryos while medium containing NAA and TDZ (thidiazuron) induceed development of shoots at stems of *M. sativa*. Roots appeared on leaves cultured on NAA and ethinyl estradiol (Hoori *et al*., 2007). Brassinosteroids and abscisic acid are also involved in the induction of callus and in some species they can replace auxin or cytokinin (Hu *et al*., 2012). Additional substances which could support maturation and conversion of somatic embryos to plantles are obtained from the extract of *Cuscuta campestris* (Amini *et al*., 2016).

Uninduced callus of alfalfa can be pretreated with different organic acids even before culture on induction medium containing 2,4-D (Nichol *et al*., 1991). The embryos produced from pretreated calli have better morphology as those arrising from untreated callus cells. Nevertheless, in general organic acid pretreatment alone can not replace auxin during callus embryogenic induction (Nichol *et al*., 1991). Next, it was found that proline, thioproline and potassium are involved in stimulation of somatic embryogenesis in *M. sativa* (Shetty and McKersie, 1993).

Low vitality of alfalfa seeds is a clear disadvantage for massive plant production and biotechnological applications (Senaratna *et al*., 1990). However, somatic embryos of *M. sativa* can be dried, stored for few months and subsequently imbibed and germinated. It was found, that phytohormone ABA can positively regulate desiccation of alfalfa somatic embryos while slow drying rate also plays an important role. Combination of both provides the best solution to achieve maximal survival rate of alfalfa somatic embryos. Moreover, tolerance to drought can be improved

by heat shock, usually showing no side effects. Triazole and uniconazole are also used, but they negatively affect growth of seedlings (Senaratna *et al*., 1989).

Generally, ABA plays important role in plant responses to unfavorable conditions, especially abiotic stresses such as drought, cold and high salinity. The highest ABA level during middle stages of seed development is associated with assembly of storage reserves. Raffinose oligosaccharides such as galactinol, raffinose and stachyose are accumulated during the late development of seeds. It was found that exogenous ABA raises levels of raffinose oligosaccharides in alfalfa somatic embryos (Blöchl *et al*., 2005).

Light quality and intensity were shown to be significant factors influencing the rate of embryo maturation. *M. sativa* somatic embryos were particularly sensitive to high light levels during the early stages of somatic embryo elongation. Full spectrum light seems to be the most suitable illumination method for growing embryos since blue, green, yellow and red filters caused lower quality of somatic embryos (Anandarajah *et al*., 1992).

2.2.5 Stable transformation of *M. sativa*

2.2.5.1 *Agrobacterium tumefaciens*-mediated transformation

Transformation of *Medicago sativa* was realized by various methods. *Agrobacterium tumefaciens*-mediated transformation is the most common one. Initial experiments optimized parameters essential for rapid production of transgenic alfalfa plants. First it was found, that succes of alfalfa transformation depends on the strain of *A. tumefaciens*. Cocultivation of stem explants from *M. sativa* with disarmed *A. tumefaciens* strain LBA4404 was made in the pilot experiment (Shahin *et al*., 1986). Du *et al.* (1994) tested four strains of *A. tumefaciens* with three *M. sativa* genotypes. One combination of genotype (petiole of C2-4 genotype) with bacteria strain A281 led to the transgenic plant.

Desgagnés *et al*. (1995) tested several combinations of alfalfa genotypes, expression vectors and bacterial strains, and also observed a strong plant genotype - bacterial strain interaction. Strain LBA4404 containing vector pGA482 and genotype 11.9 showed the highest efficiency of transformation (60%). It was also found, that length of cocultivation has influence on transformation. Prolonged period of cocultivation, until eight days, can have positive effect on transformation frequency, though suitable cocultivation period is probably genotype dependent (Austin *et al*., 1995; Samac, 1995).

Common selectable marker in transformation of *M. sativa* is *neomycin phosphotransferase II* (*nptII*) gene, which provides kanamycin resistance. Concentration of kanamycin used for selection plays an important role. It was found that kanamycin concentration up to 50 $mg \cdot l^{-1}$ inhibits growth of untransformed calli while 50 to 100 $mg \cdot l^{-1}$ can be used for selection of transformed calli, embryos and roots (Chabaud *et al*., 1988). Higher amounts of kanamycin inhibit critical stages of transformation such as callus development, embryo induction and root formation (Chabaud *et al*., 1988; Austin *et al*., 1995). Production of alfalfa transgenic lines with the bialaphos resistance gene (also called *bar* gene) that confers phosphinothricin resistance or with gene encoding resistance to antibiotic hygromycin is also possible (D'Halluin *et al*., 1989; Tabe *et al*., 1995).

Samac and Austin-Phillips (2006) described protocol for efficient stable transformation of *Medicago sativa.* They reported that 80 to100% of transformed plants regenerated via somatic embryogenesis are able to incorporate T-DNA of *A. tumefaciens*. Authors used leaves of highly regenerable genotypes of variety Regen-SY and *Agrobacterium tumefaciens* strain LBA4404. Other bacterial strains were tested, but low efficiency or low frequency of transformed plants was observed (Samac, 1995). Transgenic alfalfa plantlets can be generated 9 to 14 weeks after cocultivation with Agrobacteria.

In addition, transformation of Medicago species protoplasts using *Agrobacterium tumefaciens* and electroporation was also described (Kuchuk *et al*., 1990). However, this method did not find a wide practical application.

2.2.5.2 Other stable transformation methods

Transformation by particle bombardment

Biolistic method of alfalfa transformation by particle bombardment is not so favored as transformation mediated by *A. tumefaciens*. Nevertheless, direct introduction of DNA into alfalfa cells might save some time during preparation of transgenic plants. Ramaiah and Skinner (1997) described an effective delivery of DNA by microprojectile bombardment of pollen. Male sterile plants were pollinated with bombarded pollen to produce fertile seeds. Incorporation of *GUS* gene was confirmed by PCR and Southern blot analysis in 30% of plants obtained from fertile seeds. Southern blot data revealed multiple inserts or truncated copies of *GUS* gene. Unfortunately, some lines lost incorporated *GUS* gene while number of copies decreased after vegetative propagation. The reasons for the loss of incorporated DNA in the next generations are not well understood yet.

Pereira and Erickson (1995) reported stable nuclear transformation of *M. sativa* petiole- and stem-derived callus cells by particle bombardment. From 2035 bombarded explants, only seven transgenic plants were regenerated. Segregation of the *NPTII* gene in the crossed progeny followed a 1:1 Mendelian ratio for a single locus insertion in a heterozygous state.

Finally, protocol of alfalfa chloroplast transformation via particle bombardment was also described. Gene encoding a GREEN FLUORESCENT PROTEIN (GFP) was inserted into plastid genom. PCR and Southern blotting confirmed a presence of foreign gene, but efficiency of transformation was quite low. Occurrence of GFP in chloroplasts was observed using epifluorescence microscopy (Wei *et al*., 2011; Xing *et al*., 2014). This method could help to improve agronomically and commercially important properties of *Medicago sativa* in the future.

Transformation via vacuum infiltration

Two plant transformation approaches of *Medicago truncatula* based on vacuum infiltration were developed. The first method was based on *Arabidopsis thaliana* transformation protocol using vacuum infiltration (Bechtold *et al*., 1993). Flowering *M. truncatula* plants were infiltrated with *Agrobacterium tumefaciens* suspension. The second approach was infiltration of young *M. truncatula* seedlingswith *Agrobacterium*. It allowed simultaneous transformation of a large number of individual seedlings (Trieu *et al*., 2000). Both procedures yielded a low amount of transformants, which were genetically stable in T2 generation. Several *A. tumefaciens* strains were successfuly used, while the strain LBA4404 widely used in tissue culture transformation method of Medicago species was not approved as a suitable one (Trieu *et al*., 2000).

2.2.5.3 MTs in Medicago species

Little is known about MT dynamics and organization in legume plants. Some live-cell imaging analyses were performed on *Medicago truncatula*. Root hairs of *M. truncatula* were used for detailed visualization of MT dynamics using GFP-microtubule binding domain (MBD) and EB1-YELLOW FLUORESCENT PROTEIN (YFP) markers after Nod-factor treatments (Sieberer *et al.,* 2002; Sieberer *et al.,* 2005; Timmers *et al*., 2007). It was revealed that cortical MTs were present during the whole process of root hair development including fully developed non-growing root hairs, while endoplasmic MTs were observed in tip-growing root hairs. These endoplasmic

MTs formed 3D arrays in subapical cytoplasmic areas of root hairs (Sieberer *et al.,* 2002). After Nod-factor application, shortening of endoplasmic MTs was observed in growing root hairs whereas cortical MTs were not affected (Sieberer *et al*., 2005). It was also found, that frequency of EB1 protein labelling at MT plus ends correlated with the age of the root hair. Young and growing root hairs showed a higher number of EB1 particles as compared to older non-growing root hairs. Significant decrease in speed of moving EB1 particles was observed in root hairs of *M. truncatula* after Nod-factor treatment. Treatments with oryzalin, taxol and cytochalasin D showed that MTs are involved in root hair reorientation after Nod-factor treatment (Sieberer *et al*., 2005). Combined treatments by cytoskeletal inhibitors and Nod factors caused also higher growth rates of *M. sativa* root hairs (Weerasinghe *et al*., 2003). Application Nod-factor alone induced rapid changes in MT organization. After 3-10 min, endoplasmic and subsequently also cortical MTs were depolymerized, primarily at the proximal ends of cells. This was followed by depolymerization of most MTs after 20-30 min. Nevertheless, MT cytoskeleton reformed after 1h of Nod factor treatment (Weerasinghe *et al*., 2003). Later on, organization, bundling and polymerization of MTs in root hair tips of *M. truncatula* were studied using GFP-MBD marker (Timmers *et al*., 2007). In addition, actin cytoskeleton was visualized in interface and post-mitotic root cells and in root hairs of *M. truncatula* using molecular markers such as Plastin-GFP and GFP-mTalin (Voigt *et al.,* 2005).

Recently, a study focused on dynamic patterns of mitotic MTs in *M. sativa* roots was published. Using light-sheet fluorescence microscopy it was found that root growth rate correlated with progression of mitotic MTs during cell divison (Vyplelová *et al*., 2017).

2.2.6 MTs in *Arabidopsis thaliana*

A. thaliana is the most extensively studied model plant in cell biology, especially due to the short generation cycle, small habitus and ability to be easily cultivated under routine experimental conditions. This plant can be quite easily and efficiently genetically manipulated by transformation with *Agrobacterium tumefaciens*. Moreover, *A. thaliana* genome has been fully sequenced and large numbers of functional mutants are freely available from public sources. The most commonly used MT molecular markers including MBD of MAMMALIAN MICROTUBULE-ASSOCIATED PROTEIN 4 (MAP4) as well as markers based on tagging α- or β-tubulin isoforms

with GFP or other fluorescent proteins such as YFP, CFP (cyan), tagRFP and mCherry (red) were successfully used in *A. thaliana* (Marc *et al*., 1998; Hasezawa *et al*., 2000; Murata *et al*., 2013; Walker et al., 2007).

The root apical meristem of *A. thaliana* is regularly used for live MT imaging due to the high frequency of cell divisions (Müller *et al*., 2004; Walker *et al*., 2007; Panteris *et al*., 2011; Lipka *et al*., 2014; Rybak *et al*., 2014; Buschman *et al*., 2015; Steiner *et al*., 2016; Stöckle *et al*., 2016). Microscopic methods are also applied to study organization and dynamics of MTs in hypocotyls (Shaw *et al*., 2003; Lucas *et al*., 2011; Komis *et al*., 2014), cotyledons (Beck *et al*., 2011; Komis *et al*., 2017) or leaf petioles (Komis *et al*., 2017; Novák *et al*., 2018; Vyplelová *et al*., 2018) representing green aerial parts of *A. thaliana*.

2.3 Modern microscopic methods for studies of mitotic MTs in plants

Mitotic cell division in plants is a dynamic process playing a key role in plant morphogenesis, growth and development. Since progress of mitosis is highly sensitive to external stresses, documentation of mitotic cell division in living plants requires fast and gentle live-cell imaging microscopy methods and suitable sample preparation procedures. Following sections describe currently used advanced microscopy methods for the live-cell visualization of the entire process of plant mitosis. These methods include microscopy modalities based on light-sheet, spinning disk and Airyscan confocal laser scanning bioimaging of tissues or whole plant organs with diverse spatio-temporal resolution.

2.3.1 Light-sheet fluorescence microscopy

Quite recently, light-sheet fluorescence microscopy (LSFM) has been introduced into plant developmental biology, although the number of applications is still limited due to the difficult preparation of living plants. In general, the primary goal of LSFM is to achieve long-term observations and bioimaging of developing plants at the subcellular, cellular, tissue, organ and whole plant level under gentle environmental conditions (Maizel *et al*., 2011; Ovečka *et al*., 2015; Vyplelová *et al*., 2017). Embedding in agarose provides plant stabilization in the vertical position respecting the gravity vector. It might be, however, not physiological, especially for the upper aerial part of plant. Therefore, several modifications and optimizations of plant sample preparations were described in recent studies (Ovečka *et al*., 2015; von Wangenheim *et al*., 2017;

Vyplelová *et al*., 2017; 2018). Substantial benefit of a vertically oriented plant growing under controlled conditions favours LSFM as an advanced non-invasive microscopy technique for long-term plant developmental imaging. This method offers fast optical sectioning of the sample and free rotation of the sample for multi-angular image acquisition, thus allowing an efficient 4D (x, y, z, and t) imaging. Excitation of fluorophores occurs only within the light-sheet volume. It eliminates out-of-focus fluorophore excitation and light emission, therefore phototoxicity and photobleaching are eliminated. The total excitation energy absorbed by sample in LSFM is much lower as compared with epifluorescence and confocal scanning platforms (Ichikawa *et al*., 2014; Stelzer, 2015). From technical point of view, it is important that the focal plane of the two thin sheets of light is identical to the focal plane of the objective used to scan the sample. This allows imaging of a very thin layer of the sample without spherical aberrations. Detection of sample is perpendicular to the sheets of light. The commercial type of LSFM such as Zeiss Lightsheet Z.1 is based on a selective-plane illumination microscopy (SPIM) principle with a horizontal setup for both illumination and detection objectives. Sample is vertically placed into microscopic chamber from above and recorded by high-quality sCMOS camera (Fig. 2).

Unfortunately, LSFM data are very big and usually exceed terabyte size. This makes the storage, processing and analysis of data quite difficult. Nowadays, there are software applications that efficiently resolve data handling problems such as BigDataViewer (Pietzsch *et al*., 2015) and TeraFly (Bria *et al*., 2016).

It is important to note that live-cell imaging of dividing plant cells using LSFM is sufficient to resolve all MT arrays during mitosis and cytokinesis. Moreover, LSFM offers deep imaging of dividing cells inside of living multicellular plant organs. Good spatial and high temporal resolution of LSFM ensures recording of cell division in growing and developing plant tissues in real time in periods from a few hours to a few days.

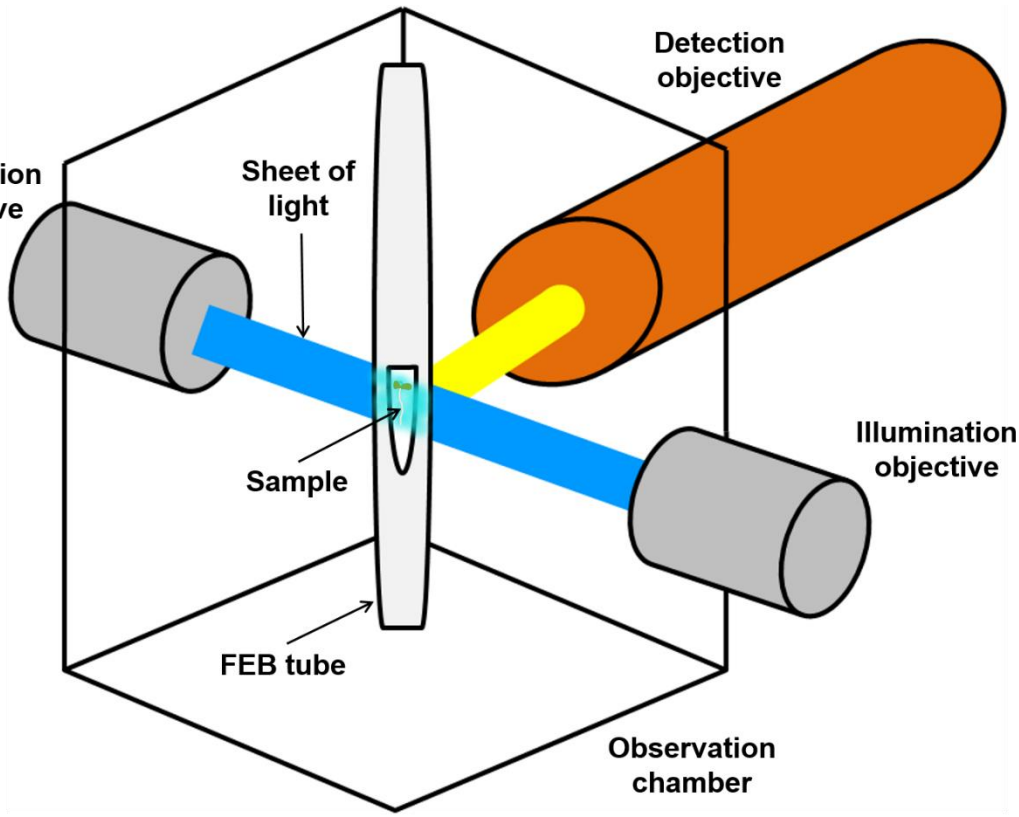

Figure 2. Principle of the LSFM. Scheme describes the arrangement of the illumination optics for generation of the light sheet, the position of the plant embedded in the FEP tube in the observation chamber and the acquisition of the image by detection objective. Adapted from Ovečka *et al*., 2015.

2.3.2 Spinning disk confocal microscopy

Spinning disk confocal microscopy (SDCM) is a high-speed method that captures optical fragments. SDCM is mostly used for short-term observation of the cytoskeleton at the cellular level or for microscopic analysis of intracellular distribution of fluorescently-labelled markers at high spatial and temporal resolution. This method is based on fast rotating disk with multiple pinholes (Nipkow disk) allowing sample illumination by thousands of light rays at the same time while a confocal image with low non-specific backgrounds is captured by high-performance chip (Fig. 3).

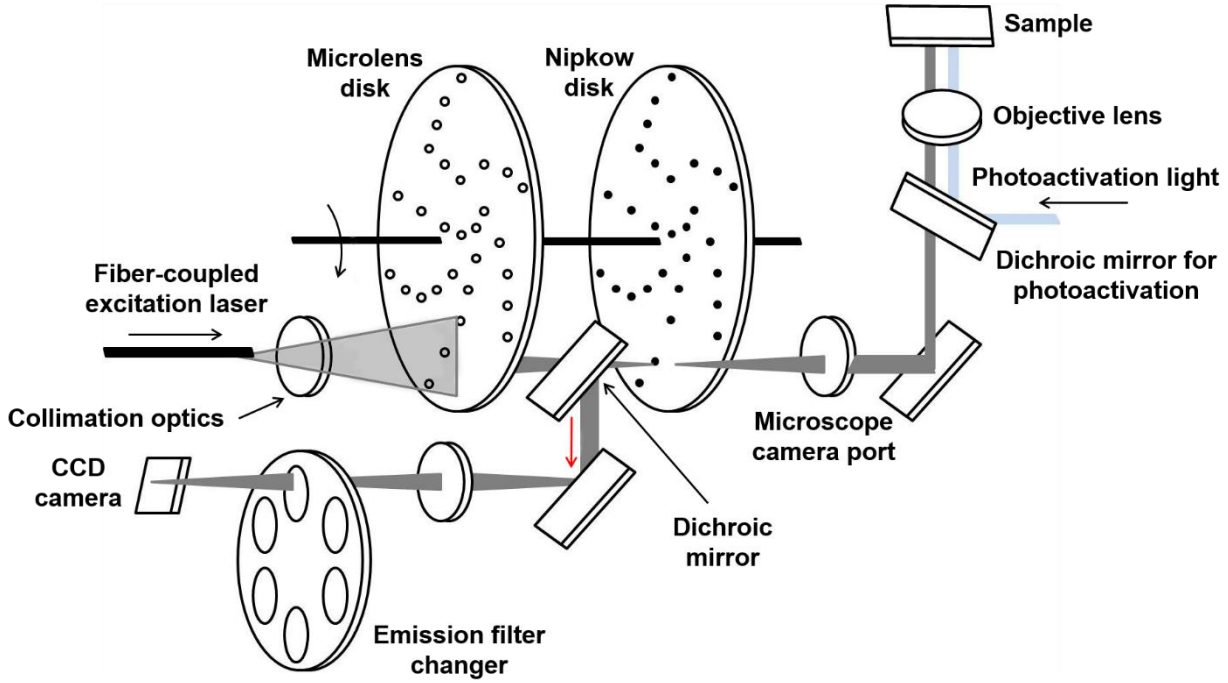

Figure 3. Principle of the SDCM. Excitation light is focused through the pinholes by lenses at microlens disk, which are aligned with the pinholes at Nipkow disk. Longer wavelength emission light returning from the sample is reflected out of the excitation light path by a dichroic mirror located between the two disks. Red arrow indicates the emission light path. Adapted from Stehbens *et al*., 2012.

A speed of scanning can be up to 1000 frames per second. SDCM produces 2D or 3D images projected with CCD or EMCCD cameras in real time. However, this method has also some disadvantages. It can cause photo-damage of the sample, especially when intensity of fluorescencein the sample is low and it is necessary to increase the intensity of illumination. Each point of sample is scanned for several hundred times and the final image is the result of many short exposures at low excitation light intensity. In contrast, for classical confocal microscopy is typical that each spot is scanned only once but delays during scanning of sample are created and high intensity of excitation light is required (Wang *et al*., 2005; Stehbens *et al*., 2012). Other limitation of SDCM is that light scattered or emitted by structures residing in regions removed from the focal plane can still reach the detector by traveling through adjacent pinholes. This artefact increases the background signal in thicker specimens, and therefore ultimately reduces the axial resolution of the system.

2.3.3 Airyscan confocal laser scanning microscopy

Airyscan confocal laser scanning microscopy (CLSM) is a modern microscopic method with improved resolution, sensitivity and speed. Airyscan operates with a hexagonally packed detector array used instead of a physical confocal pinhole aperture and unitary detector. The hexagonal design allows detecting the Airy orders separately in one snap without losing any signal. Detector has area of 32-channel gallium arsenide phosphide photomultiplier tube (GaAsP-PMT) that collects a pinhole-plane image at every scan position. Each detector element functions as a single, very small pinhole. Zoom optics can image from one up to four Airy units (AU) on the detector diameter. Airyscan is based on the fact that a fluorescence microscope will image a point-like source as an extended Airy disk (Airy pattern) (Fig. 4). This new concept dramatically improves signal by collecting light that otherwise is reduced by the confocal pinhole. The increased signal-to-noise ratio can be used to save high resolution information. Airyscan delivers 1.7x higher resolution in all three spatial dimensions and increases the signal-to-noise ratio by 4–8x compared with traditional CLSM systems with a 1-AU pinhole (Weisshart, 2014; Huff *et al*., 2015).

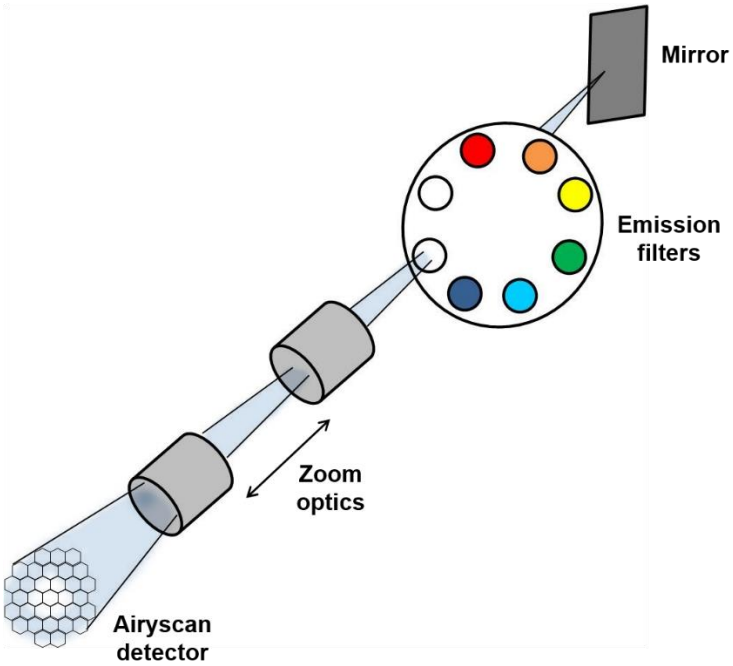

Figure 4. Principle of the Airyscan. The Airyscan detector consists of hexagonally arranged 32-channel GaAsP-PMT elements. Each element acts as its own small pinhole with positional information. The Airyscan detector is positioned in a conjugate focal plane relative to the excitation spot and uses zoom optics. Adapted from Weisshart, 2014.

3. RESULTS

3.1 Advanced microscopy methods for bioimaging of mitotic microtubules in plants

3.1.1 Abstract

Mitotic cell division in plants is a dynamic process playing a key role in plant morphogenesis, growth and development. Since progress of mitosis is highly sensitive to external stresses, documentation of mitotic cell division in living plants requires fast and gentle live-cell imaging microscopy methods and suitable sample preparation procedures. The present chapter describes, both theoretically and practically, currently used advanced microscopy methods for the live-cell visualization of the entire process of plant mitosis. These methods include microscopy modalities based on spinning disk, Airyscan confocal laser scanning and light-sheet bioimaging of tissues or whole plant organs with diverse spatio-temporal resolution. Examples are provided from studies of mitotic cell division using MT molecular markers in the model plant *A. thaliana*, and from deep imaging of mitotic MTs in robust plant samples, such as legume crop species *M. sativa*.

3.1.2 Introduction

Cellular preparations for mitotic entry in plants are marked by a dramatic reorganization of the cortical MT array to an annular cortical assembly, the PPB (Rasmussen *et al*., 2011) which is considered as a marker of the CDZ and a predictor of cell plate fusion at the parent walls (Smertenko *et al*., 2017). In this way, PPB acts as a determinant of symmetric and asymmetric cell divisions (Rasmussen *et al*., 2011). Initially, the PPB is loosely organized but progressively narrows until the perinuclear prophase spindle assembles (e.g., Vos *et al*., 2004). Thereon the PPB disassembles and the mitotic chromosome segregation starts.

Principally, the PPB is a MT array and therefore primarily consists of MTs and a wide array of MAPs with bundling (e.g., members of the MAP65 family; Li *et al*., 2017), motor (members of the kinesin superfamily; see later) and regulatory (e.g., EB1 proteins; Chan *et al*., 2003; 2005, and the HEAT repeat protein MOR1/GEM; Twell *et al*., 2002) activities. Apart from MTs and MAPs, the PPB also contains actin microfilaments which facilitate the coalescence of cortical MTs (Kojo *et al*., 2013) and several other molecules recruited on site and persisting long after the disappearance of the PPB in a continuous or discontinuous manner. Such molecules, which serve as markers of the CDZ include TAN (Walker *et al*., 2007), POK 1 and 2 (Müller *et al*., 2006),

FASS/TONNEAU2 (Camilleri *et al*., 2002), AIR9 (Buschmann *et al*., 2006), RanGAP1 (Xu *et al*., 2008) and KCBP (Buschmann *et al*., 2015). Characteristically, some mutants in corresponding genes exhibit marked CDP related phenotypes (Tab. 1 and references therein).

Segregation of duplicated genetic material between two daughter cells in the process of mitosis is a conserved feature among eukaryotes and requires the assembly of the mitotic spindle (Prosser and Pelletier, 2017). In animals and fungi, the assembly of the MT-based mitotic spindle is dominated by the occurrence of structurally defined MTOCs with MT nucleating capacity such as the centrosome (Vertii *et al*., 2016) and the spindle pole body (Kilmartin, 2014). In higher plants, however, mitotic spindle assembly is acentrosomal and its form undergoes significant changes during mitotic progression (Yamada and Goshima, 2017). The plant mitotic spindle is bipolar and it largely comprises of kinetochore MT bundles but it lacks astral MTs, possibly due to the absence of MTOCs at the spindle poles. As in the case of the PPB, several MAPs involved in MT nucleation, regulation of plus-end dynamics, MT bundling and MT-dependent motor activities as well as other proteins with regulatory functions such as protein kinases were found to be enriched in the mitotic spindle (reviewed in Yamada and Goshima, 2017).

At the end of mitosis, the mitotic spindle is replaced by the plant specific cytokinetic apparatus, the phragmoplast. The phragmoplast directs the translocation of cell wall material containing vesicles to the equatorial plane, where they fuse and form the nascent daughter plasma membrane and the cell plate. The phragmoplast expands from the cell center towards the cell periphery in a well-defined plane, which is called the CDP (Smertenko *et al*., 2017). Finally, the expanding cell plate fuses to a well-defined cortical site which is called the cell plate fusion site. This site is adjusted to a predetermined CDZ (Smertenko *et al*., 2017) which is in turn defined by the PPB (Smertenko *et al*., 2017 and references therein). Phragmoplast expansion requires the gradual disappearance of MTs from its central area and their confinement to the cell periphery through a concerted function of γ-tubulin dependent MT nucleation and MAP65 dependent MT bundling. During the process, phragmoplast positioning may be subject to corrective motions (e.g., Komis *et al*., 2017) through a navigation process probably mediated by acto-myosin cytoskeleton (e.g., Wu and Bezanilla, 2014).

Significant studies on the progressive development of the PPB, the assembly and the positioning of the mitotic spindle as well as on the centrifugal expansion of the cytokinetic phragmoplast, and the deposition of the cell plate were done in non-model plants. Most such studies were carried out

by means of transmission electron microscopy or immunofluorescence imaging (e.g., Gunning *et al*., 1978; Wick and Duniec, 1983; Samuels *et al*., 1995; Kojo *et al*., 2013) combined with the use of cytoskeletal (e.g., Panteris *et al*., 1995) or other inhibitors (e.g., Binarová *et al*., 1998) that broadly or selectively affected the above processes. The establishment of *A. thaliana* as a genetically tractable model of plant growth and development, the design of robust protocols for the generation of transgenic plants bearing appropriate fluorescent markers, and the establishment of CLSM as a routine method of imaging, allowed *in vivo* visualization of mitosis and cytokinesis in a dynamic manner. Other studies used suspension culture cells of tobacco bright yellow-2 (BY-2), a material that can be easily transformed, maintained and synchronized to provide thousands of cells in diverse mitotic stages for visualization (e.g., Granger and Cyr, 2000; Yoneda *et al*., 2005; Buschmann *et al*., 2011). However, such suspension-cultured cells lack the spatial constraints of mitotic progression found in intact tissues and they are not allowing deductions on spindle orientation and the regulation of CDP orientation necessary for pattern formation, morphogenesis and organ development in plants.

The dynamic imaging of mitosis and cytokinesis in living plant cells can convey very useful information regarding the rates of PPB narrowing (e.g., Vos *et al*., 2004; Komis *et al*., 2017) and disturbances of its formation after pharmacological (e.g., Kojo *et al*., 2014) or genetic (Komis *et al*., 2017) interference. Moreover, this approach can provide data on the duration of mitosis and the subsequent phragmoplast expansion (e.g., Beck *et al*., 2011; Komis *et al*., 2017) and it can reveal mechanisms behind mitotic and cytokinetic aberrations of appropriate mutants. Keys to successful imaging of the above processes in plants include the sufficient depth of the selected microscopy method and adequate speed of acquisition to avoid motion artefacts arising by intracellular motions of the mitotic MTs. Most importantly, the selected method should ensure the minimal exposure of the dividing cell to phototoxic excitation illumination which may delay, abort or disturb the progress of mitosis and cytokinesis or compromise the viability of the sample during imaging (see Laissue *et al*., 2017 for a critical assessment of phototoxicity during live fluorescence imaging).

The present chapter aims to summarize the bioimaging possibilities in the studies of mitotic progression *in planta* by advanced methods that were developed and commercialized over the past few years. These methods have expanded the possibilities of dissecting mitosis and cytokinesis in living plants and provided a considerable improvement of spatial and temporal resolution. High

speed and mass visualization of the mitoses can be done in whole organs such as roots or leaves with LSFM allowing imaging of subcellular details at a moderate spatial resolution. Mitosis can be followed in better spatial resolution with fast imaging modalities such as SDCM, while high-resolution methods such as Airyscan CLSM can be used to decipher fine structural details in the assembly of the PPB, the mitotic spindle and the cytokinetic phragmoplast. We are providing imaging possibilities of two different plants, the plant model *Arabidopsis thaliana* and the legume crop *Medicago sativa* which pose different challenges for sample preparation and image acquisition.

3.1.2.1 Preparation of molecular markers for the visualization of mitotic MT arrays

The *in vivo* visualization of the mitotic progress in plants requires selective molecular labelling of MTs and for this purpose three different MT molecular markers have been routinely used in related studies. The first MT marker that was introduced in plant cell biology is GFP fusion with the MBD of the non-neuronal MAP 4 (GFP-MBD; Marc *et al*., 1998). This marker has been used to report cortical MT dynamics, PPB, mitotic spindle and phragmoplast rearrangements.

Tubulin fusions with some fluorescent proteins can also be used to visualize MT dynamics during cell division and cytokinesis. Examples of such fusions include several α- and β-tubulin isoforms (such as TUA2, TUA5, TUA6 and TUB6) fused to GFP, YFP, CFP, tagRFP and mCherry (Hasezawa *et al*., 2000; Walker *et al*., 2007; Murata *et al*., 2013).

Finally, MT reporters that have been used in plant mitotic research include the plus-end binding proteins EB1a and EB1b which have been used as GFP fusions (Chan *et al*., 2003; 2005).

The expression of all of these markers is driven by the strong constitutive promoter 35S of cauliflower mosaic virus. For this reason care must be taken to avoid disturbances related to overexpression as described before and to this respect tubulin fusions are probably the best markers. MBD fusions rather could be avoided (Celler *et al*., 2016) although at moderate expression levels they can be used to follow mitotic spindle and phragmoplast dynamics (Beck *et al*., 2011).

A more thorough evaluation of microtubular markers has been presented before (Buschmann *et al*., 2010) with an account on their advantages and disadvantages. Since not all of them have been used in Arabidopsis or in studies of plant mitosis and cytokinesis, they will not be iterated here.

3.1.2.2 Use of Arabidopsis mutants to dissect mitotic progression in plants

Our knowledge on the mitotic progression in plants lags significantly behind that in animals. Nevertheless, the establishment of seed collections of Arabidopsis mutants has led to the identification of important proteins that are involved in the process and uncovered plant unique or conserved mechanisms of mitotic spindle assembly and the subsequent process of cytokinesis. Tab. 1 summarizes published work on several Arabidopsis mutants defective in mitosis, cytokinesis or CDP orientation and specifies the related defects.

Table 1. List of Arabidopsis mutants with reported mitotic and/or cytokinetic defects. Table includes only mutants somehow related to cytoskeletal regulation and excludes mutants relevant to associated processes such as membrane trafficking. Adapted from Vyplelová *et al*., 2018.

Protein	**Role**	**Accession number**	**Mutant name/ designation**	**Mutant characteristic**	**Described defect**	**Reference**
MICROTUBULE ASSOCIATED PROTEINS						
γ-tubulin (TUBG1 and TUBG2)	MT nucleation	AT3G61650 (TUBG1), AT5G05620 (TUBG2)	TUBG1^{RNAi}, *tubg1-1*, *tubg2-1*, *tubg2-2*	Downregulation of TUBG1 levels by RNA interference; *tubg1-1*, *tubg2-1* and *tubg2-2* are T-DNA insertional mutants	Aberrant mitotic spindle and phragmoplast formation	Binarová *et al*., 2006; Pastuglia *et al*., 2006
GAMMA TUBULIN COMPLEX PROTEIN 4 (GCP4)	MT nucleation	AT3G53760	amiR-GCP4	Knock-down mutant by artificial microRNA	Aberrant spindle and phragmoplast formation	Kong *et al*., 2010
GCP3-INTERACTING PROTEIN1 (GIP1) AND GIP2	MT nucleation	AT4G09550 (GIP1), AT1G73790 (GIP2)	*gip1*, *gip2*	T-DNA insertional mutants	Disorganization and malpositioning of mitotic spindle	Janski *et al*., 2012
AUGMIN SUBUNITS 1, 2, 3, 4, 5 and 7 (AUG1 to 5 and 7)	MT nucleation	AT2G41350 (AUG1), AT2G32980 (AUG2), AT5G48520 (AUG3), AT1G50710 (AUG4), AT5G38880 (AUG5), AT5G17620 (AUG7)	*aug1-1*, *aug2-1*, *aug3-1*, *aug4-1*, *aug5-1*, *aug7-1*	T-DNA insertional mutants	Abnormal mitosis and cytokinesis in dividing microspores	Ho *et al*., 2011b; Hotta *et al*., 2012
NEURAL PRECURSOR CELL EXPRESSED, DEVELOPMENTALLY DOWN-	MT nucleation	AT5G05970	*nedd1*	T-DNA insertional mutant	Abnormal mitosis and cytokinesis in dividing microspores	Zeng *et al*., 2009

REGULATED GENE 1 (NEDD1)						
ENDOSPERM DEFECTIVE1 (EDE1)	MT binding	AT2G44190	*ede1-1*	T-DNA insertional mutant	Defective cytokinesis during endosperm cellularization	Pignocchi *et al*., 2009
MAP65-1	MT bundling	AT4G26760	*map65-1-1*, *map65-1-2*	T-DNA insertional mutants expressing truncated MAP65-1	No detectable phenotype; double *map65-1 map65-2* mutants show fewer cell files in the root	Lucas *et al*., 2011; Lucas and Shaw, 2012
MAP65-2	MT bundling	AT4G26760	*map65-2-1*, *map65-2-2*	T-DNA insertional mutants expressing truncated MAP65-2	No detectable phenotype; double *map65-1 map65-2* mutants show fewer cell files in the root	Lucas *et al*., 2011; Lucas and Shaw, 2012
MAP65-3	MT bundling in mitosis/ cytokinesis	AT5G51600	*pleiade* (*ple*)*1*, *pleiade2*, *pleiade 3*	*ple1* and *ple2* are ethylmethylsulfonate (EMS)-induced mutants, while *ple3* is T-DNA insertional mutant	Incomplete cytokinesis, multinucleate cells	Müller *et al*., 2002; 2004; Söllner *et al*., 2002; Steiner *et al*., 2016
MAP65-4	MT bundling in mitosis/ cytokinesis	AT3G60840	*map65-4*	T-DNA insertional mutant expressing truncated MAP65-4	Additive to MAP65-3 depletion	Li *et al*., 2017
KATANIN p60 subunit	MT severing	AT1G80350	*ktn1-2*, *fra2*, *lue1*	*fra2* is EMS-induced point mutation expressing KATANIN with altered properties; *lue1* contains premature stop codon and expresses truncated KATANIN and *ktn1-2* is T-DNA insertional mutant disrupting KATANIN function	Aberrant PPB formation, extensive spindle rotations, prophase spindle multipolarity, elongated MTs in the phragmoplast	Panteris and Adamakis, 2012; Komis *et al*., 2017
PHRAGMOPLAST ORIENTING KINESINS 1/2	Members of the kinesin-12 class motor proteins	AT3G17360 (POK1); AT3G19050 (POK2)	*pok1-1*, *pok1-2*, *pok2-1*, *pok2-2*	All T-DNA insertional mutants showing no transcript	Aberrant CDP	Müller *et al*., 2006
ROOT SWOLLEN 7	Member of the kinesin-5 class of motor proteins	AT2G28620	*rsw7*	Point mutation, Temperature sensitive (at 30ºC) with no phenotype at permissive temperature (19ºC)	Severe spindle defects	Bannigan *et al*., 2007

KINESIN-LIKE CALMODULIN BINDING PROTEIN	Plant unique kinesin motor	AT5G65930	*zwichel* (e.g., *zwiA*)	*zwiA* is T-DNA insertional mutant	No detectable phenotype	Buschmann *et al*., 2015
ATK1	Kinesin motor	AT4G21270	*atk1-1*	Transposable element-induced mutant	Abnormal mitotic spindle formation	Marcus *et al*., 2003
ATK5	Kinesin motor	AT4G05190	*atk5-1*, *atk5-2*	T-DNA insertional mutants	Formation of mitotic spindles with broadened poles; prolongation of mitotic spindle elongation	Ambrose *et al*., 2005; Ambrose and Cyr, 2007
HINKEL, STUD	Kinesin motors	AT1G18370 (HINKEL), AT3G43210 (STUD)	*atnack1-1*, *atnack1-2*, *atnack2-1*, *atnack2-2*	T-DNA insertional mutants, there are also EMS-induced mutant alleles	Abortive cytokinesis	Strompen *et al*., 2002; Tanaka *et al*., 2004
PHRAGMOPLAST KINESIN RELATED PROTEIN1 (PAKRP1)/Kinesin-12A and PHRAGMOPLAST KINESIN RELATED PROTEIN1L/Kinesin-12B	Kinesin motors	AT4G14150 (PAKRP1), AT3G23670 (PAKRP2)	*kinesin12a-1*, *kinesin12a-2*, *kinesin12b-1*, *kinesin12b-2*	T-DNA insertional mutants	Abnormal phragmoplast formation and incomplete cytokinesis during male gametogenesis	Lee *et al*., 2007
AIR9	MT binding protein	AT2G34680	*ungud9* (*air9-9*); *haumea*; *air9-5*, *air9-27*	Both *air9-9* and *haumea* are transposon-induced deletion mutants; *air9-5* and *air9-27* are T-DNA insertional mutants	No detectable phenotype	Buschmann *et al*., 2006
END BINDING 1c	Plant specific plus end-binding protein	AT5G67270	*eb1c-2*	T-DNA insertional mutant	Abnormal mitotic spindle formation, malpositioned spindle	Komaki *et al*., 2010
MICROTUBULE ORGANIZATION 1	MT plus end regulator	AT2G35630	*mor1-1*, *mor1-2*	Both EMS-induced point mutants	Defective PPBs, spindle and phragmoplast formation	Whittington *et al*., 2001; Kawamura *et al*., 2006
TANGLED	MT binding protein	AT3G05330	*tan-csh*, *tan-mad*, *tan-riken*	T-DNA insertional mutants with absence of gene expression	Aberrant CDP	Walker *et al*., 2007
SABRE	Unknown function	AT1G58250	*kreuz und quer* (*kuq*); *sab-5*, *sab-6*, *sab-7*	*kuq* is fast proton-induced mutant while *sab-5* to *sab-7* are T-DNA insertional mutants	Oblique PPB, spindle and phragmoplast positioning; aberrant CDP	Pietra *et al*., 2013
CLIP ASSOCIATED PROTEIN (CLASP)	Regulator of MT plus-end dynamics	AT2G20190	*clasp-1*, *clasp-2*, *clasp-3*	All T-DNA insertional mutants	Oblique PPB, spindle and phragmoplast	Kirik *et al*., 2007; Pietra *et al*., 2013

					positioning; aberrant CDP	
REGULATORY PROTEINS WITH EFFECT ON MICROTUBULE ORGANIZATION						
Aurora1/2	Protein kinases	AT4G32830, AT2G25880	*aur1-1*, *aur1-2*, *aur1-3*, *aur2-1*, *aur2-2*	All T-DNA insertional mutants	Defects in formative cell divisions (aberrant CDP during divisions in lateral root primordia)	Van Damme *et al*., 2011; Boruc *et al*., 2017
ANP1-3/MKK6/MPK4	Protein kinases	AT1G09000 (ANP1), AT1G54960 (ANP2), AT3G06030 (ANP3), AT5G56580 (MKK6), AT4G01370 (MPK4)	*anp1*, *anp2*, *anp3*, *mkk6*, *mpk4*	All T-DNA insertional mutants	Incomplete cytokinesis; multinucleate cells	Krysan *et al*., 2002; Kosetsu *et al*., 2010; Beck *et al*., 2011
YODA, MPK6	Protein kinases	AT1G63700 (YODA), AT1G51660 (MKK4), AT3G21220 (MKK5), AT3G45640 (MPK3), AT2G43790 (MPK6)	*yda-1* to *yda-9* (loss-of-function), *ΔNyda* (aminotermin al deletion, gain-of-function), *mpk6-2*, *mpk6-4*	*Yda-1* to *yda-9* are EMS-induced mutants; *ΔNyda* is T-DNA insertional mutant; *mpk6-2* and *mpk6-4* are T-DNA insertional lines	Aberrant CDP	Lukowitz *et al*., 2004; Müller *et al*., 2010; Smékalová *et al*., 2014
TWO-IN-ONE (TIO)	Fused kinase; interactor of AKRP1/Kin esin-12A and PAKRP1L/ Kinesin-12B kinesin motors	AT1G50240	*Tio-3*	T-DNA insertional mutant	Abnormal phragmoplast development and cytokinesis during male gametogenesis	Oh *et al*., 2005; 2012
RanGAP1	GTPase activating protein of the Ran GTPase	AT3G63130	RanGAP1^{RNAi}	Downregulated RANGAP1 protein by RNA interference	Aberrant CDP	Xu *et al*., 2008
FASS/TONNEAU2	B regulatory subunit of type 2A protein phosphatase s	AT5G18580	*fass-5*, *fass-13*, *fass-14*, *fass-15*	*fass-5* and *fass-15* are EMS-induced, *fass-13* and *fass-14* are T-DNA insertional mutants	Absence of PPB, aberrant CDP	Camilleri *et al*., 2002; Kirik *et al*., 2012; Spinner *et al*., 2013
EXTRA SPINDLE POLES	Separase	AT4G22970	*rsw4*	Unknown; temperature sensitive		Wu *et al*., 2010; Moschou *et al*., 2013

KEULE	SEC1/Munc 18 protein	AT1G12360	*keu*^{T282}	EMS-induced point mutation	Affects MT reorganization during phragmoplast expansion	Steiner *et al.*, 2016
MODIFIER OF SNC1,7 (MOS7)	Nucleoporin	AT5G05680	*mos7-1* to *mos7-5*	T-DNA insertional mutants	Abnormal mitotic spindle formation during male gametogenesis	Park *et al.*, 2014

3.1.3 Materials

3.1.3.1 Plant transformation and crossing to introduce MT markers

Methods of MT molecular marker introduction into *A. thaliana* include either plant transformation using floral dipping into suspensions of Agrobacteria harbouring plasmids with the reporter transgene (Clough and Bent, 1998), or crossing the desirable Arabidopsis line (wild type or mutant) with another line already expressing the desirable fluorescent MT marker (e.g. Sampathkumar *et al.,* 2011). Preferable method for construct preparation is a MultiSite Gateway® technology approach. It is a fast and efficient tool based on site-specific recombination allowing simultaneous cloning of DNA fragments in predefined order and orientation. After its optimization for the use in plants a set of entry clones containing promoters, terminators and reporter genes has been created (Karimi *et al.,* 2007). Methods presented here aim to characterize MT arrays of dividing cells in wild type *A. thaliana* plants of Col-0 ecotype and in the knock-out mutant *ktn1-2*, which is deficient in the MT severing protein KATANIN 1 (Komis *et al.*, 2017). Thus, we performed live-cell imaging with transgenic *A. thaliana* plants stably expressing tubulin fluorescent marker GFP-TUA6 and transgenic *ktn1-2* mutant line with expression of GFP-TUA6 marker that was prepared by crossing of this mutant with Col-0 plants stably transformed with a *35S::TUA6:GFP* construct (Komis *et al.,* 2017).

For stable transformation of *M. sativa* we used a rapid and highly efficient method of cocultivation of leaf explants with *Agrobacterium tumefaciens* strain containing a construct carrying a transgene fused with a fluorescent marker (Samac and Austin-Phillips, 2006). We used *A. tumefaciens* strain GV3101 containing GFP-MBD MT marker (Marc *et al.,* 1998) that was prepared by a standard cloning method (Vyplelová *et al.,* 2017). Leaf explants after transformation were sequentially subcultured on media supporting callus initiation, somatic embryo formation, root and shoot development, and *in vitro* maintenance of growing plantlets (Samac and

Austin-Phillips, 2006). Selection of transformed tissues and seedlings was based on the presence of selecting herbicide marker phosphinothricin in the culture media. Transformed plants for live-cell imaging were further selected according to the presence of GFP-MBD using an epifluorescence microscope.

3.1.3.2 Preparation of plant material for light-sheet imaging of root cell mitotic progress

In general, mitotic cell divisions in plants are mostly concentrated in specialized multicellular domains, plant meristems. Cell proliferation in the root takes place within the root apical meristem, where radial root zonation consists of several cell layers important for development of various tissues (Dolan *et al.*, 1993; Baum *et al.*, 2002; Scheres *et al.*, 2002). Our understanding of how cell divisions in the root apical meristem are organized and regulated during plant growth and development thus requires microscopic imaging of dividing cells in the whole root apex with sufficient spatial and temporal resolution. Ideally, intact plants should be adapted in the microscope for long-term imaging under minimalized phototoxicity, photobleaching and proper environmental physiological conditions. A cutting edge technology fulfilling all requirements for developmental imaging under physiological conditions is represented by LSFM in animal developmental biology. LSFM has been introduced also into plant developmental biology, although the number of applications is not so high due to the more complicated preparation of living plants for long-term microscopy observations. However, substantial benefit of a vertically oriented plant (consistently with the gravity vector) prefers LSFM as an advanced microscopy technique for long-term plant developmental imaging. This method offers fast optical sectioning of the sample, restriction of the fluorophore excitation only to the thin light-sheet volume, and free rotation of the sample allowing multi-angular image acquisition. Live-cell imaging of dividing cells using LSFM is sufficient for resolving MT arrays during mitosis and cytokinesis, including deep imaging of dividing cells inside of living multicellular plant organs. Good spatial and high temporal resolution of LSFM ensures recording of cell division in growing and developing plant tissues in real time. Nevertheless, there are only very few LSFM studies on cytoskeletal proteins during plant cell division so far (Maizel *et al.,* 2011; Ovečka *et al.,* 2015; Novák *et al.,* 2016; Vyplelová *et al.,* 2017).

1. Plant root is the preferred organ for LSFM studies due to the high frequency of cell divisions and to the fact that it grows fully embedded in the culture medium. Solidified Phytagel-based culture medium containing all macro- and micro-nutrients and carbon source serves as an optimal cultivation environment for plant roots. In addition, being transparent it provides excellent optical properties (Maizel *et al.,* 2011; Ovečka *et al.,* 2015), and serves as an optimal imaging medium for LSFM. In our experiments we used a half-strength Murashige and Skoog (MS) basal salt mixture supplemented with 1% (w/v) sucrose and pH adjusted to 5.7, solidified with Phytagel at a concentration 0.6% (w/v). An alternative approach for embedding and imaging of plant samples is the use of a low-gelling-temperature agarose at appropriate concentrations (usually between 0.6% - 1.0% w/v) dissolved in water or liquid half-strength MS culture medium.

2. We prepared samples of whole intact plants in the "open system" developed for long-term live-cell imaging of *A. thaliana* seedlings (Ovečka *et al.,* 2015). Plants growing in the Phytagel–solidified culture medium were transferred to the microscope in fluorinated ethylene propylene tubes (FEP tubes). Roots grow in the culture medium inside of the FEP tube. Green parts of the plants are located in open space of the FEP tube providing access to air and light in the microscope during experiment. Alternative methods suitable for mounting *A. thaliana* plants to the light-sheet microscope supporting their growth during the imaging were also published (von Wangenheim *et al*., 2014).

3. Nourishing plants with nutrients from fresh culture medium is required, especially for long-term experiments. We use controlled perfusion of the imaging chamber with liquid half-strength MS medium without vitamins, supplemented with 1% (w/v) sucrose and pH adjusted to 5.7. Plant growth medium is filter-sterilized using a sterile syringe filter with a pore size of 0.2 μm before loading to the imaging chamber in order to prevent fungal and/or bacterial contamination.

4. Practical approaches on how to prepare plants for LSFM imaging described below are based on a published protocol optimized for *A. thaliana* (Ovečka *et al.,* 2015) and can be easily adapted for either single-cell system (e.g. cell suspension culture), or significantly thicker samples such as somatic embryos and developing plants of the legume crop plant *M. sativa*. It is applicable for both commercial and custom-built LSFM platforms.

Arabidopsis thaliana seedlings

1. Seeds of *A. thaliana* transgenic lines must be sterilized in 70% (v/v) ethanol for 2 min and subsequently in 1% (v/v) sodium hypochlorite containing 0.05% (v/v) Tween 20 for 8 min. The next step is thorough washing of the seeds (five times) with sterile MilliQ water. Sterile seeds are placed on a Petri dish filled with Phytagel-solidified half-strength MS medium. All steps of seed sterilization and plating must be done in aseptic conditions in the laminar flow box. Plates with seeds are then stored at 4°C for 2-3 days to break seed dormancy and synchronize germination. After it, plates are placed into the culture chamber at 22°C, 50% humidity and 16/8 h (light/darkness) photoperiod.

2. After germination (within 24-48 h after seed transfer to the culture chamber) seeds with ruptured testa and emerging root are transferred to round 90 × 25 mm Petri dishes filled with 80 ml of Phytagel-solidified half-strength MS medium. The thickness of culture medium should be approximately 15 mm, which is optimal for root growth and further sample preparation.

3. Two days later germinating plants with growing roots are picked up by gentle insertion of the FEP tube with an inner diameter of 2.8 mm to the culture medium enclosing the selected plant inside. The FEP tube with the plant and the culture medium inside is installed into the microscope observation chamber.

Medicago sativa roots

1. Small plantlets of *M. sativa* expressing fluorescent MT marker GFP-MBD are produced *in vitro* from somatic embryos (Vyplelová *et al.*, 2017). Well-developed somatic embryos with proliferating root pole are first selected and transferred to a new plate containing Phytagel-solidified full-strength MS medium that is at least 15 mm thick. Somatic embryos are carefully inserted vertically into the solid culture medium to ensure that the root pole will grow vertically inside the medium and the upper green part of the plant will develop in the air above the culture medium.

2. Similarly as in the case of *A. thaliana* preparation, somatic embryos are surrounded by the FEP tube, but in this case with larger inner diameter of 4.2 mm. Insertion of the FEP tube into the

culture medium must be careful enough to enclose individual somatic embryo, but not to damage the root pole. Moreover, it should provide enough surrounding culture medium inside the tube for further plant development during imaging.

3. After 1 to 2 days of somatic embryo stabilization and visual inspection of the root pole which should start elongation, such FEP tube with a germinating somatic embryo is carefully removed from the culture medium and prepared for LSFM.

Light-sheet fluorescence imaging

1. After removing from the culture plate the FEP tube with the sample is moved to the LSFM. To fix it in the sample holder, the FEP tube with *A. thaliana* plant (with inner diameter of 2.8 mm) is inserted to the glass capillary with an appropriate diameter while the FEP tube with *M. sativa* plant (with inner diameter of 4.2 mm) is inserted to the sterile plastic syringe of the 1 ml volume which was cut-open at the tip. Glass capillary or plastic syringe serve as a sample holder for fixing the sample in the microscope.

2. Imaging of plant roots described here is done with the light-sheet fluorescence microscope Z.1 (Carl Zeiss, Germany). The system is equipped with W Plan-Apochromat 20×/1.0 NA water immersion detection objective and two 10x/0.2 NA illumination objectives for left and right sample illumination. It is used for synchronized dual-side illumination and both left and right light-sheet illumination beams are modulated into a pivot scan mode.

3. Fluorescent MT markers GFP-TUA6 in *A. thaliana* and GFP-MBD in *M. sativa* are visualized with laser excitation line 488 nm and with emission filter BP505-545. Excitation intensity of the laser is set up to 2-3% of the laser intensity range available in order to minimalize photobleaching and phototoxicity. Time-lapse imaging is done by whole root image acquisition in Z-stack mode every 5 min and experiment duration is designed for a period of several hours (3-15 h). Images are recorded with the sCMOS camera (PCO.Edge, PCO AG) with exposure time of 20-50 ms per optical section.

4. Root growth rate of experimental plants during imaging is stable and fast enough that roots grow out of the field of view in the microscope. For this reason images are recorded in two or three subsequent fields of view coordinated to follow each other at the y axis in order to continuously record growing root displacement during long-term imaging experiments.

5. Acquired series of data characterizing MT arrays during cell division in x-, y-, z- and t-coordinates (Fig. 5) are edited and analysed using Zeiss Zen 2014 software (Black Version).

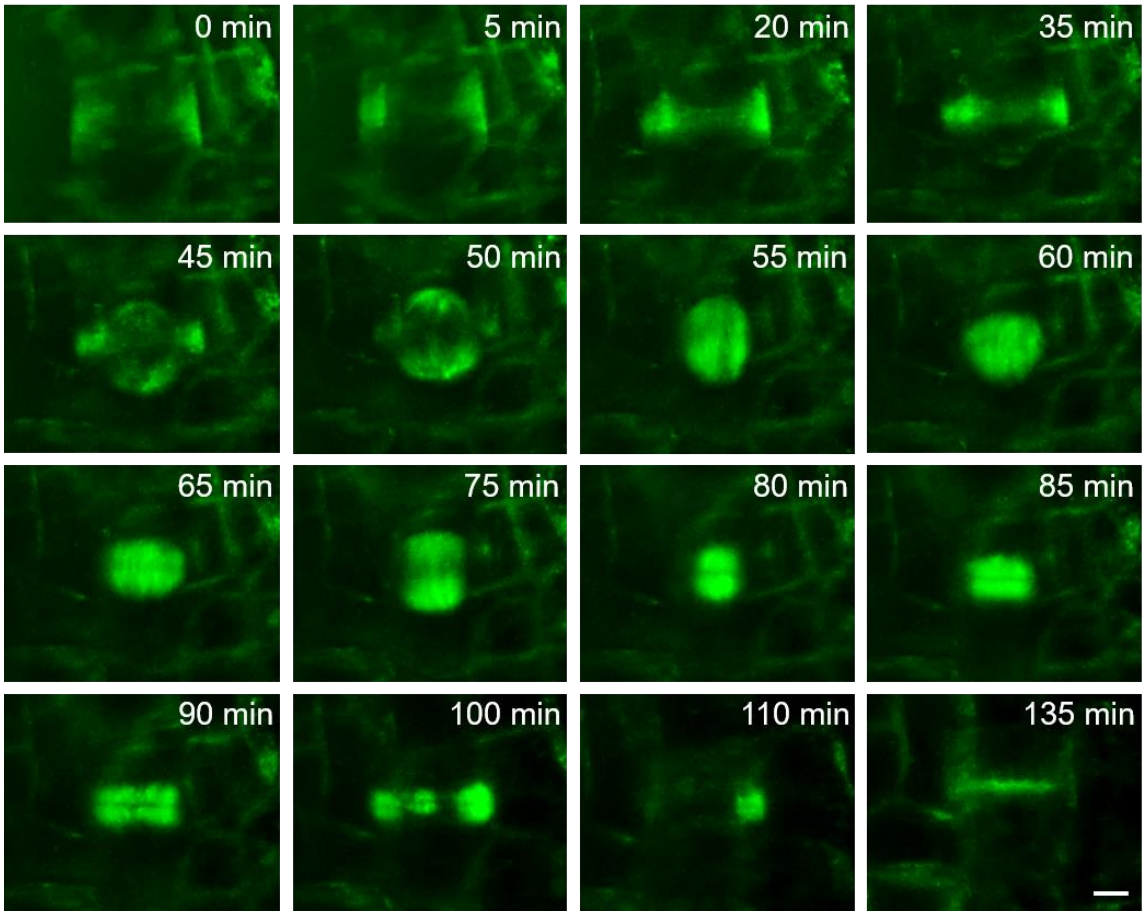

Figure 5. Time-lapse imaging of MT arrays during mitosis and cytokinesis in the root epidermal cell of *Medicago sativa* plant stably transformed with a *35S::GFP:MBD* construct using LSFM. Sequence of images showing progression of PPB narrowing and disappearance together with formation of the mitotic spindle, establishment of the phragmoplast, its centrifugal enlargement in lateral direction during the cytokinesis, final fusion of cell plate with parental cell wall and reappearance of cortical MT network in post-mitotic interphase cell. Time of the cell division progression is indicated in min. Scale bar: 5 μm. Adapted from Vyplelová *et al*., 2018.

3.1.3.3 Preparation of plant material for high speed spinning disk recording of the mitotic progress

SDCM technology is based on a rotating disk with multiple pinholes simultaneously covering multiple locations of the field of view by the excitation light. Thus the speed of imaging in this microscope is very fast, making it suitable for documentation of dynamic cellular processes, including MT dynamics in living plant cells. Several studies addressed the dynamics of cortical MT arrays in plant cells. SDCM imaging was used for characterization of MT dynamics on plus and minus ends (Shaw and Lucas, 2011), MT dynamic instability (Shaw *et al*., 2003) or MT nucleation and reorientation in *KATANIN1* mutants (Nakamura *et al*., 2010; Lindeboom *et al*., 2013). Moreover, dynamic changes of complex MT arrays during cell division were also described using SDCM quire recently (Murata *et al*., 2013; Komis *et al*., 2017). Time-lapse imaging of the entire process of mitosis brings temporal information on the duration of individual stages, including the formation of PPB, mitotic spindle and phragmoplast (Fig. 6).

1. Young seedlings of *A. thaliana* suitable for SDCM imaging are obtained from seeds 3-4 days after their germination. Before this, seeds of transgenic lines expressing an appropriate MT marker must be surface sterilized with 70% (v/v) ethanol for 2 min followed by 1% (v/v) sodium hypochlorite containing 0.05% (v/v) Tween 20 for 8 min. After plating sterile seeds on plates containing a half-strength MS medium without vitamins, with 1% (w/v) sucrose, pH adjusted to 5.7, and solidified with Phytagel at a concentration 0.6% (w/v), plates are stored for 2-4 days at 4^{o}C for stratification. Following this period plates with seeds are placed into the growth chamber at 22°C, 50% humidity and 16/8 h (light/darkness) photoperiod for germination. Plates are positioned vertically to allow straight growth of roots at the surface of solidified medium.

2. Imaging of seedlings is performed using microscopy slides prepared in the form of microchambers consisting of microscopy slide, spacers on the side of the slide made from double sided tape or parafilm, and a coverslip. Sample is thus sandwiched between slide and coverslip with a stable distance ensuring enough space for young *A. thaliana* plant. A drop of liquid half-strength MS medium is placed in the middle of the slide and one selected seedling is transferred to the drop. After closing the seedling with a coverslip the microchamber is sealed on the sides

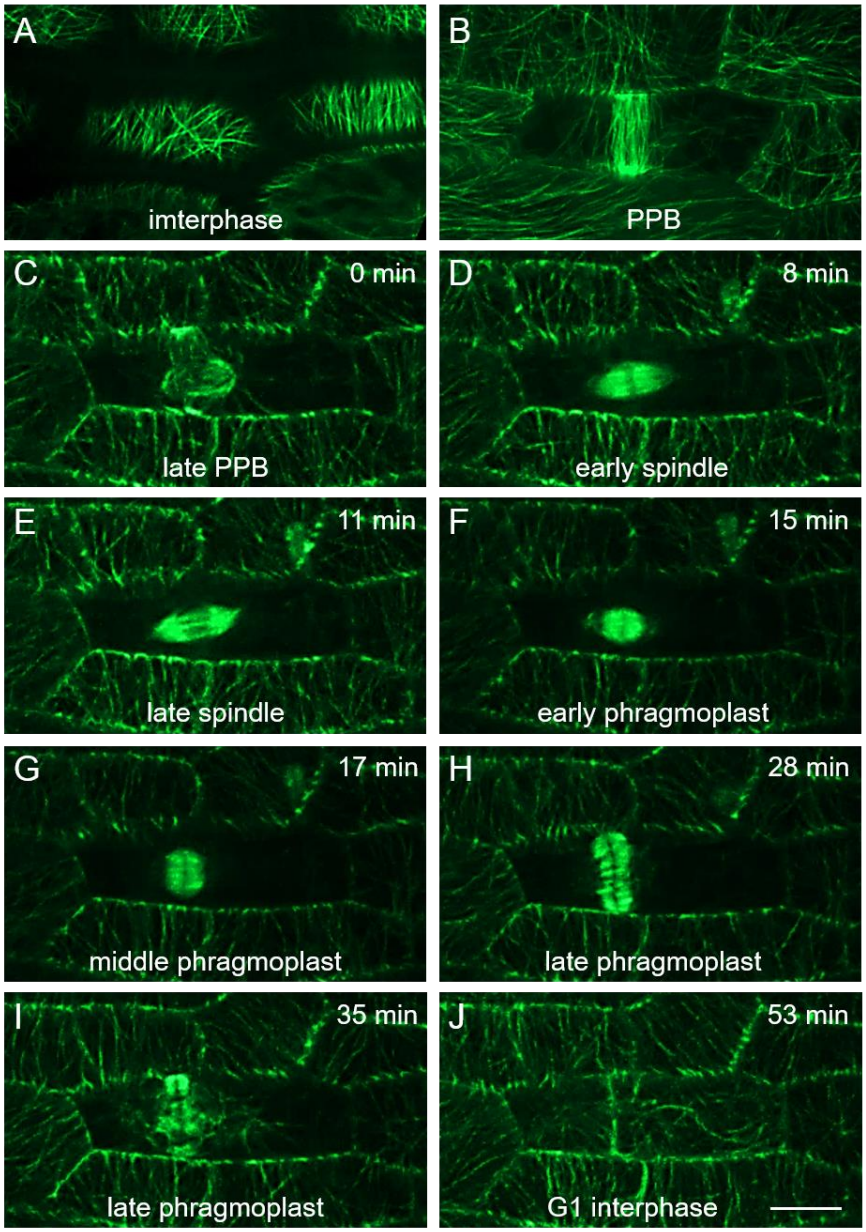

Figure 6. Time-lapse imaging of MT arrays during mitosis and cytokinesis in petiole epidermal cell of *Arabidopsis thaliana* plant stably transformed with a *35S::GFP:TUA6* construct using SDCM. Time-lapse recording of PPB narrowing from cells in interphase (A) to preprophase (B), PPB disappearance and mitotic spindle formation at prometaphase (C), mitotic spindle in metaphase and anaphase (D, E), early phragmoplast formation at telophase (F), progression of middle and late phragmoplast during cytokinesis (G, H), termination of the phragmoplast at the end of cytokinesis (I) and rearrangement of cortical MTs at the post-cytokinetic G1 phase (J). Time of the cell division progression is indicated in min. Scale bar: 100 μm. Adapted from Vyplelová *et al*., 2018.

and edges by parafilm strips to prevent evaporation of liquid half-strength MS medium during time-lapsed imaging, which may last more than 1 h. Transfer of selected plants from the sterile

culture medium to the microscopy slide should be done under sterile conditions in the laminar flow box.

3. A convenient part of young seedling possessing a high number of cells in different stages of mitotic cell division is the root tip. Young seedling plants (3-4 days after germination) are most suitable for such observations. Dividing cells in the green aerial part of *A. thaliana* plants can be found in the petiole of the young first true leaf (Fig. 6). This tissue is flat, well organized and easily accessible, but is available only later in the plant development, e.g. in 7 days old seedlings.

4. In our laboratory we operate a Cell Observer Z1 spinning disk confocal microscope (Carl Zeiss, Germany), equipped with high-resolution Evolve 512 back-thinned EM-CCD camera (Photometrics). Observation of cell division is regularly performed with an EC Plan-Neofluar 40×/1.3 NA oil immersion objective and Plan-Apochromat 63×/1.4 NA oil immersion objective. Plant samples with the MT marker GFP-TUA6 are imaged with excitation laser line 488 nm and emission filter BP525/50. For convenience, reduction of the dataset size and minimization of sample photodamage, entire z-stacks are acquired every 30 seconds, covering a period of ca. 1 h, which sufficiently covers the entire mitosis and cytokinesis. Data sets are analysed with Zeiss Zen 2014 software (Blue Version).

3.1.3.4 Imaging of plant mitotic MT arrays with the point-scanning confocal Airyscan system with improved resolution

CLSM equipped with Airyscan system represents a new application of a point-scanning imaging approach with improved resolution. The system is equipped with a 32 GaAsP detector providing high sensitivity and superior light collecting capacity. Samples can be scanned with the fast mode allowing sufficient temporal resolution during 3D spatial and temporal acquisition. Alternatively, a high-resolution mode could be used allowing improved 3D resolution for acquiring single Z-stacks. Taking into account these technical improvements, we utilized the LSM880 Airyscan microscopy platform (Zeiss Microscopy, Oberkochen, Germany) for the documentation of the mitotic progress in cells of the *ktn1-2* mutant stably expressing the MT marker GFP-TUA6 (Komis *et al*., 2017). Defects in the organization of mitotic MT arrays in dividing cells caused by mutation

in the *KATANIN1* gene were clearly documented by comparison to the corresponding control (Fig. 7).

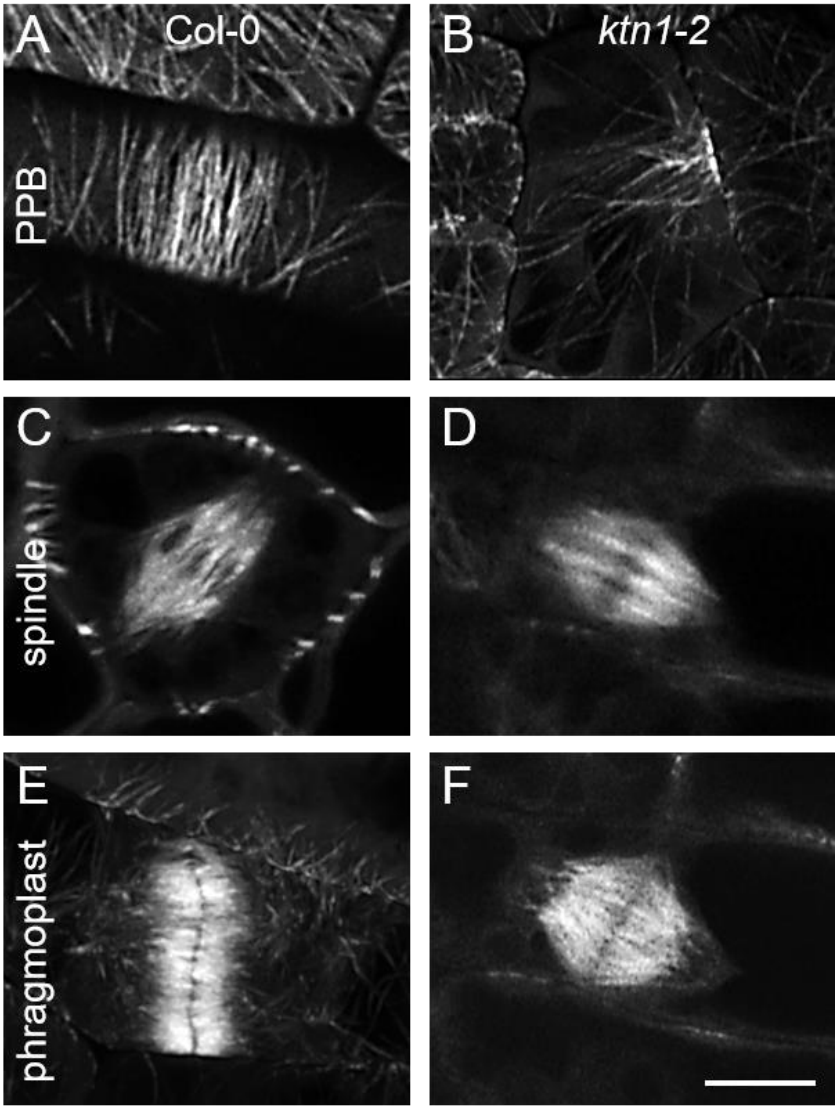

Figure 7. Comparative analysis of MT arrays during mitosis and cytokinesis of leaf petiole epidermal cells in *Arabidopsis thaliana* plants stably transformed with a *35S::GFP:TUA6* construct between wild type plants and a knock-out mutant *ktn1-2*, deficient in MT severing protein KATANIN 1 using CLSM equipped with the Airyscan system. Organization of MT arrays typical for particular cell division stages in cells of the wild type plant (A, C, E) and the *ktn1-2* mutant (B, D, F). (A, B) Narrowing of the PPB in late G2 phase of the cell cycle (preprophase stage). Note unipolar and disorganized arrangement of PPB MTs in the *ktn1-2* mutant (B). (C, D) Mitotic spindle organization, showing no structural changes between control and *ktn1-2* mutant cells. (E, F) Organization of phragmoplast MTs during cytokinesis. In comparison to control (E), phragmoplast in the *ktn1-2* mutant is abnormally shaped (F). Scale bar: 5 μm. Adapted from Vyplelová *et al*., 2018.

1. Seeds of transgenic lines expressing an appropriate MT marker (GFP-TUA6) are surface sterilized using 70% (v/v) ethanol for 2 min followed by 1% (v/v) sodium hypochlorite containing 0.05% (v/v) Tween 20 for 8 min. After washing sterile seeds are plated on the surface of half-strength MS medium without vitamins and with 1% (w/v) sucrose, pH adjusted to 5.7, solidified with Phytagel at a concentration 0.6% (w/v). Following seed stratification at 4^{o}C for 2-4 days, they are cultivated in growth chamber at 22°C, 50% humidity and 16/8 h (light/darkness) photoperiod at a vertical position to allow straight growth of roots on the surface of the solidified medium.

2. First, it is necessary to build the observation chamber using a glass slide and coverslip spaced with parafilm or double sticky tape strips. A drop of liquid half-strength MS medium is placed in the middle of the slide and one selected seedling is transferred to the drop. The sample is sandwiched between slide and coverslip with a stable distance ensuring enough space for young *A. thaliana* plant. The microchamber is sealed on the sides and edges by parafilm strips to prevent evaporation of liquid half-strength MS medium during time-lapse imaging for more than 1 h.
Note: The transfer of selected plants from the culture medium to the microscopy slide should be done under sterile conditions in the laminar flow box.

3. Epidermal petiole cells of young first true leaf are suitable for observation of cell division in the green part of *A. thaliana* plants. The most preferable plants are 6-7 days old for preparation of such sample. The plant must be entirely covered by the coverslip and young first true leaf must be positioned by abaxial (lower) leaf side parallel to the coverslip.

4. The example given here (Fig. 7) was obtained using LSM880 with Airyscan (Zeiss Microscopy, Oberkochen, Germany). We used single photon excitation with the 488 nm laser line and a 32 GaAsP detector for fluorescence detection. The superior light collecting capacity of the Airyscan and the sensitivity of the GaAsP detector allowed setting laser power to a level not exceeding 2% of the range available.Observation of dividing cells was done with Plan-Apochromat 63×/1.4 NA oil immersion objective and data sets were analysed with Zeiss Zen 2014 software (Blue Version).

3.1.4 Conclusions

Sample preparation is of paramount importance for the adequate visualization of mitosis and cytokinesis in plants. The procedures described above aim to describe preparations for high resolution time lapse imaging of mitotic dynamics by Airyscan CLSM. Additionally we provide easy to follow procedures for mounting Arabidopsis seedlings for tracking and documenting mitotic cells in the multicellular context of entire organs such as roots and leaf petioles. High resolution studies with Airyscan may be used to reveal mechanisms of spindle and phragmoplast assembly progression in living cells, while light-sheet imaging can be used to obtain information on the coordination of the mitotic process in populations of hundreds of cells, e.g. within root apical meristem.

3.2 Alfalfa root growth rate correlates with progression of microtubules during mitosis and cytokinesis as revealed by environmental light-sheet microscopy

3.2.1 Abstract

Cell division and expansion are two fundamental biological processes supporting indeterminate root growth and development of plants. Quantitative evaluations of cell divisions related to root growth analyses have been performed in several model crop and non-crop plant species, but not in important legume plant *M. sativa*. LSFM is an advanced imaging technique widely used in animal developmental biology, providing efficient fast optical sectioning under physiological conditions with considerably reduced phototoxicity and photobleaching. Long-term 4D imaging of living plants offers advantages for developmental cell biology not available in other microscopy approaches. Recently, LSFM was implemented in plant developmental biology studies, however, it is largely restricted to the model plant *A. thaliana*. Cellular and subcellular events in crop species and robust plant samples have not been studied by this method yet. Therefore we performed LSFM long-term live imaging of growing root tips of transgenic alfalfa plants expressing GFP-MBD, in order to study dynamic patterns of MT arrays during mitotic cell division. Quantitative evaluations of cell division progress in the two root tissues (epidermis and cortex) clearly indicate that root growth rate is correlated with duration of cell division in alfalfa roots. Our results favour non-invasive environmental LSFM as one of the most suitable methods for qualitative and quantitative cellular and developmental imaging of living transgenic legume crops.

3.2.2 Introduction

Plant growth and development is directed by key biological processes establishing proper morphogenetic pattern. Among them, cell division plays an indispensable role. Cell divisions in the root meristem are followed by subsequent cellular expansion in the root elongation zone and ensure sustained development of roots. Plant mitotic cell division is dynamic process controlled by rearrangements of MTs that are gradually transformed into different MT arrays during mitosis and cytokinesis. Before the onset of cell division, cortical MTs are narrowing to form the PPB defining the CDP (Rasmussen *et al.,* 2011). After nuclear envelope breakdown and the initiation of the mitotic process, MTs form the mitotic spindle responsible for chromosome partitioning into daughter cells during mitosis (Vos *et al.,* 2004; Marcus *et al.,* 2005; Azimzadeh *et al.,* 2008). This bipolar spindle is formed with its long axis oriented perpendicularly to the PPB plane (Van Damme, 2007; 2009). During cytokinesis the bipolar

spindle is transformed into the phragmoplast. Phragmoplast serves as a guide for cell plate assembly and the subsequent formation of new cell wall separating two daughter cells (Lee and Liu, 2013).

Complex analyses of cell division and elongation patterns during primary root growth and development were mostly performed in model plants such as Arabidopsis (e.g. Beemster and Baskin, 1998; Beemster *et al.,* 2002; Lavrekha *et al.,* 2017), maize (e.g. Sacks *et al.,* 1997), barley (e.g. Kirschner *et al.,* 2017), tobacco (e.g. Pasternak *et al.,* 2017) and rice (e.g. Rebouillat *et al.,* 2009; Ni *et al.,* 2014). These studies were mostly based on 3D reconstruction analyses from fixed plant samples. Functional studies on dynamics of MTs during mitotic cell division were almost exclusively conducted in two model species, Arabidopsis and tobacco. The MT cytoskeleton in living plant cells can be visualized using several MT-specific molecular reporters. One such reporter is the GFP fusion with the MBD of the MAP4 (GFP-MBD). Dynamics, reorientation and reorganization of cortical MTs with GFP-MBD as a molecular MT marker was originally studied using CLSM in living epidermal cells (Marc *et al.,* 1998).

Nowadays there are several microscopic approaches to study MTs in living plant cells of model plant species during cell division. CLSM and SDCM are most popular ones. From practical point of view, dimensions of tobacco BY-2 and Arabidopsis suspension cells, as well as easily cultured Arabidopsis seedling plants facilitate utilization of conventional microscopy methods for live-cell imaging of mitotic MTs in dividing cells. Another important aspect of microscopic cell division studies on model plants is availability of firmly established transformation protocols and protein tagging approaches in Arabidopsis and tobacco. Some of these studies analysed stem cell divisions (Campilho *et al.,* 2006) and determined the role of MAP65-1 phosphorylation in cell cycle progression (Boruc *et al.,* 2017) in the Arabidopsis root, visualized Arabidopsis zygote cell divisions (Kimata *et al.,* 2016), described MT arrays during cell division of Arabidopsis suspension cells (Calder *et al.,* 2015), or visualized PPB (Dhonukshe and Gadella, 2003), mitotic spindle (Dhonukshe *et al.,* 2006; Gaillard *et al.,* 2008) and phragmoplast (Murata *et al.,* 2013) in dividing tobacco BY-2 cells. Further, Arabidopsis γ-tubulin double mutants *tubg1-1* and *tubg2-1* expressing GFP-MBD MT marker showed abnormal spindles, asymmetric phragmoplasts and disorganization of cortical MT arrays (Pastuglia *et al.,* 2006). Time-lapse live-cell imaging using CLSM was used to document abnormalities of mitotic MT arrays and to monitor the duration of mitosis in *anp2anp3* and *mpk4* mutants (Beck *et al.,* 2011). Arabidopsis *fh1-1* mutant expressing GFP-MBD showed increased instability of MTs (Rosero *et al.,* 2016). SDCM was used mostly to study dynamics of cortical MT arrays. Bundling of cortical MTs and speed of MT growth and shortening on

plus and minus ends were studied in living hypocotyl cells of Arabidopsis (Shaw and Lucas, 2011) while dynamic MT nucleation of cortical arrays has been done in Arabidopsis wild type, *katanin* and *gcp2-1* mutants (Nakamura *et al.,* 2010).

Nevertheless, environmental and long-term imaging are compromised in such conventional microscopic methods as CLSM and SDCM because living model plants are exposed to several stresses (artificial horizontal position, tight microscopic chamber with limited nutrients and pressure between microscopic slides) and suffer from high energy illumination causing undesirable phototoxicity and photodamage. In comparison to Arabidopsis, crop species including alfalfa typically have more robust habitus and their roots are thicker because they consist from more tissue layers. Consequently, mounting of the whole alfalfa seedlings to classical horizontally-positioned microscopy stage is more challenging and affects fitness of such samples during long-term experiments. Obviously, microscopic techniques like CLSM and SDCM also suffer from serious limitations in imaging depth. Finally, all commercial CLSM and SDCM platforms are based on horizontal stages, not allowing for living plants to be observed normally oriented with respect to the gravity vector. All these disadvantages can be avoided by using LSFM. Optical sectioning of the sample with excitation sheet of light is very fast. Importantly, excitation of fluorophores is restricted within the light-sheet volume, which effectively eliminates out-of-focus fluorescence and bleaching. Emitted fluorescence light is detected by independent orthogonally-positioned detection objective. Focal plane of the light-sheet is harmonized with the focal plane of the detection objective and thus, very thin layer of the sample is detected by spherical aberration-free imaging. Sample can be freely rotated with respect to the light-sheet plane illumination allowing multi-angular image acquisition. Fast imaging mode of LSFM ensures that imaged cells are illuminated with very low level of excitation energy (Stelzer, 2015). Finally, in some custom-made and commercial LSFM platforms, sample loading can be done vertically allowing typical gravitropic growth of plants during the course of imaging. All these technical benefits bring LSFM to the forefront of current standards for proper spatial, temporal and physiological imaging of developmental processes. So far the applications of LSFM in plants have been preferentially restricted to the developmental imaging of primary or lateral roots in Arabidopsis (Maizel *et al.,* 2011; Lucas *et al.,* 2013; Rosquete *et al.,* 2013; Vermeer *et al.,* 2014; Ovečka *et al.,* 2015; von Wangenheim *et al.,* 2016). Subcellular localizations of cytoskeletal components by LSFM in Arabidopsis are very few, and include structure and dynamics of both MT and actin cytoskeleton in different organs (Ovečka *et al.,* 2015), cell division in root epidermis (Maizel *et al.,* 2011) and

developmental imaging of EB1c in cells of different tissues and developmental zones of the root tip (Novák *et al.,* 2016).

Generally, studies on cellular distributions of fluorescently-labelled proteins in *M. sativa* are more difficult due to the limited availability of established molecular tools and efficient transformation techniques. In contrast to Arabidopsis and tobacco, there are only scarce reports on cytoskeletal dynamics during cell division in *Medicago sativa*. It is known that transitions between G1/S and G2/M phases are controlled by cyclin-dependent Ser/Thr kinases, among others also by *M. sativa* kinase CDKB2;1 (Joubès *et al.,* 2000). This kinase is activated in mitotic cells and it is localized in PPB, perinuclear ring in early prophase, mitotic spindle and phragmoplast (Mészáros *et al.,* 2000). Activity of CDKB2;1 is controlled by protein PP2A which affects MT organization during the mitosis (Ayaydin *et al.,* 2000). However, both organization and dynamics of MTs was characterized only in developing and Nod factor-treated root hairs of *M. truncatula* (Sieberer *et al.,* 2002; 2005; Timmers *et al.,* 2007). In addition, actin cytoskeleton was visualized in interface and post-mitotic root cells and in root hairs using Plastin-GFP and GFP-mTalin in *M. truncatula* (Voigt *et al.,* 2005). Here we employed for the first time LSFM for long-term live-cell imaging of GFP-tagged MTs in thicker roots of a legume crop plant. We performed quantitative study of root growth rate and duration of individual mitotic stages in diverse tissues of robust roots of transgenic *M. sativa* plants originating from somatic embryogenesis that carried GFP-MBD MT marker. We show positive correlation between root growth rate and dynamic patterns of MT arrays in dividing cells during continuous root development.

3.2.3 Materials and Methods

3.2.3.1 Stable transformation of *Medicago sativa*

M. sativa stable transformation has been performed with *Agrobacterium tumefaciens* strain GV3101 containing construct carrying MBD of MAP4 fused to GFP driven by constitutive 35S promoter. N-terminal GFP fusion with rifampicin and kanamycin resistance was prepared by classical cloning method in pCB302 vector with herbicide phosphinothricin as the selection marker *in planta*. Phosphinothricin has been added to each subculture medium to control successful transformation. The transformation procedure was performed according to protocol for efficient transformation of alfalfa described by Samac and Austin-Phillips (2006). Highly responsive cultivar Regen SY (RSY; Bingham, 1991) of *M. sativa* has been selected. Well-developed leaves at the third node from the shoot apex were used as a source plant

material. Leaves explanted from plants were surface sterilized, cut in half and wounded on the surface with sterile scalpel blade. They were incubated with overnight grown *A. tumefaciens* culture with cell density between 0.6 and 0.8 at A_{600} nm for 30 min. Formation of calli and somatic embryos as well as induction and development of shoots and roots were achieved by transferring culture on the appropriate media (Schenk and Hildebrant medium for *A. tumefaciens* inoculation, Gamborg medium for cocultivation, callus initiation and embryo formation and Murashige and Skoog media for plant rooting, development and maintenance) for appropriate time in the culture chamber at 22°C, 50% humidity and 16/8 h light/dark photoperiod (Samac and Austin-Phillips, 2006). Regenerated plants were maintained on media with selective phosphinothricin marker and tested for the presence of GFP fusion proteins using fluorescence microscope. Transgenic *M. sativa* plants were further clonally propagated *in vitro* via somatic embryogenesis from leaf explants. Received somatic embryos stably expressing *35S::GFP:MBD* construct were used in further experiments.

3.2.3.2 Plant material and sample preparation for LSFM imaging

Transgenic somatic embryos carrying *35S::GFP:MBD* construct with well-developed root poles were separated, individually transferred and inserted vertically into solidified Murashige and Skoog-based root and plant development medium (MMS) or into Murashige and Skoog plant maintaining medium (MS). Embryos were enclosed from the upper part by FEP tube with an inner diameter of 4.2 mm and wall thickness of 0.2 mm (Wolf-Technik, Germany). FEP tubes were inserted into the culture medium carefully to enclose individual somatic embryo and surrounding medium inside of the tube. After 1 to 2 days of somatic embryo stabilization and after visual inspection of the root pole which was starting elongation, such FEP tube with somatic embryo was carefully removed from culture medium and prepared for LSFM. Sample was prepared according to the "open system" protocol for long-term live-cell imaging of *A. thaliana* seedlings described by Ovečka *et al*. (2015), with a modification in the respect that *M. sativa* roots are thicker than *A. thaliana* roots. The block of the culture medium inside of the FEP tube serves as holder of the sample and simultaneously also as root growing medium. Upper green part of the somatic embryo and later on developing plantlet was in open space of the FEP tube with the access to air. Thus, the root was able to grow inside of the microscope chamber without stress during long-term experiments. After removing from the culture plate FEP tube with the sample was inserted into sterile plastic syringe (with 1 ml volume and an inner diameter of app. 5 mm), which was cut-open at the tip before use. Plastic syringe was

used for fixing the sample in sample holder of the microscope. Sample holder with the sample was placed into observation chamber of the microscope tempered to 22°C using Peltier heating/cooling system. Before insertion of the sample to the microscope somatic embryo in the solidified culture medium was ejected slightly out of the FEP tube to the extent that root in the block of solidified culture medium was directly loaded into appropriate liquid medium (MMS or MS) in the microscope chamber. FEP tube was still holding the sample, but was no more surrounding the root part of the plant, which enhanced considerably quality of root deep imaging. To prevent contamination during long-term imaging, liquid medium filling the observation chamber was filter-sterilized using a sterile syringe filter. FEP tube was sterilized using 70% ethanol and dried out before use. After insertion of the sample to the observation chamber of the light-sheet microscope and 30 min stabilization, it was prepared for imaging.

3.2.3.3 LSFM

Long-term fluorescence live-cell imaging was done with the light-sheet Z.1 system (Carl Zeiss, Germany), equipped with W Plan-Apochromat 20×/1.0 NA water immersion detection objective (Carl Zeiss, Germany) and two LSFM 10x/0.2 NA illumination objectives (Carl Zeiss, Germany). Samples were imaged using dual-side illumination by a light-sheet modulated with a pivot scan mode. GFP-MBD was visualized with excitation line 488 nm and with emission filter BP505-545. Laser excitation intensity did not exceed 3% of the laser intensity range available. Image acquisition was done every 5 min in Z-stack mode for a period of 3-12 h. Scaling of images in x, y and z dimensions was 0.152 x 0.152 x 0.469 µm. Images were scanned in two or three views coordinated to follow each other in y axis to record root growth in long-term imaging and to prevent the movement of the growing root out of the field of only one field of view. Images were recorded with the PCO.Edge camera (PCO AG, Germany) with the exposure time 20 ms or 50 ms per optical section.

3.2.3.4 Measurements and statistical analyses

Time-lapsed images of growing roots in x-, y-, z- and t-dimensions were acquired using Zen 2014 software, black edition (Carl Zeiss, Germany). Images in the .czi format were transformed to 2D images using Maximum intensity projection function. Subsets of data containing individual dividing cells were created either with defined x- and y- dimensions from maximum intensity projection images or from original data with defined x-, y- and z- dimensions. Root

growth rate and displacement of individual cells in growing roots (representing a displacement distance of dividing cell in growing root in respect to the growth medium, Baskin, 2013) were recorded from the stage of mitotic spindle formation till the phragmoplast disappearance as well as width of PPB were measured using Line function of the Zen 2014 software. Duration of individual mitotic stages in min (stages of PPB, spindle and phragmoplast) in dividing cells was measured using Coordinate function of the Zen 2014 software. The initial stage of the measurement started at a progressive PPB narrowing which was defined by PPB width when it was in the range of 2 – 4 μm.

For measurement of duration of mitotic and cytokinetic stages only transverse cell divisions were selected. All parameters were measured and evaluated separately for epidermis and the first outer layer of cortex. Data from 9 individual roots were collected. After quantitative evaluation, measured roots were divided into three groups according to the root growth rate.

Final statistical data evaluation and plotting were done with Microsoft Excel software. Statistical significance was carried out using program STATISTICA 12 (StatSoft) according to one-way ANOVA and subsequent Fisher´s LSD test at the level of significance of $p < 0.05$.

3.2.4 Results

3.2.4.1 Germination of *M. sativa* somatic embryos

LSFM imaging was performed on roots of transgenic *M. sativa* plants originating from somatic embryos. After completion of somatic embryogenesis and after maturation, further development of somatic embryos required “germination”, characterized by proliferation on the root pole. This was initiated by transfer of mature somatic embryos from a hormone-free to a root and plant development (MMS) inducing medium. Somatic embryos with already proliferating roots were transferred directly to plant maintaining (MS) medium. Each somatic embryo has been transferred to MMS (or MS) medium individually in such way so that the root pole of somatic embryo was carefully inserted vertically into the solidified culture medium. This ensured that further growth of the root would continue inside of the medium and in vertical orientation. Upon activation of root growth as defined by its visible elongation, such “germinating” somatic embryos were prepared for light-sheet microscopy using FEP tubes.

3.2.4.2 Root growth rate

Whole plantlets growing in a cylinder of solidified culture medium inside of FEP tubes were placed to the light-sheet microscope. However, due to the bulkiness of the samples, only the apical part of the root was selected for time-lapse imaging. Root growth inside of the light-sheet microscope was recorded in 5 min intervals. Due to the displacement of the continuously growing root tip out of the selected field of view, images were recorded in two or three axially overlapping fields of view. Each field of view was 292.46 x 292.46 μm and thus, recording of root growth in two successive fields of view provided a frame 580 μm long within which we were able to measure root elongation. Based on the variability among characterized roots, their elongation speed was measured over time periods ranging from 3 to 12 h. Most likely due to the somaclonal variability during somatic embryogenesis, nine individual root tips which were taken into account elongated at different extents and so they were classified into three different groups (Fig. 8A-D) according to their root growth rate. Roots showing root growth rate in the range between 0.7 – 1.4 $\mu m.min^{-1}$ were characterized as fast-growing roots (Fig. 8A, D, E; Video S1), roots with growth rate in the range of 0.2 – 0.5 $\mu m.min^{-1}$ were characterized as medium-growing roots (Fig. 8B, D, E; Video S2) and roots with growth rate less than 0.2 $\mu m.min^{-1}$ were characterized as fast-growing roots (Fig. 8C, D, E; Video S3). Measurement of the growth distance of representative roots from each group over a period of 3 h during LSFM imaging yielded values ranging between 145.1 μm for a fast-growing root (Fig. 8A) to 67.1 μm for a medium-growing root (Fig. 8B) and 32.6 μm for a slow-growing root (Fig. 8C). Selection of individual roots according to their root growth rate (Fig. 8D) was taken into consideration in all further quantitative analyses. Analysis of correlation between increase in length of growing roots and a given recording time during time-lapse light-sheet imaging clearly revealed different root growth rate of fast-growing, medium-growing and slow-growing roots (Fig. 8E), giving proof for distribution of analysed roots into three different groups for further quantitative analyses.

3.2.4.3 Determination of cell division stages

The aim of our study was analysis of dynamic properties of MT arrays during cell division in root apical meristem, a tissue exhibiting active and coordinated mitotic activity. To visualize MT arrays during individual cell division stages in intact transgenic *M. sativa* plants originating from somatic embryos, we performed subcellular localization of MBD tagged with GFP.

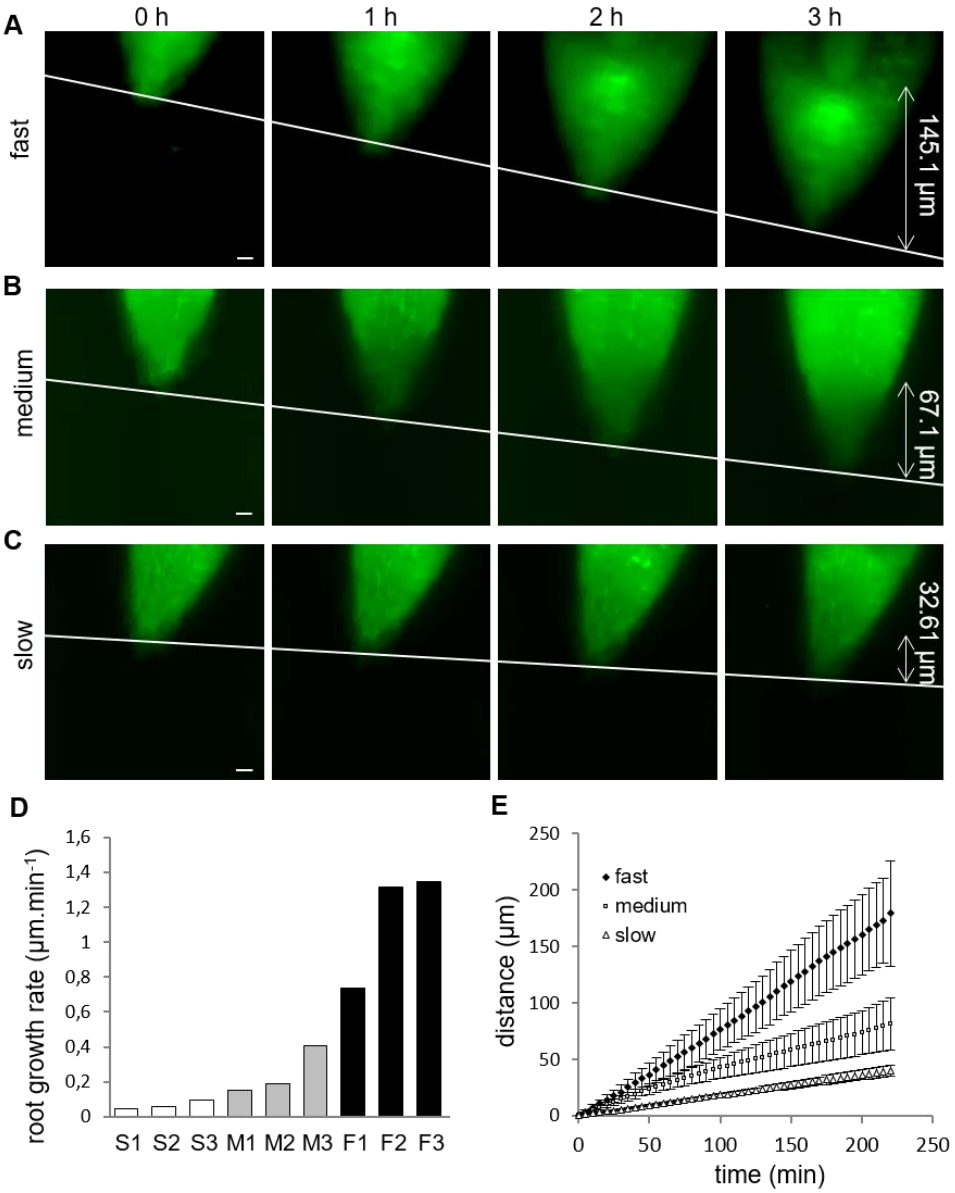

Figure 8. Root growth rate of *M. sativa* somatic embryo-derived plantlets, expressing *35S::GFP:MBD* construct. (A-C) LSFM imaging of root growth over the period of 3 h. Based on the root growth rate, roots were sub-divided into three different groups. Representative examples of a fast-growing root, grown in a distance of 145.1 µm in 3 h (A), a medium-growing root, grown in a distance of 67.1 µm in 3 h (B) and a slow-growing root, grown in a distance of 32.6 µm in 3 h (C). Double-pointed arrows with appropriate values on the right side of images show recorded distance in µm. White line indicates displacement of the root tip in individual time points of the measurement. (D) Bar chart illustrating distribution of measured individual roots according to their root growth rate. White bars represent slow-growing roots (S1, S2, S3), grey bars represent medium-growing roots (M1, M2, M3) and black bars represent fast-growing roots (F1, F2, F3). (E) Time course of primary root growth showing a correlation between average length increase of fast-growing (♦), medium-growing (□) and slow-growing (Δ) roots and recording time from time-lapse light-sheet imaging at 5 min intervals. Bars = 20 µm (A-C). Adapted from Vyplelová *et al*., 2017.

Progression of cells through the cell division was analyzed on the basis of quantification of the duration of individual cell division stages. Particular transition points characterizing the duration of individual cell division stages (Fig. 9) were identified according to Smertenko *et al.* (2017). The initial stage of the measurement in preprophase and prophase, when progressive PPB narrowing occurs, was defined from the point when width of the PPB was in the range of 2 – 4 μm (Fig. 9A). Transition from preprophase and prophase stage of cell division to mitotic division (prometaphase stage) was defined by the observation of PPB remnants and early mitotic spindle formation (Fig. 9B). PPB stage duration was thus defined from PPB narrowing at late G2 phase (Fig. 9A) to PPB disappearance at prometaphase (Fig. 9B). Stage of mitotic spindle lasted from PPB disappearance and early mitotic spindle formation during prometaphase and finished by last stage of mitotic spindle presence at telophase (Fig. 9C). After disappearance of the mitotic spindle further stages during cytokinesis were formations of early (disk) and late (ring and discontinuous) phragmoplasts (Fig. 9D, E).

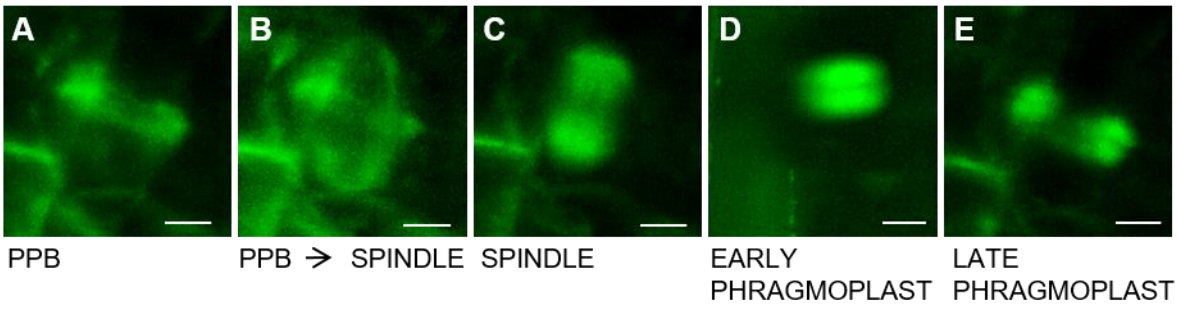

Figure 9. **Stages and transition points of cell division in root epidermis and cortex of *M. sativa* plants expressing *35S::GFP:MBD* construct based on time-lapse LSFM imaging.** (A) PPB narrowing at the preprophase stage of cell division. (B) Transition point from preprophase to prometaphase of cell division characterized by last PPB presence and early stage of mitotic spindle formation. (C) Typical mitotic spindle stage of cell division (shown is anaphase). (D) Early phragmoplast stage of cell division. (E) Late phragmoplast stage of cell division. Shown is typical example of cell division from medium-growing root. Bars = 5 μm. Adapted from Vyplelová *et al*., 2017.

For quantitative analysis, both early and late phragmoplast stages together were considered as one common stage (phragmoplast stage).

We analyzed cell division in the epidermis and the first outer cell layer of the root cortex of the root meristematic zone. To reveal if there are some differences or not between these two cell layers, we first characterized their behaviour during root elongation growth. In addition to measuring the root elongation extend during the recording time, which was used for the calculation of the root growth rate, we measured also the distance, in which selected dividing

cells in epidermis and first outer cortex were displaced along with growing roots. Each dividing cell was tracked down during root elongation and the distance of its displacement (in respect to the growth medium) from the point of mitotic spindle formation until the end of cell division (disappearance of late phragmoplast) was recorded. Results (Fig. 10, 11) corroborated the data of root growth rate (Fig. 8D). Distances in which selected dividing cells were displaced in individual roots showed the same pattern of distribution into three different groups of roots (Fig. 11A, B). Similar results were obtained when the rate of displacement of dividing cells in $\mu m.min^{-1}$ was measured during the recording of root growth (Fig. 11C, D). Importantly, displacement of dividing cells (Fig. 11A, B) during the recording of root growth showed no differences between epidermal (Fig. 11A, C) and first outer cortex cell layer (Fig. 11B, D). Comparison of duration time of individual cell division stages showed several differences

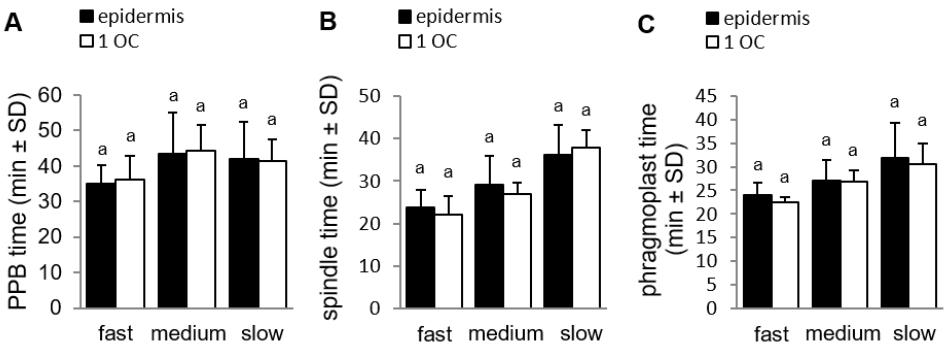

Figure 10. Comparison of duration time of individual cell division stages between epidermis and first outer cortex (1 OC) cell layer. (A) Average PPB stage duration in the preprophase and prophase stages of cell division in epidermis and first outer cortex for fast-growing, medium-growing and slow-growing roots. (B) Average mitotic spindle stage duration from prometaphase to telophase during cell division in epidermis and first outer cortex for fast-growing, medium-growing and slow-growing roots. (C) Average phragmoplast stage duration in cytokinesis of the cell division in epidermis and first outer cortex for fast-growing, medium-growing and slow-growing roots. Letters above the bars represent statistical significance according to one-way ANOVA test at $P < 0.05$. Adapted from Vyplelová *et al*., 2017.

between fast-, medium- and slow-growing roots. Different times were recorded in PPB stage duration (Fig. 12A), mitotic spindle stage duration (Fig. 12B) and phragmoplast stage duration (Fig. 12C). Consistently with previous results comparing epidermis with first outer cortex layer (Fig. 11), also duration time of individual cell division stages showed no considerable differences between epidermis and first outer cortex cell layer (Fig. 10).

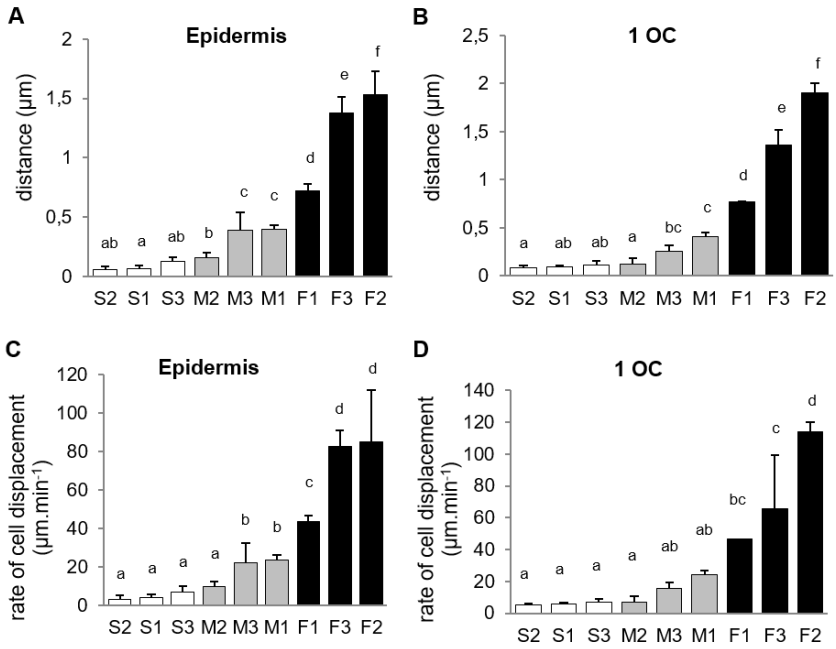

Figure 11. Displacement of dividing cells in epidermis and first outer cortex (1 OC) cell layer during the recording of root growth. (A-B) Average distance, in which dividing cells were displaced in growing roots in respect to the growth medium. Selected dividing cells were tracked down from the time of mitotic spindle formation till the end of cell division in root epidermis (A) and in first outer cortex cell layer (B). Data of the measured distances were normalized to the time period of 60 min. (C-D) Average rate of displacement of dividing cells in growing roots in root epidermis (C) and in first outer cortex cell layer (D). Rate of displacement was calculated from distance, in which dividing cells were displaced during the recording of root growth in respect to the growth medium and from time required for completion of cell division, starting from mitotic spindle formation till the phragmoplast disappearance. Distribution of measured individual roots is shown from shortest to longest average values for slow-growing (S1, S2, S3, white bars), medium-growing (M1, M2, M3, grey bars) and fast-growing roots (F1, F2, F3, black bars). Different letters above the bars represent statistical significance according to one-way ANOVA test at $P < 0.05$. Adapted from Vyplelová *et al*., 2017.

Based on these evidences, data from individual dividing cells in epidermis and first outer cortex were combined together in each root and analysed together in further quantitative analyses.

3.2.4.4 Duration time of individual cell division stages

Time-lapse LSFM imaging of growing roots of transgenic alfalfa plants in 5 min intervals over a period of several hours allowed recording of cells in the meristematic zone and at different stages of cell division. In particular, cells with established PPB (at late G2 phase) were monitored and their entrance to the cell division was documented in time. Preprophase and

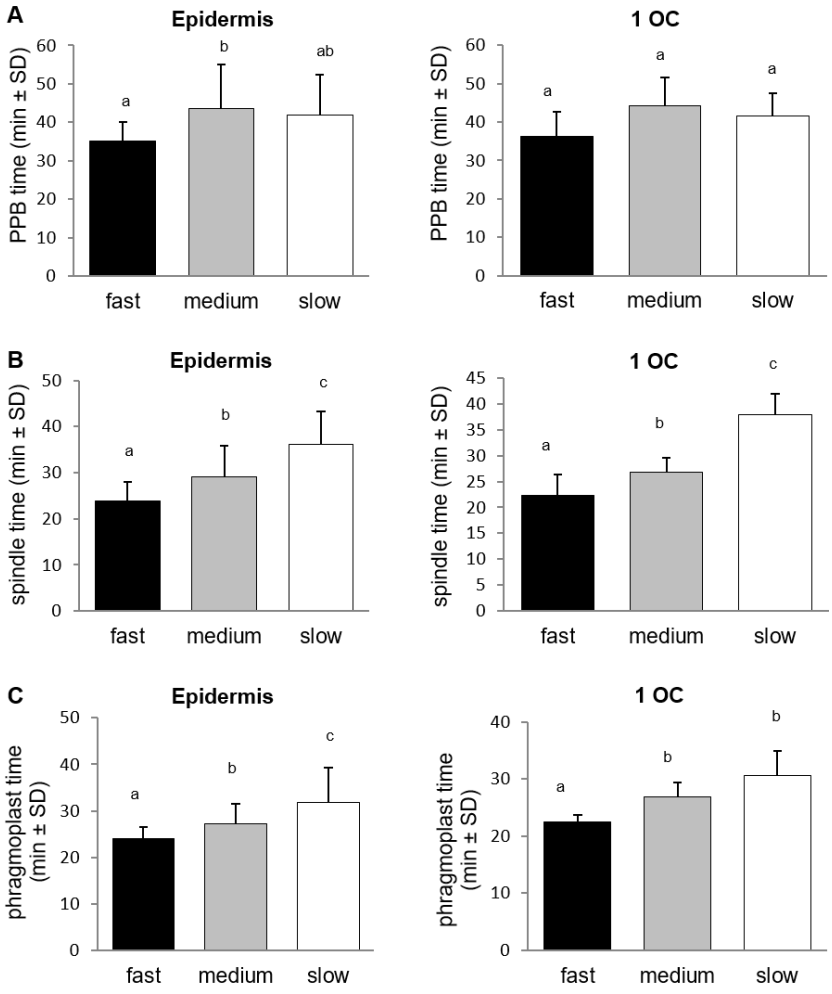

Figure 12. Comparison of duration time of individual cell division stages between epidermis and first outer cortex (1 OC) cell layer. (A) Average PPB stage duration in the preprophase and prophase stages of cell division in epidermis and first outer cortex. (B) Average mitotic spindle stage duration from prometaphase to telophase during cell division in epidermis and first outer cortex. (C) Average phragmoplast stage duration in cytokinesis of the cell division in epidermis and first outer cortex. Black bars represent fast-growing roots, grey bars represent medium-growing roots and white bars represent slow-growing roots. Different letters above the bars represent statistical significance according to one-way ANOVA test at $P < 0.05$. Adapted from Vyplelová *et al*., 2017.

prophase stage of the cell division was identified from the stage of progressive PPB narrowing when PPB width was in the range of 2-4 μm. This time point has been set up as time 0 min. Recording of preprophase and prophase stage finished by PPB disappearance in cells entering mitosis with starting of mitotic spindle formation in prometaphase. Time-lapse recording of this stage in 5 min intervals revealed its duration for 35-40 min. Interestingly, in roots with different root growth rate this duration was different (Fig. 13A-C). In average, preprophase and prophase stage of cell division was fastest in fast-growing roots, while duration of this stage did not differ between medium-growing and slow-growing roots (Fig. 13D).

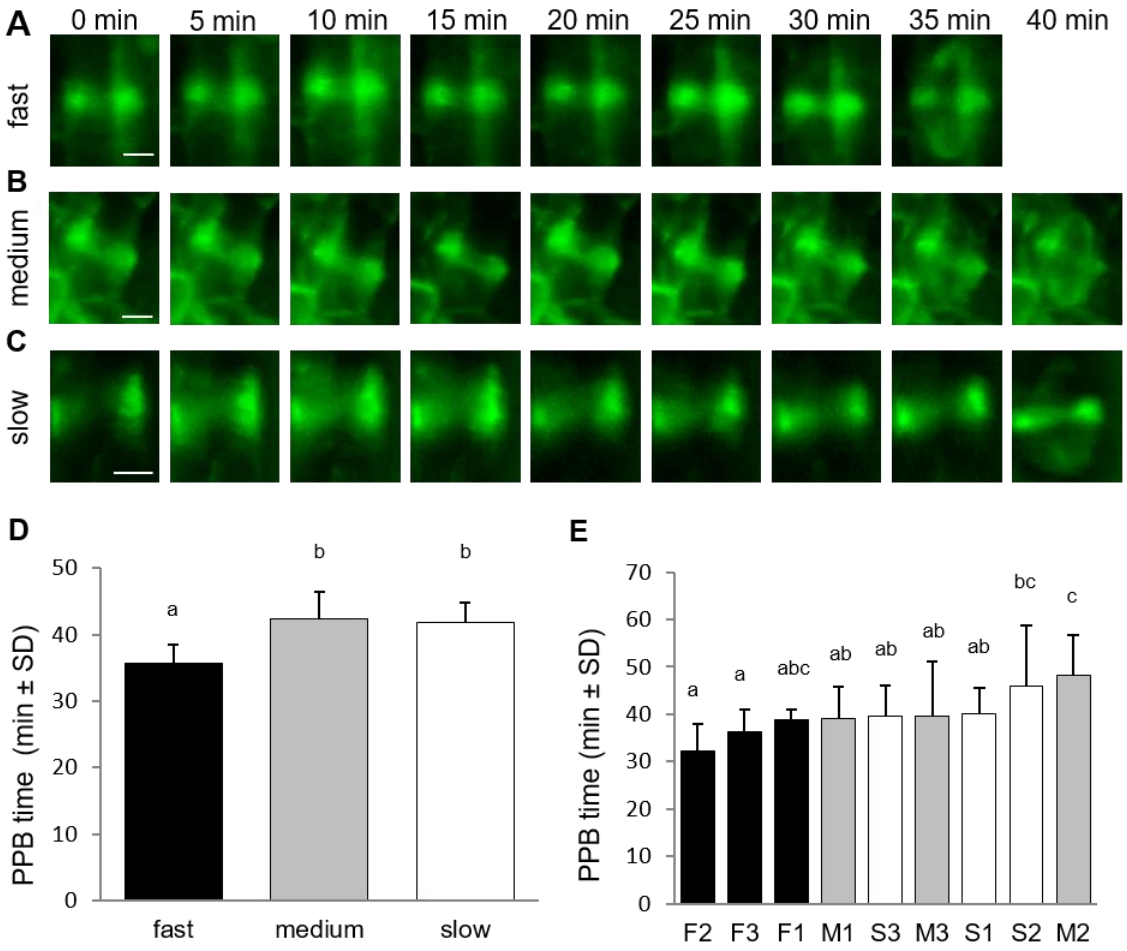

Figure 13. Duration of the preprophase and prophase stage of the cell division. (A-C) Series of stills from time-lapse light-sheet imaging of dividing cells in root epidermis and cortex of *M. sativa* plants expressing *35S::GFP:MBD* construct. Sequence of preprophase and prophase stage starting from PPB narrowing and finishing by last stage of PPB presence and early mitotic spindle formation. Progress of the preprophase and prophase stage is shown for fast-growing roots (A), medium-growing roots (B) and slow-growing roots (C). Series of images were recorded in 5 min intervals from the stage of cell division when progressive PPB narrowing was defined by PPB width in the range of 2-4 μm (time 0 min). (D) Average duration time of preprophase and prophase stage of cell division in all roots of fast-growing, medium-growing and slow-growing group of roots. (E) Average duration time of preprophase and prophase stage in all dividing cells of individual roots. Roots are arranged from shortest to longest average duration time of preprophase and prophase stage. Black bars represent fast-growing roots (F1, F2, F3), grey bars represent medium-growing roots (M1, M2, M3) and white bars represent slow-growing roots (S1, S2, S3). Different letters above the bars represent statistical significance according to one-way ANOVA test at $P < 0.05$. Bars = 5 μm (A-C). Adapted from Vyplelová *et al*., 2017.

Basically the same results were obtained after comparison of preprophase and prophase stage duration in individual roots (Fig. 13E).

Stage of mitotic spindle was measured from disappearance of the PPB with simultaneous mitotic spindle formation through metaphase and anaphase to mitotic spindle disappearance at late anaphase. Measurement revealed that termination of the mitotic spindle stage at late

anaphase was different among three groups of roots differing in their growth rate (Fig. 14A-C). The average duration time of this stage revealed that it was shortest in fast-growing roots, significantly longer in medium-growing roots and the longest in slow-growing roots (Fig. 14D). Comparison of mitotic spindle duration in individual roots confirmed this observation, showing shortest duration of this stage in fast-growing roots and longest duration in slow-growing roots (Fig. 14E).

Duration of the phragmoplast stage was determined from mitotic spindle disappearance at late anaphase with the formation of early (disk) phragmoplast to disappearance of late (ring and discontinuous) phragmoplast at the end of cytokinesis. Consistent with the duration of previous cell division stages the termination of phragmoplast expansion also occurred at different time among the three groups of roots differing in their growth rate (Fig. 15A-C). The average duration time of phragmoplast stage was shortest in fast-growing roots, significantly longer in medium-growing roots and the longest in slow-growing roots (Fig. 15D). Comparison of phragmoplast stage duration in individual roots confirmed this observation (Fig. 15E).

3.2.4.5 Correlation between duration of cell division stages and root growth rate

To reveal possible relationship between speed of root growth and duration of cell division in root apical meristem we analysed correlations between duration of individual cell division stages and root growth rates. Three groups of roots with different root growth rates were analysed separately. Cross-comparison of average root growth rate with average duration of PPB (Fig. 16A), mitotic spindle (Fig. 16B) and phragmoplast (Fig. 16C) stages revealed different tendency. Recorded data were arranged in clusters, distinctly separating groups of fast-growing, medium-growing and slow-growing roots (Fig. 16A-C). Overall data from all individual dividing cells showing duration time of the PPB (Fig. 16D), mitotic spindle (Fig. 16E) and phragmoplast (Fig. 16F) stages correlated very well with the root growth rates, and confirmed clear separation of fast-growing roots from the rest. Particularly values for roots F2 and F3 (Fig. 8D) segregated separately in the upper part of the graphs (Fig. 16D-F).

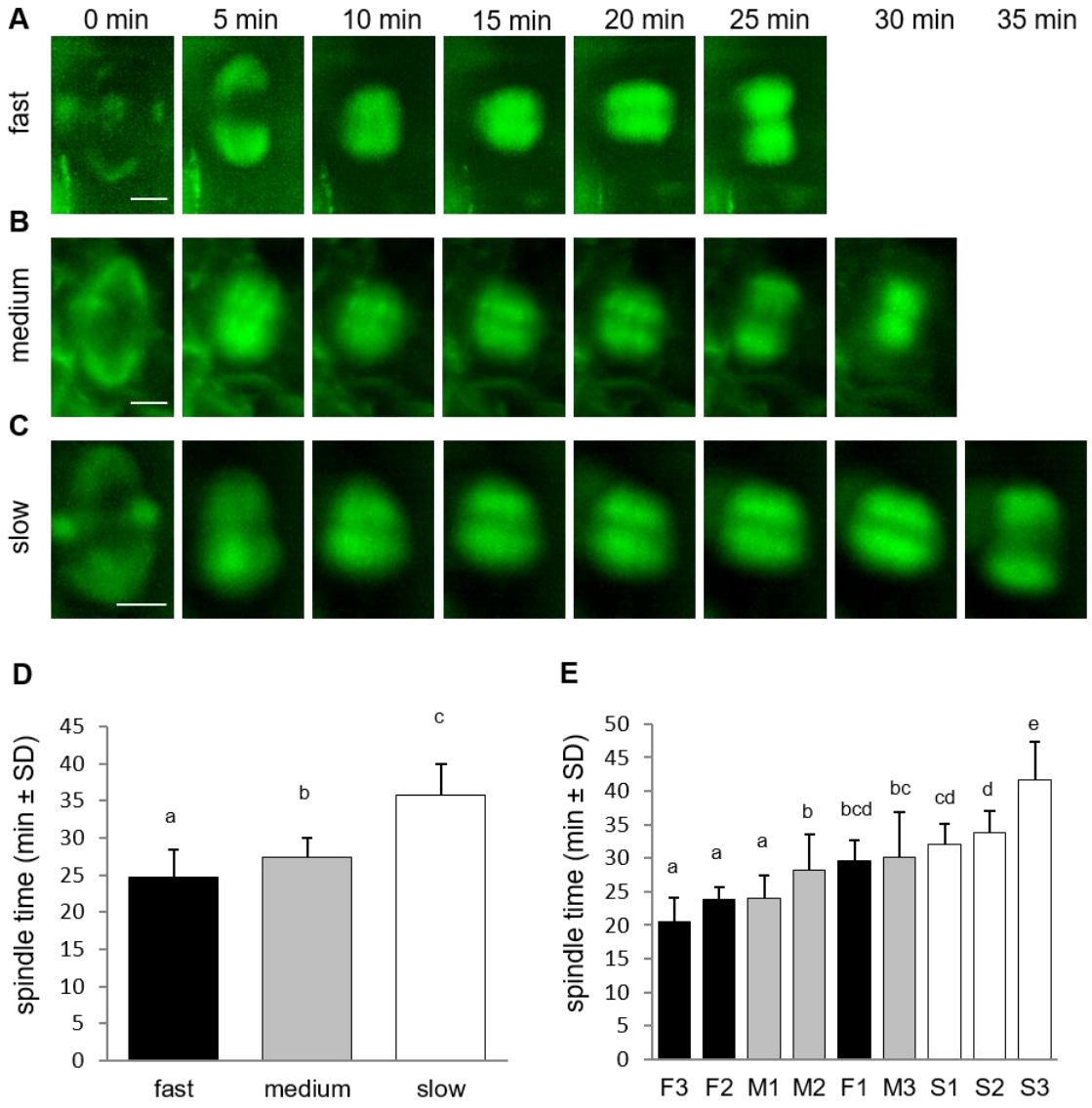

Figure 14. Duration of the mitotic spindle stage from prometaphase to telophase during the cell division. (A-C) Series of stills from time-lapse light-sheet imaging of dividing cells in root epidermis and cortex of *M. sativa* plants expressing *35S::GFP:MBD* construct. Sequence of prometaphase, metaphase, anaphase and telophase stages starting from PPB disappearance and mitotic spindle formation at prometaphase and finishing by last stage of mitotic spindle presence at telophase. Progress of the mitotic spindle stages is shown for fast-growing roots (A), medium-growing roots (B) and slow-growing roots (C). Series of images were recorded in 5 min intervals from the PPB disappearance and mitotic spindle formation at prometaphase (time 0 min). (D) Average duration time of mitotic spindle (prometaphase, metaphase, anaphase and telophase) stages of cell division in all roots of fast-growing, medium-growing and slow-growing group of roots. (E) Average duration time of mitotic spindle (prometaphase, metaphase, anaphase and telophase) stages in all dividing cells of individual roots. Roots are arranged from shortest to longest average duration time of mitotic spindle. Black bars represent fast-growing roots (F1, F2, F3), grey bars represent medium-growing roots (M1, M2, M3) and white bars represent slow-growing roots (S1, S2, S3). Different letters above the bars represent statistical significance according to one-way ANOVA test at $P < 0.05$. Bars = 5 μm (A-C). Adapted from Vyplelová *et al*., 2017.

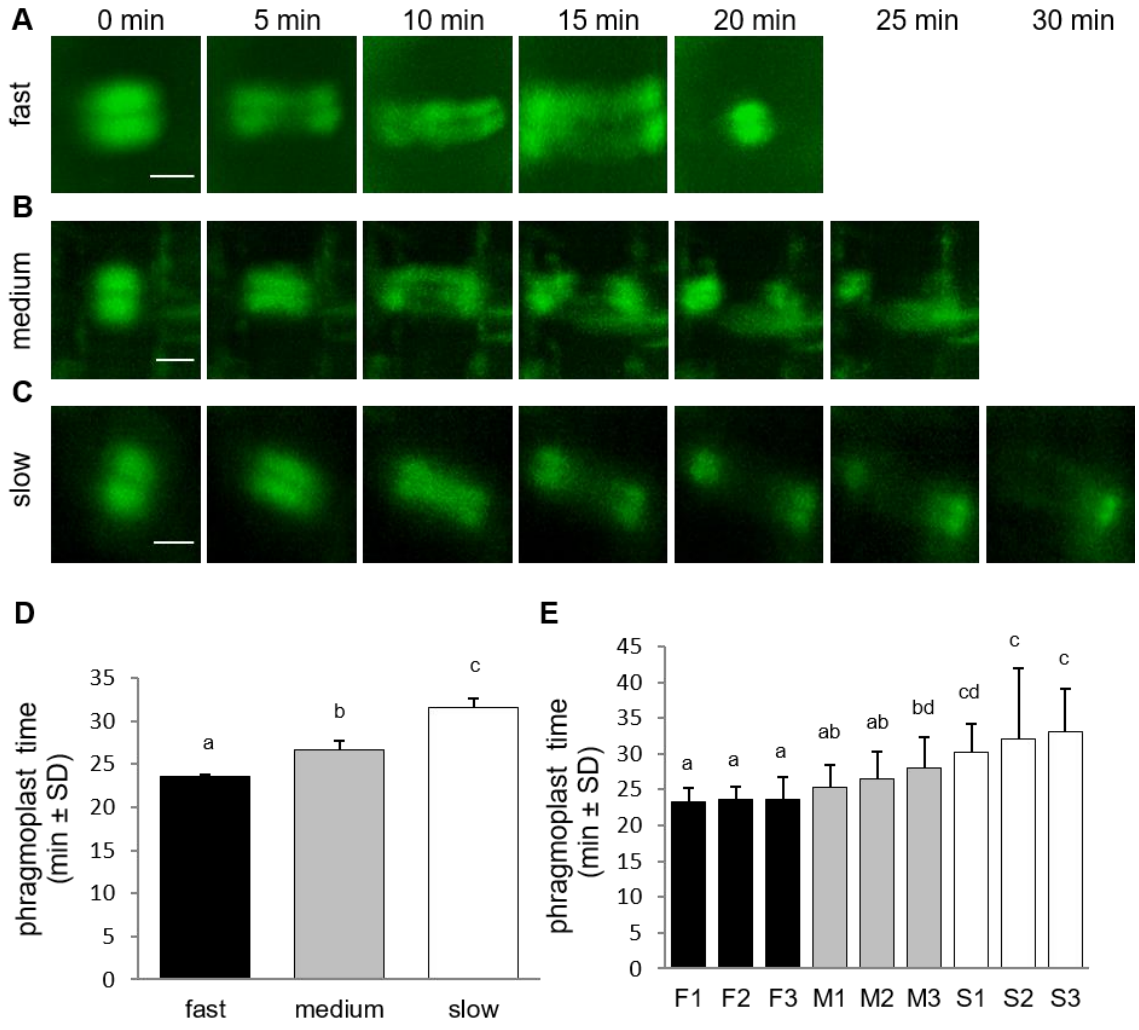

Figure 15. Duration of the phragmoplast stage of the cell division. (A-C) Series of stills from time-lapse light-sheet imaging of dividing cells in root epidermis and cortex of *M. sativa* plants expressing *35S::GFP:MBD* construct. Sequence of phragmoplast stages is shown for fast-growing roots (A), medium-growing roots (B) and slow-growing roots (C). Series of images were recorded in 5 min intervals from the stage of early phragmoplast formation (time 0 min). (D) Average duration time of phragmoplast stage of cell division in all roots of fast-growing, medium-growing and slow-growing group of roots. (E) Average duration time of phragmoplast stage in all dividing cells of individual roots. Roots are arranged from shortest to longest average duration time of phragmoplast. Black bars represent fast-growing roots (F1, F2, F3), grey bars represent medium-growing roots (M1, M2, M3) and white bars represent slow-growing roots (S1, S2, S3). Different letters above the bars represent statistical significance according to one-way ANOVA test at $P < 0.05$. Bars = 5 µm (A-C). Adapted from Vyplelová *et al*., 2017.

Segregation of values measured in medium- and slow-growing roots, correlating PPB, mitotic spindle and phragmoplast stages with root growth rates into clusters is also obvious, although less pronounced as for fast-growing roots (Fig. 16D-G).

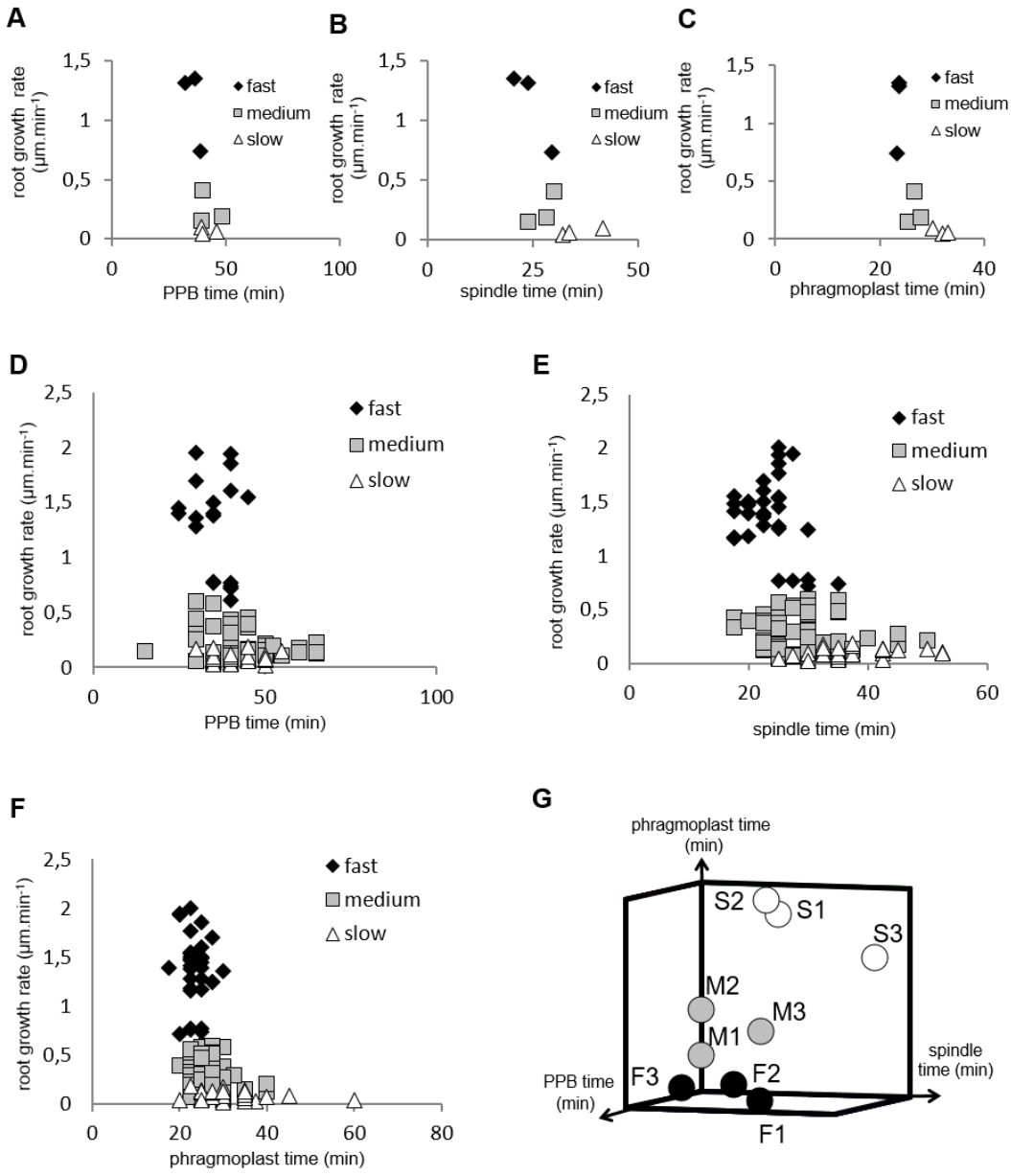

Figure 16. Two- and three-dimensional visualization of data clusters for duration time of individual cell division stages in fast-growing, medium-growing and slow-growing roots according to root growth rate. (A-C) Distribution of clusters for average duration time of the PPB stage (A), mitotic spindle stage (B) and phragmoplast stage (C) according to root growth rate in three fast-growing (♦), three medium-growing (□) and three slow-growing (Δ) roots. (D-F) Distribution of clusters for duration time of the PPB stage (D), mitotic spindle stage (E) and phragmoplast stage (F) according to root growth rate in all individual dividing cells of the fast-growing (♦), medium-growing (□) and slow-growing (Δ) roots. (G) Visualization of data clustering for three fast-growing (F1, F2, F3), three medium-growing (M1, M2, M3) and three slow-growing (S1, S2, S3) roots according to cross-correlation between average duration time of the PPB stage, mitotic spindle stage and phragmoplast stage. Adapted from Vyplelová *et al*., 2017.

In general, the extend of correlation between root growth rate and duration time of the PPB (Fig. 16D), mitotic spindle (Fig. 16E) and phragmoplast (Fig. 16F) stages in all dividing cells of fast-, medium- and slow-growing roots is rather low, as documented by trends of correlation lines and values of correlation coefficients (Fig. 17). Degree of correlation is rather low also for duration time of individual cell division stages compared between each other, namely between PPB and mitotic spindle (Fig. 18A), PPB and phragmoplast (Fig. 18B) and also between mitotic spindle and phragmoplast (Fig. 18C). Negative slope of correlation lines (Fig. 17) indicates a tendency to prolong cell division stages with reducing root growth rates. Thus, clustering of data recorded from individual cell division stages (Fig. 16A-F) and clear separation of these clusters in fast-, medium- and slow-growing roots according to cross-correlation between average duration time of the PPB, mitotic spindle and phragmoplast stages (Fig. 16G) represents crucial aspect of our quantitative evaluation. Collectively, these results suggest correlative regulation of cell division duration depending on the speed of root growth.

3.2.5 Discussion and conclusions

Cell division is key regulatory component of plant morphogenesis and development and one of the most frequently studied biological processes in the plant biology. Monitoring cell divisions in living multicellular plant organs require real time microscopy approach for long-term observation of intact plants that are adapted to proper physiological conditions. Live-cell LSFM imaging of dividing cells could ideally resolve details of cytoskeletal division machinery with high temporal resolution. Moreover, four dimensional monitoring of cell division in organ-, tissue- and cell type-specific context is required for fundamental understanding of cell division regulation during plant growth and development. Nowadays, different microscopy methods are used to study cell division in genetically, developmentally and microscopically-tractable plant model species. Critically important, however, is the adaptation of currently available microscopy techniques for routine live-cell developmental imaging of living robust plant samples, such as crop species. Together with application of efficient protocols for stable transformation of crop species, it should be based on implementation of new approaches, tools and concepts enabling scientific progress in plant cell imaging.

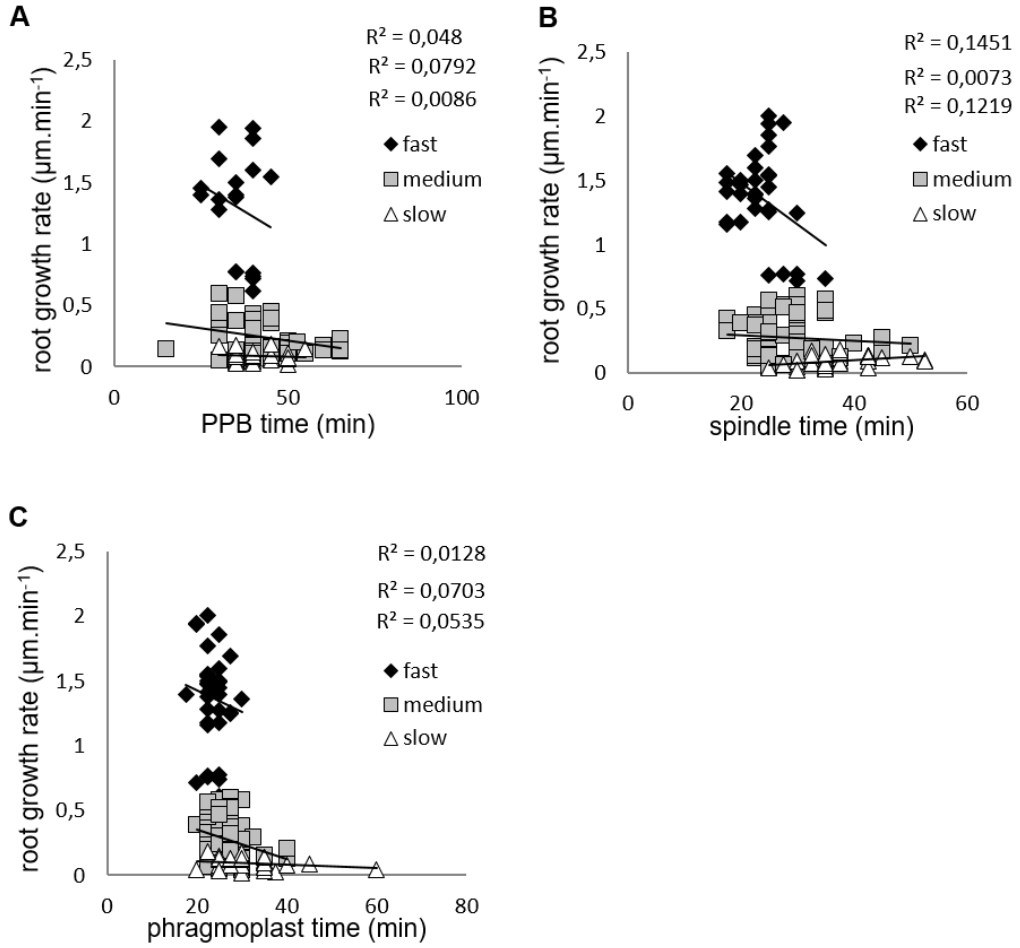

Figure 17. Correlations between root growth rate and duration time of the PPB stage, mitotic spindle stage and phragmoplast stage of dividing cells. (A) Distribution of clusters, correlation lines and correlation coefficients for duration time of the PPB stage in all recorded dividing cells of fast-growing (♦), medium-growing (□) and slow-growing (Δ) roots according to root growth rate. (B) Distribution of clusters, correlation lines and correlation coefficients for duration time of the mitotic spindle stage in all recorded dividing cells of fast-growing (♦), medium-growing (□) and slow-growing (Δ) roots according to root growth rate. (C) Distribution of clusters, correlation lines and correlation coefficients for duration time of the phragmoplast stage in all recorded dividing cells of fast-growing (♦), medium-growing (□) and slow-growing (Δ) roots according to root growth rate. Adapted from Vyplelová *et al*., 2017.

Progression of cell division in plant cells is regulated by particular MT structures, such as PPB, mitotic spindle and phragmoplast. These MT arrays are involved in CDP orientation, symmetry of cell division, segregation of nuclear material into two new cell nuclei and partitioning of cytoplasmic space of dividing cell into two daughter cells. Organization and dynamics of MTs during individual mitotic and cytokinetic stages control the progression of cell division. MT-dependent functions during cell division are mediated by modulators of MT organization and dynamics, such as MAPs, EB1 proteins and MT severing proteins.

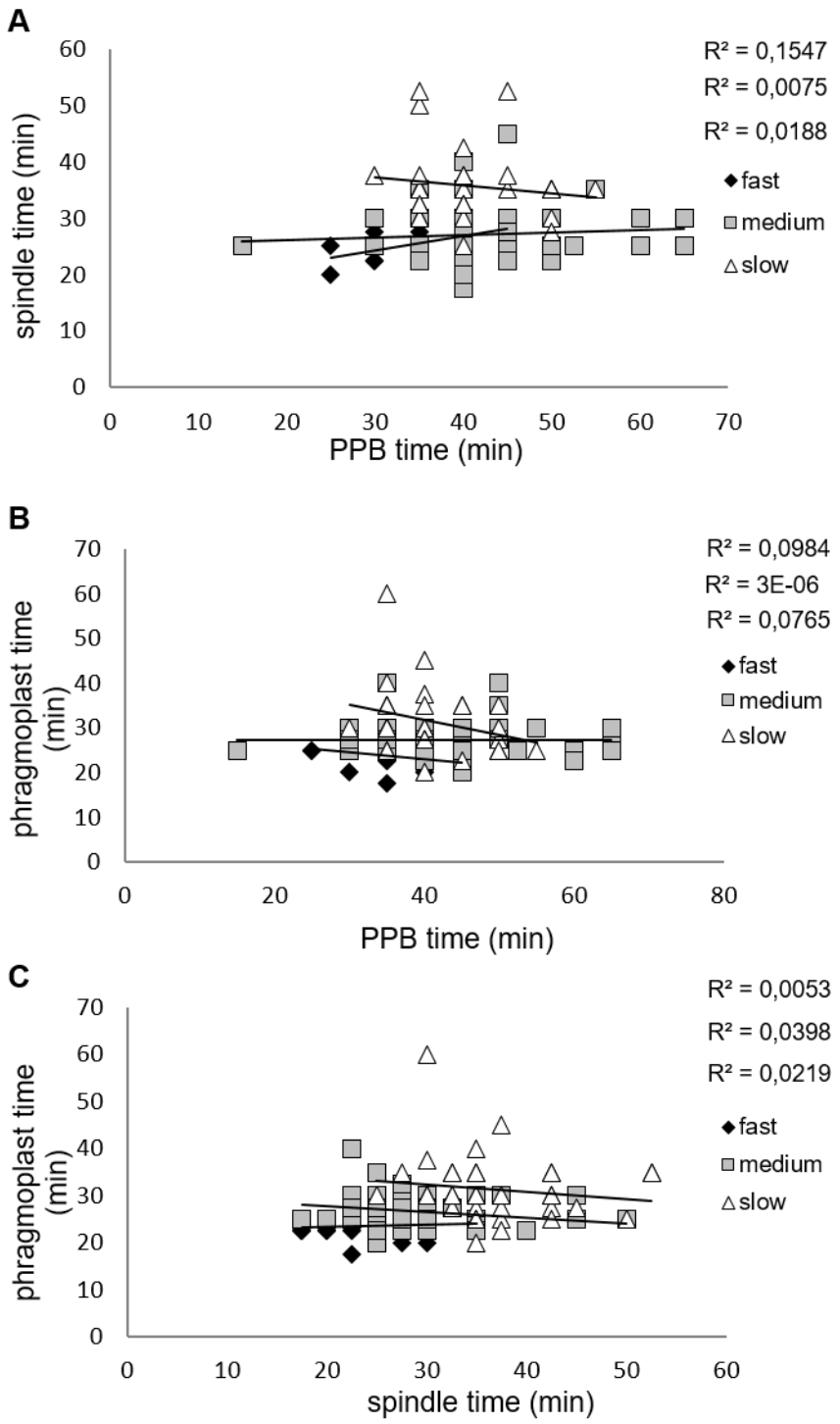

Figure 18. Correlations between duration time of individual cell division stages in all measured dividing cells. (A) Correlations between duration time of the PPB stage and mitotic spindle stage in fast-growing (♦), medium-growing (□) and slow-growing (Δ) roots. (B) Correlations between duration time of the PPB stage and phragmoplast stage in fast-growing (♦), medium-growing (□) and slow-growing (Δ) roots. (C) Correlations between duration time of the mitotic spindle stage and phragmoplast stage in fast-growing (♦), medium-growing (□) and slow-growing (Δ) roots. Adapted from Vyplelová *et al*., 2017.

Study of MAPs from the MAP65 protein family (van Damme *et al.*, 2004; Chang *et al.*, 2005; Mao *et al.*, 2005; Smertenko *et al.*, 2006; Ho *et al.*, 2011a; 2012) and EB1 proteins (Chan *et al.*, 2003; 2005; Komaki *et al.*, 2010) in their interactions with spindle and phragmoplast MTs promoted considerably our understanding how MTs are organized and how their dynamic properties regulate cell division progress and duration.

Roles of MT-severing proteins were traditionally connected to dynamic reorganization of cortical MT arrays. Recent study on knock-out mutant *ktn1-2* revealed that KATANIN 1 contributes to PPB formation and maturation, and is involved in the positioning of the mitotic spindle and the phragmoplast (Komis *et al.*, 2017). An important scientific question will be how complex MT network well described in models operates in legume crop species. Starting to address this question in *M. sativa*, we characterized MT arrays during the progress of mitotic cell division and sustained root growth. Main motivation of our study was to collect relevant data at near environmental condition, ensuring stress- and artefact-free imaging of living legume plant that is not interfering with normal plant growth and development. This was possible by implementation of LSFM and proper sample preparation protocols into live developmental imaging of alfalfa plants.

Progress of mitotic cell division, distribution of mitoses within the root meristematic zone and cessation of mitotic activity in the root transition zone are tissue-specifically regulated. It has been shown that cells of the cortex and epidermis quit cell division earlier than cells of the endodermis and central cylinder tissues (Baluška *et al.*, 1990; Schmidt *et al.*, 2014). Duration of the PPB stage can be considerably long, as compared to the duration of other subsequent cell division stages during mitosis (Dhonukshe and Gadella, 2003; Vos *et al.*, 2004; Komis *et al.*, 2017). Alterations in the duration of the phragmoplast expansion have been observed in the Arabidopsis *mpk4* mutant, which is devoid of the mitogen-activated protein kinase 4 (MPK4). This stage of the cell division was considerably delayed in comparison to control plants (Beck *et al.*, 2011). Herein, we recorded and quantitatively evaluated duration time of PPB, mitotic spindle and phragmoplast during cell division of epidermal and cortex cells in root meristem of transgenic *M. sativa*. Results suggested that duration time of cell division stages was different in roots with different growth rates. PPB stage was shortest in fast-growing roots, characterized by root growth rate of 0.7 – 1.4 $\mu m.min^{-1}$, similarly as duration time of mitotic spindle and phragmoplast. Stages of mitosis and cytokinesis lasted significantly longer time in medium-growing roots with root growth rate of 0.2 – 0.5 $\mu m.min^{-1}$ and duration of these stages was the longest in slow-growing roots with growth rate less than 0.2 $\mu m.min^{-1}$.

Quantitative kinematic study of primary root growth among 18 different ecotypes of *A. thaliana* revealed considerable variations, functionally linking root growth rate with cell cycle regulation. Along with variation in mature cortical cell length and number of dividing cells, also cell cycle duration contributed considerably to the observed variations in root growth rate (Beemster *et al.*, 2002). Because the rate of cell division and the rate of cell production (defined as number of dividing cells and variation in their cell cycle duration) should be principally distinguished (reviewed by Baskin, 2000), determination of root growth rate ideally combines the spatial profile of cell length, cell velocity, relative elongation rate and cell division rate (Beemster and Baskin, 1998; Baskin, 2000). Functional interconnections of these critical parameters are obvious under unfavourable and stress environmental conditions. Responses of *A. thaliana* roots to temperature changes lead to alterations in the meristem length, which was compensated by changes in the cell length within the elongation zone or by changes in division rate helping to maintain equilibrated cell flux within the root meristem (Yang *et al.*, 2017). Although it is generally assumed that durations of individual mitotic and cytokinetic stages correlate only indirectly with total cell cycle duration, statistically evaluated parameters in *M. sativa* confirmed *vice versa* correlation of root growth rate with speed of these mitotic and cytokinetic stages in the root meristem. In principle, reduction in root growth rate was reflected by the prolongation of mitotic and cytokinetic stages. Such data were not available in crop species *M. sativa* before.

Moreover, the present study is the first one to provide large-scale imaging and quantitative characterization of cell divisions in the growing robust root of *M. sativa* using developmental live-cell imaging. This was achieved by advanced LSFM, providing suitable technological and physiological tool for developmental live-cell imaging of dividing cells in plant material with high spatial and excellent temporal resolution. LSFM is mesoscopic imaging method, overcoming several critical problems regarding the proper preparation and long-term maintenance of living plant samples. Low phototoxicity allows monitoring of Arabidopsis root growth for long time under physiological conditions (Maizel *et al.*, 2011; Ovečka *et al.*, 2015). Potential of LSFM for developmental imaging of mitotic MT arrays during cell division is obvious, although it was so far utilized only in three studies on Arabidopsis. Previously, cell division in growing primary roots in long-term time-lapse experiments was observed in Arabidopsis plants carrying MT molecular markers GFP-MBD (Maizel *et al.*, 2011) or GFP-TUA5 (Ovečka *et al.*, 2015). LSFM was also used for characterization of tissue-specific and developmentally-regulated distribution of nuclear levels of GFP-tagged EB1c protein expressed under the control of native *EB1c* promoter. Quantitative correlation analysis revealed

relationship between nuclear size and EB1c expression levels in diverse tissues like epidermis, cortex and endodermis, and in different developmental zones including meristematic, transition and elongation zone of *A. thaliana* roots (Novák *et al.*, 2016). In this study we performed dynamic imaging of mitotic MT arrays in robust *M. sativa* growing roots using LSFM. For this purpose, we prepared stably transformed lines of *M. sativa* carrying molecular MT marker GFP-MBD and evaluated MT organization and dynamics during cell division of both epidermal and cortical root cells. Quantitative evaluation of cell division duration time was based on characterization of individual cell division stages, namely PPB, mitotic spindle and phragmoplast. The study clearly revealed an important link between duration of cell division in the root meristematic cells and root growth rates in *M. sativa*. These results suggest that spatio-temporal organization of MT-dependent cell divisions in the root meristem significantly contribute to the root growth rates. Importantly, LSFM is broadly applicable to any genetically modified and fluorescently labelled model legume species such as *M. truncatula* and *Lotus japonicus* as well as to agriculturally important legumes such as soybean, fava bean, pea or chickpea. Moreover, it is potentially interesting also for biotechnological applications such as *M. sativa* lines with RNAi-mediated genetic downregulation of stress-induced mitogen activated protein kinase kinase (SIMKK), an important component of signal transduction cascades in alfalfa (Bekešová *et al.*, 2015), or crop transgenic lines with genetically manipulated cytoskeleton (Komis *et al*., 2015). Considering big potential of LSFM for deep imaging, it can be adapted and used to study interactions of legume roots expressing diverse subcellular markers (including MTs) with beneficial microbes such as Rhizobia and mycorrhizal fungi.

Conclusively, previous achievements on Arabidopsis together with data presented in this study demonstrate a high potential of LSFM in developmental live-cell imaging of mitotic cytoskeletal arrays in diverse plant species. High temporal and good spatial resolution combined with non-invasive and gentle live-cell imaging of cell divisions during growth and development of *M. sativa* roots favour light-sheet microscopy as the most promising imaging method for the future developmental bioimaging and characterization of robust crop species.

4. GENERAL CONCLUSIONS

The present Ph.D. thesis addresses aspects of the plant cytoskeleton, giving special emphasis on the role of MTs during the mitosis. The main aim of the work was the application of novel microscopic approaches and visualization methods in the study of mitotic microtubular structures such as PPB, mitotic spindle and phragmoplast. The thesis consists of three parts. The first part summarizes the existing basic knowledge on the plant cytoskeleton, with special attention being payed to the organization and dynamics of MTs. This section also includes important information on the large number of MAPs identified mainly in the model plant organism *A. thaliana* and their crucial role in the particular stages of cell division. Overall, mitosis is a highly dynamic process in which extensive reorganization of MTs occurs. Therefore, the selection of suitable method for preparation of plant material and application of appropriate visualization method is a key point in the successful study of microtubular system during the mitosis.

In the second part, the procedure of sample preparation was methodically described for three modern microscopic methods such as LSFM, SDCM and Airyscan CLSM. Due to the high speed imaging of SDCM and high resolution and sensitivity of Airyscan CLSM in combination with the additional Airyscan detector, significantly improving signal-to-noise ratio, both methods are suitable for the fast live-cell imaging during the short-term experiments. In addition, LSFM represents a potent tool for long-term plant imaging in real time due to the physiological vertical orientation of sample and low phototoxicity during imaging.

Last part of the thesis was devoted the use of LSFM for 4D long-term live deep-imaging of *M. sativa* roots expressing *35S::GFP:MBD* construct as genetically encoded MT marker. Optimization of sample preparation was important for obtaining of good quality resolution during the visualization of mitotic MT arrays in two different cell layers, the epidermis and the first outer layer of cortex. Based on the growth parameters, in total nine *M. sativa* roots were divided into three groups designed as fast-, medium- and slow-growing roots. Growth rates of individual roots, growth rates of elongating cells and duration of particular mitotic stages were measured and analyzed. It was observed that the durations of PPB, mitotic spindle and phragmoplast stages were shortest in the fast-growing roots, while in slow-growing roots all mitotic stages persisted for the longest period of time. Duration of PPB stage in medium- and slow-growing was approximately the same. Importantly, a positive correlation between the root growth rate and the duration of cell division in the *M. sativa* roots was found. Thus, LSFM

proved to be an efficient method for imaging of robust roots of legume species such as *M. sativa*.

5. REFERENCES

Akhmanova A, Steinmetz MO. Tracking the ends: a dynamic protein network controls the fate of microtubule tips. *Nat Rev Mol Cell Biol* 2008; 9: 309 – 322.

Alberts B, Johnson A, Lewis J, Raff M, Roberts K, Walter P. The cell cycle. In Molecular biology of the cell, 5th edition. Editors Anderson M, Granum S, Garland Science, NY, 2008, 1053 – 1114.

Ambrose JC, Cyr R. Mitotic spindle organization by the preprophase band. *Mol Plant* 2008; 1: 950 – 960.

Ambrose JC, Cyr R. The kinesin ATK5 functions in early spindle assembly in Arabidopsis. *Plant Cell* 2007; 19: 226 – 236.

Ambrose JC, Li W, Marcus A, Ma H, Cyr R. A minus-end-directed kinesin with plus-end tracking protein activity is involved in spindle morphogenesis. *Mol Biol Cell* 2005; 16: 1584 – 1592.

Ambrose JC, Shoji T, Kotzer AM, Pighin JA, Wasteneys GO. The Arabidopsis CLASP gene encodes a microtubule-associated protein involved in cell expansion and division. *Plant Cell* 2007; 19: 2763 – 2775.

Amini M, Deljou A, Nabiabad HS. Improvement of in vitro embryo maturation, plantlet regeneration and transformation efficiency from alfalfa (*Medicago sativa* L.) somatic embryos using *Cuscuta campestris* extract. *Physiol Mol Biol Plants* 2016; 22: 321 – 330.

Ammirato PV. The regulation of somatic embryo development in plant cell cultures: suspension culture techniques and hormone requirements. *Nat Biotechnol* 1983; 1: 68 – 73.

Anandarajah K, McKersie BD. Influence of plating density, sucrose and light during development on the germination and vigour of *Medicago sativa* L. somatic embryos after desiccation. *Seed Sci Res* 1992; 2: 133 – 140.

Arnold MFF, Penterman J, Shabab M, Chen EJ, Walker GC. Important late stage symbiotic role of the *Sinorhizobium meliloti* exopolysaccharide succinoglycan. *J Bacteriol* 2018; pii: JB.00665-17. doi: 10.1128/JB.00665-17

Asada T, Kuriyama R, Shibaoka H. TKRP125, a kinesin-related protein involved in the centrosome-independent organization of the cytokinetic apparatus in tobacco BY-2 cells. *J Cell Sci* 1997; 110: 179 – 189.

Atanassov A, Brown DC. Plant regeneration from suspension culture and mesophyll protoplasts of *Medicago sativa* L. *Plant Cell Tissue Organ Cult* 1984; 3: 149 – 162.

Austin S, Bingham ET, Mathews DE, Shahan MN, Will J, Burgess RR. Production and field performance of transgenic alfalfa (*Medicago sativa* L.) expressing alpha-amylase and manganese-depent lignin peroxidase. *Euphytica* 1995; 85: 381 – 393.

Ayaydin F, Vissi E, Mészáros T, Miskolczi P, Kovács I, Fehér A, Dombrádi V, Erdödi F, Gergely P, Dudits D. Inhibition of serine/threonine-specific protein phosphatases causes premature activation of cdc2MsF kinase at G2/M transition and early mitotic microtubule organisation in alfalfa. *Plant J* 2000; 23: 85 – 96.

Azimzadeh J, Nacry P, Christodoulidou A, Drevensek S, Camilleri C, Amiour N, Parcy F, Pastuglia M, Bouchez D. Arabidopsis TONNEAU1 proteins are essential for preprophase band formation and interact with centrin. *Plant Cell* 2008; 20: 2146 – 2159.

Baluška F, Kubica S, Hauskrecht M. Postmitotic 'isodiametric' cell growth in the maize root apex. *Planta* 1990; 181: 269 – 274.

Baluška F, Salaj J, Mathur J, Braun M, Jasper F, Šamaj J, Chua NH, Barlow PW, Volkmann D. Root hair formation: F-actin-dependent tip growth is initiated by local assembly of profilin-supported F-actin meshworks accumulated within expansin-enriched bulges. *Dev Biol* 2000; 227: 618 – 632.

Bannigan A, Scheible WR, Lukowitz W, Fagerstrom C, Wadsworth P, Somerville C, Baskin TI. A conserved role for kinesin-5 in plant mitosis. *J Cell Sci* 2007; 120: 2819 – 2827.

Barbulova A, Iantcheva A, Zhiponova M, Vlahova M, Atanassov A. Establishment of emryogenic potential of economically important bulgarian alfalfa cultivars (*Medicago sativa* L.). *Biotechnol Biotechnol Eq* 2002; 16: 55 – 63.

Baskin TI. On the constancy of cell division rate in the root meristem. *Plant Mol Biol* 2000; 43: 545 – 554.

Baskin TI. Patterns of root growth acclimation: constant processes, changing boundaries. *Wiley Interdiscip Rev Dev Biol* 2013; 2: 65 – 73.

Baum SF, Dubrovsky JG, Rost TL. Apical organization and maturation of the cortex and vascular cylinder in *Arabidopsis thaliana* (Brassicaceae) roots. *Am J Bot* 2002; 89: 908 – 920.

Bechtold N, Ellis J, Pelletier G. In planta *Agrobacterium* mediated gene transfer by infiltration of adult *Arabidopsis thaliana* plants. *C R Acad Scl Pans, Life Scl* 1993; 316: 1194 – 1199.

Beck M, Komis G, Ziemann A, Menzel D, Samaj J. Mitogen-activated protein kinase 4 is involved in the regulation of mitotic and cytokinetic microtubule transitions in *Arabidopsis thaliana*. *New Phytol* 2011; 189: 1069 – 1083.

Beemster GT, Baskin TI. Analysis of cell division and elongation underlying the developmental acceleration of root growth in *Arabidopsis thaliana*. *Plant Physiol* 1998; 116: 1515 – 1526.

Beemster GT, De Vusser K, De Tavernier E, De Bock K, Inzé D. Variation in growth rate between Arabidopsis ecotypes is correlated with cell division and A-type cyclin-dependent kinase activity. *Plant Physiol* 2002; 129: 854 – 864.

Bekešová S, Komis G, Křenek P, Vyplelová P, Ovečka M, Luptovčiak I, Illés P, Kuchařová A, Šamaj J. Monitoring protein phosphorylation by acrylamide pendant Phos-Tag™ in various plants. *Front Plant Sci* 2015; 6: 336. doi: 10.3389/fpls.2015.00336.

Bezanilla M, Gladfelter AS, Kovar DR, Lee WL. Cytoskeletal dynamics: a view from the membrane. *J Cell Biol* 2015; 209: 329 – 337.

Bi EF, Lutkenhaus J. FtsZ ring structure associated with division in *Escherichia coli*. *Nature* 1991; 354: 161 – 164.

Binarová P, Cenklová V, Hause B, Kubátová E, Lysák M, Doležel J, Bögre L, Dráber P. Nuclear γ-tubulin during acentriolar plant mitosis. *Plant Cell* 2000; 12: 433 – 442.

Binarová P, Cenklová V, Procházková J, Doskočilová A, Volc J, Vrlík M, Bögre L. γ -tubulin is essential for acentrosomal microtubule nucleation and coordination of late mitotic events in *Arabidopsis*. *Plant Cell* 2006; 18: 1199 – 1212.

Binarová P, Dolezel J, Draber P, Heberle-Bors E, Strnad M, Bögre L. Treatment of *Vicia faba* root tip cells with specific inhibitors to cyclin-dependent kinases leads to abnormal spindle formation. *Plant J* 1998; 16: 697 – 707.

Bingham ET, Hurley LV, Kaatz DM, Saunders JW. Breeding alfalfa which regenerates from callus tissue in culture. *Crop Sci* 1975; 15: 719 – 721.

Bingham ET. Registration of alfalfa hybrid Regen-SY germplasm for tissue culture and transformation research. *Crop Sci* 1991; 31: 1098 doi:10.2135/cropsci1991.0011183X003100040075x.

Blaydes DF. Interaction of kinetin and various inhibitors in the growth of soybean tissue. *Physiol Plant* 1966; 19: 748 – 753.

Blöchl A, Grenier-de March G, Sourdioux M, Peterbauer T, Richter A. Induction of raffinose oligosaccharide biosynthesis by abscisic acid in somatic embryos of alfalfa (*Medicago sativa* L.). *Plant Sci* 2005; 168: 1075 – 1082.

Boruc J, Weimer AK, Stoppin-Mellet V, Mylle E, Kosetsu K, Cedeño C, Jaquinod M, Njo M, De Milde L, Tompa P, Gonzalez N, Inzé D, Beeckam T, Vantard M, Van Damme D. Phosphorylation of MAP65-1 by Arabidopsis Aurora kinases is required for efficient cell cycle progression. *Plant Physiol* 2017; 173: 582 – 599.

Bria A, Iannello G, Onofri L, Peng H. TeraFly: real-time three-dimensional visualization and annotation of terabytes of multidimensional volumetric images. *Nat Methods* 2016; 13: 192 – 194.

Brown DCW, Atanassov A. Role of genetic backroung in somatic embryogenesis in *Medicago*. *Plant Cell Tissue Organ Cult* 1985; 4: 111 – 122.

Burk DH, Liu B, Zhong R, Morrison WH, Ye ZH. A katanin-like protein regulates normal cell wall biosynthesis and cell elongation. *Plant Cell* 2001; 13: 807 – 827.

Buschmann H, Chan J, Sanchez-Pulido L, Andrade-Navarro MA, Doonan JH, Lloyd CW. Microtubule-associated AIR9 recognizes the cortical division site at preprophase and cell-plate insertion. *Curr Biol* 2006; 16: 1938 – 1943.

Buschmann H, Dols J, Kopischke S, Peña EJ, Andrade-Navarro MA, Heinlein M, Szymanski DB, Zachgo S, Doonan JH, Lloyd CW. Arabidopsis KCBP interacts with AIR9 but stays in the cortical division zone throughout mitosis via its MyTH4-FERM domain. *J Cell Sci* 2015; 128: 2033 – 2046.

Buschmann H, Green P, Sambade A, Doonan JH, Lloyd CW. Cytoskeletal dynamics in interphase, mitosis and cytokinesis analysed through *Agrobacterium*-mediated transient transformation of tobacco BY-2 cells. *New Phytol* 2011; 190: 258 – 267.

Buschmann H, Sambade A, Pesquet E, Calder G, Lloyd CW. Microtubule dynamics in plant cells. *Methods Cell Biol* 2010; 97: 373 – 400.

Calder G, Hindle C, Chan J, Shaw P. An optical imaging chamber for viewing living plant cells and tissues at high resolution for extended periods. *Plant Methods* 2015; 11:22. doi: 10.1186/s13007-015-0065-7.

Camilleri C, Azimzadeh J, Pastuglia M, Bellini C, Grandjean O, Bouchez D. The Arabidopsis *TONNEAU2* gene encodes a putative novel protein phosphatase 2A regulatory subunit essential for the control of the cortical cytoskeleton. *Plant Cell* 2002; 14: 833 – 845.

Campilho A, Garcia B, Toorn HV, Wijk HV, Campilho A, Scheres B. Time-lapse analysis of stem-cell divisions in the *Arabidopsis thaliana* root meristem. *Plant J* 2006; 48: 619 – 627.

Celler K, Fujita M, Kawamura E, Ambrose C, Herburger K, Holzinger A, Wasteneys GO. Microtubules in Plant Cells: Strategies and methods for immunofluorescence, transmission electron microscopy and live cell imaging. *Methods Mol Biol* 2016; 1365: 155 – 184.

Chabaud M, Passiatore JE, Cannon F, Buchanan-Wollaston V. Parameters affecting the frequency of kanamycin resistant alfalfa obtained by *Agrobacterium tumefaciens* mediated transformation. *Plant Cell Rep* 1988; 7: 512 – 516.

Chan J, Calder G, Fox S, Lloyd C. Localization of the microtubule end binding protein EB1 reveals alternative pathways of spindle development in Arabidopsis suspension cells. *Plant Cell* 2005; 17: 1737 – 1748.

Chan J, Calder GM, Doonan JH, Lloyd CW. EB1 reveals mobile microtubule nucleation sites in *Arabidopsis*. *Nat Cell Biol* 2003; 5: 967 – 971.

Chang HY, Smertenko AP, Igarashi H, Dixon DP, Hussey PJ. Dynamic interaction of NtMAP65-1a with microtubules *in vivo*. *J Cell Sci* 2005; 118: 3195 – 3201.

Chen THH, Marowitch J, Thompson BG. Genotypic effects on somatic embryogenesis and plant regeneration from callus cultures of alfalfa. *Plant Cell Tissue Organ Cult* 1987; 8: 73 – 81.

Chichili GR, Rodgers W. Cytoskeleton-membrane interactions in membrane raft structure. *Cell Mol Life Sci* 2009; 66: 2319 – 2328.

Clough SJ, Bent AF. Floral dip: a simplified method for *Agrobacterium*-mediated transformation of *Arabidopsis thaliana*. *Plant J* 1998; 16: 735 – 743.

Coudreuse D, Nurse P. Driving the cell cycle with a minimal CDK control network. *Nature* 2010; 468: 1074 – 1079.

Crea F, Bellucci M, Damiani F, Arcioni S. Genetic control of somatic embryogenesis in alfalfa (*Medicago sativa* L. cv. Adriana). *Euphytica* 1995; 81: 151 – 155.

Cyr RJ. Microtubules in plant morphogenesis: Role of the Cortical Array. *Annu Rev Cell Biol* 1994; 10: 153 – 180.

D´Halluin K, Botterman J, de Greef W. Engineering of herbicide-resistant alfalfa and evaluation under field conditions. *Crop Sci* 1989; 30: 866 – 871.

Demidov D, Van Damme D, Geelen D, Blattner FR, Houben A. Identification and dynamics of two classes of aurora-like kinases in Arabidopsis and other plants. *Plant Cell* 2005; 17: 836 – 848.

Denchev P, Velcheva M, Atanassov A. A new approach to direct somatic embryogenesis in *Medicago*. *Plant Cell Rep* 1991; 10: 338 – 341.

Desai A, Mitchison TJ. Microtubule polymerization dynamics. *Annu Rev Cell Dev Biol* 1997; 13: 83 – 117.

Desgagnés R, Laberge S, Allard G, Khoudi H, Castonguay Y, Lapointe J, Michaud R, Vézina LP. Genetic transformation of commercial breeding of alfalfa (*Medicago sativa*). *Plant Cell Tissue Organ Cult* 1995; 42: 129 – 140.

Dhonukshe P, Gadella TW Jr. Alteration of microtubule dynamic instability during preprophase band formation revealed by yellow fluorescent protein-CLIP170 microtubule plus-end labeling. *Plant Cell* 2003; 15: 597 – 611.

Dhonukshe P, Vischer N, Gadella TW Jr. Contribution of microtubule growth polarity and flux to spindle assembly and functioning in plant cells. *J Cell Sci* 2006; 119: 3193 – 3205.

Dibbayawan TP, Harper JD, Marc J. A γ-tubulin antibody against a plant peptide sequence localises to cell division-specific microtubule arrays and organelles in plants. *Micron* 2001; 32: 671 – 678.

Dijak M, Brown DCW. Patterns of direct and indirect embryogenesis from mesophyll protoplasts of *Medicago sativa*. *Plant Cell Tissue Organ Cult* 1987; 9: 121 – 130.

Dixit R, Cyr RJ. Spatio-temporal relationship between nuclear-envelope breakdown and preprophase band disappearance in cultured tobacco cells. *Protoplasma* 2002; 219: 116 – 121.

Dolan L, Janmaat K, Willemsen V, Linstead P, Poethig S, Roberts K, Scheres B. Cellular organisation of the *Arabidopsis thaliana* root. *Development* 1993; 119: 71 – 84.

Dryková D, Cenklová V, Sulimenko V, Volc J, Dráber P, Binarová P. Plant γ-tubulin interacts with αβ-tubulin dimers and forms membrane-associated complexes. *Plant Cell* 2003; 15: 465 – 480.

Du S, Erickson L, Bowley S. Effect of plant genotype on the transformation of cultivated alfalfa (*Medicago sativa*) by *Agrobacterium tumefaciens*. *Plant Cell Rep* 1994; 13: 330 – 334.

Dudits D, Bögre L, Györgyey J. Molecular and cellular approaches to the analysis of plant embryo development from somatic cells *in vitro*. *J Cell Sci* 1991; 99: 475 – 484.

Dunsch AK, Hammond D, Lloyd J, Schermelleh L, Gruneberg U, Barr FA. Dynein light chain 1 and a spindle-associated adaptor promote dynein asymmetry and spindle orientation. *J Cell Biol* 2012; 198: 1039 – 1054.

Erickson HP. Evolution of the cytoskeleton. *BioEssays* 2007; 29: 668 – 677.

Fache V, Gaillard J, Van Damme D, Geelen D, Neumann E, Stoppin-Mellet V, Vantard M. Arabidopsis kinetochore fiber-associated MAP65-4 cross-links microtubules and promotes microtubule bundle elongation. *Plant Cell* 2010; 22: 3804 – 3815.

Fowler JE, Quatrano RS. Plant cell morphogenesis: plasma membrane interactions with the cytoskeleton and cell wall. *Annu Rev Cell Dev Biol* 1997; 13: 697 – 743.

Gage DJ, Bobo T, Long SR. Use of green fluorescent protein to visualize the early events of symbiosis between *Rhizobium meliloti* and alfalfa (*Medicago sativa*). *J Bacteriol* 1996; 178: 7159 – 7166.

Gaillard J, Neumann E, Van Damme D, Stoppin-Mellet V, Ebel C, Barbier E, Geelen D, Vantard M. Two microtubule-associated proteins of Arabidopsis MAP65s promote antiparallel microtubule bundling. *Mol Biol Cell* 2008; 19: 4534 – 4544.

Gavin RH. Microtubule-microfilament synergy in the cytoskeleton. *Int Rev Cytol* 1997; 173: 207 – 242.

Goddard RH, Wick SM, Silflow CD, Snustad DP. Microtubule components of the plant cell cytoskeleton. *Plant Physiol* 1994; 104: 1 – 6.

Goode BL, Drubin DG, Barnes G. Functional cooperation between the mikrotubule and actin cytockeletons. *Curr Opin Cell Biol* 2000; 12: 63 – 71.

Granger CL, Cyr RJ. Microtubule reorganization in tobacco BY-2 cells stably expressing GFP-MBD. *Planta* 2000; 210: 502 – 509.

Gruss OJ, Carazo-Salas RE, Schatz CA, Guarguaglini G, Kast J, Wilm M, Le Bot N, Vernos I, Karsenti E, Mattaj IW. Ran induces spindle assembly by reversing the inhibitory effect of importin alpha on TPX2 activity. *Cell* 2001; 104: 83 – 93.

Gunawardane RN, Lizarraga SB, Wiese C, Wilde A, Zheng Y. γ-Tubulin complexes and their role in microtubule nucleation. *Curr Top Dev Biol* 2000; 49: 55 – 73.

Gunning BE, Hardham AR, Hughes JE. Pre-prophase bands of microtubules in all categories of formative and proliferative cell division in *Azolla* roots. *Planta* 1978; 143: 145 – 160.

Hall Q, Cannon MC. The cell wall hydroxyproline-rich glycoprotein RSH is essential for normal embryo development in Arabidopsis. *Plant Cell* 2002; 14: 1161 – 1172.

Hamada T, Igarashi H, Itoh TJ, Shimmen T, Sonobe S. Characterization of a 200 kDa microtubule-associated protein of tobacco BY-2 cells, a member of the XMAP215/MOR1 family. *Plant Cell Physiol* 2004; 45: 1233 – 1242.

Hamada T. Microtubule-associated proteins in higher plants. *J Plant Res* 2007; 120: 79 – 98.

Hasezawa S, Ueda K, Kumagai F. Time-sequence observations of microtubule dynamics throughout mitosis in living cell suspensions of stable transgenic Arabidopsis--direct evidence for the origin of cortical microtubules at M/G1 interface. *Plant Cell Physiol* 2000; 41: 244 – 250.

Hashimoto T. Microtubules in plants. *Arabidopsis Book* 2015; 13: e0179.

Heese M, Gansel X, Sticher L, Wick P, Grebe M, Granier F, Jürgens G. Functional characterization of the KNOLLE-interacting t-SNARE AtSNAP33 and its role in plant cytokinesis. *J Cell Biol* 2001; 155: 239 – 250.

Hemerly A, Engler JA, Bergounioux C, Van Montagu M, Engler G, Inzé D, Ferreira P. Dominant negative mutants of the Cdc2 kinase uncouple cell division from iterative plant development. *EMBO J* 1995; 14: 3925 – 3936.

Henderson IR, Jacobsen SE. Epigenetic inheritance in plants. *Nature* 2007; 447: 418 – 424.

Hepler PK, Vidali L, Cheung AY. Polarized cell growth in higher plants. *Annu Rev Cell Dev Biol* 2001; 17: 159 – 187.

Hernandéz-Fernandéz MM, Christie BR. Inheritance of somatic embryogenesis in alfalfa (*Medicago sativa* L.). *Genome* 1989; 32: 318 – 321.

Hindson S, McElroy AR, Portelance C. Media and genotype effects on the development and conversion of somatic alfalfa (*Medicago sativa* L.) embryos. *In Vitro Cell Dev Biol Plant* 1998; 34: 181 – 184.

Ho CM, Hotta T, Guo F, Roberson RW, Lee YR, Liu B. Interaction of antiparallel microtubules in the phragmoplast is mediated by the microtubule-associated protein MAP65-3 in Arabidopsis. *Plant Cell* 2011a; 23: 2909 – 2923.

Ho CM, Hotta T, Kong Z, Zeng CJ, Sun J, Lee YR, Liu B. Augmin plays a critical role in organizing the spindle and phragmoplast microtubule arrays in *Arabidopsis*. *Plant Cell* 2011b; 23: 2606 – 2618.

Ho CM, Lee YR, Kiyama LD, Dinesh-Kumar SP, Liu B. *Arabidopsis* microtubule-associated protein MAP65-3 cross-links antiparallel microtubules toward their plus ends in the phragmoplast via its distinct C-terminal microtubule binding domain. *Plant Cell* 2012; 24: 2071 – 2085.

Hong W, Deng W, Xie J. The structure, function, and regulation of *Mycobacterium* FtsZ. *Cell Biochem Biophys* 2013; 65: 97 – 105.

Hoori F, Ehsanpour AA, Mostajeran A. Comparison of somatic embryogenesis in *Medicago sativa* and *Medicago truncatula*. *Pak J Biol Sci* 2007; 10: 481 – 485.

Hotta T, Kong Z, Ho CM, Zeng CJ, Horio T, Fong S, Vuong T, Lee YR, Liu B. Characterization of the Arabidopsis augmin complex uncovers its critical function in the assembly of the acentrosomal spindle and phragmoplast microtubule arrays. *Plant Cell* 2012; 24: 1494 – 1509.

Hu X, Zhang CR, Xie H, Huang X, Chen YF, Huang XL. The expression of a new HD-Zip II gene, *MSHB1*, involving the inhibitory effect of thidiazuron on somatic embryogenic competence in alfalfa (*Medicago sativa* L. cv. Jinnan) callus. *Acta Physiol Plant* 2012; 34: 1067 – 1074.

Huff J. The Airyscan detector from Zeiss: confocal imaging with improved signal-to-noise ratio and super-resolution. *Nat Methods* 2015; 12.

Hush JM, Wadsworth P, Callaham DA, Hepler PK. Quantification of microtubule dynamics in living plant cells using fluorescence redistribution after photobleaching. *J Cell Sci* 1994; 107: 775 – 784.

Hyman AA, Chrétien D, Arnal I, Wade RH. Structural changes accompanying GTP hydrolysis in microtubules: information from a slowly hydrolyzable analogue guanylyl-(alpha,beta)-methylene-diphosphonate. *J Cell Biol* 1995; 128: 117 – 125.

Ichikawa T, Nakazato K, Keller PJ, Kajiura-Kobayashi H, Stelzer EH, Mochizuki A, Nonaka S. Live imaging and quantitative analysis of gastrulation in mouse embryos using light-sheet microscopy and 3D tracking tools. *Nat Protoc* 201; 9: 575 – 585.

Janski N, Masoud K, Batzenschlager M, Herzog E, Evrard JL, Houlné G, Bourge M, Chabouté ME, Schmita AC. The GCP3-Interacting Proteins GIP1 and GIP2 are required for γ-tubulin complex protein localization, spindle integrity and chromosomal stability. *Plant Cell* 2012; 24: 1171 – 1187.

Jorgensen P, Tyers M. How cells coordinate growth and division. *Curr Biol* 2004; 14: 1014 – 1027.

Joubès J, Chevalier C, Dudits D, Heberle-Bors E, Inzé D, Umeda M, Renaudin JP. CDK-related protein kinases in plants. *Plant Mol Biol* 2000; 43: 607 – 620.

Kao KN, Michayluk MR. Embryoid formation in alfalfa cell suspension cultures from different plants. *In Vitro Cell Dev Biol Plant* 1981; 17: 645 – 648.

Kao KN, Michayluk MR. Plant regeneration from mesophyll protoplasts of alfalfa. *Z Pflanzenphysiol* 1980; 96: 135 – 141.

Kao YL, Deavours BE, Phelps KK, Walker RA, Reddy ASN. Bundling of microtubules by motor and tail domains of a kinesin-like calmodulin-binding protein from *Arabidopsis*: Regulation by Ca2+/calmodulin. *Biochem Biophys Res Commun* 2000; 267: 201 – 207.

Karimi M, Bleys A, Vanderhaeghen R, Hilson P. Building blocks for plant gene assembly. *Plant Physiol* 2007; 145: 1183 – 1191.

Katsuta J, Hashiguchi Y, Shibaoka H. The role of the cytoskeleton in positioning of the nucleus in premitotic tobacco BY-2 cells. *J Cell Sci* 1990; 95: 413 – 422.

Katsuta J, Shibaoka H. The roles of the cytoskeleton and the cell wall in nuclear positioning in tobacco BY-2 cells. *Plant Cell Physiol* 1988; 29: 403 – 413.

Kawamura E, Himmelspach R, Rashbrooke MC, Whittington AT, Gale KR, Collings DA, Wasteneys GO. MICROTUBULE ORGANIZATION 1 regulates structure and function of microtubule arrays during mitosis and cytokinesis in the Arabidopsis root. *Plant Physiol* 2006; 140: 102 – 114.

Kawamura E, Wasteneys GO. MOR1, the *Arabidopsis thaliana* homologue of Xenopus MAP215, promotes rapid growth and shrinkage, and suppresses the pausing of microtubules in vivo. *J Cell Sci* 2008; 121: 4114 – 4123.

Ketelaar T. The actin cytoskeleton in root hairs: all is fine at the tip. *Curr Opin Plant Biol* 2013; 16: 749 – 756.

Kielly GA, Bowley SR. Genetic control of somatic embryogenesis in alfalfa. *Genome* 1992; 35: 474 – 477.

Kikkawa M. Big steps toward understanding dynein. *J Cell Biol* 2013; 202: 15 – 23.

Kilmartin JV (2014). Lessons from yeast: the spindle pole body and the centrosome. *Philos Trans R Soc Lond B Biol Sci* 2014; 369: 20130456.

Kimata Y, Higaki T, Kawashima T, Kurihara D, Sato Y, Yamada T, Hasezawa S, Berger F, Higashiyama T, Ueda M. Cytoskeleton dynamics control the first asymmetric cell division in *Arabidopsis* zygote. *Proc Natl Acad Sci USA* 2016; 113: 14157-14162.

Kirik A, Ehrhardt DW, Kirik V. *TONNEAU2/FASS* regulates the geometry of microtubule nucleation and cortical array organization in interphase Arabidopsis cells. *Plant Cell* 2012; 24: 1158 – 1170.

Kirik V, Herrmann U, Parupalli C, Sedbrook JC, Ehrhardt DW, Hülskamp M. CLASP localizes in two discrete patterns on cortical microtubules and is required for cell morphogenesis and cell division in Arabidopsis. *J Cell Sci* 2007; 120: 4416 – 4425.

Kirschner GK, Stahl Y, Von Korff M, Simon R. Unique and conserved features of the barley root meristem. *Front Plant Sci* 2017; 8:1240. doi: 10.3389/fpls.2017.01240.

Klotz J, Nick P. A novel actin-microtubule cross-linking kinesin, NtKCH, functions in cell expansion and division. *New Phytol* 2012; 193: 576 – 589.

Kojo KH, Higaki T, Kutsuna N, Yoshida Y, Yasuhara H, Hasezawa S. Roles of cortical actin microfilament patterning in division plane orientation in plants. *Plant Cell Physiol* 2013; 54: 1491 – 1503.

Kojo KH, Yasuhara H, Hasezawa S. Time-sequential observation of spindle and phragmoplast orientation in BY-2 cells with altered cortical actin microfilament patterning. *Plant Signal Behav* 2014; 9: e29579.

Komaki S, Abe T, Coutuer S, Inzé D, Russinova E, Hashimoto T. Nuclear-localized subtype of end-binding 1 protein regulates spindle organization in Arabidopsis. *J Cell Sci* 2010; 123: 451 – 459.

Komis G, Luptovciak I, Doskocilova A, Samaj J. Biotechnological aspects of cytoskeletal regulation in plants. *Biotechnol Adv* 2015; 33: 1043 – 1062.

Komis G, Luptovčiak I, Ovečka M, Samakovli D, Šamajová O, Šamaj J. Katanin effects on dynamics of cortical microtubules and mitotic arrays in *Arabidopsis thaliana* revealed by advanced live-cell imaging. *Front Plant Sci* 2017; 8: 866.

Komis G, Mistrik M, Šamajová O, Doskočilová A, Ovečka M, Illés P, Bartek J, Šamaj J. Dynamics and organization of cortical microtubules as revealed by superresolution structured illumination microscopy. *Plant Physiol* 2014; 165: 129 – 148.

Kong Z, Hotta T, Lee YR, Horio T, Liu B. The γ- tubulin complex protein GCP4 is required for organizing functional microtubule arrays in *Arabidopsis thaliana*. *Plant Cell* 2010; 22: 191 – 204.

Kosetsu K, Matsunaga S, Nakagami H, Colcombet J, Sasabe M, Soyano T, Takahashi Y, Hirt H, Machida Y. The MAP kinase MPK4 is required for cytokinesis in *Arabidopsis thaliana*. *Plant Cell* 2010; 22: 3778 – 3790.

Kropf DL, Bisgrove SR, Hable WE. Cytoskeletal control of polar growth in plant cells. *Curr Opin Cell Biol* 1998; 10: 117 – 122.

Krysan PJ, Jester PJ, Gottwald JR, Sussman MR. An Arabidopsis mitogen-activated protein kinase kinase kinase gene family encodes essential positive regulators of cytokinesis. *Plant Cell* 2002; 14: 1109 – 1120.

Kuchuk N, Komarnitski I, Shakhovsky A, Gleba Y. Genetic transformation of *Medicago* species by *Agrobacterium tumefaciens* and electroporation of protoplasts. *Plant Cell Rep* 1990; 8: 660 – 663.

Lai FM, McKersie BD. Regulation of starch and protein accumulation in alfalfa (*Medicago sativa* L.) somatic embryos. *Plant Sci* 1994a; 100: 211 – 219.

Lai FM, McKersie BD. Regulation of storage protein synthesis by nitrogen and sulfur nutrients in alfalfa (*Medicago sativa* L.) somatic embryos. *Plant Sci* 1994b; 103: 209 – 221.

Laissue PP, Alghamdi RA, Tomancak P, Reynaud EG, Shroff H. Assessing phototoxicity in live fluorescence imaging. *Nat Methods* 2017; 14: 657 – 661.

Larkin P. Somaclonal variation: history, method and meaning. *Iowa State J Res* 1987; 61: 393 – 434.

Lauber MH, Waizenegger I, Steinmann T, Schwarz H, Mayer U, Hwang I, Lukowitz W, Jürgens G. The Arabidopsis KNOLLE protein is a cytokinesis-specific syntaxin. *J Cell Biol* 1997; 139: 1485 – 1493.

Lavrekha VV, Pasternak T, Ivanov VB, Palme K, Mironova VV. 3D analysis of mitosis distribution highlights the longitudinal zonation and diarch symmetry in proliferation activity of the *Arabidopsis thaliana* root meristem. *Plant J* 2017; 92: 834 – 845.

Ledbetter MC, Porter KR. Morphology of microtubules of plant cells. *Science* 1964; 144: 872 – 874.

Lee YR, Li Y, Liu B. Two Arabidopsis phragmoplast-associated kinesins play a critical role in cytokinesis during male gametogenesis. *Plant Cell* 2007; 19: 2595 – 2605.

Lee YR, Liu B. The rise and fall of the phragmoplast microtubule array. *Curr Opin Plant Biol* 2013; 16: 757 – 763.

Li H, Sun B, Sasabe M, Deng X, Machida Y, Lin H, Julie Lee YR, Liu B. Arabidopsis MAP65-4 plays a role in phragmoplast microtubule organization and marks the cortical cell division site. *New Phytol* 2017; 215: 187 – 201.

Li R, Gundersen GG. Beyond polymer polarity: how the cytoskeleton builds a polarized cell. *Nat Rev Mol Cell Biol* 2008; 9: 860 – 873.

Li Y, Shen Y, Cai C, Zhong C, Zhu L, Yuan M, Ren H. The type II Arabidopsis formin14 interacts with microtubules and microfilaments to regulate cell division. *Plant Cell* 2010; 22: 2710 – 2726.

Limpens E, Franken C, Smit P, Willemse J, Bisseling T, Geurts R. LysM domain receptor kinases regulating Rhizobial Nod factor-induced infection. *Science* 2003; 302: 630 – 633.

Lindeboom JJ, Nakamura M, Hibbel A, Shundyak K, Gutierrez R, Ketelaar T, Emons AM, Mulder BM, Kirik V, Ehrhardt DW. A mechanism for reorientation of cortical microtubule arrays driven by microtubule severing. *Science* 2013; 342: 1245533. doi: 10.1126/science.1245533.

Lipka E, Gadeyne A, Stöckle D, Zimmermann S, De Jaeger G, Ehrhardt DW, Kirik V, Van Damme D, Müller S. The Phragmoplast-orienting kinesin-12 class proteins translate the positional information of the preprophase band to establish the cortical division zone in *Arabidopsis thaliana*. *Plant Cell* 2014; 26: 2617 – 2632.

Litz RE, Gray DJ. Somatic embryogenesis for agricultural improvement. *World J Microbiol Biotechnol* 1995; 11: 416 – 425.

Liu B, Hotta T, Ho CMK, Lee YRJ. Microtubule organization in the phragmoplast. *Plant Cytoskeleton* 2011; 2: 207 – 225.

Lu DY, Davey MR, Cocking EC. A comparison of the cultural behaviour of protoplasts from leaves, cotyledons and roots of *Medicago sativa*. *Plant Sci Lett* 1983; 31: 87 – 99.

Lucas JR, Courtney S, Hassfurder M, Dhingra S, Bryant A, Shaw SL. Microtubule-associated proteins MAP65-1 and MAP65-2 positively regulate axial cell growth in etiolated Arabidopsis hypocotyls. *Plant Cell* 2011; 23: 1889 – 1903.

Lucas JR, Shaw SL. MAP65-1 and MAP65-2 promote cell proliferation and axial growth in Arabidopsis roots. *Plant J* 2012; 71: 454 – 463.

Lucas M, Kenobi K, von Wangenheim D, Voβ U, Swarup K, De Smet I, Van Damme D, Lawrence T, Péret B, Moscardi E, Barbeau D, Godin C, Salt D, Guyomarc'h S, Stelzer EH, Maizel A, Laplaze L, Bennett MJ. Lateral root morphogenesis is dependent on the mechanical properties of the overlaying tissues. *Proc Natl Acad Sci USA* 2013; 110: 5229 – 5234.

Lukowitz W, Roeder A, Parmenter D, Somerville C. A MAPKK kinase gene regulates extra-embryonic cell fate in Arabidopsis. *Cell* 2004; 116: 109 – 119.

Luptovčiak I, Komis G, Takáč T, Ovečka M, Šamaj J. Katanin: A sword cutting microtubules for cellular, developmental and physiological purposes. *Front Plant Sci* 2017; 8:1982.

Maiato H, Sampaio P, Sunkel CE. Microtubule-associated proteins and their essential roles during mitosis. *Int Rev Cytol* 2004; 241: 53 – 153.

Maizel A, von Wangenheim D, Federici F, Haseloff J, Stelzer EH. High-resolution live imaging of plant growth in near physiological bright conditions using light sheet fluorescence microscopy. *Plant J* 2011; 68: 377 – 385.

Mandelkow EM, Mandelkow E, Milligan RA. Microtubule dynamics and microtubule caps: a time-resolved cryo-electron microscopy study. *J Cell Biol* 1991; 114: 977 – 991.

Mao G, Chan J, Calder G, Doonan JH, Lloyd CW. Modulated targeting of GFP-AtMAP65-1 to central spindle microtubules during division. *Plant J* 2005; 43: 469 – 478.

Marc J, Granger CL, Brincat J, Fisher DD, Kao TH, McCubbin AG, Cyr RJ. A *GFP-MAP4* reporter gene for visualizing cortical microtubule rearrangements in living epidermal cells. *Plant Cell* 1998; 10: 1927-1939.

Marcus AI, Dixit R, Cyr RJ. Narrowing of the preprophase microtubule band is not required for cell division plane determination in cultured plant cells. *Protoplasma* 2005; 226: 169 – 174.

Marcus AI, Li W, Ma H, Cyr RJ. A kinesin mutant with an atypical bipolar spindle undergoes normal mitosis. *Mol Biol Cell* 2003; 14: 1717 – 1726.

McClinton RS, Chandler JS, Callis J. cDNA isolation, characterization, and protein intracellular localization of a katanin-like p60 subunit from *Arabidopsis thaliana*. *Protoplasma* 2001; 216: 181 – 190.

McClinton RS, Sung ZR. Organization of cortical microtubules at the plasma membrane in Arabidopsis. *Planta* 1997; 201: 252 – 260.

McCurdy DW, Kovar DR, Staiger CJ. Actin and actin-binding proteins in higher plants. *Protoplasma* 2001; 215: 89 – 104.

McDonald HB, Stewart RJ, Goldstein LS. The kinesin-like *ncd* protein of Drosophila is a minus end-directed microtubule motor. *Cell* 1990; 63: 1159 – 1165.

Meagher RB, Williamson RE. The plant cytoskeleton. In: Arabidopsis. Meyerowitz E, Somerville C (eds). Cold Spring Harbor Laboratory Press, Cold Spring Harbor, NY, 1994, 1049 – 1084.

Mészáros T, Miskolczi P, Ayaydin F, Pettkó-Szandtner A, Peres A, Magyar Z, Horváth GV, Bakó L, Fehér A, Dudits D. Multiple cyclin-dependent kinase complexes and phosphatases control G2/M progression in alfalfa cells. *Plant Mol Biol* 2000; 43: 595 – 605.

Mimori-Kiyosue Y, Grigoriev I, Lansbergen G, Sasaki H, Matsui C, Severin F, Galjart N, Grosveld F, Vorobjev I, Tsukita S, Akhmanova A. CLASP1 and CLASP2 bind to EB1 and regulate microtubule plus-end dynamics at the cell cortex. *J Cell Biol* 2005; 168: 141 – 153.

Mitten DH, Sato SJ, Skokut TA. In vitro regenerative potential of alfalfa germplasm sources. *Crop Sci* 1983; 24: 943 – 954.

Moschou PN, Smertenko AP, Minina EA, Fukada K, Savenkov EI, Robert S, Hussey PJ, Bozhkov PV. The caspase-related protease separase (extra spindle poles) regulates cell polarity and cytokinesis in Arabidopsis. *Plant Cell* 2013; 25: 2171 – 2186.

Müller J, Beck M, Mettbach U, Komis G, Hause G, Menzel D, Samaj J. Arabidopsis MPK6 is involved in cell division plane control during early root development, and localizes to the pre-prophase band, phragmoplast, trans-Golgi network and plasma membrane. *Plant J* 2010; 61: 234 – 248.

Müller S, Fuchs E, Ovecka M, Wysocka-Diller J, Benfey PN, Hauser MT. Two new loci, PLEIADE and HYADE, implicate organ-specific regulation of cytokinesis in Arabidopsis. *Plant Physiol* 2002; 130: 312 – 324.

Müller S, Han S, Smith LG. Two kinesins are involved in the spatial control of cytokinesis in *Arabidopsis thaliana*. *Curr Biol* 2006; 16: 888 – 894.

Müller S, Smertenko A, Wagner V, Heinrich M, Hussey PJ, Hauser MT. The plant microtubule-associated protein AtMAP65-3/PLE is essential for cytokinetic phragmoplast function. *Curr Biol* 2004; 14: 412 – 417.

Murata T, Hasebe M. Microtubule-dependent microtubule nucleation in plant cells. *J Plant Res* 2007; 120: 73 – 78.

Murata T, Sano T, Sasabe M, Nonaka S, Higashiyama T, Hasezawa S, Machida Y, Hasebe M. Mechanism of microtubule array expansion in the cytokinetic phragmoplast. *Nat Commun* 2013; 4: 1967.

Murata T, Sonobe S, Baskin TI, Hyodo S, Hasezawa S, Nagata T, Horio T, Hasebe M. Microtubule-dependent microtubule nucleation based on recruitment of γ-tubulin in higher plants. *Nat Cell Biol* 2005; 7: 961 – 968.

Nakamura M, Ehrhardt DW, Hashimoto T. Microtubule and katanin-dependent dynamics of microtubule nucleation complexes in the acentrosomal Arabidopsis cortical array. *Nat Cell Biol* 2010; 12: 1064 – 1070.

Ni J, Shen Y, Zhang Y, Wu P. Definition and stabilisation of the quiescent centre in rice roots. *Plant Biol* 2014; 16: 1014 – 1019.

Nichol JW, Slade D, Viss P, Stuart DA. Effect of organic acid pretreatment on the regeneration and development (conversion) of whole plants from callus cultures of alfalfa, *Medicago sativa* L. *Plant Sci* 1991; 79: 181 – 192.

Nick P. Signals, motors, morphogenesis: the cytoskeleton in plant development. *Plant Biol* 1999; 1: 169 – 179.

Nogami A, Mineyuki Y. Loosening of a preprophase band of microtubules in onion (Allium cepa L.) root tip cells by kinase inhibitors. *Cell Struct Funct* 1999; 24: 419 – 424.

Novák D, Kuchařová A, Ovečka M, Komis G, Šamaj J. Developmental nuclear localization and quantification of GFP-tagged EB1c in Arabidopsis root using light-sheet microscopy. *Front Plant Sci* 2016; 6: 1187. doi: 10.3389/fpls.2015.01187.

Novák D, Vadovič P, Ovečka M, Šamajová O, Komis G, Colcombet J, Šamaj J. Gene expression pattern and protein localization of Arabidopsis phospholipase D alpha 1 revealed by ddvanced light-sheet and super-resolution microscopy. *Front Plant Sci* 2018; 9: 371. doi: 10.3389/fpls.2018.00371.wu

Novák FJ, Konečná D. Somatic embryogenesis in callus and cell suspension cultures of alfalfa (*Medicago sativa* L.). *Z Pflanzenphysiol* 1982; 105: 279 – 284.

Oakley BR, Oakley CE, Yoon Y, Jung MK. Gamma-tubulin is a component of the spindle pole body that is essential for microtubule function in *Aspergillus nidulans*. *Cell* 1990; 61: 1289 – 1301.

Oh SA, Allen T, Kim GJ, Sidorova A, Borg M, Park SK, Twell D. Arabidopsis Fused kinase and the kinesin-12 subfamily constitute a signalling module required for phragmoplast expansion. *Plant J* 2012; 72: 308 – 319.

Oh SA, Johnson A, Smertenko A, Rahman D, Park SK, Hussey PJ, Twell D. A divergent cellular role for the FUSED kinase family in the plant-specific cytokinetic phragmoplast. *Curr Biol* 2005; 15: 2107 – 2111.

Otegui M, Staehelin LA. Cytokinesis in flowering plants: more than one way to divide a cell. *Curr Opin Plant Biol* 2000; 3: 493–502.

Ovečka M, Vaškebová L, Komis G, Luptovčiak I, Smertenko A, Šamaj J. Preparation of plants for developmental and cellular imaging by light-sheet microscopy. *Nat Protoc* 2015; 10: 1234 – 1247.

Paluh JL, Nogales E, Oakley BR, McDonald K, Pidoux AL, Cande WZ. A mutation in γ-tubulin alters microtubule dynamics and organization and is synthetically lethal with the kinesin-like protein pkl1p. *Mol Biol Cell* 2000; 11: 1225 – 1239.

Panteris E, Adamakis ID, Voulgari G, Papadopoulou G. A role for katanin in plant cell division: microtubule organization in dividing root cells of *fra2* and *lue1 Arabidopsis thaliana* mutants. *Cytoskeleton* 2011; 68: 401 – 413.

Panteris E, Adamakis ID. Aberrant microtubule organization in dividing root cells of p60-katanin mutants. *Plant Signal Behav* 2012; 7: 16 – 18.

Panteris E, Apostolakos P, Galatis B. The effect of taxol on Triticum preprophase root cells: preprophase microtubule band organization seems to depend on new microtubule assembly. *Protoplasma* 1995; 186: 72 – 78.

Paredez AR, Somerville CR, Ehrhardt DW. Visualization of cellulose synthase demonstrates functional association with microtubules. *Science* 2006; 312: 1491 – 1495.

Park GT, Frost JM, Park JS, Kim TH, Lee JS, Oh SA, Twell D, Brooks JS, Fischer RL, Choi Y. Nucleoporin MOS7/Nup88 is required for mitosis in gametogenesis and seed development in Arabidopsis. *Proc Natl Acad Sci USA* 2014; 111: 18393 – 18398.

Pasternak T, Haser T, Falk T, Ronneberger O, Palme K, Otten L. A 3D digital atlas of the *Nicotiana tabacum* root tip and its use to investigate changes in the root apical meristem induced by the Agrobacterium 6b oncogene. *Plant J* 2017; 92: 31 – 42.

Pastuglia M, Azimzadeh J, Goussot M, Camilleri C, Belcram K, Evrard JL, Schmit AC, Guerche P, Bouchez D. γ-Tubulin is essential for microtubule organization and development in Arabidopsis. *Plant Cell* 2006; 18: 1412 – 1425.

Pereira LF, Erickson L. Stable transformation of alfalfa (*Medicago sativa* L.) by particle bombardment. *Plant Cell Rep* 1995; 14: 290 – 293.

Pickett-Heaps JD, Northcote DH. Organization of microtubules and endoplasmic reticulum during mitosis and cytokinesis in wheat meristems. *J Cell Sci* 1966; 1: 109 – 120.

Pietra S, Gustavsson A, Kiefer C, Kalmbach L, Hörstedt P, Ikeda Y, Stepanova AN, Alonso JM, Grebe M. Arabidopsis SABRE and CLASP interact to stabilize cell division plane orientation and planar polarity. *Nat Commun* 2013; 4: 2779.

Pietzsch T, Saalfeld S, Preibisch S, Tomancak P. BigDataViewer: visualization and processing for large image data sets. *Nat Methods* 2016; 12: 481 – 483.

Pignocchi C, Minns GE, Nesi N, Koumproglou R, Kitsios G, Benning C, Lloyd CW, Doonan JH, Hills MJ. ENDOSPERM DEFECTIVE1 Is a Novel Microtubule-Associated Protein Essential for Seed Development in Arabidopsis. *Plant Cell* 2009; 21: 90 – 105.

Prosser SL, Pelletier L. Mitotic spindle assembly in animal cells: a fine balancing act. *Nat Rev Mol Cell Biol* 2017; 18: 187 – 201.

Qi R, John PCL. Expression of genomic AtCYCD2;1 in Arabidopsis induces cell division at smaller cell sizes: Implications for the control of plant growth. *Plant Physiol* 2007; 144: 1587 – 1597.

Radović J, Sokolović D, Marković J. Alfalfa – most important perennial forage legume in animal husbandry. *Biotechnol Anim Husb* 2009; 25: 465 - 475.

Rai MK, Akhtar N, Jaiswal VS. Somatic embryogenesis and plant regeneration in *Psidium guajava* L. cv. Banarasi local. *Sci Hortic* 2007; 113: 129 – 133.

Ramaiah SM, Skinner DZ. Particle bombardment: A simple and efficient method of alfalfa (*Medicago sativa* L.) pollen transformation. *Curr Sci* 1997; 73: 674 – 682.

Rashmi R, Sarkar M, Vikramaditya. Cultivaton of alfalfa (*Medicago sativa* L.). *Anc Sci Life* 1997; 17: 117 – 119.

Rasmussen CG, Humphries JA, Smith LG. Determination of symmetric and asymmetric division planes in plant cells. *Annu Rev Plant Biol* 2011; 62: 387 – 409.

Rasmussen CG, Wright AJ, Muller S. The role of the cytoskeleton and associated proteins in determination of the plant cell division plane. *Plant J* 2013, 75: 258 – 269.

Raynaud-Messina B, Merdes A. γ-tubulin complexes and microtubule organization. *Curr Opin Cell Biol* 2007; 19: 24 – 30.

Rebouillat J, Dievart A, Verdeil JL, Escoute J, Giese G, Breitler JC, Gantet P, Espeout S, Guiderdoni E, Périn C. Molecular genetics of rice root development. *Rice* 2009; 2: 15 – 34.

Reisch B, Bingham ET. The genetic control of bud formation from callus cultures of diploid alfalfa. *Plant Sci Lett* 1980; 20: 71 – 77.

Ren H, Xiang Y. The function of actin-binding proteins in pollen tube growth. *Protoplasma* 2007; 230: 171 – 182.

Rice LM, Montabana EA, Agard DA. The lattice as allosteric effector: structural studies of alphabeta- and gamma-tubulin clarify the role of GTP in microtubule assembly. *Proc Natl Acad Sci USA* 2008; 105: 5378 – 5383.

Rosero A, Oulehlová D, Stillerová L, Schiebertová P, Grunt M, Žárský V, Cvrčková F. Arabidopsis FH1 formin affects cotyledon pavement cell shape by modulating cytoskeleton dynamics. *Plant Cell Physiol* 2016; 57: 488 – 504.

Rosquete MR, von Wangenheim D, Marhavý P, Barbez E, Stelzer EH, Benková E, Maizel A, Kleine-Vehn J. An auxin transport mechanism restricts positive orthogravitropism in lateral roots. *Curr Biol* 2013; 23: 817 – 822.

Rybak K, Steiner A, Synek L, Klaeger S, Kulich I, Facher E, Wanner G, Kuster B, Zarsky V, Persson S, Assaad FF. Plant cytokinesis is orchestrated by the sequential action of the TRAPPII and exocyst tethering complexes. *Dev Cell* 2014; 29: 607 – 620.

Sabelli PA, Larkins BA. The Development of endosperm in grasses. *Plant Physiol* 2009; 149: 14 – 26.

Sablin EP, Case RB, Dai SC, Hart CL, Ruby A, Vale RD, Fletterick RJ. Direction determination in the minus-end-directed kinesin motor ncd. *Nature* 1998; 395: 813 – 816.

Sacks MM, Silk WK, Burman P. Effect of water stress on cortical cell division rates within the apical meristem of primary roots of maize. *Plant Physiol* 1997; 114: 519 – 527.

Samac DA, Austin-Phillips S. Alfalfa (*Medicago sativa L.*). *Methods Mol Biol* 2006; 343: 301 – 311.

Samac DA, Temple SJ. Development and utilization of transformation in *Medicago* species. In Genetically modified crops. Their development, uses and risks. Editors Liang GH, Skinner DZ. The Haworth Press, NY, 2004, 165 – 202.

Samac DA. Strain specificity in transformation of alfalfa by *Agrobacterium tumefaciens*. *Plant Cell Tissue Organ Cult* 1995; 43: 271 – 277.

Šamaj J, Baluška F, Voigt B, Schlicht M, Volkmann D, Menzel D. Endocytosis, actin cytoskeleton and signaling. *Plant Physiol* 2004; 135: 1150 – 1161.

Šamaj J, Ovečka M, Hlavacka A, Lecourieux F, Meskiene I, Lichtscheidl I, Lenart P, Salaj J, Volkmann D, Bögre L, Baluška F, Hirt H. Involvement of the mitogen-activated protein kinase SIMK in regulation of root hair tip growth. *EMBO J* 2002; 21: 3296 – 3306.

Šamaj J, Ovečka M, Hlavacka A, Lecourieux F, Meskiene I, Lichtscheidl I, Lenart P, Salaj J, Volkmann D, Bögre L, Baluška F, Hirt H. Involvement of MAP kinase SIMK and actin cytoskeleton in the regulation of root hair tip growth. *Cell Biol Int* 2003; 27: 257 – 259.

Sampathkumar A, Lindeboom JJ, Debolt S, Gutierrez R, Ehrhardt DW, Ketelaar T, Persson S. Live cell imaging reveals structural associations between the actin and microtubule cytoskeleton in Arabidopsis. *Plant Cell* 2011; 23: 2302 – 2313.

Samuels AL, Giddings TH Jr, Staehelin LA. Cytokinesis in tobacco BY-2 and root tip cells: a new model of cell plate formation in higher plants. *J Cell Biol* 1995; 130: 1345 – 1357.

Sano T, Higaki T, Oda Y, Hayashi T, Hasezawa S. Appearance of actin microfilament 'twin peaks' in mitosis and their function in cell plate formation, as visualized in tobacco BY-2 cells expressing GFP–fimbrin. *Plant J* 2005; 44: 595 – 605.

Saunders JW, Bingham ET. Growth regulator effects on bud initiation in callus cultures of *Medicago sativa*. *Amer J Bot* 1975; 62: 850 – 855.

Saunders JW, Bingham ET. Production of alfalfa plants from callus tissue. *Crop Sci* 1972; 12: 804 – 808.

Scheres B, Benfey P, Dolan L. Root development. *Arabidopsis Book* 2002; 1: e0101.

Schmidt T, Pasternak T, Liu K, Blein T, Aubry-Hivet D, Dovzhenko A, Duerr J, Teale W, Ditengou FA, Burkhardt H, Ronneberger O, Palme K. The iRoCS Toolbox--3D analysis of the plant root apical meristem at cellular resolution. *Plant J* 2014; 77: 806 – 814.

Schmit AC. Acentrosomal microtubule nucleation in higher plants. *Int Rev Cytol* 2002; 220: 257 – 289.

Seagull RW, Falconer M, Weerdenburg CA. Microfilaments: dynamic arrays in higher plant cells. *J Cell Biol* 1987; 104: 995 – 1004.

Senaratna T, McKersie BD, Bowley SR. Artificial seeds of alfalfa (*Medicago sativa* L.). Induction of desiccation tolerance in somatic embryos. *In Vitro Cell Dev Biol Plant* 1990; 26: 85 – 90.

Senaratna T, McKersie BD, Bowley SR. Deiccation tolerance of alfalfa (*Medicago sativa* L.) somatic embryos. Influence of abscisic acid, stress pretreatments and drying rates. *Plant Sci* 1989; 65: 253 – 259.

Setién I, Fuertes-Mendizabal T, González A, Aparicio-Tejo PM, González-Murua C, González-Moro MB, Estavillo JM. High irradiance improves ammonium tolerance in wheat plants by increasing N assimilation. *J Plant Physiol* 2013; 170: 758 – 771.

Shahin EA, Spielmann A, Sukhapinda K, Simpson RB, Yashar M. Transformation of cultivated alfalfa using disarmed *Agrobacterium tumefaciens*. *Crop Sci* 1986; 26: 1235 – 1239.

Shaw SL, Kamyar R, Ehrhardt DW. Sustained microtubule treadmilling in Arabidopsis cortical arrays. *Science* 2003; 300: 1715 – 1718.

Shaw SL, Lucas J. Intrabundle microtubule dynamics in the Arabidopsis cortical array. *Cytoskeleton* 2011; 68: 56 – 67.

Shetty K, McKersie BD. Proline, thioproline and potassium mediated stimulation of somatic embryogenesis in alfalfa (*Medicago sativa* L.). *Plant Sci* 1993; 88: 185 – 193.

Sieberer BJ, Timmers AC, Emons AM. Nod factors alter the microtubule cytoskeleton in *Medicago truncatula* root hairs to allow root hair reorientation. *Mol Plant Microbe Interact* 2005; 18: 1195 – 1204.

Sieberer BJ, Timmers AC, Lhuissier FG, Emons AM. Endoplasmic microtubules configure the subapical cytoplasm and are required for fast growth of *Medicago truncatula* root hairs. *Plant Physiol* 2002; 130: 977 – 988.

Smékalová V, Luptovčiak I, Komis G, Šamajová O, Ovečka M, Doskočilová A, Takáč T, Vadovič P, Novák O, Pechan T, Ziemann A, Košútová P, Šamaj J. Involvement of YODA and mitogen activated protein kinase 6 in Arabidopsis post-embryogenic root development through auxin up-regulation and cell division plane orientation. *New Phytol* 2014; 203: 1175 – 1193.

Smertenko A, Assaad F, Baluška F, Bezanilla M, Buschmann H, Drakakaki G, Hauser MT, Janson M, Mineyuki Y, Moore I, Müller S, Murata T, Otegui MS, Panteris E, Rasmussen C, Schmit AC, Šamaj J, Samuels L, Staehelin LA, Van Damme D, Wasteneys G, Žárský V. Plant Cytokinesis: Terminology for structures and processes. *Trends Cell Biol* 2017; 27: 885 – 894.

Smertenko A, Bozhkov PV. Somatic embryogenesis: life and death processes during apical-basal patterning. *J Exp Bot* 2014; 65: 1343 – 1360.

Smertenko A, Franklin-Tong VE. Organisation and regulation of the cytoskeleton in plant programmed cell death. *Cell Death Differ* 2011; 18: 1263 – 1270.

Smertenko AP, Chang HY, Sonobe S, Fenyk SI, Weingartner M, Bögre L, Hussey PJ. Control of the AtMAP65-1 interaction with microtubules through the cell cycle. *J Cell Sci* 2006; 119: 3227 – 3237.

Smertenko AP, Chang HY, Wagner V, Kaloriti D, Fenyk S, Sonobe S, Lloyd C, Hauser MT, Hussey PJ. The Arabidopsis microtubule-associated protein AtMAP65-1: molecular analysis of its microtubule bundling activity. *Plant Cell* 2004; 16: 2035 – 2047.

Smith LG. Cytoskeletal control of plant cell shape: getting the fine points. *Curr Opin Cell Biol* 2003; 6: 63 – 73.

Söllner R, Glässer G, Wanner G, Somerville CR, Jürgens G, Assaad FF. Cytokinesis-defective mutants of Arabidopsis. *Plant Physiol* 2002; 129: 678 – 690.

Spinner L, Gadeyne A, Belcram K, Goussot M, Moison M, Duroc Y, Eeckhout D, De Winne N, Schaefer E, Van De Slijke E, Persiau G, Witters E, Gevaert K, De Jaeger G, Bouchez D, Van Damme D, Pastuglia M. A protein phosphatase 2A complex spatially controls plant cell division. *Nat Commun* 2013; 4:1863.

Stehbens S, Pemble H, Murrow L, Wittmann T. Imaging intracellular protein dynamics by spinning disk confocal microscopy. *Methods Enzymol* 2012; 504: 293 – 313.

Steiner A, Rybak K, Altmann M, McFarlane HE, Klaeger S, Nguyen N, Facher E, Ivakov A, Wanner G, Kuster B, Persson S, Braun P, Hauser MT, Assaad FF. Cell cycle-regulated PLEIADE/AtMAP65-3 links membrane and microtubule dynamics during plant cytokinesis. *Plant J* 2016; 88: 531 – 541.

Stelzer EH. Light-sheet fluorescence microscopy for quantitative biology. *Nat Methods* 2015; 12: 23 – 26.

Steward FC, Mapes MO, Mears K. Growth and organized development of cultured cells. II. Organization in cultures grown from freely suspend cells. *Am J Bot* 1958; 45: 705 – 708.

Stöckle D, Herrmann A, Lipka E, Lauster T, Gavidia R, Zimmermann S, Müller S. Putative RopGAPs impact division plane selection and interact with kinesin-12 POK1. *Nat Plants* 2016; 2: 16120. doi: 10.1038/nplants.2016.120.

Stoppin V, Vantard M, Schmit AC, Lambert AM. Isolated plant nuclei nucleate microtubule assembly: the nuclear surface in higher plants has centrosome-like activity. *Plant Cell* 1994; 6: 1099 – 1106.

Strahl H, Burmann F, Hamoen LW. The actin homologue MreB organizes the bacterial cell membrane. *Nat Commun* 2014; 5: 3442.

Strompen G, El Kasmi F, Richter S, Lukowitz W, Assaad FF, Jürgens G, Mayer U. The Arabidopsis *HINKEL* gene encodes a kinesin-related protein involved in cytokinesis and is expressed in a cell cycle-dependent manner. *Curr Biol* 2002; 12: 153 – 158.

Stuart DA, Nelsen J, Nichol JW. Expression of 7S and 11S alfalfa seed storage proteins in somatic embryos. *J Plant Physiol* 1988; 132: 134 – 139.

Suprasanna P, Rao PS. Somatic embryogenesis in crop plants. In: Ramana Rao TV, Kothari IL (eds) Plant structure and morphogenesis. Sardar Patel University, Vallabh Vidyanagar, India, 1997, 29 – 35.

Suzaki T, Yoro E, Kawagucchi. Leguminous plants: Inventors of root nodules to accommodate symbiotic bacteria. *Int Rev Cell Mol Biol* 2015; 316: 111 – 158.

Tabe LM, Wardley-Richardson T, Ceriotti A, Aryan A, McNabb W, Moore A, Higgins TJV. A biotechnological approach to improving the nutritive value of alfalfa. *J Anim Sci* 1995; 73: 2752 – 2759.

Takeuchi M, Karahara I, Kajimura N, Takaoka A, Murata K, Misaki K, Yonemura S, Staehelin LA, Mineyuki Y. Single microfilaments mediate the early steps of microtubule bundling during preprophase band formation in onion cotyledon epidermal cells. *Mol Biol Cell* 2016; 27: 1809–1820.

Tanaka H, Ishikawa M, Kitamura S, Takahashi Y, Soyano T, Machida C, Machida Y. The *AtNACK1/HINKEL* and *STUD/TETRASPORE/AtNACK2* genes, which encode functionally redundant kinesins, are essential for cytokinesis in Arabidopsis. *Genes Cells* 2004; 9: 1199 – 1211.

Tian CF, Garnerone AM, Mathieu-Demaziere C, Masson-Boivin C, Batut J. Plant-activated bacterial receptor adenylate cyclases modulate epidermal infection in Sinorhizobium meliloti – Medicago symbiosis. *Plant Biol* 2012; 17: 6751–6756.

Tilney LG, Bryan J, Bush DJ, Fujiwara K, Mooseker MS, Murphy DB, Snyder DH. Microtubules: evidence for 13 protofilaments. *J Cell Biol* 1973, 59: 267 – 275.

Timmers AC, Vallotton P, Heym C, Menzel D. Microtubule dynamics in root hairs of *Medicago truncatula*. *Eur J Cell Biol* 2007; 86: 69 – 83.

Traas JA, Doonan JH, Rawlins DJ, Shaw PJ, Watts J, Lloyd CW. An actin network is present in the cytoplasm throughout the cell cycle of carrot cells and associates with the dividing nucleus. *J Cell Biol* 1987; 105: 387 – 395.

Trieu AT, Burleigh SH, Kardailsky IV, Maldonado-Mendoza IE, Versaw WK, Blaylock LA, Shin H, Chiou TJ, Katagi H, Dewbre GR, Weigel D, Harrison MJ. Transformation of *Medicago truncatula* via infiltration of seedlings or flowering plants with *Agrobacterium*. *Plant J* 2000; 22: 531 – 541.

Twell D, Park SK, Hawkins TJ, Schubert D, Schmidt R, Smertenko A, Hussey PJ. MOR1/GEM1 has an essential role in the plant-specific cytokinetic phragmoplast. *Nat Cell Biol* 2002; 4: 711 – 714.

Udvardi M, Poole PS. Transport and metabolism in legume-Rhizobia symbioses. *Annu Rev Plant Biol* 2013; 64: 781 – 805.

Vahdati K, Bayat S, Ebrahimzadeh H, Jariteh M, Mirmasoumi M. Effect of exogenous ABA on somatic embryo maturation and germination in Persian walnut (*Juglans regia* L.). *Plant Cell Tissue Organ Cult* 2008; 93: 163 – 171.

Van Damme D, Coutuer S, De Rycke R, Bouget FY, Inzé D, Geelen D. Somatic cytokinesis and pollen maturation in Arabidopsis depend on TPLATE, which has domains similar to coat proteins. *Plant Cell* 2006; 18: 3502 – 3518.

Van Damme D, De Rybel B, Gudesblat G, Demidov D, Grunewald W, De Smet I, Houben A, Beeckman T, Russinova E. Arabidopsis α Aurora kinases function in formative cell division plane orientation. *Plant Cell* 2011; 23: 4013 – 4024.

Van Damme D, Gadeyne A, Vanstraelen M, Inzé D, Van Montagu MC, De Jaeger G, Russinova E, Geelen D. Adaptin-like protein TPLATE and clathrin recruitment during plant somatic cytokinesis occurs via two distinct pathways. *Proc Natl Acad Sci USA* 2011; 108: 615 – 620.

Van Damme D, Van Poucke K, Boutant E, Ritzenthaler C, Inzé D, Geelen D. In vivo dynamics and differential microtubule-binding activities of MAP65 proteins. *Plant Physiol* 2004; 136: 3956 – 3967.

Van Damme D, Vanstraelen M, Geelen D. Cortical division zone establishment in plant cells. *Trends Plant Sci* 2007; 12: 458 – 464.

Van Damme D. Division plane determination during plant somatic cytokinesis. *Curr Opin Plant Biol* 2009; 12: 745 – 751.

Vanstraelen M, Van Damme D, De Rycke R, Mylle E, Inzé D, Geelen D. Cell cycle-dependent targeting of a kinesin at the plasma membrane demarcates the division site in plant cells. *Curr Biol* 2006; 16: 308 – 314.

Vasil IK. Progress in the regeneration and genetic manipulation of cereal crops. *Nat Biotechnol* 1988; 6: 397 – 402.

Vaughan KT. Microtubule plus ends, motors, and traffic of Golgi membranes. *Biochim Biophys Acta* 2005; 1744: 316 – 324.

Vermeer JEM, von Wangenheim D, Barberon M, Lee Y, Stelzer EHK, Maizel A, Geldner N. A spatial accommodation by neighboring cells is required for organ initiation in Arabidopsis. *Science* 2014; 343: 178 – 183.

Vertii A, Hehnly H, Doxsey S. The centrosome, a multitalented renaissance organelle. *Cold Spring Harb Perspect Biol* 2016; 8. pii: a025049.

Vidali L, Hepler PK. Actin and pollen tube growth. *Protoplasma* 2001; 215: 64 – 76.

Voigt B, Timmers ACJ, Šamaj J, Müller J, Baluška F, Menzel D. GFP-FABD2 fusion construct allows in vivo visualization of the dynamic actin cytoskeleton in all cells of Arabidopsis seedlings. *Eur J Cell Biol* 2005; 84: 595 – 608.

Volkmann D, Baluška F. Actin cytoskeleton in plants: from transport networks to signaling networks. *Microsc Res Tech* 1999; 47: 135 – 154.

Von Arnold S, Sabala I, Bozhkov P, Dyachok J, Filonova L. Developmental pathways of somatic embryogenesis. *Plant Cell Tissue Organ Cult* 2002; 69: 233 – 249.

von Wangenheim D, Daum G, Lohmann JU, Stelzer EK, Maizel A. Live imaging of Arabidopsis development. *Methods Mol Biol* 2014; 1062: 539 – 550.

von Wangenheim D, Fangerau J, Schmitz A, Smith RS, Leitte H, Stelzer EH, Maizel A. Rules and self-organizing properties of post-embryonic plant organ cell division patterns. *Curr Biol* 2016; 26: 439 – 449.

von Wangenheim D, Hauschild R, Friml J. Light sheet fluorescence microscopy of plant roots growing on the surface of a gel. *J Vis Exp* 2017; 119. doi: 10.3791/55044

Vos JW, Dogterom M, Emons AM. Microtubules become more dynamic but not shorter during preprophase band formation: a possible "search-and-capture" mechanism for microtubule translocation. *Cell Motil Cytoskeleton* 2004; 57: 246 – 258.

Vos JW, Pieuchot L, Evrard JL, Janski N, Bergdoll M, de Ronde D, Perez LH, Sardon T, Vernos I, Schmit AC. The plant TPX2 protein regulates prospindle assembly before nuclear envelope breakdown. *Plant Cell* 2008; 20: 2783 – 2797.

Vyplelová P, Ovečka M, Komis G, Šamaj J. Advanced microscopy methods for bioimaging of mitotic microtubules in plants. *Methods Cell Biol* 2018; in press. doi.org/10.1016/bs.mcb.2018.03.019.

Vyplelová P, Ovečka M, Šamaj J. Alfalfa root growth rate correlates with progression of microtubules during mitosis and cytokinesis as revealed by environmental light-sheet microscopy. *Front Plant Sci* 2017; 8: 1870. doi: 10.3389/fpls.2017.01870.

Wade RH, Hyman AA. Microtubule structure and dynamics. *Curr Opin Cell Biol* 1997; 9: 12 – 17.

Wade RH. On and around microtubules: An overview. *Mol Biotechnol* 2009; 43: 177 – 191.

Walker KL, Müller S, Moss D, Ehrhardt DW, Smith LG. Arabidopsis TANGLED identifies the division plane throughout mitosis and cytokinesis. *Curr Biol* 2007; 17: 1827 – 1836.

Wang E, Babbey CM, Dunn KW. Performance comparison between the high-speed Yokogawa spinning disc confocal system and single-point scanning confocal systems. *J Microsc* 2005; 218: 148 – 159.

Wasteneys GO. Microtubule organization in the green kingdom: chaos or selforder?. *J Cell Sci* 2002; 115: 1345 – 1354.

Weerasinghe RR, Collings DA, Johannes E, Allen NS. The distributional changes and role of microtubules in Nod factor-challenged *Medicago sativa* root hairs. *Planta* 2003; 218: 276 – 287.

Wei Z, Liu Y, Lin C, Wang Y, Cai Q, Dong Y, Xing S. Transformation of alfalfa chloroplasts and expression of green fluorescent protein in a forage crop. *Biotechnol Lett* 2011; 33: 2487 – 2494.

Weisshart K. The basic principle of Airyscanning. *Zeiss technology note* 2014.

Whittington AT, Vugrek O, Wei KJ, Hasenbein NG, Sugimoto K, Rashbrooke MC, Wasteneys GO. MOR1 is essential for organizing cortical microtubules in plants. *Nature* 2001; 411: 610 – 613.

Wick SM, Duniec J. Immunofluorescence microscopy of tubulin and microtubule arrays in plant cells. I. Preprophase band development and concomitant appearance of nuclear envelope-associated tubulin. *J Cell Biol* 1983; 97: 235 – 243.

Wiese C, Zheng Y. Microtubule nucleation: γ-tubulin and beyond. *J Cell Sci* 2006; 119: 4143 – 4153.

Wittmann T, Wilm M, Karsenti E, Vernos I. TPX2, A novel xenopus MAP involved in spindle pole organization. *J Cell Biol* 2000; 149: 1405 – 1418.

Wu S, Scheible WR, Schindelasch D, Van Den Daele H, De Veylder L, Baskin TI. A conditional mutation in *Arabidopsis thaliana* separase induces chromosome non-disjunction, aberrant morphogenesis and cyclin B1;1 stability. *Development* 2010; 137: 953 – 961.

Wu SZ, Bezanilla M. Myosin VIII associates with microtubule ends and together with actin plays a role in guiding plant cell division. *Elife* 2014; 3: doi: 10.7554/eLife.03498.

Xing S, Wei Z, Wang Y, Liu Y, Lin C. Integration and expression of *gfp* in the plastid of *Medicago sativa* L. *Methods Mol Biol* 2014; 1132: 375 – 387.

Xu T, Qu Z, Yang X, Qin X, Xiong J, Wang Y, Ren D, Liu G. A cotton kinesin GhKCH2 interacts with both microtubules and microfilaments. *Biochem J* 2009; 421: 171 – 180.

Xu XM, Zhao Q, Rodrigo-Peiris T, Brkljacic J, He CS, Müller S, Meier I. RanGAP1 is a continuous marker of the Arabidopsis cell division plane. *Proc Natl Acad Sci USA* 2008; 105: 18637 – 18642.

Yamada M, Goshima G. Mitotic spindle assembly in land plants: Molecules and mechanisms. *Biology (Basel)* 2017; 6: 6.

Yamagishi M, Shigematsu H, Yokoyama T, Kikkawa M, Sugawa M, Aoki M, Shirouzu M, Yajima J, Nitta R. Structural basis of backwards motion in kinesin-1-kinesin-14 chimera: Implication for kinesin-14 motility. *Structure* 2016; 24: 1322 – 1334.

Yang X, Dong G, Palaniappan K, Mi G, Baskin TI. Temperature-compensated cell production rate and elongation zone length in the root of *Arabidopsis thaliana*. *Plant Cell Environ* 2017; 40: 264 – 276.

Yasuhara H, Oe Y. TMBP200, a XMAP215 homologue of tobacco BY-2 cells, has an essential role in plant mitosis. *Protoplasma* 2011; 248: 493 – 502.

Yoneda A, Akatsuka M, Hoshino H, Kumagai F, Hasezawa S. Decision of spindle poles and division plane by double preprophase bands in a BY-2 cell line expressing GFP-tubulin. *Plant Cell Physiol* 2005; 46: 531 – 538.

Yuan M, Shaw PJ, Warn RM, Lloyd CW. Dynamic reorientation of cortical microtubules, from transverse to longitudinal, in living plant cells. *Proc Natl Acad Sci USA* 1994; 91: 6050 – 6053.

Zeng CJ, Lee YR, Liu B. The WD40 repeat protein NEDD1 functions in microtubule organization during cell division in *Arabidopsis thaliana*. *Plant Cell* 2009; 21: 1129 – 1140.

Zhang H, Dawe RK. Mechanisms of plant spindle formation. *Chromosome Res* 2011; 19: 335 – 344.

Zhu L, Zhang Y, Kang E, Xu Q, Wang M, Rui Y, Liu B, Yuan M, Fu Y. MAP18 regulates the direction of pollen tube growth in Arabidopsis by modulating F-actin organization. *Plant Cell* 2013; 25: 851 – 867.

6. ABBREVIATIONS

1 OC	first outer cortex
2,4,5-T	2,4,5-trichlorophenoxyacetid acid
2,4-D	2,4-dichlorophenoxyacetid acid
ABA	abscisic acid
ABP	actin binding protein
ADF	actin depolymerizing factor
AF	actin filament
AFH14	*A. thaliana* FORMIN 14
AIR9	AUXIN-INDUCED IN ROOT cultures 9
air9-5, air9-27	mutants of *AUXIN-INDUCED IN ROOT* cultures 9
anp1, anp2, anp3	mutants of *A. thaliana* homologue of *NUCLEUS AND PHRAGMOPLAST ASSOCIATED KINASE*
anp2anp3	double mutant of *A. thaliana* homologue of *NUCLEUS AND PHRAGMOPLAST ASSOCIATED KINASE*
ARP2/3	ACTIN-RELATED PROTEINS 2/3
ATK1	*A. thaliana* KINESIN 1
atk1-1	mutant of *A. thaliana KINESIN 1*
ATK5	*A. thaliana* KINESIN 5
atk5, atk5-1, atk5-2	mutants of *A. thaliana KINESIN 5*
AU	Airy units
AUG1	AUGMIN 1
aug1-1	mutant of *AUGMIN 1*
AUG2	AUGMIN 2
aug2-1	mutant of *AUGMIN 2*
AUG3	AUGMIN 3
aug3-1	mutant of *AUGMIN 3*
AUG4	AUGMIN 4
aug4-1	mutant of *AUGMIN 4*
AUG5	AUGMIN 5
aug5-1	mutant of *AUGMIN 5*
AUG6	AUGMIN 6
AUG7	AUGMIN 7
aug7-1	mutant of *AUGMIN 7*
AUG8	AUGMIN 8

aur1-1, aur1-2, aur1-3	mutants of *AURORA 1*
aur2-1, aur2-2	mutants of *AURORA 2*
BY-2	tobacco cultivar Bright Yellow - 2
CDKB2;1	cyclin-dependent kinase B2;1
CDP	cell division plane
CDZ	cortical division zone
CFP	CYAN FLUORESCENT PROTEIN
CLASP	CLIP-ASSOCIATED PROTEIN
clasp, clasp-1, clasp-2, clasp-3	mutants of *CLIP-ASSOCIATED PROTEIN*
CLSM	confocal laser scanning microscopy
Col-0	*A. thaliana* ecotype Columbia-0
CPA	4-chlorophenoxyacetic acid
EB1	END-BINDING PROTEIN 1
EB1a	END-BINDING PROTEIN 1a
EB1b	END-BINDING PROTEIN 1b
EB1c	END-BINDING PROTEIN 1c
eb1c-2	mutant of *END-BINDING PROTEIN 1c*
EDE1	ENDOSPERM DEFECTIVE 1
ede1-1	mutant of *ENDOSPERM DEFECTIVE 1*
EMS	ethylmethylsulfonate
F-actin	filamentous actin
fass-5, fass-13, fass-14, fass-15	mutants of *FASS/TONNEAU2*
FEP tubes	fluorinated ethylene propylene tubes
fh1-1	mutant of *FORMIN-LIKE PROTEIN 1*
fra2	*fragile fiber 2*, mutant of *KATANIN 1*
GaAsP-PMT	gallium arsenide phosphide photomultiplier tube
G-actin	globular actin
GCP2	γ-TUBULIN COMPLEX PROTEIN 2
GCP3	γ-TUBULIN COMPLEX PROTEIN 3
GCP4	γ-TUBULIN COMPLEX PROTEIN 4
GFP	GREEN FLUORESCENT PROTEIN
GhKCH2	*Gossypium hirsutum* kinesin with a calponin homology domain
GIP1	GCP3-INTERACTING PROTEIN 1
gip1	mutant of *GCP3-INTERACTING PROTEIN 1*
GIP2	GCP3-INTERACTING PROTEIN 2
gip2	mutant of *GCP3-INTERACTING PROTEIN 2*

GUS	β-glucuronidase
IAA	indole-3-acetic acid
IT	infection thread
KCBP	KINESIN-LIKE CALMODULIN-BINDING PROTEIN
KCH	kinesin with a calponin homology domain
keu	mutant of *KEULE*
ktn1-2	mutant of *KATANIN 1*
LSFM	light-sheet fluorescence microscopy
lue1	*luciferase super-expressor 1*, mutant of *KATANIN 1*
MAP	microtubule-associated protein
MAP4	MAMMALIAN MICROTUBULE-ASSOCIATED PROTEIN 4
MAP65	MICROTUBULE-ASSOCIATED PROTEIN 65
MAP65-1	MICROTUBULE-ASSOCIATED PROTEIN 65-1
map65-1-1, map65-1-2	mutants of *MICROTUBULE-ASSOCIATED PROTEIN 65-1*
MAP65-2	MICROTUBULE-ASSOCIATED PROTEIN 65-2
map65-2-1, map65-2-2	mutants of *MICROTUBULE-ASSOCIATED PROTEIN 65-2*
MAP65-3	MICROTUBULE-ASSOCIATED PROTEIN 65-3
MAP65-4	MICROTUBULE-ASSOCIATED PROTEIN 65-4
MAP65-4	mutant of *MICROTUBULE-ASSOCIATED PROTEIN 65-4*
MAP70	MICROTUBULE-ASSOCIATED PROTEIN 70
MAPKs	MITOGEN-ACTIVATED PROTEIN KINASEs
MAPs	microtubule-associated proteins
MBD	microtubule-binding domain
MOR1	MICROTUBULE ORGANIZATION 1
mor1, mor1-1, mor1-2	mutants of *MICROTUBULE ORGANIZATION 1*
MOS7	MODIFIER OF SNC1,7
mos7-1, mos7-2, mos7-3, mos7-4, mos7-5	mutants of *MODIFIER OF SNC1,7*
MPK4	MITOGEN-ACTIVATED PROTEIN KINASE 4
mpk4	mutant of *MITOGEN-ACTIVATED PROTEIN KINASE 4*
MPK6	MITOGEN-ACTIVATED PROTEIN KINASE 6

mpk6-2, mpk6-4	mutants of *MITOGEN-ACTIVATED PROTEIN KINASE 6*
MS medium	Murashige and Skoog medium
MT	microtubule
MTOC	microtubule organizing center
MyTH4-FERM	N-terminal myosin tail homology 4 and band4.1, ezrin, radixin, moesin domain
NAA	1-naphthaleneacetic acid
nedd1	mutant of *NEURAL PRECURSOR CELL EXPRESSED, DEVELOPMENTALLY DOWN-REGULATED 1*
NEDD1	NEURAL PRECURSOR CELL EXPRESSED, DEVELOPMENTALLY DOWN-REGULATED 1
nptII	*neomycin phosphotransferase II* gene
NtKCH	*Nicotiana tabacum* kinesin with a calponin homology domain
PAKRP1	PHRAGMOPLAST KINESIN RELATED PROTEIN 1
PAKRP1L	PHRAGMOPLAST KINESIN RELATED PROTEIN 1L
PCR	polymerase chain reaction
ple	*pleiade*, mutants of *MICROTUBULE-ASSOCIATED PROTEIN 65-3*
pleiade1, pleiade2, pleiade 3	mutants of *MICROTUBULE-ASSOCIATED PROTEIN 65-3*
POK1	PHRAGMOPLAST ORIENTING KINESIN 1
pok1-1, pok1-2	mutants of *PHRAGMOPLAST ORIENTING KINESIN 1*
POK2	PHRAGMOPLAST ORIENTING KINESIN 2
pok2-1, pok2-2	mutants of *PHRAGMOPLAST ORIENTING KINESIN 2*
PPA2	phosphatase 2A
PPB	preprophase band
RanGAP1	Ran GTPase ACTIVATING PROTEIN 1
RFP	RED FLUORESCENT PROTEIN
RSH	ROOT-SHOOT-HYPOCOTYL-DEFECTIVE PROTEIN
rsw4, rsw7	mutant of *ROOT SWOLLEN 7*

RSY	*M. sativa* cultivar Regen SY
sab, sab-5, sab-6, sab-7	mutants of *SABRE*
SDCM	spinning disk confocal microscopy
SIMKK	stress-induced mitogen activated protein kinase kinase
SPIM	selective-plane illumination microscopy
TAN	TANGLED
tan, tan-csh, tan-mad, tan-riken	mutants of *TANGLED*
TDZ	thidiazuron
TIO	TWO-IN-ONE
tio-3	mutant of *TWO-IN-ONE*
TMBP200	tobacco MICROTUBULE-BINDING PROTEIN 200
TON1	TONNEAU 1
ton1, ton2	mutants of *TONNEAU 1*
TPX2	TARGETING PROTEIN for Xklp2
TRMs	TON1 RECRUITING MOTIF PROTEINS
TTP	complex consisting of TONNEAU1, TONNEAU1 RECRUITING MOTIF PROTEINS and phosphatase 2A
TUA2	α-tubulin isoform 2
TUA5	α-tubulin isoform 5
TUA6	α-tubulin isoform 6
TUB6	β-tubulin isoform 6
TUBG1	γ-tubulin 1
tubg1-1	mutant of *γ-tubulin 1*
TUBG2	γ-tubulin 2
tubg2-1, tubg2-2	mutants of *γ-tubulin 2*
Xklp2	Xenopus KINESIN-LIKE PROTEIN 2
yda-1 to *yda-9*	mutants of *YODA*
YFP	YELLOW FLUORESCENT PROTEIN

7. CURICULUM VITAE

Personal data

First name and surname:	Petra Illésová (Vyplelová)
Title:	Mgr.
Date of birth:	1st of March 1988
Place of birth:	Přerov
Address:	Bayerova 1504/6, 750 02, Přerov
Nationality:	Czech
E-mail:	petra.illesova@upol.cz
Current position:	PhD. Student/Academic scientist Department of Cell Biology Centre of the Region Haná for Biotechnological and Agricultural Research Faculty of Science Palacký University Olomouc Šlechtitelů 27, 783 71, Olomouc Czech Republic

Education

Ph.D. study in Biochemistry 2014 – present

Palacký University Olomouc

Title of Ph.D. thesis: New microscopic methods for studies of plant cytoskeleton

Master´s program in Biochemistry 2012 – 2014

Palacký University in Olomouc

Title of Master thesis: Detection of MAP kinases with TEY motif in barley cultivated under conditionsof abiotic stress

Bachelor´s program in Applied Biochemistry 2007 – 2012

Masaryk University in Brno

Title of Bachelor thesis: Compare concentrations of sodium and potassium by direct and indirect potentiometry and flame photometry

Employment

Ph.D. student 2014 – August 2016

Ph.D. student/Academic scientist September 2016 – present

Department of Cell Biology, Centre of the Region Haná for Biotechnological and Agricultural Research (CRH), Faculty of Science, Palacký University in Olomouc

Research internship

University in Bielefeld February – April 2018

CeBiTec – Centre for Biotechnology

Prof. Dr. Karsten Niehaus

Project participation

"Proteomic analysis of Arabidopsis MAPK mutants." (IGA_PrF_2013_011), position: diploma student.

"Biological and molecular analysis of selected MAPKs during abiotic stress." (IGA_PrF_2014_033), position: diploma student/ Ph.D. student.

"Microscopic study of MAPKs and cytoskeleton in Arabidopsis and Medicago." (IGA_PrF_ 2015_0153), position: Ph.D. student

"Application of proteomics to study microtubule cleavage using katanin in Arabidopsis." (IGA_PrF_2016_012), position: Ph.D. student

"Revisiting microtubule organization during plant cell division, growth and morphogenesis by superresolution microscopy." (Czech Science Foundation GA ČR, project Nr. 16-24313S), position: Ph.D. student

Teaching

KBC/GFP Plant GFP Technologies 2014

KBC/GFP Plant GFP Technologies 2015

CRH/MM Microscopic methods and their application in biotechnology 2015

CRH/MM Microscopic methods and their application in biotechnology 2016

Mentoring

1. Viktor Janouch
   Study branch: Biotechnology and Gene engineering
   Title of bachelor thesis: Optimization of *in vitro* cultivation conditions of *Medicago sativa* (defended in June 2018)
2. Jiří Sojka
   Study branch: Biotechnology and Gene engineering
   Title of bachelor thesis: Measurement of abundance and activity of the MAP kinases in the transgenic plants of *Medicago sativa* (defended in June 2018)

Fields of interest

Molecular cell and developmental plant biology with main focus on the cytoskeleton in *Medicago sativa* plants and their deep-imaging using light-sheet microscopy.

List of publications:

1. Vyplelová P, Ovečka M, Komis G, Šamaj J. Advanced microscopy methods for bioimaging of mitotic microtubules in plants. *Methods in Cell Biology* 2018; in press. https://doi.org/10.1016/bs.mcb.2018.03.019.

2. Vyplelová P*, Ovečka M*, Šamaj J. Alfalfa root growth rate correlates with progression of microtubules during mitosis and cytokinesis as revealed by environmental light-sheet microscopy. *Frontiers in Plant Science* 2017; 8: 1870. * joined first authors.

3. Bekešová S, Komis G, Křenek P, Vyplelová P, Ovečka M, Luptovčiak I, Illés P, Kuchařová A, Šamaj J**.** Monitoring protein phosphorylation by acrylamide pendant Phos-Tag™ in various plants. *Frontiers in Plant Science* 2015; 6: 336.

4. Křenek P, Niks RE, Vels A, Vyplelová P, Šamaj J. Genome-wide analysis of the barley MAPK gene family and its expression patterns in relation to *Puccinia hordei* infection. Acta Physiologia Plantarum 2015; 37: 1 – 16.

List of posters on conferences:

1. Vyplelová P, Ovečka M, Šamaj J. Contribution of cell division rates to the speed of root growth in *Medicago sativa*. Biotechnology of Plant Products: Green For Good IV, 2017, Olomouc, Czech Republic.
2. Šamajová O, Ovečka M, Takáč T, Vyplelová P, Komis G, Bekešová S, Luptovčiak I, Vadovič P, Hirt H, Šamaj J. Salt stress-induced subcellular kinase relocation and enhanced seedling sensitivity to salt induced by overexpression of Medicago SIMKK in Arabidopsis. 12th International Congress of Cell Biology, 2016, Prague, Czech Republic.
3. Ovečka M, Takáč T, Vyplelová P, Komis G, Bekešová S, Luptovčiak I, Vadovič P, Šamajová O, Hirt H, Šamaj J. Overexpression of Medicago mitogen-activated protein kinase kinase SIMKK in Arabidopsis causes salt stress-induced subcellular relocation and enhanced salt sensitivity. 17th European Congress of Biotechnology, 2016, Krakow, Poland.
4. Vyplelová P, Bekešová S, Komis G, Křenek P, Ovečka M, Luptovčiak I, Illés P, Kuchařová A, Šamaj J. Monitoring protein phosphorylation by acrylamide pendant Phos-Tag™ in various plants. Plant Biotechnology: Green For Good III, 2015, Olomouc, Czech Republic.

8. SUPPLEMENTS

Supplementary Videos

Video S1. Light-sheet imaging of fast-growing root of *M. sativa* stably expressing a GFP-MBD microtubule marker. Root was recorded for a time period of 3 h. Video was produced from time-lapse image acquisition of every 5 min and is presented in the speed of 10 fps.

Video S2. Light-sheet imaging of medium-growing root of *M. sativa* stably expressing a GFP-MBD microtubule marker. Root was recorded for a time period of 3 h. Video was produced from time-lapse image acquisition of every 5 min and is presented in the speed of 10 fps.

Video S3. Light-sheet imaging of slow-growing root of *M. sativa* stably expressing a GFP-MBD microtubule marker. Root was recorded for a time period of 3 h. Video was produced from time-lapse image acquisition of every 5 min and is presented in the speed of 10 fps.

Book chapter

Advanced microscopy methods for bioimaging of mitotic microtubules in plants.

Illésová (Vyplelová) P, Ovečka M, Komis G, Šamaj J.

Methods in Cell Biology 2018; in press. https://doi.org/10.1016/bs.mcb.2018.03.019

IF 1,306

Advanced microscopy methods for bioimaging of mitotic microtubules in plants

Petra Vyplelová, Miroslav Ovečka, George Komis, Jozef Šamaj[1]

Department of Cell Biology, Centre of the Region Haná for Biotechnological and Agricultural Research, Palacký University Olomouc, Olomouc, Czech Republic

[1]*Corresponding author: e-mail address: jozef.samaj@upol.cz*

CHAPTER OUTLINE

Methods in Cell Biology, ISSN 0091-679X, https://doi.org/10.1016/bs.mcb.2018.03.019

Abstract

Mitotic cell division in plants is a dynamic process playing a key role in plant morphogenesis, growth, and development. Since progress of mitosis is highly sensitive to external stresses, documentation of mitotic cell division in living plants requires fast and gentle live-cell imaging microscopy methods and suitable sample preparation procedures. This chapter describes, both theoretically and practically, currently used advanced microscopy methods for the live-cell visualization of the entire process of plant mitosis. These methods include microscopy modalities based on spinning disk, Airyscan confocal laser scanning, structured illumination, and light-sheet bioimaging of tissues or whole plant organs with diverse spatiotemporal resolution. Examples are provided from studies of mitotic cell division using microtubule molecular markers in the model plant *Arabidopsis thaliana*, and from deep imaging of mitotic microtubules in robust plant samples, such as legume crop species *Medicago sativa*.

1 INTRODUCTION

Cellular preparations for mitotic entry in plants are marked by a dramatic reorganization of the cortical microtubule array to an annular cortical assembly, the microtubule preprophase band (PPB; Rasmussen, Humphries, & Smith, 2011) which is considered as a marker of the cortical division zone and a predictor of cell plate fusion at the parent walls (Smertenko et al., 2017). In this way, PPB acts as a determinant of symmetric and asymmetric cell divisions (Rasmussen et al., 2011). Initially, the PPB is loosely organized but progressively narrows until the perinuclear prophase spindle assembles (e.g., Vos, Dogterom, & Emons, 2004). Thereon the PPB disassembles and the mitotic chromosome segregation starts.

Principally, the PPB is a microtubule array and therefore primarily consists of microtubules and a wide array of microtubule-associated proteins with bundling (e.g., members of the MAP65 family; Li et al., 2017), motor (members of the kinesin superfamily; see later), and regulatory (e.g., End Binding 1 proteins; Chan, Calder, Doonan, & Lloyd, 2003; Chan, Calder, Fox, & Lloyd, 2005, and the HEAT repeat protein MOR1/GEM; Twell et al., 2002) activities. Apart from microtubules and microtubule-associated proteins, the PPB also contains actin microfilaments which facilitate the coalescence of cortical microtubules (Kojo et al., 2013) and several other molecules recruited on site and persisting long after the disappearance of the PPB in a continuous or discontinuous manner. Such molecules which serve as markers of the cortical division zone include TANGLED (Walker, Müller, Moss, Ehrhardt, & Smith, 2007), PHRAGMOPLAST-ORIENTING KINESINS 1 and 2 (Müller, Han, & Smith, 2006), FASS/TONNEAU2 (Camilleri et al., 2002), AIR9 (Buschmann et al., 2006), RanGAP1 (Xu et al., 2008), and KINESIN-LIKE CALMODULIN-BINDING PROTEIN (Buschmann et al., 2015). Characteristically, some mutants in corresponding genes exhibit marked cell division plane (CDP)-related phenotypes (Table 1 and references therein).

Table 1 List of *Arabidopsis* Mutants With Reported Mitotic and/or Cytokinetic Defects

Protein	Role	Accession Number	Mutant Name/ Designation	Mutant Characteristic	Described Defect	References
Microtubule-associated proteins						
γ-Tubulin (TUBG1 and TUBG2)	Microtubule nucleation	AT3G61650 (TUBG1), AT5G05620 (TUBG2)	TUBG1^{RNAi}, *tubg1-1*, *tubg2-1*, *tubg2-2*	Downregulation of TUBG1 levels by RNA interference; *tubg1-1*, *tubg2-1*, and *tubg2-2* are T-DNA insertional mutants	Aberrant mitotic spindle and phragmoplast formation	Binarová et al. (2006) and Pastuglia et al. (2006)
GAMMA TUBULIN COMPLEX PROTEIN 4 (GCP4)	Microtubule nucleation	AT3G53760	amiR-GCP4	Knockdown mutant by artificial microRNA	Aberrant mitotic spindle and phragmoplast formation	Kong, Hotta, Lee, Horio, and Liu (2010)
GCP3-INTERACTING PROTEIN1 (GIP1) and GIP2	Microtubule nucleation	AT4G09550 (GIP1), AT1G73790 (GIP2)	*gip1*, *gip2*	T-DNA insertional mutants	Disorganization and malpositioning of mitotic spindle	Janski et al. (2012)
AUGMIN SUBUNITS 1, 2, 3, 4, 5, and 7 (AUG1–5 and 7)	Microtubule nucleation	AT2G41350 (AUG1), AT2G32980 (AUG2), AT5G48520 (AUG3), AT1G50710 (AUG4), AT5G38880 (AUG5), AT5G17620 (AUG7)	*aug1-1*, *aug2-1*, *aug3-1*, *aug4-1*, *aug5-1*, *aug7-1*	T-DNA insertional mutants	Abnormal mitosis and cytokinesis in dividing microspores	Ho et al. (2011) and Hotta et al. (2012)
NEURAL PRECURSOR CELL EXPRESSED, DEVELOPMENTALLY DOWNREGULATED GENE 1 (NEDD1)	Microtubule nucleation	AT5G05970	*nedd1*	T-DNA insertional mutant	Abnormal mitosis and cytokinesis in dividing microspores	Zeng, Lee, and Liu (2009)
ENDOSPERM DEFECTIVE1 (EDE1)	Microtubule binding	AT2G44190	*ede1-1*	T-DNA insertional mutant	Defective cytokinesis during endosperm cellularization	Pignocchi et al. (2009)

Continued

Table 1 List of *Arabidopsis* Mutants With Reported Mitotic and/or Cytokinetic Defects—cont'd

Protein	Role	Accession Number	Mutant Name/ Designation	Mutant Characteristic	Described Defect	References
MAP65-1	Microtubule bundling	AT4G26760	*map65-1-1* and *map65-1-2*	T-DNA insertional mutants expressing truncated MAP65-1	No detectable phenotype; double *map65-1 map65-2* mutants show fewer cell files in the root	Lucas and Shaw (2012) and Lucas et al. (2011)
MAP65-2	Microtubule bundling	AT4G26760	*map65-2-1* and *map65-2-2*	T-DNA insertional mutants expressing truncated MAP65-2	No detectable phenotype; double *map65-1 map65-2* mutants show fewer cell files in the root	Lucas and Shaw (2012) and Lucas et al. (2011)
MAP65-3	Microtubule bundling in mitosis/ cytokinesis	AT5G51600	*pleiade* (*ple*) *1*, *pleiade2*, and *pleiade 3*	*ple1* and *ple2* are ethylmethylsulfonate (EMS)-induced mutants, while *ple3* is T-DNA insertional mutant	Incomplete cytokinesis, multinucleate cells	Müller et al. (2002, 2004), Söllner et al. (2002) and Steiner et al. (2016)
MAP65-4	Microtubule bundling in mitosis/ cytokinesis	AT3G60840	*map65-4*	T-DNA insertional mutant expressing truncated MAP65-4	Additive to MAP65-3 depletion	Li et al. (2017)
KATANIN p60 subunit	Microtubule severing	AT1G80350	*ktn1-2*, *fra2*, *lue1*	*fra2* is EMS-induced point mutation expressing KATANIN with altered properties; *lue1* contains premature stop codon and expresses truncated KATANIN and *ktn1-2* is T-DNA insertional mutant disrupting KATANIN function	Aberrant PPB formation, extensive mitotic spindle rotations, prophase mitotic spindle multipolarity, elongated microtubules in the phragmoplast	Komis et al. (2017) and Panteris and Adamakis (2012)

PHRAGMOPLAST-ORIENTING KINESINS 1/2	Members of the kinesin-12 class motor proteins	AT3G17360 (POK1); AT3G19050 (POK2)	*pok1-1*, *pok1-2*, *pok2-1*, *pok2-2*	All T-DNA insertional mutants showing no transcript	Aberrant CDP	Müller et al. (2006)
ROOT SWOLLEN 7	Member of the kinesin-5 class of motor proteins	AT2G28620	*rsw7*	Point mutation, temperature sensitive (at 30°C) with no phenotype at permissive temperature (19°C)	Severe mitotic spindle defects	Bannigan et al. (2007)
KINESIN-LIKE CALMODULIN-BINDING PROTEIN	Plant unique kinesin motor	AT5G65930	*zwichel* (e.g., *zwiA*)	*zwiA* is T-DNA insertional mutant	No detectable phenotype	Buschmann et al. (2015)
ATK1	Kinesin motor	AT4G21270	*atk1-1*	Transposable element-induced mutant	Abnormal mitotic spindle formation	Marcus, Li, Ma, and Cyr (2003)
ATK5	Kinesin motor	AT4G05190	*atk5-1*, *atk5-2*	T-DNA insertional mutants	Formation of mitotic spindles with broadened poles; prolongation of mitotic spindle elongation	Ambrose and Cyr (2007) and Ambrose, Li, Marcus, Ma, and Cyr (2005)
HINKEL, STUD	Kinesin motors	AT1G18370 (HINKEL), AT3G43210 (STUD)	*atnack1-1*, *atnack1-2*, *atnack2-1*, *atnack2-2*	T-DNA insertional mutants, there are also EMS-induced mutant alleles	Abortive cytokinesis	Strompen et al. (2002) and Tanaka et al. (2004)
PHRAGMOPLAST KINESIN-RELATED PROTEIN1 (PAKRP1)/ kinesin-12A and PHRAGMOPLAST KINESIN-RELATED PROTEIN1L/ kinesin-12B	Kinesin motors	AT4G14150 (PAKRP1), AT3G23670 (PAKRP2)	*kinesin12a-1*, *kinesin12a-2*, *kinesin12b-1*, *kinesin12b-2*	T-DNA insertional mutants	Abnormal phragmoplast formation and incomplete cytokinesis during male gametogenesis	Lee, Li, and Liu (2007)

Continued

Table 1 List of *Arabidopsis* Mutants With Reported Mitotic and/or Cytokinetic Defects—cont'd

Protein	Role	Accession Number	Mutant Name/ Designation	Mutant Characteristic	Described Defect	References
AIR9	Microtubule-binding protein	AT2G34680	*ungud9* (*air9-9*); *haumea*; *air9-5*; *air9-27*	Both *air9-9* and *haumea* are transposon-induced deletion mutants; *air9-5* and *air9-27* are T-DNA insertional mutants	No detectable phenotype	Buschmann et al. (2006)
END BINDING 1c	Plant-specific plus end-binding protein	AT5G67270	*eb1c-2*	T-DNA insertional mutant	Abnormal mitotic spindle formation, malpositioned spindle	Komaki et al. (2010)
MICROTUBULE ORGANIZATION 1	Microtubule plus end regulator	AT2G35630	*mor1-1* and *mor1-2*	Both EMS-induced point mutants	Defective PPBs, mitotic spindle and phragmoplast formation	Kawamura et al. (2006) and Whittington et al. (2001)
TANGLED	Microtubule-binding protein	AT3G05330	*tan-csh*, *tan-mad*, *tan-riken*	T-DNA insertional mutants with absence of gene expression	Aberrant CDP	Walker et al. (2007)
SABRE	Unknown function	AT1G58250	*kreuz und quer* (*kuq*); *sab-5*, *sab-6*, *sab-7*	*kuq* is fast proton-induced mutant while *sab-5* to *sab-7* are T-DNA insertional mutants	Oblique PPB, mitotic spindle and phragmoplast positioning; aberrant CDP	Pietra et al. (2013)
CLIP-ASSOCIATED PROTEIN (CLASP)	Regulator of microtubule plus-end dynamics	AT2G20190	*clasp-1*, *clasp-2*, *clasp-3*	All T-DNA insertional mutants	Oblique PPB, mitotic spindle and phragmoplast positioning; aberrant CDP	Kirik et al. (2007) and Pietra et al. (2013)

Regulatory proteins with effect on microtubule organization

Aurora1/2	Protein kinases	AT4G32830 and AT2G25880	*aur1-1*, *aur1-2*, *aur1-3*; *aur2-1*, *aur2-2*	All T-DNA insertional mutants	Defects in formative cell divisions (aberrant CDP during divisions in lateral root primordia)	Boruc et al. (2017) and Van Damme et al. (2011)
ANP1–3/MKK6/MPK4	Protein kinases	AT1G09000 (ANP1), AT1G54960 (ANP2), AT3G06030 (ANP3), AT5G56580 (MKK6), AT4G01370 (MPK4)	*anp1*, *anp2*, *anp3*, *mkk6*, *mpk4*	All T-DNA insertional mutants	Incomplete cytokinesis; multinucleate cells	Beck, Komis, Ziemann, Menzel, and Šamaj (2011), Kosetsu et al. (2010), and Krysan, Jester, Gottwald, and Sussman, (2002)
YODA, MPK6	Protein kinases	AT1G63700 (YODA), AT1G51660 (MKK4), AT3G21220 (MKK5), AT3G45640 (MPK3), AT2G43790 (MPK6)	*yda-1* to *yda-9* (loss-of-function), *ΔNyda* (aminoterminal deletion, gain-of-function), *mpk6-2*, *mpk6-4*	*Yda-1* to *yda-9* are EMS-induced mutants; *ΔNyda* is T-DNA insertional mutant; *mpk6-2* and *mpk6-4* are T-DNA insertional lines	Aberrant CDP	Lukowitz, Roeder, Parmenter, and Somerville (2004), Müller et al. (2010), and Smékalová et al. (2014)
TWO-IN-ONE (TIO)	Fused kinase; interactor of AKRP1/kinesin-12A and PAKRP1L/kinesin-12B kinesin motors	AT1G50240	*Tio-3*	T-DNA insertional mutant	Abnormal phragmoplast development and cytokinesis during male gametogenesis	Oh et al. (2005, 2012)

Continued

Table 1 List of *Arabidopsis* Mutants With Reported Mitotic and/or Cytokinetic Defects—cont'd

Protein	Role	Accession Number	Mutant Name/ Designation	Mutant Characteristic	Described Defect	References
RanGAP1	GTPase-activating protein of the Ran GTPase	AT3G63130	RanGAP1^{RNAi}	Downregulated RANGAP1 protein by RNA interference	Aberrant CDP	Xu et al. (2008)
FASS/TONNEAU2	B regulatory subunit of type 2A protein phosphatases	AT5G18580	*fass-5*, *fass-13*, *fass-14*, *fass-15*	*fass-5* and *fass-15* are EMS-induced, *fass-13* and *fass-14* are T-DNA insertional mutants	Absence of PPB, aberrant CDP	Camilleri et al. (2002), Kirik, Ehrhardt, and Kirik (2012), and Spinner et al. (2013)
EXTRA SPINDLE POLES	Separase	AT4G22970	*rsw4*	Unknown; temperature sensitive		Moschou et al. (2013) and Wu et al. (2010)
KEULE	SEC1/Munc18 protein	AT1G12360	*keu*^{T282}	EMS-induced point mutation	Affects microtubule reorganization during phragmoplast expansion	Steiner et al. (2016)
MODIFIER OF SNC1,7 (MOS7)	Nucleoporin	AT5G05680	*mos7-1* to *mos7-5*	T-DNA insertional mutants	Abnormal mitotic spindle formation during male gametogenesis	Park et al. (2014)

Table includes only mutants somehow related to cytoskeletal regulation and excludes mutants relevant to associated processes such as membrane trafficking.

Segregation of duplicated genetic material between two daughter cells in the process of mitosis is a conserved feature among eukaryotes and requires the assembly of the mitotic spindle (Prosser & Pelletier, 2017). In animals and fungi, the assembly of the microtubule-based mitotic spindle is dominated by the occurrence of structurally defined microtubule-organizing centers (MTOCs) with microtubule-nucleating capacity such as the centrosome (Vertii, Hehnly, & Doxsey, 2016) and the spindle pole body (Kilmartin, 2014). In higher plants, however, mitotic spindle assembly is acentrosomal and its form undergoes significant changes during mitotic progression (Yamada & Goshima, 2017). The plant mitotic spindle is bipolar and it largely comprises of kinetochore microtubule bundles but it lacks astral microtubules, possibly due to the absence of MTOCs at the spindle poles. As in the case of the PPB, several microtubule-associated proteins involved in microtubule nucleation, regulation of plus-end dynamics, microtubule bundling, and microtubule-dependent motor activities as well as other proteins with regulatory functions such as protein kinases were found to be enriched in the mitotic spindle (reviewed in Yamada & Goshima, 2017).

At the end of mitosis, the mitotic spindle is replaced by the plant-specific cytokinetic apparatus, the phragmoplast. The phragmoplast directs the translocation of cell wall material containing vesicles to the equatorial plane, where they fuse and form the nascent daughter plasma membrane and the cell plate. The phragmoplast expands from the cell center toward the cell periphery in a well-defined plane, which is called the CDP (Smertenko et al., 2017). Finally, the expanding cell plate fuses to a well-defined cortical site, which is called the cell plate fusion site. This site is adjusted to a predetermined cortical division zone (Smertenko et al., 2017), which is in turn defined by the PPB (Smertenko et al., 2017 and references therein). Phragmoplast expansion requires the gradual disappearance of microtubules from its central area and their confinement to the cell periphery through a concerted function of γ-tubulin-dependent microtubule nucleation and MAP65-dependent microtubule bundling. During the process, phragmoplast positioning may be subject to corrective motions (e.g., Komis et al., 2017) through a navigation process probably mediated by actomyosin cytoskeleton (e.g., Wu & Bezanilla, 2014).

Significant studies on the progressive development of the preprophase microtubule band, the assembly and the positioning of the mitotic spindle as well as on the centrifugal expansion of the cytokinetic phragmoplast, and the deposition of the cell plate were done in nonmodel plants. Most such studies were carried out by means of transmission electron microscopy or immunofluorescence imaging (e.g., Gunning, Hardham, & Hughes, 1978; Kojo et al., 2013; Samuels, Giddings, & Staehelin, 1995; Wick & Duniec, 1983) combined with the use of cytoskeletal (e.g., Panteris, Apostolakos, & Galatis, 1995) or other inhibitors (e.g., Binarová et al., 1998) that broadly or selectively affected the above processes. The establishment of *Arabidopsis thaliana* as a genetically tractable model of plant growth and development, the design of robust protocols for the generation

of transgenic plants bearing appropriate fluorescent markers, and the establishment of confocal laser scanning microscopy as a routine method of imaging allowed in vivo visualization of mitosis and cytokinesis in a dynamic manner. Other studies used suspension culture cells of tobacco bright yellow-2 (BY-2), a material that can be easily transformed, maintained, and synchronized to provide thousands of cells in diverse mitotic stages for visualization (e.g., Buschmann, Green, Sambade, Doonan, & Lloyd, 2011; Granger & Cyr, 2000; Yoneda, Akatsuka, Hoshino, Kumagai, & Hasezawa, 2005). However, such suspension-cultured cells lack the spatial constraints of mitotic progression found in intact tissues and they are not allowing deductions on spindle orientation and the regulation of CDP orientation necessary for pattern formation, morphogenesis, and organ development in plants.

The dynamic imaging of mitosis and cytokinesis in living plant cells can convey very useful information regarding the rates of PPB narrowing (e.g., Komis et al., 2017; Vos et al., 2004) and disturbances of its formation after pharmacological (e.g., Kojo, Yasuhara, & Hasezawa, 2014) or genetic (Komis et al., 2017) interference. Moreover, this approach can provide data on the duration of mitosis and the subsequent phragmoplast expansion (e.g., Beck et al., 2011; Komis et al., 2017), and it can reveal mechanisms behind mitotic and cytokinetic aberrations of appropriate mutants. Keys to successful imaging of the above processes in plants include the sufficient depth of the selected microscopy method and adequate speed of acquisition to avoid motion artifacts arising by intracellular motions of the mitotic microtubules. Most importantly, the selected method should ensure the minimal exposure of the dividing cell to phototoxic excitation illumination which may delay, abort, or disturb the progress of mitosis and cytokinesis or compromise the viability of the sample during imaging (see Laissue, Alghamdi, Tomancak, Reynaud, & Shroff, 2017 for a critical assessment of phototoxicity during live fluorescence imaging).

This chapter aims to summarize the bioimaging possibilities in the studies of mitotic progression in planta by advanced methods that were developed and commercialized over the past few years. These methods have expanded the possibilities of dissecting mitosis and cytokinesis in living plants and provided a considerable improvement of spatial and temporal resolution. High speed and mass visualization of the mitoses can be done in whole organs such as roots or leaves with light-sheet fluorescent microscopy (LSFM) allowing imaging of subcellular details at a moderate spatial resolution. Mitosis can be followed in better spatial resolution with fast imaging modalities such as spinning disk microscopy, while high-resolution methods such as Airyscan confocal microscopy and superresolution methods such as structured illumination microscopy (SIM) can be used to decipher fine structural details in the assembly of the PPB, the mitotic spindle, and the cytokinetic phragmoplast. We are providing imaging possibilities of two different plants, the plant model *A. thaliana* and the legume crop *Medicago sativa* which pose different challenges for sample preparation and image acquisition.

2 PREPARATION OF MOLECULAR MARKERS FOR THE VISUALIZATION OF MITOTIC MICROTUBULE ARRAYS

The in vivo visualization of the mitotic progress in plants requires selective molecular labeling of microtubules and for this purpose three different microtubule molecular markers have been routinely used in related studies. The first microtubule marker that was introduced in plant cell biology is a green fluorescent protein (GFP) fusion with the microtubule-binding domain (MBD) of the nonneuronal mammalian microtubule-associated protein 4 (GFP-MBD; Marc et al., 1998). This marker has been used to report cortical microtubule dynamics, PPB, mitotic spindle, and phragmoplast rearrangements.

Tubulin fusions with some fluorescent proteins can also be used to visualize microtubule dynamics during cell division and cytokinesis. Examples of such fusions include several α- and β-tubulin isoforms (such as TUA2, TUA5, TUA6, and TUB6) fused to GFP, YFP, CFP, tagRFP, and mCherry (Hasezawa, Ueda, & Kumagai, 2000; Murata et al., 2013; Walker et al., 2007).

Finally, microtubule reporters that have been used in plant mitotic research include the plus-end-binding proteins EB1a and EB1b which have been used as GFP fusions (Chan et al., 2003, 2005).

The expression of all of these markers is driven by the strong constitutive promoter 35S of cauliflower mosaic virus. For this reason care must be taken to avoid disturbances related to overexpression as described before and to this respect tubulin fusions are probably the best markers. MBD fusions rather could be avoided (Celler et al., 2016) although at moderate expression levels they can be used to follow mitotic spindle and phragmoplast dynamics (Beck et al., 2011).

A more thorough evaluation of microtubular markers has been presented before (Buschmann, Sambade, Pesquet, Calder, & Lloyd, 2010) with an account on their advantages and disadvantages. Since not all of them have been used in *Arabidopsis* or in studies of plant mitosis and cytokinesis, they will not be iterated here.

3 USE OF *ARABIDOPSIS* MUTANTS TO DISSECT MITOTIC PROGRESSION IN PLANTS

Our knowledge on the mitotic progression in plants lags significantly behind that in animals. Nevertheless, the establishment of seed collections of *Arabidopsis* mutants has led to the identification of important proteins that are involved in the process and uncovered plant unique or conserved mechanisms of mitotic spindle assembly and the subsequent process of cytokinesis. Table 1 summarizes published work on several *Arabidopsis* mutants defective in mitosis, cytokinesis, or CDP orientation and specifies the related defects.

4 MATERIALS

4.1 PLANT TRANSFORMATION AND CROSSING TO INTRODUCE MICROTUBULE MARKERS

Methods of microtubule molecular marker introduction into *A. thaliana* include either plant transformation using floral dipping into suspensions of Agrobacteria harboring plasmids with the reporter transgene (Clough & Bent, 1998), or crossing the desirable *Arabidopsis* line (wild type or mutant) with another line already expressing the desirable fluorescent microtubule marker (e.g., Sampathkumar et al., 2011). Preferable method for construct preparation is a MultiSite Gateway® technology approach. It is a fast and efficient tool based on site-specific recombination allowing simultaneous cloning of DNA fragments in predefined order and orientation. After its optimization for the use in plants, a set of entry clones containing promoters, terminators, and reporter genes has been created (Karimi, Bleys, Vanderhaeghen, & Hilson, 2007). Methods presented here aim to characterize microtubule arrays of dividing cells in wild-type *A. thaliana* plants of Col-0 ecotype and in the knockout mutant *ktn1-2*, which is deficient in the microtubule severing protein KATANIN 1 (Komis et al., 2017). Thus, we performed live-cell imaging with transgenic *A. thaliana* plants stably expressing tubulin fluorescent marker GFP-TUA6 and transgenic *ktn1-2* mutant line with expression of GFP-TUA6 marker that was prepared by crossing of this mutant with Col-0 plants stably transformed with a *35S*::*TUA6:GFP* construct (Komis et al., 2017).

For stable transformation of *M. sativa*, we used a rapid and highly efficient method of cocultivation of leaf explants with *Agrobacterium tumefaciens* strain containing a construct carrying a transgene fused with a fluorescent marker (Samac & Austin-Phillips, 2006). We used *A. tumefaciens* strain GV3101 containing GFP-MBD microtubule marker (Marc et al., 1998) that was prepared by a standard cloning method (Vyplelová, Ovečka, & Šamaj, 2017). Leaf explants after transformation were sequentially subcultured on media supporting callus initiation, somatic embryo formation, root and shoot development, and in vitro maintenance of growing plantlets (Samac & Austin-Phillips, 2006). Selection of transformed tissues and seedlings was based on the presence of selecting herbicide marker phosphinothricin in the culture media. Transformed plants for live-cell imaging were further selected according to the presence of GFP-MBD using an epifluorescence microscope.

4.2 PREPARATION OF PLANT MATERIAL FOR LIGHT-SHEET IMAGING OF ROOT CELL MITOTIC PROGRESS

In general, mitotic cell divisions in plants are mostly concentrated in specialized multicellular domains, plant meristems. Cell proliferation in the root takes place within the root apical meristem, where radial root zonation consists of several cell layers important for development of various tissues (Baum, Dubrovsky, & Rost, 2002; Dolan et al., 1993; Scheres, Benfey, & Dolan, 2002). Our understanding of

how cell divisions in the root apical meristem are organized and regulated during plant growth and development thus requires microscopic imaging of dividing cells in the whole root apex with sufficient spatial and temporal resolution. Ideally, intact plants should be adapted in the microscope for long-term imaging under minimalized phototoxicity, photobleaching, and proper environmental physiological conditions. A cutting-edge technology fulfilling all requirements for developmental imaging under physiological conditions is represented by LSFM in animal developmental biology. LSFM has been introduced also into plant developmental biology, although the number of applications is not so high due to the more complicated preparation of living plants for long-term microscopy observations. However, substantial benefit of a vertically oriented plant (consistently with the gravity vector) prefers LSFM as an advanced microscopy technique for long-term plant developmental imaging. This method offers fast optical sectioning of the sample, restriction of the fluorophore excitation only to the thin light-sheet volume, and free rotation of the sample allowing multiangular image acquisition. Live-cell imaging of dividing cells using LSFM is sufficient for resolving microtubule arrays during mitosis and cytokinesis, including deep imaging of dividing cells inside of living multicellular plant organs. Good spatial and high temporal resolution of LSFM ensures recording of cell division in growing and developing plant tissues in real time. Nevertheless, there are only very few LSFM studies on cytoskeletal proteins during plant cell division so far (Maizel, von Wangenheim, Federici, Haseloff, & Stelzer, 2011; Novák, Kuchařová, Ovečka, Komis, & Šamaj, 2016; Ovečka et al., 2015; Vyplelová et al., 2017).

1. Plant root is the preferred organ for LSFM studies due to the high frequency of cell divisions and to the fact that it grows fully embedded in the culture medium. Solidified Phytagel-based culture medium containing all macro- and micronutrients and carbon source serves as an optimal cultivation environment for plant roots. In addition, being transparent it provides excellent optical properties (Maizel et al., 2011; Ovečka et al., 2015) and serves as an optimal imaging medium for LSFM. In our experiments, we used a half-strength Murashige and Skoog (MS) basal salt mixture supplemented with 1% (w/v) sucrose and pH adjusted to 5.7, solidified with Phytagel at a concentration 0.6% (w/v). An alternative approach for embedding and imaging of plant samples is the use of a low-gelling-temperature agarose at appropriate concentrations (usually between 0.6% and 1.0% (w/v)) dissolved in water or liquid half-strength MS culture medium.
2. We prepared samples of whole intact plants in the "open system" developed for long-term live-cell imaging of *A. thaliana* seedlings (Ovečka et al., 2015). Plants growing in the Phytagel-solidified culture medium were transferred to the microscope in fluorinated ethylene propylene tubes (FEP tubes). Roots grow in the culture medium inside of the FEP tube. Green parts of the plants are located in open space of the FEP tube providing access to air and light in the microscope during experiment. Alternative methods suitable for mounting *A. thaliana* plants to the light-sheet microscope supporting their growth

during the imaging were also published (de Luis Balaguer et al., 2016, von Wangenheim, Daum, Lohmann, Stelzer, & Maizel, 2014).

3. Nourishing plants with nutrients from fresh culture medium is required, especially for long-term experiments. We use controlled perfusion of the imaging chamber with liquid half-strength MS medium without vitamins, supplemented with 1% (w/v) sucrose and pH adjusted to 5.7. Plant growth medium is filter-sterilized using a sterile syringe filter with a pore size of 0.2 µm before loading to the imaging chamber in order to prevent fungal and/or bacterial contamination.
4. Practical approaches on how to prepare plants for LSFM imaging described later are based on a published protocol optimized for *A. thaliana* (Ovečka et al., 2015) and can be easily adapted for either single-cell system (e.g., cell suspension culture), or significantly thicker samples such as somatic embryos and developing plants of the legume crop plant *M. sativa*. It is applicable for both commercial and custom-built LSFM platforms.

4.2.1 A. thaliana *seedlings*

1. Seeds of *A. thaliana* transgenic lines must be sterilized in 70% (v/v) ethanol for 2 min and subsequently in 1% (v/v) sodium hypochlorite containing 0.05% (v/v) Tween 20 for 8 min. The next step is thorough washing of the seeds (five times) with sterile MilliQ water. Sterile seeds are placed on a Petri dish filled with Phytagel-solidified half-strength MS medium. All steps of seed sterilization and plating must be done in aseptic conditions in the laminar flow box. Plates with seeds are then stored at 4°C for 2–3 days to break seed dormancy and synchronize germination. After it, plates are placed into the culture chamber at 22°C, 50% humidity, and 16/8 h (light/darkness) photoperiod.
2. After germination (within 24–48 h after seed transfer to the culture chamber) seeds with ruptured testa and emerging root are transferred to round 90 × 25 mm Petri dishes filled with 80 mL of Phytagel-solidified half-strength MS medium. The thickness of culture medium should be approximately 15 mm, which is optimal for root growth and further sample preparation.
3. Two days later germinating plants with growing roots are picked up by gentle insertion of the FEP tube with an inner diameter of 2.8 mm to the culture medium enclosing the selected plant inside. The FEP tube with the plant and the culture medium inside is installed into the microscope observation chamber.

4.2.2 M. sativa *seedlings*

1. Small plantlets of *M. sativa* expressing fluorescent microtubule marker GFP-MBD are produced in vitro from somatic embryos (Vyplelová et al., 2017). Well-developed somatic embryos with proliferating root pole are first selected and transferred to a new plate containing Phytagel-solidified full-strength MS medium that is at least 15-mm thick. Somatic embryos are carefully inserted vertically into the solid culture medium to ensure that the root pole will grow

vertically inside the medium and the upper green part of the plant will develop in the air above the culture medium.

2. Similarly as in the case of *A. thaliana* preparation, somatic embryos are surrounded by the FEP tube, but in this case with larger inner diameter of 4.2 mm. Insertion of the FEP tube into the culture medium must be careful enough to enclose individual somatic embryo, but not to damage the root pole. Moreover, it should provide enough surrounding culture medium inside the tube for further plant development during imaging.
3. After 1–2 days of somatic embryo stabilization and visual inspection of the root pole which should start elongation, such FEP tube with a germinating somatic embryo is carefully removed from the culture medium and prepared for LSFM.

4.2.3 Light-sheet fluorescence imaging

1. After removing from the culture plate the FEP tube with the sample is moved to the light-sheet microscope. To fix it in the sample holder, the FEP tube with *A. thaliana* plant (with inner diameter of 2.8 mm) is inserted to the glass capillary with an appropriate diameter, while the FEP tube with *M. sativa* plant (with inner diameter of 4.2 mm) is inserted to the sterile plastic syringe of the 1 mL volume which was cut-open at the tip. Glass capillary or plastic syringe serves as a sample holder for fixing the sample in the microscope.
2. Imaging of plant roots described here is done with the light-sheet fluorescence microscope Z.1 (Carl Zeiss Microscopy, Germany). The system is equipped with W Plan-Apochromat 20 ×/1.0 NA water immersion detection objective and two 10 ×/0.2 NA illumination objectives for left and right sample illumination. It is used for synchronized dual-side illumination and both left and right light-sheet illumination beams are modulated into a pivot scan mode.
3. Fluorescent microtubule markers GFP-TUA6 in *A. thaliana* and GFP-MBD in *M. sativa* are visualized with laser excitation line 488 nm and with emission filter BP505–545. Excitation intensity of the laser is set up to 2%–3% of the laser intensity range available in order to minimalize photobleaching and phototoxicity. Time-lapse imaging is done by whole root image acquisition in *Z*-stack mode every 5 min and experiment duration is designed for a period of several hours (3–15 h). Images are recorded with the sCMOS camera (PCO.Edge, PCO AG) with exposure time of 20–50 ms per optical section.
4. Root growth rate of experimental plants during imaging is stable and fast enough that roots grow out of the field of view in the microscope. For this reason, images are recorded in two or three subsequent fields of view coordinated to follow each other at the *y* axis in order to continuously record growing root displacement during long-term imaging experiments.
5. Acquired series of data characterizing microtubule arrays during cell division in *x*-, *y*-, *z*-, and *t*-coordinates (Fig. 1) are edited and analyzed using Zeiss Zen 2014 software (Black Version).

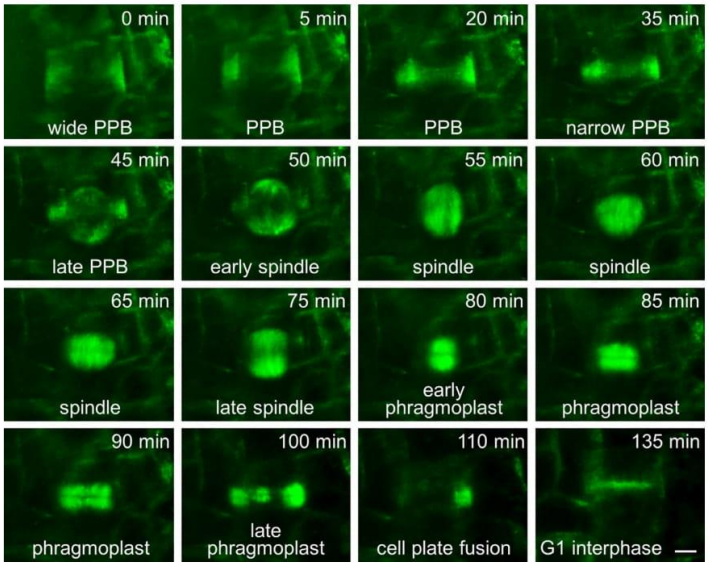

FIG. 1

Time-lapse imaging of microtubule arrays during mitosis and cytokinesis in the root epidermal cell of *Medicago sativa* plant stably transformed with a *35S::GFP:MBD* construct using light-sheet fluorescence microscopy. Sequence of images showing progression of PPB narrowing and disappearance together with formation of the mitotic spindle, establishment of the phragmoplast, its centrifugal enlargement in lateral direction during the cytokinesis, final fusion of cell plate with parental cell wall, and reappearance of cortical microtubule network in postmitotic interphase cell. Time of the cell division progression is indicated in minutes. Scale bar: 5 μm.

4.3 PREPARATION OF PLANT MATERIAL FOR HIGH-SPEED SPINNING DISK RECORDING OF THE MITOTIC PROGRESS

Spinning disk confocal microscope technology is based on a rotating disk with multiple pinholes simultaneously covering multiple locations of the field of view by the excitation light. Thus, the speed of imaging in this microscope is very fast, making it suitable for documentation of dynamic cellular processes, including microtubule dynamics in living plant cells. Several studies addressed the dynamics of cortical microtubule arrays in plant cells. Spinning disk confocal microscope imaging was used for characterization of microtubule dynamics on plus and minus ends (Shaw & Lucas, 2011), microtubule dynamic instability (Shaw, Kamyar, & Ehrhardt, 2003) or microtubule nucleation, and reorientation in *KATANIN1* mutants (Lindeboom

et al., 2013; Nakamura, Ehrhardt, & Hashimoto, 2010). Moreover, dynamic changes of complex microtubule arrays during cell division were also described using spinning disk confocal microscopy quire recently (Komis et al., 2017; Murata et al., 2013). Time-lapse imaging of the entire process of mitosis brings temporal information on the duration of individual stages, including the formation of PPB, mitotic spindle, and phragmoplast (Fig. 2).

1. Young seedlings of *A. thaliana* suitable for spinning disk confocal microscopy imaging are obtained from seeds 3–4 days after their germination. Before this, seeds of transgenic lines expressing an appropriate microtubule marker must be surface sterilized with 70% (v/v) ethanol for 2 min followed by 1% (v/v) sodium hypochlorite containing 0.05% (v/v) Tween 20 for 8 min. After plating sterile seeds on plates containing a half-strength MS medium without vitamins, with 1% (w/v) sucrose, pH adjusted to 5.7, and solidified with Phytagel at a concentration 0.6% (w/v), plates are stored for 2–4 days at 4°C for stratification. Following this period plates with seeds are placed into the growth chamber at 22°C, 50% humidity, and 16/8 h (light/darkness) photoperiod for germination. Plates are positioned vertically to allow straight growth of roots at the surface of solidified medium.
2. Imaging of seedlings is performed using microscopy slides prepared in the form of microchambers consisting of microscopy slide, spacers on the side of the slide made from double sided tape or parafilm, and a coverslip. Sample is thus sandwiched between slide and coverslip with a stable distance ensuring enough space for young *A. thaliana* plant. A drop of liquid half-strength MS medium is placed in the middle of the slide and one selected seedling is transferred to the drop. After closing the seedling with a coverslip, the microchamber is sealed on the sides and edges by parafilm strips to prevent evaporation of liquid half-strength MS medium during time-lapsed imaging, which may last more than 1 h. Transfer of selected plants from the sterile culture medium to the microscopy slide should be done under sterile conditions in the laminar flow box.
3. A convenient part of young seedling possessing a high number of cells in different stages of mitotic cell division is the root tip. Young seedling plants (3–4 days after germination) are most suitable for such observations. Dividing cells in the green aerial part of *A. thaliana* plants can be found in the petiole of the young first true leaf (Fig. 2). This tissue is flat, well organized, and easily accessible, but it is available only later in the plant development, e.g., in 7-days-old seedlings.
4. In our laboratory, we operate a Cell Observer Z1 spinning disk confocal microscope (Carl Zeiss Microscopy), equipped with high-resolution Evolve 512 back-thinned EM-CCD camera (Photometrics). Observation of cell division is regularly performed with an EC Plan-Neofluar 40 ×/1.3 NA oil immersion objective and Plan-Apochromat 63 ×/1.4 NA oil immersion objective. Plant samples with the microtubule marker GFP-TUA6 are imaged with excitation laser line 488 nm and emission filter BP525/50. For convenience, reduction of the

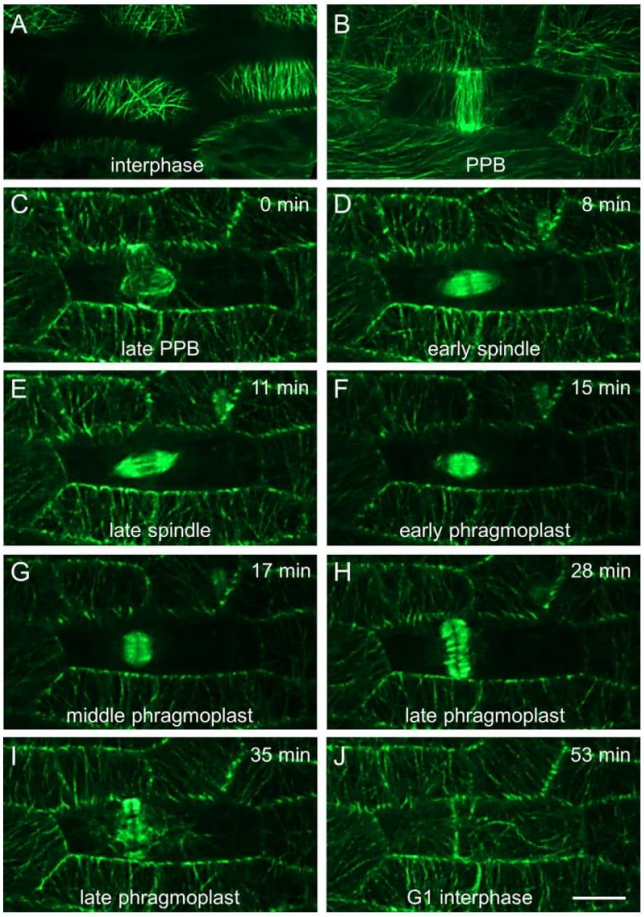

FIG. 2

Time-lapse imaging of microtubule arrays during mitosis and cytokinesis in petiole epidermal cell of *Arabidopsis thaliana* plant stably transformed with a *35S::GFP:TUA6* construct using spinning disk microscopy. Time-lapse recording of PPB narrowing from cells in interphase (A) to preprophase (B), PPB disappearance and mitotic spindle formation at prometaphase (C), mitotic spindle in metaphase and anaphase (D and E), early phragmoplast formation at telophase (F), progression of middle and late phragmoplast during cytokinesis (G and H), termination of the phragmoplast at the end of cytokinesis (I), and rearrangement of cortical microtubules at the postcytokinetic G1 phase (J). Time of the cell division progression is indicated in minutes. Scale bar: 100 μm.

dataset size and minimization of sample photodamage, entire Z-stacks are acquired every 30 s, covering a period of ca. 1 h, which sufficiently covers the entire mitosis and cytokinesis. Data sets are analyzed with Zeiss Zen 2014 software (Blue Version).

4.4 IMAGING OF PLANT MITOTIC MICROTUBULE ARRAYS WITH THE POINT-SCANNING CONFOCAL AIRYSCAN SYSTEM WITH IMPROVED RESOLUTION

Confocal laser scanning microscopy (CLSM) equipped with Airyscan system represents a new application of a point-scanning imaging approach with improved resolution. The system is equipped with a 32 GaAsP detector providing high sensitivity and superior light-collecting capacity. Samples can be scanned with the fast mode allowing sufficient temporal resolution during 3D spatial and temporal acquisition. Alternatively, a high-resolution mode could be used allowing improved 3D resolution for acquiring single Z-stacks. Taking into account these technical improvements, we utilized the LSM880 Airyscan microscopy platform (Carl Zeiss Microscopy) for the documentation of the mitotic progress in cells of the *ktn1-2* mutant stably expressing the microtubule marker GFP-TUA6 (Komis et al., 2017). Defects in the organization of mitotic microtubule arrays in dividing cells caused by mutation in the *KATANIN1* gene were clearly documented by comparison to the corresponding control (Fig. 3).

1. Seeds of transgenic lines expressing an appropriate microtubule marker (GFP-TUA6) are surface sterilized using 70% (v/v) ethanol for 2 min followed by 1% (v/v) sodium hypochlorite containing 0.05% (v/v) Tween 20 for 8 min. After washing, sterile seeds are plated on the surface of half-strength MS medium without vitamins and with 1% (w/v) sucrose, pH adjusted to 5.7, solidified with Phytagel at a concentration 0.6% (w/v). Following seed stratification at 4°C for 2–4 days, they are cultivated in growth chamber at 22°C, 50% humidity, and 16/8 h (light/darkness) photoperiod at a vertical position to allow straight growth of roots on the surface of the solidified medium.
2. First, it is necessary to build the observation chamber using a glass slide and coverslip spaced with parafilm or double sticky tape strips. A drop of liquid half-strength MS medium is placed in the middle of the slide and one selected seedling is transferred to the drop. The sample is sandwiched between slide and coverslip with a stable distance ensuring enough space for young *A. thaliana* plant. The microchamber is sealed on the sides and edges by parafilm strips to prevent evaporation of liquid half-strength MS medium during time-lapse imaging for more than 1 h. *Note*: The transfer of selected plants from the culture medium to the microscopy slide should be done under sterile conditions in the laminar flow box.
3. Epidermal petiole cells of young first true leaf are suitable for observation of cell division in the green part of *A. thaliana* plants. The most preferable plants are

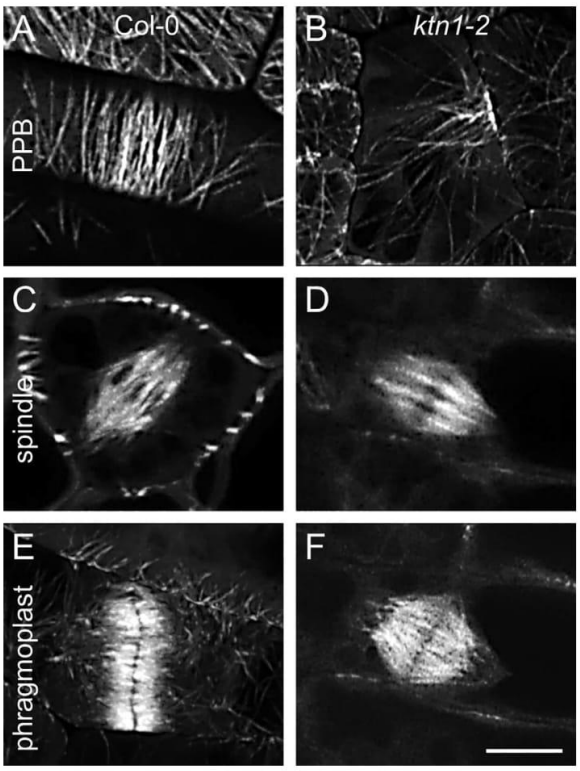

FIG. 3

Comparative analysis of microtubule arrays during mitosis and cytokinesis of leaf petiole epidermal cells in *Arabidopsis thaliana* plants stably transformed with a *35S::GFP:TUA6* construct between wild type plants and a knockout mutant *ktn1-2*, deficient in microtubule severing protein KATANIN 1 using confocal laser scanning microscopy equipped with the Airyscan system. Organization of microtubule arrays typical for particular cell division stages in cells of the wild type plant (A, C, and E) and the *ktn1-2* mutant (B, D, and F). (A and B) Narrowing of the preprophase band (PPB) in late G2 phase of the cell cycle (preprophase stage). Note unipolar and disorganized arrangement of PPB microtubules in the *ktn1-2* mutant (B). (C and D) Mitotic spindle organization, showing no structural changes between control and *ktn1-2* mutant cells. (E and F) Organization of phragmoplast microtubules during cytokinesis. In comparison to control (E), phragmoplast in the *ktn1-2* mutant is abnormally shaped (F). Scale bar: 5μm.

6–7 days old for preparation of such sample. The plant must be entirely covered by the coverslip and young first true leaf must be positioned by abaxial (lower) leaf side parallel to the coverslip.

4. The example given here (Fig. 3) was obtained using LSM880 with Airyscan (Carl Zeiss Microscopy). We used single-photon excitation with the 488 nm laser line and a 32 GaAsP detector for fluorescence detection. The superior light-collecting capacity of the Airyscan and the sensitivity of the GaAsP detector allowed setting laser power to a level not exceeding 2% of the range available. Observation of dividing cells was done with Plan-Apochromat 63 ×/1.4 NA oil immersion objective and data sets were analyzed with Zeiss Zen 2014 software (Blue Version).

4.5 HIGH-RESOLUTION IMAGING OF THE PLANT MITOTIC APPARATUS

Superresolution methods such as SIM, stochastic optical reconstruction microscopy, or stimulated emission depletion microscopy have been used to visualize details in the structure of the mitotic apparatus or its components at the three dimensions in fixed and immunolabeled animal cells (e.g., Dunsch et al., 2012; Wynne & Funabiki, 2016), while such studies are largely absent from the plant field. Owing to the temporal restrictions of image acquisition and the limited depth of imaging of superresolution methods in the existing commercially available superresolution platforms, the dynamic imaging of the mitotic and cytokinetic process has been very scarce. In a relevant study, spindle dynamics have been reported at high acquisition frame rates, albeit using a custom-built TIRF-SIM setup (Kner, Chhun, Griffis, Winoto, & Gustafsson, 2009). In any case, it is possible to acquire two-dimensional high-resolution snapshots showing details in the organization of the PPB, the mitotic spindle, and the phragmoplast (Fig. 4). Later, we describe easy-to-follow steps for such snapshot acquisition of *A. thaliana* dividing cells.

1. Surface sterilize and plate seeds of any wild-type or mitotic mutant harboring an appropriate microtubule marker. After stratification at 4°C for 2–4 days, Petri dishes with plated seeds can be placed in an appropriate environmental chamber to allow growth. Seeds can be allowed to germinate and grow under full exposure to light conditions of the chamber or they may grow in full darkness to promote etiolation after covering the Petri dish with aluminium foil. In the latter case etiolated seedlings are very thin, devoid of chlorophyll, and therefore constitute a more friendly material for sample mounting and imaging by SIM (Komis et al., 2014).
2. High numbers of dividing cells can be found in the root tip and the cotyledons of relatively young seedlings (i.e., 3–4 days after germination) while in older seedlings (over 7 days after germination) a good source of dividing cells is the petiole of the young first true leaf.
3. In case young seedlings are selected, those can be placed on a drop of liquid half-strength MS medium and sandwiched between glass slide and coverslip spaced

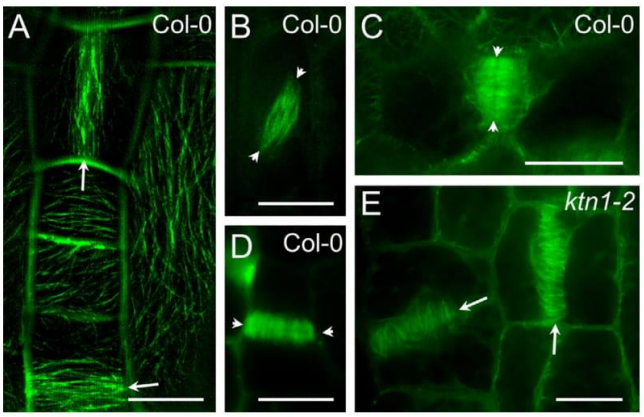

FIG. 4

Imaging mitosis and cytokinesis by structured illumination microscopy in living, dividing cells of *Arabidopsis thaliana* plants stably transformed with a *35S::GFP:TUA6* construct. (A) Two preprophase petiole cells with a variable degree in PPB organization (*arrows*). (B) A prometaphase lateral root cap cell with a clearly defined, oblique mitotic spindle (*arrowheads* denote the spindle poles). (C and D) Early (C) and late (D) cytokinetic cotyledon epidermal cells showing phragmoplasts at different stages. *Arrowheads* mark the equatorial plane. (E) Abnormal persistence of midplane microtubules (*arrows*) in postcytokinetic petiole epidermal cells of *ktn1-2* mutant. All scale bars: 10 μm.

by double sticky tape. If older seedlings are to be used, they should also be mounted as above but it will be necessary to position the cotyledons with the aid of fine forceps, in order to reveal and expose the petiole(s) as near to the coverslip surface as possible. This should be done under a dissection microscope in sterile conditions. When seedlings are young they can be adequately wetted by the aqueous half-strength MS medium, minimizing the possibility of spherical aberrations during image acquisition. Aerial parts of older seedlings, especially cotyledons and leaves, are poorly wetted and for this reason it is suggested to mount such material in oxygen saturated perfluorocarbon such as perfluorodecalin (Littlejohn, Gouveia, Edner, Smirnoff, & Love, 2010; Littlejohn et al., 2014). In both cases care must be taken to position the plant sample at the center of the observation chamber.

4. Glassware and solutions used to prepare the sample should be exceptionally clean before mounting the observation chamber on the microscope stage. Follow standard procedures for cleaning coverslips and glass slides and make sure that oil immersion objectives will be free of dust and residual immersion oil before starting the observation experiment. Coverslips and glass slides can be cleaned by fuming nitric acid, washed with an excess of high purity water, and stored under absolute ethanol until use.

5. Switch on the microscope and computer and start the associated software. We operate a Zeiss Elyra PS.1 platform with 63 ×/1.40 NA, 100 ×/1.46 NA, and 100 ×/1.57 NA oil immersion objectives coupled to a Definite Focus 2 device and an sCMOS camera (PCO.Edge 5.5, PCO AG, 2560 × 2160 pixels, pixel size 6.5 μm × 6.5 μm) running under Zeiss Zen 2014 software (Black Version). Place sample on the microscope stage and setup the imaging experiment. Select appropriate laser line (for GFP we use 488 nm excitation line and for RFP or mCherry we use a 561 nm laser line) and matching filter cubes. The Zen software allows choosing between 3 and 5 grating pattern rotations and standard 5 phase shifts. Since the highest quality of snapshot images is required, select 5 rotations. Finally, set appropriate laser power and camera exposure time. As a rule of thumb, laser power and camera exposure time should be set to the minimum values that allow a high signal-to-noise ratio and the clear imaging of cytoskeletal structures over a relatively dark background.
6. Locate dividing cells, focus carefully, and activate the Definite Focus device to make sure that the focus will remain stable during the acquisition. This is particularly important at camera times of ca. 350–500 ms which are necessary for imaging samples with low expression levels of the microtubule marker (e.g., Fig. 4). Total acquisition time (for 5 grid rotations and 5 phase shifts, i.e., 25 individual images for a single snapshot) can be between 8 and 12 s. It is also necessary to see the grid lines and their movements during the acquisition as this empirically means that the cytoskeletal structures are well modulated with the light pattern and they will be adequately resolved in the final reconstructed image.
7. Proceed to image reconstruction and quality control according to previously published procedures (Demmerle et al., 2017; Komis et al., 2015).
8. It is important to note that the above sample preparation guidelines are platform independent and can be easily used to other existing commercial SIM microscopes (Komis et al., 2015).

5 CONCLUSIONS

Sample preparation is of paramount importance for the adequate visualization of mitosis and cytokinesis in plants. The procedures described earlier aim to describe preparations for high-resolution time-lapse imaging of mitotic dynamics by Airyscan CLSM and for characterizing the organization of mitotic microtubules by SIM at the single-cell level. Additionally, we provide easy to follow procedures for mounting *Arabidopsis* seedlings for tracking and documenting mitotic cells in the multicellular context of entire organs such as roots and leaf petioles. High-resolution studies with Airyscan and SIM may be used to reveal mechanisms of spindle and phragmoplast assembly progression in living cells, while light-sheet imaging can be used to obtain information on the coordination of the mitotic process in populations of hundreds of cells, e.g., within root apical meristem.

ACKNOWLEDGMENTS

We cordially acknowledge Katarína Takáčová and Pavlína Floková for their help with plant care. This work was funded by Grant No. LO1204 (Sustainable development of research in the Centre of the Region Haná) from the National Program of Sustainability I, MEYS, Czech Republic.

REFERENCES

Ambrose, J. C., & Cyr, R. (2007). The kinesin ATK5 functions in early spindle assembly in *Arabidopsis*. *Plant Cell*, *19*, 226–236.

Ambrose, J. C., Li, W., Marcus, A., Ma, H., & Cyr, R. (2005). A minus-end-directed kinesin with plus-end tracking protein activity is involved in spindle morphogenesis. *Molecular Biology of the Cell*, *16*, 1584–1592.

Bannigan, A., Scheible, W.-R., Lukowitz, W., Fagerstrom, C., Wadsworth, P., Somerville, C., et al. (2007). A conserved role for kinesin-5 in plant mitosis. *Journal of Cell Science*, *120*, 2819–2827.

Baum, S. F., Dubrovsky, J. G., & Rost, T. L. (2002). Apical organization and maturation of the cortex and vascular cylinder in *Arabidopsis thaliana* (*Brassicaceae*) roots. *American Journal of Botany*, *89*, 908–920.

Beck, M., Komis, G., Ziemann, A., Menzel, D., & Šamaj, J. (2011). Mitogen-activated protein kinase 4 is involved in the regulation of mitotic and cytokinetic microtubule transitions in *Arabidopsis thaliana*. *New Phytologist*, *189*, 1069–1083.

Binarová, P., Cenklová, V., Procházková, J., Doskočilová, A., Volc, J., Vrlík, M., et al. (2006). γ-Tubulin is essential for acentrosomal microtubule nucleation and coordination of late mitotic events in *Arabidopsis*. *Plant Cell*, *18*, 1199–1212.

Binarová, P., Doležel, J., Draber, P., Heberle-Bors, E., Strnad, M., & Bögre, L. (1998). Treatment of *Vicia faba* root tip cells with specific inhibitors to cyclin-dependent kinases leads to abnormal spindle formation. *The Plant Journal*, *16*, 697–707.

Boruc, J., Weimer, A. K., Stoppin-Mellet, V., Mylle, E., Kosetsu, K., Cedeño, C., et al. (2017). Phosphorylation of MAP65-1 by Arabidopsis Aurora kinases is required for efficient cell cycle progression. *Plant Physiology*, *173*, 582–599.

Buschmann, H., Chan, J., Sanchez-Pulido, L., Andrade-Navarro, M. A., Doonan, J. H., & Lloyd, C. W. (2006). Microtubule-associated AIR9 recognizes the cortical division site at preprophase and cell-plate insertion. *Current Biology*, *16*, 1938–1943.

Buschmann, H., Dols, J., Kopischke, S., Peña, E. J., Andrade-Navarro, M. A., Heinlein, M., et al. (2015). *Arabidopsis* KCBP interacts with AIR9 but stays in the cortical division zone throughout mitosis via its MyTH4-FERM domain. *Journal of Cell Science*, *128*, 2033–2046.

Buschmann, H., Green, P., Sambade, A., Doonan, J. H., & Lloyd, C. W. (2011). Cytoskeletal dynamics in interphase, mitosis and cytokinesis analysed through *Agrobacterium*-mediated transient transformation of tobacco BY-2 cells. *New Phytologist*, *190*, 258–267.

Buschmann, H., Sambade, A., Pesquet, E., Calder, G., & Lloyd, C. W. (2010). Microtubule dynamics in plant cells. *Methods in Cell Biology*, *97*, 373–400.

Camilleri, C., Azimzadeh, J., Pastuglia, M., Bellini, C., Grandjean, O., & Bouchez, D. (2002). The Arabidopsis *TONNEAU2* gene encodes a putative novel protein phosphatase 2A

regulatory subunit essential for the control of the cortical cytoskeleton. *Plant Cell*, *14*, 833–845.

Celler, K., Fujita, M., Kawamura, E., Ambrose, C., Herburger, K., Holzinger, A., et al. (2016). Microtubules in plant cells: Strategies and methods for immunofluorescence, transmission electron microscopy and live cell imaging. In R. Gavin (Ed.), *Methods in molecular biology: Vol. 1365. Cytoskeleton methods and protocols* (pp. 155–184). New York, NY: Humana Press.

Chan, J., Calder, G. M., Doonan, J. H., & Lloyd, C. W. (2003). EB1 reveals mobile microtubule nucleation sites in *Arabidopsis*. *Nature Cell Biology*, *11*, 967–971.

Chan, J., Calder, G., Fox, S., & Lloyd, C. (2005). Localization of the microtubule end binding protein EB1 reveals alternative pathways of spindle development in Arabidopsis suspension cells. *Plant Cell*, *17*, 1737–1748.

Clough, S. J., & Bent, A. F. (1998). Floral dip: A simplified method for *Agrobacterium*-mediated transformation of *Arabidopsis thaliana*. *The Plant Journal*, *16*, 735–743.

de Luis Balaguer, M. A., Ramos-Pezzotti, M., Rahhal, M. B., Melvina, C. E., Johannes, E., Horn, T. J., et al. (2016). Multi-sample Arabidopsis growth and imaging chamber (MAGIC) for long term imaging in the ZEISS Lightsheet Z.1. *Developmental Biology*, *419*, 19–25.

Demmerle, J., Innocent, C., North, A. J., Ball, G., Müller, M., & Miron, E. (2017). Strategic and practical guidelines for successful structured illumination microscopy. *Nature Protocols*, *12*, 988–1010.

Dolan, L., Janmaat, K., Willemsen, V., Linstead, P., Poethig, S., Roberts, K., et al. (1993). Cellular organisation of the *Arabidopsis thaliana* root. *Development*, *119*, 71–84.

Dunsch, A. K., Hammond, D., Lloyd, J., Schermelleh, L., Gruneberg, U., & Barr, F. A. (2012). Dynein light chain 1 and a spindle-associated adaptor promote dynein asymmetry and spindle orientation. *Journal of Cell Biology*, *198*, 1039–1054.

Granger, C. L., & Cyr, R. J. (2000). Microtubule reorganization in tobacco BY-2 cells stably expressing GFP-MBD. *Planta*, *210*, 502–509.

Gunning, B. E., Hardham, A. R., & Hughes, J. E. (1978). Pre-prophase bands of microtubules in all categories of formative and proliferative cell division in *Azolla* roots. *Planta*, *143*, 145–160.

Hasezawa, S., Ueda, K., & Kumagai, F. (2000). Time-sequence observations of microtubule dynamics throughout mitosis in living cell suspensions of stable transgenic *Arabidopsis*-direct evidence for the origin of cortical microtubules at M/G1 interface. *Plant and Cell Physiology*, *41*, 244–250.

Ho, C. M., Hotta, T., Kong, Z., Zeng, C. J., Sun, J., Lee, Y. R., et al. (2011). Augmin plays a critical role in organizing the spindle and phragmoplast microtubule arrays in *Arabidopsis*. *Plant Cell*, *23*, 2606–2618.

Hotta, T., Konq, Z., Ho, C. M., Zenq, C. J., Horio, T., Fonq, S., et al. (2012). Characterization of the *Arabidopsis* augmin complex uncovers its critical function in the assembly of the acentrosomal spindle and phragmoplast microtubule arrays. *Plant Cell*, *24*, 14494–14509.

Janski, N., Masoud, K., Batzenschlager, M., Herzog, E., Evrard, J. L., Houlné, G., et al. (2012). The GCP3-interacting proteins GIP1 and GIP2 are required for γ-tubulin complex protein localization, spindle integrity, and chromosomal stability. *Plant Cell*, *24*, 1171–1187.

Karimi, M., Bleys, A., Vanderhaeghen, R., & Hilson, P. (2007). Building blocks for plant gene assembly. *Plant Physiology*, *145*, 1183–1191.

Kawamura, E., Himmelspach, R., Rashbrooke, M. C., Whittington, A. T., Gale, K. R., Collings, D. A., et al. (2006). MICROTUBULE ORGANIZATION 1 regulates structure and function of microtubule arrays during mitosis and cytokinesis in the Arabidopsis root. *Plant Physiology*, *140*, 102–114.

Kilmartin, J. V. (2014). Lessons from yeast: The spindle pole body and the centrosome. *Philosophical Transactions of the Royal Society of London. Series B, Biological Sciences*, *369*, 20130456. https://doi.org/10.1098/rstb.2013.0456.

Kirik, A., Ehrhardt, D. W., & Kirik, V. (2012). *TONNEAU2/FASS* regulates the geometry of microtubule nucleation and cortical array organization in interphase *Arabidopsis* cells. *Plant Cell*, *24*, 1158–1170.

Kirik, V., Herrmann, U., Parupalli, C., Sedbrook, J. C., Ehrhardt, D. W., & Hülskamp, M. (2007). CLASP localizes in two discrete patterns on cortical microtubules and is required for cell morphogenesis and cell division in *Arabidopsis*. *Journal of Cell Science*, *120*, 4416–4425.

Kner, P., Chhun, B. B., Griffis, E. R., Winoto, L., & Gustafsson, M. G. (2009). Super-resolution video microscopy of live cells by structured illumination. *Nature Methods*, *6*, 339–342.

Kojo, K. H., Higaki, T., Kutsuna, N., Yoshida, Y., Yasuhara, H., & Hasezawa, S. (2013). Roles of cortical actin microfilament patterning in division plane orientation in plants. *Plant and Cell Physiology*, *54*, 1491–1503.

Kojo, K. H., Yasuhara, H., & Hasezawa, S. (2014). Time-sequential observation of spindle and phragmoplast orientation in BY-2 cells with altered cortical actin microfilament patterning. *Plant Signaling & Behavior, 9*, e29579.

Komaki, S., Abe, T., Coutuer, S., Inzé, D., Russinova, E., & Hashimoto, T. (2010). Nuclear-localized subtype of end-binding 1 protein regulates spindle organization in *Arabidopsis*. *Journal of Cell Science*, *123*, 451–459.

Komis, G., Luptovčiak, I., Ovečka, M., Samakovli, D., Šamajová, O., & Šamaj, J. (2017). Katanin effects on dynamics of cortical microtubules and mitotic arrays in *Arabidopsis thaliana* revealed by advanced live-cell imaging. *Frontiers in Plant Science*, *8*, 866.

Komis, G., Mistrik, M., Šamajová, O., Doskočilová, A., Ovečka, M., Illés, P., et al. (2014). Dynamics and organization of cortical microtubules as revealed by superresolution structured illumination microscopy. *Plant Physiology*, *165*, 129–148.

Komis, G., Mistrik, M., Šamajová, O., Ovečka, M., Bartek, J., & Šamaj, J. (2015). Superresolution live imaging of plant cells using structured illumination microscopy. *Nature Protocols*, *10*, 1248–1263.

Kong, Z., Hotta, T., Lee, Y. R., Horio, T., & Liu, B. (2010). The γ-tubulin complex protein GCP4 is required for organizing functional microtubule arrays in *Arabidopsis thaliana*. *Plant Cell*, *22*, 191–204.

Kosetsu, K., Matsunaga, S., Nakagami, H., Colcombet, J., Sasabe, M., Soyano, T., et al. (2010). The MAP kinase MPK4 is required for cytokinesis in *Arabidopsis thaliana*. *Plant Cell*, *22*, 3778–3790.

Krysan, P. J., Jester, P. J., Gottwald, J. R., & Sussman, M. R. (2002). An Arabidopsis mitogen-activated protein kinase kinase kinase gene family encodes essential positive regulators of cytokinesis. *Plant Cell*, *14*, 1109–1120.

Laissue, P. P., Alghamdi, R. A., Tomancak, P., Reynaud, E. G., & Shroff, H. (2017). Assessing phototoxicity in live fluorescence imaging. *Nature Methods*, *14*, 657–661.

Lee, Y. R., Li, Y., & Liu, B. (2007). Two *Arabidopsis* phragmoplast-associated kinesins play a critical role in cytokinesis during male gametogenesis. *Plant Cell*, *19*, 2595–2605.

Li, H., Sun, B., Sasabe, M., Deng, X., Machida, Y., Lin, H., et al. (2017). Arabidopsis MAP65-4 plays a role in phragmoplast microtubule organization and marks the cortical cell division site. *New Phytologist*, *215*, 187–201.

Lindeboom, J. J., Nakamura, M., Hibbel, A., Shundyak, K., Gutierrez, R., Ketelaar, T., et al. (2013). A mechanism for reorientation of cortical microtubule arrays driven by microtubule severing. *Science, 342*, e1245533.

Littlejohn, G. R., Gouveia, J. D., Edner, C., Smirnoff, N., & Love, J. (2010). Perfluorodecalin enhances in vivo confocal microscopy resolution of *Arabidopsis thaliana* mesophyll. *New Phytologist*, *186*, 1018–1025.

Littlejohn, G. R., Mansfield, J. C., Christmas, J. T., Witterick, E., Fricker, M. D., Grant, M. R., et al. (2014). An update: Improvements in imaging perfluorocarbon-mounted plant leaves with implications for studies of plant pathology, physiology, development and cell biology. *Frontiers in Plant Science*, *5*, 140.

Lucas, J. R., Courtney, S., Hassfurder, M., Dhingra, S., Bryant, A., & Shaw, S. L. (2011). Microtubule-associated proteins MAP65-1 and MAP65-2 positively regulate axial cell growth in etiolated Arabidopsis hypocotyls. *Plant Cell*, *23*, 1889–1903.

Lucas, J. R., & Shaw, S. L. (2012). MAP65-1 and MAP65-2 promote cell proliferation and axial growth in Arabidopsis roots. *The Plant Journal*, *71*, 454–463.

Lukowitz, W., Roeder, A., Parmenter, D., & Somerville, C. (2004). A MAPKK kinase gene regulates extra-embryonic cell fate in *Arabidopsis*. *Cell*, *116*, 109–119.

Maizel, A., von Wangenheim, D., Federici, F., Haseloff, J., & Stelzer, E. H. K. (2011). High-resolution live imaging of plant growth in near physiological bright conditions using light sheet fluorescence microscopy. *The Plant Journal*, *68*, 377–385.

Marc, J., Granger, C. L., Brincat, J., Fisher, D. D., Kao, T.-H., McCubbin, A. G., et al. (1998). A *GFP-MAP4* reporter gene for visualizing cortical microtubule rearrangements in living epidermal cells. *Plant Cell*, *10*, 1927–1940.

Marcus, A. I., Li, W., Ma, H., & Cyr, R. J. (2003). A kinesin mutant with an atypical bipolar spindle undergoes normal mitosis. *Molecular Biology of the Cell*, *14*, 1717–1726.

Moschou, P. N., Smertenko, A. P., Minina, E. A., Fukada, K., Savenkov, E. I., Robert, S., et al. (2013). The caspase-related protease separase (extra spindle poles) regulates cell polarity and cytokinesis in *Arabidopsis*. *Plant Cell*, *25*, 2171–2186.

Müller, J., Beck, M., Mettbach, U., Komis, G., Hause, G., Menzel, D., et al. (2010). Arabidopsis MPK6 is involved in cell division plane control during early root development, and localizes to the pre-prophase band, phragmoplast, trans-Golgi network and plasma membrane. *The Plant Journal*, *61*, 234–248.

Müller, S., Fuchs, E., Ovečka, M., Wysocka-Diller, J., Benfey, P. N., & Hauser, M. T. (2002). Two new loci, *PLEIADE* and *HYADE*, implicate organ-specific regulation of cytokinesis in Arabidopsis. *Plant Physiology*, *130*, 312–324.

Müller, S., Han, S., & Smith, L. G. (2006). Two kinesins are involved in the spatial control of cytokinesis in *Arabidopsis thaliana*. *Current Biology*, *16*, 888–894.

Müller, S., Smertenko, A., Wagner, V., Heinrich, M., Hussey, P. J., & Hauser, M. T. (2004). The plant microtubule-associated protein AtMAP65-3/PLE is essential for cytokinetic phragmoplast function. *Current Biology*, *14*, 412–417.

Murata, T., Sano, T., Sasabe, M., Nonaka, S., Higashiyama, T., Hasezawa, S., et al. (2013). Mechanism of microtubule array expansion in the cytokinetic phragmoplast. *Nature Communications*, *4*, 1967.

Nakamura, M., Ehrhardt, D. W., & Hashimoto, T. (2010). Microtubule and katanin-dependent dynamics of microtubule nucleation complexes in the acentrosomal *Arabidopsis* cortical array. *Nature Cell Biology*, *12*, 1064–1070.

Novák, D., Kuchařová, A., Ovečka, M., Komis, G., & Šamaj, J. (2016). Develomental nuclear localization and quantification of GFP-tagged EB1c in *Arabidopsis* root using light-sheet microscopy. *Frontiers in Plant Science*, *6*, 1187.

Oh, S. A., Allen, T., Kim, G. J., Sidorova, A., Borg, M., Park, S. K., et al. (2012). Arabidopsis fused kinase and the kinesin-12 subfamily constitute a signalling module required for phragmoplast expansion. *The Plant Journal*, *72*, 308–319.

Oh, S. A., Johnson, A., Smertenko, A., Rahman, D., Park, S. K., Hussey, P. J., et al. (2005). A divergent cellular role for the FUSED kinase family in the plant-specific cytokinetic phragmoplast. *Current Biology*, *15*, 2107–2111.

Ovečka, M., Vaškebová, L., Komis, G., Luptovčiak, I., Smertenko, A., & Šamaj, J. (2015). Preparation of plants for developmental and cellular imaging by light-sheet microscopy. *Nature Protocols*, *10*, 1234–1247.

Panteris, E., & Adamakis, I. D. (2012). Aberrant microtubule organization in dividing root cells of p60-katanin mutants. *Plant Signaling & Behavior*, *7*, 16–18.

Panteris, E., Apostolakos, P., & Galatis, B. (1995). The effect of taxol on *Triticum* preprophase root cells: Preprophase microtubule band organization seems to depend on new microtubule assembly. *Protoplasma*, *186*, 72–78.

Park, G. T., Frost, J. M., Park, J. S., Kim, T. H., Lee, J. S., Oh, S. A., et al. (2014). Nucleoporin MOS7/Nup88 is required for mitosis in gametogenesis and seed development in *Arabidopsis*. *Proceedings of the National Academy of Sciences of the United States of America*, *111*, 18393–18398.

Pastuglia, M., Azimzadeh, J., Goussot, M., Camilleri, C., Belcram, K., Evrard, J. L., et al. (2006). γ-Tubulin is essential for microtubule organization and development in *Arabidopsis*. *Plant Cell*, *18*, 1412–1425.

Pietra, S., Gustavsson, A., Kiefer, C., Kalmbach, L., Hörstedt, P., Ikeda, Y., et al. (2013). *Arabidopsis SABRE* and *CLASP* interact to stabilize cell division plane orientation and planar polarity. *Nature Communications*, *4*, 2779.

Pignocchi, C., Minns, G. E., Nesi, N., Koumproglou, R., Kitsios, G., Benning, C., et al. (2009). ENDOSPERM DEFECTIVE1 is a novel microtubule-associated protein essential for seed development in *Arabidopsis*. *Plant Cell*, *21*, 90–105.

Prosser, S. L., & Pelletier, L. (2017). Mitotic spindle assembly in animal cells: A fine balancing act. *Nature Reviews Molecular Cell Biology*, *18*, 187–201.

Rasmussen, C. G., Humphries, J. A., & Smith, L. G. (2011). Determination of symmetric and asymmetric division planes in plant cells. *Annual Review of Plant Biology*, *62*, 387–409.

Samac, D. A., & Austin-Phillips, S. (2006). Alfalfa (*Medicago sativa* L.). In K. Wang (Ed.), *Methods in molecular biology: Agrobacterium protocols: Vol. 1223* (pp. 301–311). New York, NY: Springer. https://doi.org/10.1007/978-1-4939-1695-5_17.

Sampathkumar, A., Lindeboom, J. J., Debolt, S., Gutierrez, R., Ehrhardt, D. W., Ketelaar, T., et al. (2011). Live cell imaging reveals structural associations between the actin and microtubule cytoskeleton in *Arabidopsis*. *Plant Cell*, *23*, 2302–2313.

Samuels, A. L., Giddings, T. H., Jr., & Staehelin, L. A. (1995). Cytokinesis in tobacco BY-2 and root tip cells: A new model of cell plate formation in higher plants. *Journal of Cell Biology*, *130*, 1345–1357.

Scheres, B., Benfey, P., & Dolan, L. (2002). Root development. *The Arabidopsis Book, 1*, e0101.

Shaw, S. L., Kamyar, R., & Ehrhardt, D. W. (2003). Sustained microtubule treadmilling in *Arabidopsis* cortical arrays. *Science*, *300*, 1715–1718.

Shaw, S. L., & Lucas, J. (2011). Intrabundle microtubule dynamics in the *Arabidopsis* cortical array. *Cytoskeleton*, *68*, 56–67.

Smékalová, V., Luptovčiak, I., Komis, G., Šamajová, O., Ovečka, M., Doskočilová, A., et al. (2014). Involvement of YODA and mitogen activated protein kinase 6 in Arabidopsis post-embryogenic root development through auxin up-regulation and cell division plane orientation. *New Phytologist*, *203*, 1175–1193.

Smertenko, A., Assaad, F., Baluška, F., Bezanilla, M., Buschmann, H., Drakakaki, G., et al. (2017). Plant cytokinesis: Terminology for structures and processes. *Trends in Cell Biology*, *27*, 885–894.

Söllner, R., Glässer, G., Wanner, G., Somerville, C. R., Jürgens, G., & Assaad, F. F. (2002). Cytokinesis-defective mutants of Arabidopsis. *Plant Physiology*, *129*, 678–690.

Spinner, L., Gadeyne, A., Belcram, K., Goussot, M., Moison, M., Duroc, Y., et al. (2013). A protein phosphatase 2A complex spatially controls plant cell division. *Nature Communications*, *4*, 1863.

Steiner, A., Rybak, K., Altmann, M., McFarlane, H. E., Klaeger, S., Nguyen, N., et al. (2016). Cell cycle-regulated PLEIADE/AtMAP65-3 links membrane and microtubule dynamics during plant cytokinesis. *The Plant Journal*, *88*, 531–541.

Strompen, G., El Kasmi, F., Richter, S., Lukowitz, W., Assaad, F. F., Jürgens, G., et al. (2002). The *Arabidopsis HINKEL* gene encodes a kinesin-related protein involved in cytokinesis and is expressed in a cell cycle-dependent manner. *Current Biology*, *22*, 153–158.

Tanaka, H., Ishikawa, M., Kitamura, S., Takahashi, Y., Soyano, T., Machida, C., et al. (2004). The *AtNACK1/HINKEL* and *STUD/TETRASPORE/AtNACK2* genes, which encode functionally redundant kinesins, are essential for cytokinesis in *Arabidopsis*. *Genes to Cells*, *9*, 1199–1211.

Twell, D., Park, S. K., Hawkins, T. J., Schubert, D., Schmidt, R., Smertenko, A., et al. (2002). MOR1/GEM1 has an essential role in the plant-specific cytokinetic phragmoplast. *Nature Cell Biology*, *4*, 711–714.

Van Damme, D., De Rybel, B., Gudesblat, G., Demidov, D., Grunewald, W., De Smet, I., et al. (2011). Arabidopsis α aurora kinases function in formative cell division plane orientation. *Plant Cell*, *23*, 4013–4024.

Vertii, A., Hehnly, H., & Doxsey, S. (2016). The centrosome, a multitalented renaissance organelle. *Cold Spring Harbor Perspectives in Biology*, *8*, a025049. https://doi.org/10.1101/cshperspect.a025049.

von Wangenheim, D., Daum, G., Lohmann, J. U., Stelzer, E. K., & Maizel, A. (2014). Live imaging of Arabidopsis development. *Methods in Molecular Biology*, *1062*, 539–550.

Vos, J. W., Dogterom, M., & Emons, A. M. (2004). Microtubules become more dynamic but not shorter during preprophase band formation: A possible "search-and-capture" mechanism for microtubule translocation. *Cell Motility and the Cytoskeleton*, *57*, 246–258.

Vyplelová, P., Ovečka, M., & Šamaj, J. (2017). Alfalfa root growth rate correlates with progression of microtubules during mitosis and cytokinesis as revealed by environmental light-sheet microscopy. *Frontiers in Plant Science*, *8*, 1870.

Walker, K. L., Müller, S., Moss, D., Ehrhardt, D. W., & Smith, L. G. (2007). Arabidopsis TANGLED identifies the division plane throughout mitosis and cytokinesis. *Current Biology*, *17*, 1827–1836.

Whittington, A. T., Vugrek, O., Wei, K. J., Hasenbein, N. G., Sugimoto, K., Rashbrooke, M. C., et al. (2001). MOR1 is essential for organizing cortical microtubules in plants. *Nature*, *411*, 610–613.

Wick, S. M., & Duniec, J. (1983). Immunofluorescence microscopy of tubulin and microtubule arrays in plant cells. I. Preprophase band development and concomitant appearance of nuclear envelope-associated tubulin. *Journal of Cell Biology*, *97*, 235–243.

Wu, S. Z., & Bezanilla, M. (2014). Myosin VIII associates with microtubule ends and together with actin plays a role in guiding plant cell division. *eLife, 3*, 03498. https://doi.org/10.7554/eLife.03498.

Wu, S., Scheible, W. R., Schindelasch, D., Van Den Daele, H., De Veylder, L., & Baskin, T. I. (2010). A conditional mutation in *Arabidopsis thaliana* separase induces chromosome non-disjunction, aberrant morphogenesis and cyclin B1;1 stability. *Development*, *137*, 953–961.

Wynne, D. J., & Funabiki, H. (2016). Heterogeneous architecture of vertebrate kinetochores revealed by three-dimensional superresolution fluorescence microscopy. *Molecular Biology of the Cell*, *27*, 3395–3404.

Xu, X. M., Zhao, Q., Rodrigo-Peiris, T., Brkljacic, J., He, C. S., Müller, S., et al. (2008). RanGAP1 is a continuous marker of the *Arabidopsis* cell division plane. *Proceedings of the National Academy of Sciences of the United States of America*, *105*, 18637–18642.

Yamada, M., & Goshima, G. (2017). Mitotic spindle assembly in land plants: Molecules and mechanisms. *Biology*, *6*, 6. https://doi.org/10.3390/biology6010006.

Yoneda, A., Akatsuka, M., Hoshino, H., Kumagai, F., & Hasezawa, S. (2005). Decision of spindle poles and division plane by double preprophase bands in a BY-2 cell line expressing GFP-tubulin. *Plant and Cell Physiology*, *46*, 531–538.

Zeng, C. J., Lee, Y. R., & Liu, B. (2009). The WD40 repeat protein NEDD1 functions in microtubule organization during cell division in *Arabidopsis thaliana*. *Plant Cell*, *21*, 1129–1140.

Research article

Alfalfa root growth rate correlates with progression of microtubules during mitosis and cytokinesis as revealed by environmental light-sheet microscopy.

Illésová (Vyplelová) P*, Ovečka M*, Šamaj J.

Frontiers in Plant Science 2017; 8: 1870. * joined first authors

IF 4,298

frontiers in Plant Science

ORIGINAL RESEARCH
published: 30 October 2017
doi: 10.3389/fpls.2017.01870

Alfalfa Root Growth Rate Correlates with Progression of Microtubules during Mitosis and Cytokinesis as Revealed by Environmental Light-Sheet Microscopy

*Petra Vyplelová†, Miroslav Ovečka† and Jozef Šamaj**

Department of Cell Biology, Centre of the Region Haná for Biotechnological and Agricultural Research, Palacký University Olomouc, Olomouc, Czechia

OPEN ACCESS

Edited by:
Diane C. Bassham,
Iowa State University, United States

Reviewed by:
Frantisek Baluska,
University of Bonn, Germany
Taras P. Pasternak,
Albert Ludwigs University of Freiburg, Germany

****Correspondence:***
Jozef Šamaj
jozef.samaj@upol.cz

†These authors have contributed equally to this work.

Specialty section:
This article was submitted to Plant Cell Biology, a section of the journal Frontiers in Plant Science

Received: *22 August 2017*
Accepted: *13 October 2017*
Published: *30 October 2017*

Citation:
Vyplelová P, Ovečka M and Šamaj J (2017) Alfalfa Root Growth Rate Correlates with Progression of Microtubules during Mitosis and Cytokinesis as Revealed by Environmental Light-Sheet Microscopy. Front. Plant Sci. 8:1870. doi: 10.3389/fpls.2017.01870

Cell division and expansion are two fundamental biological processes supporting indeterminate root growth and development of plants. Quantitative evaluations of cell divisions related to root growth analyses have been performed in several model crop and non-crop plant species, but not in important legume plant *Medicago sativa*. Light-sheet fluorescence microscopy (LSFM) is an advanced imaging technique widely used in animal developmental biology, providing efficient fast optical sectioning under physiological conditions with considerably reduced phototoxicity and photobleaching. Long-term 4D imaging of living plants offers advantages for developmental cell biology not available in other microscopy approaches. Recently, LSFM was implemented in plant developmental biology studies, however, it is largely restricted to the model plant *Arabidopsis thaliana*. Cellular and subcellular events in crop species and robust plant samples have not been studied by this method yet. Therefore we performed LSFM long-term live imaging of growing root tips of transgenic alfalfa plants expressing the fluorescent molecular marker for the microtubule-binding domain (GFP-MBD), in order to study dynamic patterns of microtubule arrays during mitotic cell division. Quantitative evaluations of cell division progress in the two root tissues (epidermis and cortex) clearly indicate that root growth rate is correlated with duration of cell division in alfalfa roots. Our results favor non-invasive environmental LSFM as one of the most suitable methods for qualitative and quantitative cellular and developmental imaging of living transgenic legume crops.

Keywords: cell division, developmental imaging, light-sheet microscopy, *Medicago sativa*, microtubules, root growth, transgenic crops

INTRODUCTION

Plant growth and development is directed by key biological processes establishing proper morphogenetic pattern. Among them, cell division plays an indispensable role. Cell divisions in the root meristem are followed by subsequent cellular expansion in the root elongation zone and ensure sustained development of roots. Plant mitotic cell division is dynamic process controlled by rearrangements of microtubules that are gradually transformed into different microtubule

arrays during mitosis and cytokinesis. Before the onset of cell division, cortical microtubules are narrowing to form the preprophase band (PPB) defining the cell division plane (Rasmussen et al., 2011). After nuclear envelope breakdown and the initiation of the mitotic process, microtubules form the mitotic spindle responsible for chromosome partitioning into daughter cells during mitosis (Vos et al., 2004; Marcus et al., 2005; Azimzadeh et al., 2008). This bipolar spindle is formed with its long axis oriented perpendicularly to the PPB plane (Van Damme et al., 2007; Van Damme, 2009). During cytokinesis the bipolar spindle is transformed into the phragmoplast. Phragmoplast serves as a guide for cell plate assembly and the subsequent formation of new cell wall separating two daughter cells (Lee and Liu, 2013).

Complex analyses of cell division and elongation patterns during primary root growth and development were mostly performed in model plants such as Arabidopsis (e.g., Beemster and Baskin, 1998; Beemster et al., 2002; Lavrekha et al., 2017), maize (e.g., Sacks et al., 1997), barley (e.g., Kirschner et al., 2017), tobacco (e.g., Pasternak et al., 2017) and rice (e.g., Rebouillat et al., 2009; Ni et al., 2014). These studies were mostly based on 3D reconstruction analyses from fixed plant samples. Functional studies on dynamics of microtubules during mitotic cell division were almost exclusively conducted in two model species, Arabidopsis and tobacco. The microtubule cytoskeleton in living plant cells can be visualized using several microtubule-specific molecular reporters. One such reporter is the green fluorescent protein (GFP) fusion with the microtubule binding domain (MBD) of the mammalian microtubule-associated protein 4 (MAP4; GFP-MBD). Dynamics, reorientation, and reorganization of cortical microtubules with GFP-MBD as a molecular microtubule marker was originally studied using laser scanning confocal microscope in living epidermal cells (Marc et al., 1998).

Nowadays there are several microscopic approaches to study microtubules in living plant cells of model plant species during cell division. Confocal laser scanning microscopy (CLSM) and spinning disk (SD) microscopy are most popular ones. From practical point of view, dimensions of tobacco BY-2 and Arabidopsis suspension cells, as well as easily cultured Arabidopsis seedling plants facilitate utilization of conventional microscopy methods for live-cell imaging of mitotic microtubules in dividing cells. Another important aspect of microscopic cell division studies on model plants is availability of firmly established transformation protocols and protein tagging approaches in Arabidopsis and tobacco. Some of these studies analyzed stem cell divisions (Campilho et al., 2006) and determined the role of MAP65-1 phosphorylation in cell cycle progression (Boruc et al., 2017) in the Arabidopsis root, visualized Arabidopsis zygote cell divisions (Kimata et al., 2016), described microtubule arrays during cell division of Arabidopsis suspension cells (Calder et al., 2015), or visualized preprophase band (Dhonukshe and Gadella, 2003), mitotic spindle (Dhonukshe et al., 2006; Gaillard et al., 2008), and phragmoplast (Murata et al., 2013) in dividing tobacco BY-2 cells. Further, Arabidopsis γ-tubulin double mutants *tubg1-1* and *tubg2-1* expressing GFP-MBD microtubule marker showed abnormal spindles, asymmetric phragmoplasts, and disorganization of cortical microtubule arrays (Pastuglia et al., 2006). Time-lapse live cell imaging using CLSM was used to document abnormalities of mitotic microtubule arrays and to monitor the duration of mitosis in *anp2anp3* and *mpk4* mutants (Beck et al., 2011). Arabidopsis *fh1-1* mutant expressing GFP-MBD showed increased instability of microtubules (Rosero et al., 2016). SD microscopy was used mostly to study dynamics of cortical microtubule arrays. Bundling of cortical microtubules and speed of microtubule growth and shortening on plus and minus ends were studied in living hypocotyl cells of Arabidopsis (Shaw and Lucas, 2011) while dynamic microtubule nucleation of cortical arrays has been done in Arabidopsis wild type, *katanin* and *gcp2-1* mutants (Nakamura et al., 2010).

Nevertheless, environmental and long-term imaging are compromised in such conventional microscopic methods as CLSM and SD because living model plants are exposed to several stresses (artificial horizontal position, tight microscopic chamber with limited nutrients, and pressure between microscopic slides) and suffer from high energy illumination causing undesirable phototoxicity and photodamage. In comparison to Arabidopsis, crop species including alfalfa typically have more robust habitus and their roots are thicker because they consist from more tissue layers. Consequently, mounting of the whole alfalfa seedlings to classical horizontally-positioned microscopy stage is more challenging and affects fitness of such samples during long-term experiments. Obviously, microscopic techniques like CLSM and SD also suffer from serious limitations in imaging depth. Finally, all commercial CLSM and SD platforms are based on horizontal stages, not allowing for living plants to be observed normally oriented with respect to the gravity vector. All these disadvantages can be avoided by using light-sheet fluorescence microscopy (LSFM). Optical sectioning of the sample with excitation sheet of light is very fast. Importantly, excitation of fluorophores is restricted within the light-sheet volume, which effectively eliminates out-of-focus fluorescence and bleaching. Emitted fluorescence light is detected by independent orthogonally-positioned detection objective. Focal plane of the light-sheet is harmonized with the focal plane of the detection objective and thus, very thin layer of the sample is detected by spherical aberration-free imaging. Sample can be freely rotated with respect to the light-sheet plane illumination allowing multi-angular image acquisition. Fast imaging mode of LSFM ensures that imaged cells are illuminated with very low level of excitation energy (Stelzer, 2015). Finally, in some custom-made and commercial LSFM platforms, sample loading can be done vertically allowing typical gravitropic growth of plants during the course of imaging. All these technical benefits bring LSFM to the forefront of current standards for proper spatial, temporal and physiological imaging of developmental processes. So far the applications of LSFM in plants have been preferentially restricted to the developmental imaging of primary or lateral roots in Arabidopsis (Maizel et al., 2011; Lucas et al., 2013; Rosquete et al., 2013; Vermeer et al., 2014; Ovečka et al., 2015; von Wangenheim et al., 2016). Subcellular localizations of cytoskeletal components by LSFM in Arabidopsis are very few, and include structure and dynamics of both microtubule and

actin cytoskeleton in different organs (Ovečka et al., 2015), cell division in root epidermis (Maizel et al., 2011) and developmental imaging of EB1c in cells of different tissues and developmental zones of the root tip (Novák et al., 2016).

Generally, studies on cellular distributions of fluorescently-labeled proteins in *M. sativa* are more difficult due to the limited availability of established molecular tools and efficient transformation techniques. In contrast to Arabidopsis and tobacco, there are only scarce reports on cytoskeletal dynamics during cell division in *Medicago sativa*. It is known that transitions between G1/S and G2/M phases are controlled by cyclin-dependent Ser/Thr kinases, among others also by *M. sativa* kinase CDKB2;1 (Joubès et al., 2000). This kinase is activated in mitotic cells and it is localized in PPB, perinuclear ring in early prophase, mitotic spindle, and phragmoplast (Mészáros et al., 2000). Activity of CDKB2;1 is controlled by protein phosphatase PP2A which affects microtubule organization during the mitosis (Ayaydin et al., 2000). However, both organization and dynamics of microtubules was characterized only in developing and Nod factor-treated root hairs of *Medicago truncatula* (Sieberer et al., 2002, 2005; Timmers et al., 2007). In addition, actin cytoskeleton was visualized in interface and post-mitotic root cells and in root hairs using Plastin-GFP and GFP-mTalin in *M. truncatula* (Voigt et al., 2005). Here we employed for the first time LSFM for long-term live cell imaging of GFP-tagged microtubules in thicker roots of a legume crop plant. We performed quantitative study of root growth rate and duration of individual mitotic stages in diverse tissues of robust roots of transgenic *M. sativa* plants originating from somatic embryogenesis that carried GFP-MBD microtubule marker. We show positive correlation between root growth rate and dynamic patterns of microtubule arrays in dividing cells during continuous root development.

MATERIALS AND METHODS

Stable Transformation of *Medicago sativa*

M. sativa stable transformation has been performed with *Agrobacterium tumefaciens* strain GV3101 containing construct carrying microtubule-binding domain (MBD) of the mammalian MICROTUBULE-ASSOCIATED PROTEIN 4 (MAP4) fused to GFP driven by constitutive 35S promoter. N-terminal GFP fusion with rifampicin and kanamycin resistance was prepared by classical cloning method in pCB302 vector with herbicide phosphinothricin as the selection marker *in planta*. Phosphinothricin has been added to each subculture medium to control successful transformation. The transformation procedure was performed according to protocol for efficient transformation of alfalfa described by Samac and Austin-Phillips (2006). Highly responsive cultivar Regen SY (RSY; Bingham, 1991) of *M. sativa* has been selected. Well-developed leaves at the third node from the shoot apex were used as a source plant material. Leaves explanted from plants were surface sterilized, cut in half and wounded on the surface with sterile scalpel blade. They were incubated with overnight grown *A. tumefaciens* culture with cell density between 0.6 and 0.8 at A_{600} nm for 30 min. Formation of calli and somatic embryos as well as induction and development of shoots and roots were achieved by transferring culture on the appropriate media (Schenk and Hildebrant medium for *A. tumefaciens* inoculation, Gamborg medium for cocultivation, callus initiation and embryo formation and Murashige and Skoog media for plant rooting, development and maintenance) for appropriate time in the culture chamber at 22°C, 50% humidity and 16/8 h light/dark photoperiod (Samac and Austin-Phillips, 2006). Regenerated plants were maintained on media with selective phosphinothricin marker and tested for the presence of GFP fusion proteins using fluorescence microscope. Transgenic *M. sativa* plants were further clonally propagated *in vitro* via somatic embryogenesis from leaf explants. Received somatic embryos stably expressing *35S::GFP:MBD* construct were used in further experiments.

Plant Material and Sample Preparation for Light-Sheet Microscopy Imaging

Transgenic somatic embryos carrying *35S::GFP:MBD* construct with well-developed root poles were separated, individually transferred and inserted vertically into solidified Murashige and Skoog-based root and plant development medium (MMS) or into Murashige and Skoog plant maintaining medium (MS). Embryos were enclosed from the upper part by fluorinated ethylene propylene (FEP) tube with an inner diameter of 4.2 mm and wall thickness of 0.2 mm (Wolf-Technik, Germany). FEP tubes were inserted into the culture medium carefully to enclose individual somatic embryo and surrounding medium inside of the tube. After 1–2 days of somatic embryo stabilization and after visual inspection of the root pole which was starting elongation, such FEP tube with somatic embryo was carefully removed from culture medium and prepared for light-sheet microscopy. Sample was prepared according to the "open system" protocol for long-term live-cell imaging of *Arabidopsis thaliana* seedlings described by Ovečka et al. (2015), with a modification in the respect that *M. sativa* roots are thicker than *A. thaliana* roots. The block of the culture medium inside of the FEP tube serves as holder of the sample and simultaneously also as root growing medium. Upper green part of the somatic embryo and later on developing plantlet was in open space of the FEP tube with the access to air. Thus, the root was able to grow inside of the microscope chamber without stress during long-term experiments. After removing from the culture plate FEP tube with the sample was inserted into sterile plastic syringe (with 1 ml volume and an inner diameter of ∼5 mm), which was cut-open at the tip before use. Plastic syringe was used for fixing the sample in sample holder of the microscope. Sample holder with the sample was placed into observation chamber of the microscope tempered to 22°C using Peltier heating/cooling system. Before insertion of the sample to the microscope somatic embryo in the solidified culture medium was ejected slightly out of the FEP tube to the extent that root in the block of solidified culture medium was directly loaded into appropriate liquid medium (MMS or MS) in the microscope chamber. FEP tube was still holding the sample, but was no more surrounding the root part of the plant, which enhanced considerably quality of root deep imaging. To prevent

contamination during long-term imaging, liquid medium filling the observation chamber was filter-sterilized using a sterile syringe filter. FEP tube was sterilized using 70% ethanol and dried out before use. After insertion of the sample to the observation chamber of the light-sheet microscope and 30 min stabilization, it was prepared for imaging.

Light-Sheet Microscopy

Long-term fluorescence live-cell imaging was done with the light-sheet Z.1 system (Carl Zeiss, Germany), equipped with W Plan-Apochromat 20×/1.0 NA water immersion detection objective (Carl Zeiss, Germany) and two LSFM 10x/0.2 NA illumination objectives (Carl Zeiss, Germany). Samples were imaged using dual-side illumination by a light-sheet modulated with a pivot scan mode. GFP-MBD was visualized with excitation line 488 nm and with emission filter BP505-545. Laser excitation intensity did not exceed 3% of the laser intensity range available. Image acquisition was done every 5 min in Z-stack mode for a period of 3–12 h. Scaling of images in x, y, and z dimensions was 0.152 × 0.152 × 0.469 μm. Images were scanned in two or three views coordinated to follow each other in y axis to record root growth in long-term imaging and to prevent the movement of the growing root out of the field of only one field of view. Images were recorded with the PCO.Edge camera (PCO AG, Germany) with the exposure time 20 or 50 ms per optical section.

Measurements and Statistical Analyses

Time-lapsed images of growing roots in x-, y-, z-, and t-dimensions were acquired using Zen 2014 software, black edition (Carl Zeiss, Germany). Images in the czi format were transformed to 2D images using Maximum intensity projection function. Subsets of data containing individual dividing cells were created either with defined x- and y- dimensions from maximum intensity projection images or from original data with defined x-, y-, and z- dimensions. Root growth rate and displacement of individual cells in growing roots (representing a displacement distance of dividing cell in growing root in respect to the growth medium, Baskin, 2013) were recorded from the stage of mitotic spindle formation till the phragmoplast disappearance as well as width of PPB were measured using Line function of the Zen 2014 software. Duration of individual mitotic stages in min (stages of PPB, spindle and phragmoplast) in dividing cells was measured using Coordinate function of the Zen 2014 software. The initial stage of the measurement started at a progressive PPB narrowing which was defined by PPB width when it was in the range of 2–4 μm.

For measurement of duration of mitotic and cytokinetic stages only transverse cell divisions were selected. All parameters were measured and evaluated separately for epidermis and the first outer layer of cortex. Data from 9 individual roots were collected. After quantitative evaluation, measured roots were divided into three groups according to the root growth rate.

Final statistical data evaluation and plotting were done with Microsoft Excel software. Statistical significance was carried out using program STATISTICA 12 (StatSoft) according to one-way ANOVA and subsequent Fisher's LSD test at the level of significance of $P < 0.05$.

RESULTS

Germination of *M. sativa* Somatic Embryos

Light-sheet microscopy imaging was performed on roots of transgenic *M. sativa* plants originating from somatic embryos. After completion of somatic embryogenesis and after maturation, further development of somatic embryos required "germination," characterized by proliferation on the root pole. This was initiated by transfer of mature somatic embryos from a hormone-free to a root and plant development (MMS) inducing medium. Somatic embryos with already proliferating roots were transferred directly to plant maintaining (MS) medium. Each somatic embryo has been transferred to MMS (or MS) medium individually in such way so that the root pole of somatic embryo was carefully inserted vertically into the solidified culture medium. This ensured that further growth of the root would continue inside of the medium and in vertical orientation. Upon activation of root growth as defined by its visible elongation, such "germinating" somatic embryos were prepared for light-sheet microscopy using FEP tubes.

Root Growth Rate

Whole plantlets growing in a cylinder of solidified culture medium inside of FEP tubes were placed to the light-sheet microscope. However, due to the bulkiness of the samples, only the apical part of the root was selected for time-lapse imaging. Root growth inside of the light-sheet microscope was recorded in 5 min intervals. Due to the displacement of the continuously growing root tip out of the selected field of view, images were recorded in two or three axially overlapping fields of view. Each field of view was 292.46 × 292.46 μm and thus, recording of root growth in two successive fields of view provided a frame 580 μm long within which we were able to measure root elongation. Based on the variability among characterized roots, their elongation speed was measured over time periods ranging from 3 to 12 h. Most likely due to the somaclonal variability during somatic embryogenesis, nine individual root tips which were taken into account elongated at different extents and so they were classified into three different groups (**Figures 1A–D**) according to their root growth rate. Roots showing root growth rate in the range between 0.7 and 1.4 $\mu m.min^{-1}$ were characterized as fast-growing roots (**Figures 1A,D,E**; **Video S1**), roots with growth rate in the range of 0.2–0.5 $\mu m.min^{-1}$ were characterized as medium-growing roots (**Figures 1B,D,E**; **Video S2**) and roots with growth rate $< 0.2\,\mu m.min^{-1}$ were characterized as slow-growing roots (**Figures 1C–E**; **Video S3**). Measurement of the growth distance of representative roots from each group over a period of 3 h during light-sheet microscopy imaging yielded values ranging between 145.1 μm for a fast-growing root (**Figure 1A**) to 67.1 μm for a medium-growing root (**Figure 1B**) and 32.6 μm for a slow-growing root (**Figure 1C**). Selection of individual roots according to their root growth rate (**Figure 1D**) was taken into consideration in all further

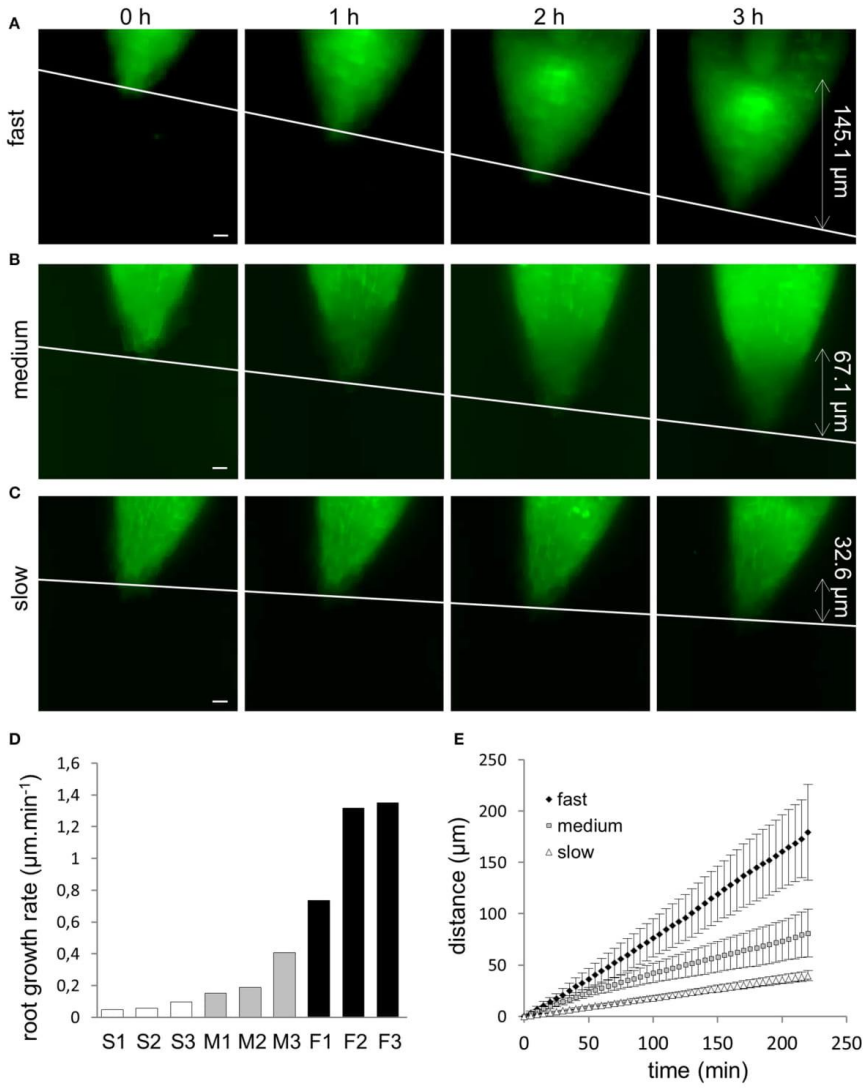

FIGURE 1 | Root growth rate of *Medicago sativa* somatic embryo-derived plantlets, expressing *35S::GFP:MBD* construct. **(A–C)** Light-sheet microscopy imaging of root growth over the period of 3 h. Based on the root growth rate, roots were sub-divided into three different groups. Representative examples of a fast-growing root, grown in a distance of 145.1 µm in 3 h **(A)**, a medium-growing root, grown in a distance of 67.1 µm in 3 h **(B)** and a slow-growing root, grown in a distance of 32.6 µm in 3 h **(C)**. Double-pointed arrows with appropriate values on the right side of images show recorded distance in µm. White line indicates displacement of the root tip in individual time points of the measurement. **(D)** Bar chart illustrating distribution of measured individual roots according to their root growth rate. White bars represent slow-growing roots (S1, S2, S3), gray bars represent medium-growing roots (M1, M2, M3) and black bars represent fast-growing roots (F1, F2, F3). **(E)** Time course of primary root growth showing a correlation between average length increase of fast-growing (♦), medium-growing (□) and slow-growing (Δ) roots and recording time from time-lapse light-sheet imaging at 5 min intervals. Bars = 20 µm **(A–C)**.

quantitative analyses. Analysis of correlation between increase in length of growing roots and a given recording time during time-lapse light-sheet imaging clearly revealed different root growth rate of fast-growing, medium-growing, and slow-growing roots (**Figure 1E**), giving proof for distribution of analyzed roots into three different groups for further quantitative analyses.

Determination of Cell Division Stages

The aim of our study was analysis of dynamic properties of microtubule arrays during cell division in root apical meristem, a tissue exhibiting active and coordinated mitotic activity. To visualize microtubule arrays during individual cell division stages in intact transgenic *M. sativa* plants originating from somatic embryos, we performed subcellular localization of MBD tagged with GFP. Progression of cells through the cell division was analyzed on the basis of quantification of the duration of individual cell division stages. Particular transition points characterizing the duration of individual cell division stages (Figure S1) were identified according to Smertenko et al. (2017). The initial stage of the measurement in preprophase and prophase, when progressive PPB narrowing occurs, was defined from the point when width of the PPB was in the range of 2–4 μm (Figure S1a). Transition from preprophase and prophase stage of cell division to mitotic division (prometaphase stage) was defined by the observation of PPB remnants and early mitotic spindle formation (Figure S1b). PPB stage duration was thus defined from PPB narrowing at late G2 phase (Figure S1a) to PPB disappearance at prometaphase (Figure S1b). Stage of mitotic spindle lasted from PPB disappearance and early mitotic spindle formation during prometaphase and finished by last stage of mitotic spindle presence at telophase (Figure S1c). After disappearance of the mitotic spindle further stages during cytokinesis were formations of early (disk) and late (ring and discontinuous) phragmoplasts (Figures S1d,e). For quantitative analysis, both early and late phragmoplast stages together were considered as one common stage (phragmoplast stage).

We analyzed cell division in the epidermis and the first outer cell layer of the root cortex of the root meristematic zone. To reveal if there are some differences or not between these two cell layers, we first characterized their behavior during root elongation growth. In addition to measuring the root elongation extend during the recording time, which was used for the calculation of the root growth rate, we measured also the distance, in which selected dividing cells in epidermis and first outer cortex were displaced along with growing roots. Each dividing cell was tracked down during root elongation and the distance of its displacement (in respect to the growth medium) from the point of mitotic spindle formation until the end of cell division (disappearance of late phragmoplast) was recorded. Results (**Figure 2**, Figure S2) corroborated the data of root growth rate (**Figure 1D**). Distances in which selected dividing cells were displaced in individual roots showed the same pattern of distribution into three different groups of roots (Figures S2a,b). Similar results were obtained when the rate of displacement of dividing cells in $\mu m.min^{-1}$ was measured during the recording of root growth (Figures S2c,d). Importantly, displacement of dividing cells (Figures S2a,b) during the recording of root growth showed no differences between epidermal (Figures S2a,c) and first outer cortex cell layer (Figure S2b,d). Comparison of duration time of individual cell division stages showed several differences between fast-, medium- and slow-growing roots. Different times were recorded in PPB stage duration (Figure S3a), mitotic spindle stage duration (Figure S3b) and phragmoplast stage duration (Figure S3c). Consistently with previous results comparing epidermis with first outer cortex layer (Figure S2), also duration time of individual cell division stages showed no considerable differences between epidermis and first outer cortex cell layer (**Figure 2**). Based on these evidences, data from individual dividing cells in epidermis and first outer cortex were

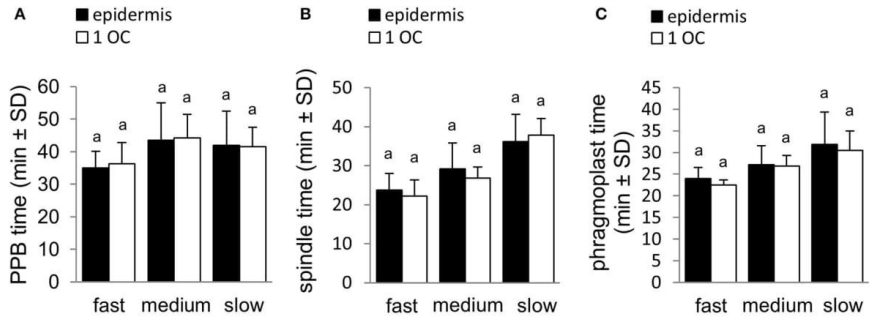

FIGURE 2 | Comparison of duration time of individual cell division stages between epidermis and first outer cortex (1 OC) cell layer. **(A)** Average PPB stage duration in the preprophase and prophase stages of cell division in epidermis and first outer cortex for fast-growing, medium-growing and slow-growing roots. **(B)** Average mitotic spindle stage duration from prometaphase to telophase during cell division in epidermis and first outer cortex for fast-growing, medium-growing and slow-growing roots. **(C)** Average phragmoplast stage duration in cytokinesis of the cell division in epidermis and first outer cortex for fast-growing, medium-growing and slow-growing roots. Letters above the bars represent statistical significance according to one-way ANOVA test at $P < 0.05$.

combined together in each root and analyzed together in further quantitative analyses.

Duration Time of Individual Cell Division Stages

Time-lapse LSFM imaging of growing roots of transgenic alfalfa plants in 5 min intervals over a period of several hours allowed recording of cells in the meristematic zone and at different stages of cell division. In particular, cells with established PPB (at late G2 phase) were monitored and their entrance to the cell division was documented in time. Preprophase and prophase stage of the cell division was identified from the stage of progressive PPB narrowing when PPB width was in the range of 2–4 μm. This time point has been set up as time 0 min. Recording of preprophase and prophase stage finished by PPB disappearance in cells entering mitosis with starting of mitotic spindle formation in prometaphase. Time-lapse recording of this stage in 5 min intervals revealed its duration for 35–40 min. Interestingly, in roots with different root growth rate this duration was different (**Figures 3A–C**). In average, preprophase and prophase stage of cell division was fastest in fast-growing roots, while duration of this stage did not differ between medium-growing and slow-growing roots (**Figure 3D**). Basically the same results were obtained after comparison of preprophase and prophase stage duration in individual roots (**Figure 3E**).

Stage of mitotic spindle was measured from disappearance of the PPB with simultaneous mitotic spindle formation through metaphase and anaphase to mitotic spindle disappearance at telophase. Measurement revealed that termination of the mitotic spindle stage at telophase was different among three groups of roots differing in their growth rate (**Figures 4A–C**). The average duration time of this stage revealed that it was shortest in fast-growing roots, significantly longer in medium-growing roots and the longest in slow-growing roots (**Figure 4D**). Comparison of mitotic spindle duration in individual roots confirmed this observation, showing shortest duration of this stage in fast-growing roots and longest duration in slow-growing roots (**Figure 4E**).

Duration of the phragmoplast stage was determined from mitotic spindle disappearance at telophase with the formation of early (disk) phragmoplast to disappearance of late (ring and discontinuous) phragmoplast at the end of cytokinesis. Consistent with the duration of previous cell division stages the termination of phragmoplast expansion also occurred at different time among the three groups of roots differing in their growth rate (**Figures 5A–C**). The average duration time of phragmoplast stage was shortest in fast-growing roots, significantly longer in medium-growing roots and the longest in slow-growing roots (**Figure 5D**). Comparison of phragmoplast stage duration in individual roots confirmed this observation (**Figure 5E**).

Correlation between Duration of Cell Division Stages and Root Growth Rate

To reveal possible relationship between speed of root growth and duration of cell division in root apical meristem we analyzed correlations between duration of individual cell division stages and root growth rates. Three groups of roots with different root growth rates were analyzed separately. Cross-comparison of average root growth rate with average duration of PPB (**Figure 6A**), mitotic spindle (**Figure 6B**), and phragmoplast (**Figure 6C**) stages revealed different tendency. Recorded data were arranged in clusters, distinctly separating groups of fast-growing, medium-growing and slow-growing roots (**Figures 6A–C**). Overall data from all individual dividing cells showing duration time of the PPB (**Figure 6D**), mitotic spindle (**Figure 6E**), and phragmoplast (**Figure 6F**) stages correlated very well with the root growth rates, and confirmed clear separation of fast-growing roots from the rest. Particularly values for roots F2 and F3 (**Figure 1D**) segregated separately in the upper part of the graphs (**Figures 6D–F**). Segregation of values measured in medium- and slow-growing roots, correlating PPB, mitotic spindle, and phragmoplast stages with root growth rates into clusters is also obvious, although less pronounced as for fast-growing roots (**Figures 6D–G**). In general, the extend of correlation between root growth rate and duration time of the PPB (**Figure 6D**), mitotic spindle (**Figure 6E**), and phragmoplast (**Figure 6F**) stages in all dividing cells of fast-, medium- and slow-growing roots is rather low, as documented by trends of correlation lines and values of correlation coefficients (**Figure 7**). Degree of correlation is rather low also for duration time of individual cell division stages compared between each other, namely between PPB and mitotic spindle (**Figure 8A**), PPB and phragmoplast (**Figure 8B**) and also between mitotic spindle and phragmoplast (**Figure 8C**). Negative slope of correlation lines (**Figure 7**) indicates a tendency to prolong cell division stages with reducing root growth rates. Thus, clustering of data recorded from individual cell division stages (**Figures 6A–F**) and clear separation of these clusters in fast-, medium-, and slow-growing roots according to cross-correlation between average duration time of the PPB, mitotic spindle, and phragmoplast stages (**Figure 6G**) represents crucial aspect of our quantitative evaluation. Collectively, these results suggest correlative regulation of cell division duration depending on the speed of root growth.

DISCUSSION

Cell division is key regulatory component of plant morphogenesis and development and one of the most frequently studied biological processes in the plant biology. Monitoring cell divisions in living multicellular plant organs require real time microscopy approach for long-term observation of intact plants that are adapted to proper physiological conditions. Live cell LSFM imaging of dividing cells could ideally resolve details of cytoskeletal division machinery with high temporal resolution. Moreover, four dimensional monitoring of cell division in organ-, tissue-, and cell type-specific context is required for fundamental understanding of cell division regulation during plant growth and development. Nowadays, different microscopy methods are used to study cell division in genetically, developmentally and microscopically-tractable plant model species. Critically important, however, is the adaptation

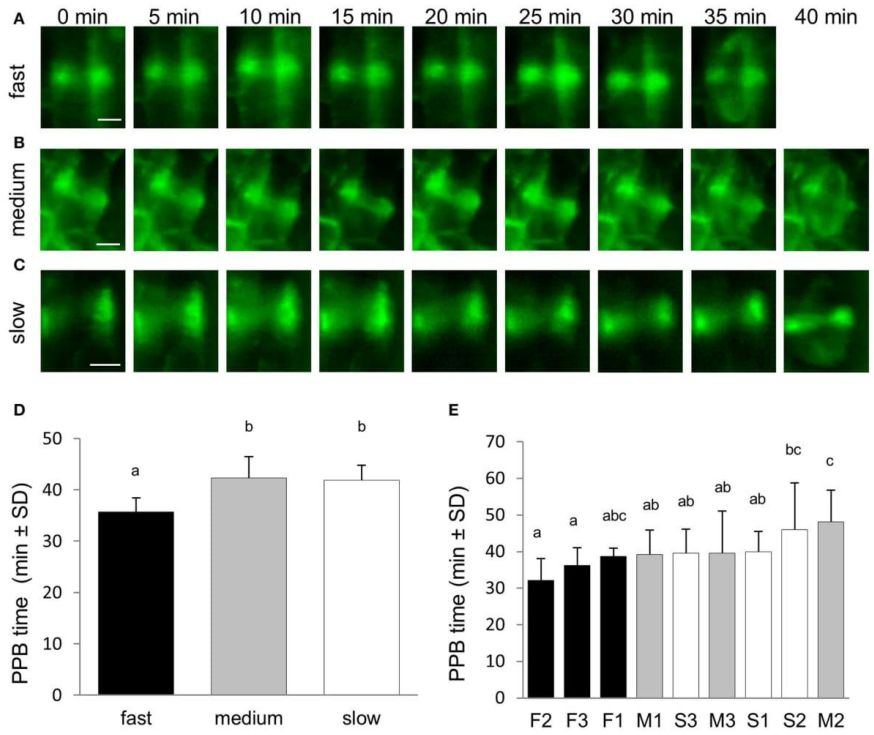

FIGURE 3 | Duration of the preprophase and prophase stage of the cell division. **(A–C)** Series of stills from time-lapse light-sheet imaging of dividing cells in root epidermis and cortex of *M. sativa* plants expressing *35S::GFP:MBD* construct. Sequence of preprophase and prophase stage starting from PPB narrowing and finishing by last stage of PPB presence and early mitotic spindle formation. Progress of the preprophase and prophase stage is shown for fast-growing roots **(A)**, medium-growing roots **(B)**, and slow-growing roots **(C).** Series of images were recorded in 5 min intervals from the stage of cell division when progressive PPB narrowing was defined by PPB width in the range of 2–4 μm (time 0 min). **(D)** Average duration time of preprophase and prophase stage of cell division in all roots of fast-growing, medium-growing and slow-growing group of roots. **(E)** Average duration time of preprophase and prophase stage in all dividing cells of individual roots. Roots are arranged from shortest to longest average duration time of preprophase and prophase stage. Black bars represent fast-growing roots (F1, F2, F3), gray bars represent medium-growing roots (M1, M2, M3) and white bars represent slow-growing roots (S1, S2, S3). Different letters above the bars represent statistical significance according to one-way ANOVA test at $P < 0.05$. Bars = 5 μm **(A–C)**.

of currently available microscopy techniques for routine live cell developmental imaging of living robust plant samples, such as crop species. Together with application of efficient protocols for stable transformation of crop species, it should be based on implementation of new approaches, tools and concepts enabling scientific progress in plant cell imaging.

Progression of cell division in plant cells is regulated by particular microtubule structures, such as PPB, mitotic spindle, and phragmoplast. These microtubule arrays are involved in cell division plane orientation, symmetry of cell division, segregation of nuclear material into two new cell nuclei and partitioning of cytoplasmic space of dividing cell into two daughter cells. Organization and dynamics of microtubules during individual mitotic and cytokinetic stages control the progression of cell division. Microtubule-dependent functions during cell division are mediated by modulators of microtubule organization and dynamics, such as microtubule-associated proteins (MAPs), End-binding 1 (EB1) proteins, and microtubule severing proteins. Study of MAPs from the MAP65 protein family (Van Damme et al., 2004; Chang et al., 2005; Mao et al., 2005; Smertenko et al., 2006; Ho et al., 2011, 2012) and EB1 proteins (Chan et al., 2003, 2005; Komaki et al., 2009) in their interactions with spindle and phragmoplast microtubules promoted considerably our understanding how microtubules are organized and how their dynamic properties regulate cell division progress and duration. Roles of microtubule-severing proteins were traditionally connected to dynamic reorganization of cortical microtubule arrays. Recent study on knock-out

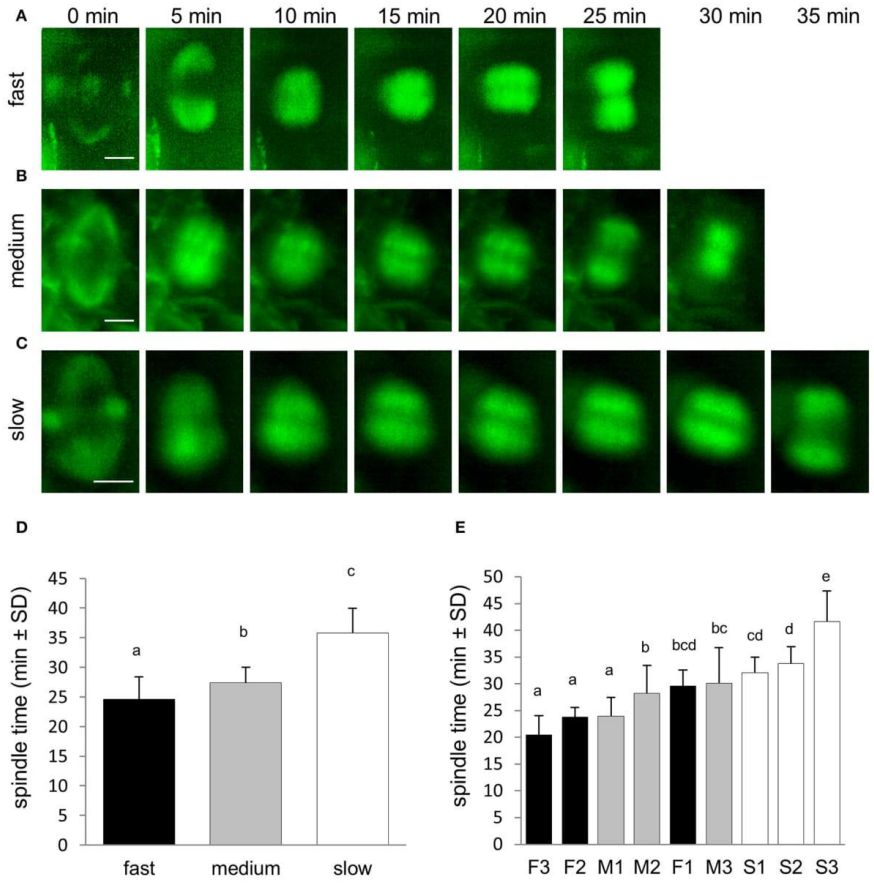

FIGURE 4 | Duration of the mitotic spindle stage from prometaphase to telophase during the cell division. **(A–C)** Series of stills from time-lapse light-sheet imaging of dividing cells in root epidermis and cortex of *M. sativa* plants expressing *35S::GFP:MBD* construct. Sequence of prometaphase, metaphase, anaphase and telophase stages starting from PPB disappearance and mitotic spindle formation at prometaphase and finishing by last stage of mitotic spindle presence at telophase. Progress of the mitotic spindle stages is shown for fast-growing roots **(A)**, medium-growing roots **(B)**, and slow-growing roots **(C)**. Series of images were recorded in 5 min intervals from the PPB disappearance and mitotic spindle formation at prometaphase (time 0 min). **(D)** Average duration time of mitotic spindle (prometaphase, metaphase, anaphase, and telophase) stages of cell division in all roots of fast-growing, medium-growing and slow-growing group of roots. **(E)** Average duration time of mitotic spindle (prometaphase, metaphase, anaphase, and telophase) stages in all dividing cells of individual roots. Roots are arranged from shortest to longest average duration time of mitotic spindle. Black bars represent fast-growing roots (F1, F2, F3), gray bars represent medium-growing roots (M1, M2, M3) and white bars represent slow-growing roots (S1, S2, S3). Different letters above the bars represent statistical significance according to one-way ANOVA test at $P < 0.05$. Bars = 5 μm **(A–C)**.

mutant *ktn1-2* revealed that KATANIN 1 contributes to PPB formation and maturation, and is involved in the positioning of the mitotic spindle and the phragmoplast (Komis et al., 2017). An important scientific question will be how complex microtubule network well described in models operates in legume crop species. Starting to address this question in *M. sativa*, we characterized microtubule arrays during the progress of mitotic cell division and sustained root growth. Main motivation of our study was to collect relevant data at near environmental condition, ensuring stress- and artifact-free imaging of living legume plant that is not interfering with normal plant growth and development. This was possible by implementation of LSFM and proper sample preparation protocols into live developmental imaging of alfalfa plants.

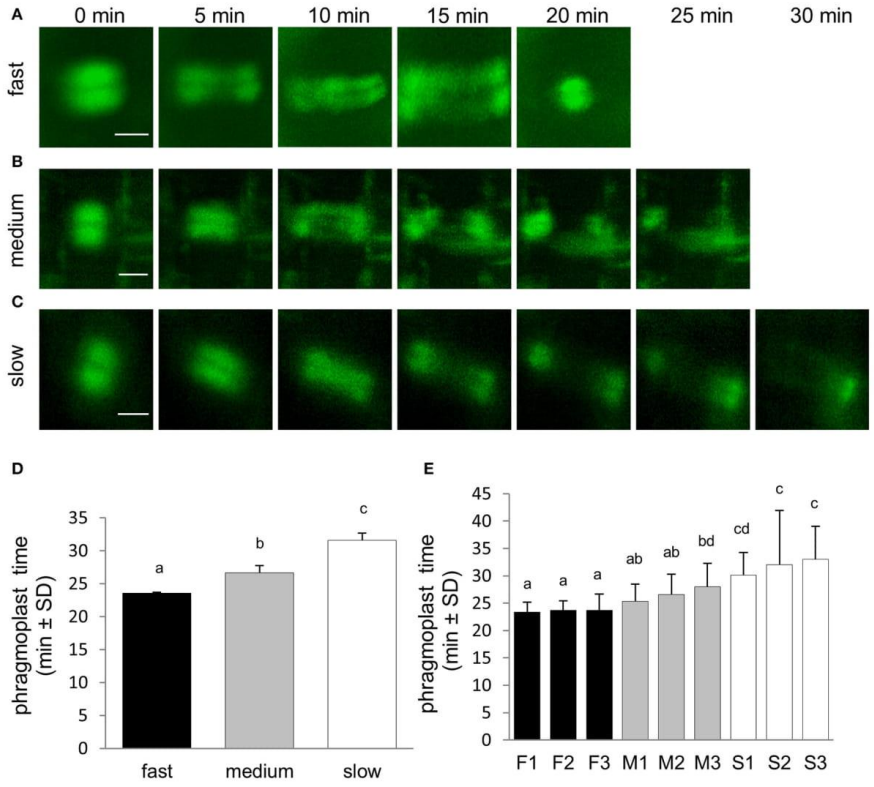

FIGURE 5 | Duration of the phragmoplast stage of the cell division. **(A–C)** Series of stills from time-lapse light-sheet imaging of dividing cells in root epidermis and cortex of *M. sativa* plants expressing *35S::GFP:MBD* construct. Sequence of phragmoplast stages is shown for fast-growing roots **(A)**, medium-growing roots **(B)** and slow-growing roots **(C)**. Series of images were recorded in 5 min intervals from the stage of early phragmoplast formation (time 0 min). **(D)** Average duration time of phragmoplast stage of cell division in all roots of fast-growing, medium-growing, and slow-growing group of roots. **(E)** Average duration time of phragmoplast stage in all dividing cells of individual roots. Roots are arranged from shortest to longest average duration time of phragmoplast. Black bars represent fast-growing roots (F1, F2, F3), gray bars represent medium-growing roots (M1, M2, M3) and white bars represent slow-growing roots (S1, S2, S3). Different letters above the bars represent statistical significance according to one-way ANOVA test at $P < 0.05$. Bars = 5 μm **(A–C)**.

Progress of mitotic cell division, distribution of mitoses within the root meristematic zone and cessation of mitotic activity in the root transition zone are tissue-specifically regulated. It has been shown that cells of the cortex and epidermis quit cell division earlier than cells of the endodermis and central cylinder tissues (Baluška et al., 1990; Schmidt et al., 2014). Duration of the PPB stage can be considerably long, as compared to the duration of other subsequent cell division stages during mitosis (Dhonukshe and Gadella, 2003; Vos et al., 2004; Komis et al., 2017). Alterations in the duration of the phragmoplast expansion have been observed in the Arabidopsis *mpk4* mutant, which is devoid of the mitogen activated protein kinase 4. This stage of the cell division was considerably delayed in comparison to control plants (Beck et al., 2011). Herein, we recorded and quantitatively evaluated duration time of PPB, mitotic spindle, and phragmoplast during cell division of epidermal and cortex cells in root meristem of transgenic *M. sativa*. Results suggested that duration time of cell division stages was different in roots with different growth rates. PPB stage was shortest in fast-growing roots, characterized by root growth rate of 0.7–1.4 $\mu m.min^{-1}$, similarly as duration time of mitotic spindle and phragmoplast. Stages of mitosis and cytokinesis lasted significantly longer time in medium-growing roots with root growth rate of 0.2–0.5 $\mu m.min^{-1}$ and duration of these stages was the longest in slow-growing roots with growth rate $< 0.2\ \mu m.min^{-1}$.

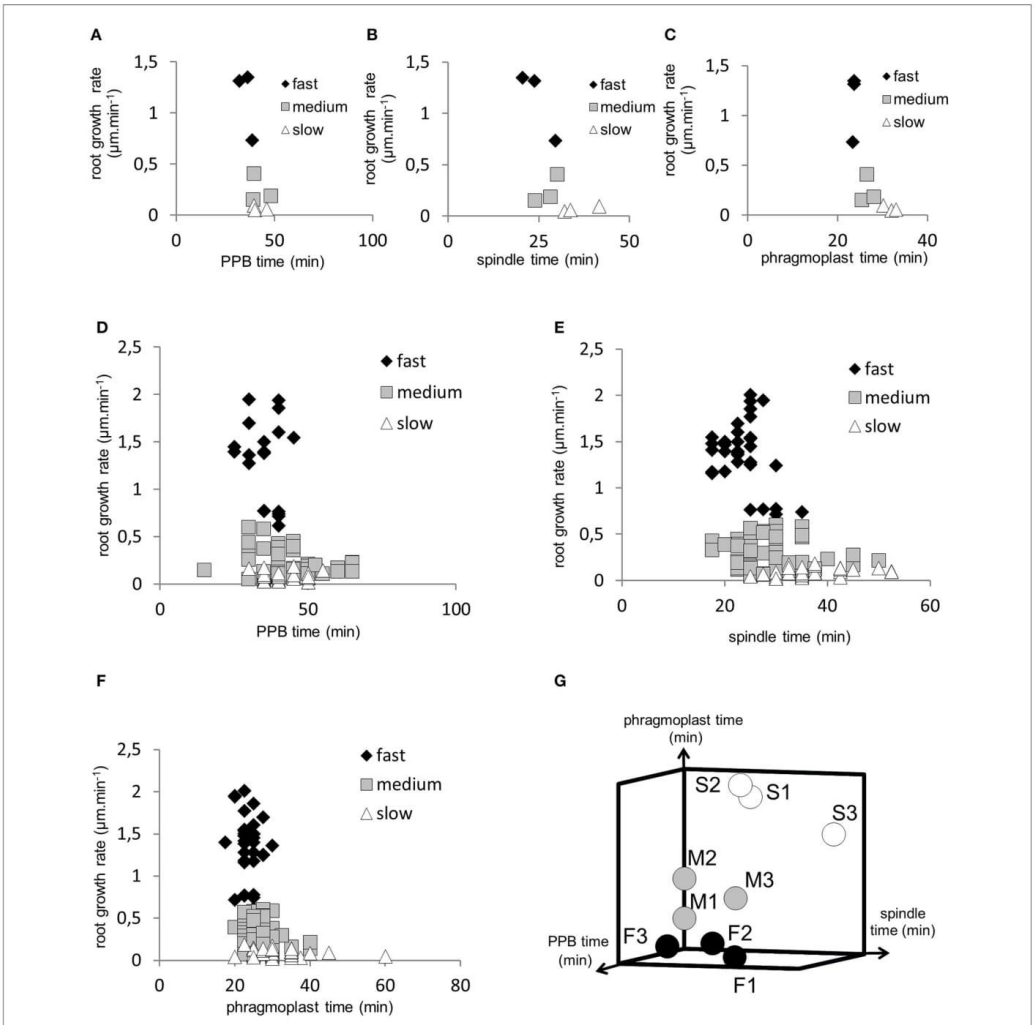

FIGURE 6 | Two- and three-dimensional visualization of data clusters for duration time of individual cell division stages in fast-growing, medium-growing and slow-growing roots according to root growth rate. **(A–C)** Distribution of clusters for average duration time of the PPB stage **(A)**, mitotic spindle stage **(B)** and phragmoplast stage **(C)** according to root growth rate in three fast-growing (♦), three medium-growing (□) and three slow-growing (△) roots. **(D–F)** Distribution of clusters for duration time of the PPB stage **(D)**, mitotic spindle stage **(E)** and phragmoplast stage **(F)** according to root growth rate in all individual dividing cells of the fast-growing (♦), medium-growing (□) and slow-growing (△) roots. **(G)** Visualization of data clustering for three fast-growing (F1, F2, F3), three medium-growing (M1, M2, M3) and three slow-growing (S1, S2, S3) roots according to cross-correlation between average duration time of the PPB stage, mitotic spindle stage and phragmoplast stage.

Quantitative kinematic study of primary root growth among 18 different ecotypes of *A. thaliana* revealed considerable variations, functionally linking root growth rate with cell cycle regulation. Along with variation in mature cortical cell length and number of dividing cells, also cell cycle duration contributed considerably to the observed variations in root growth rate (Beemster et al., 2002). Because the rate of cell division and the rate of cell production (defined as number of dividing cells

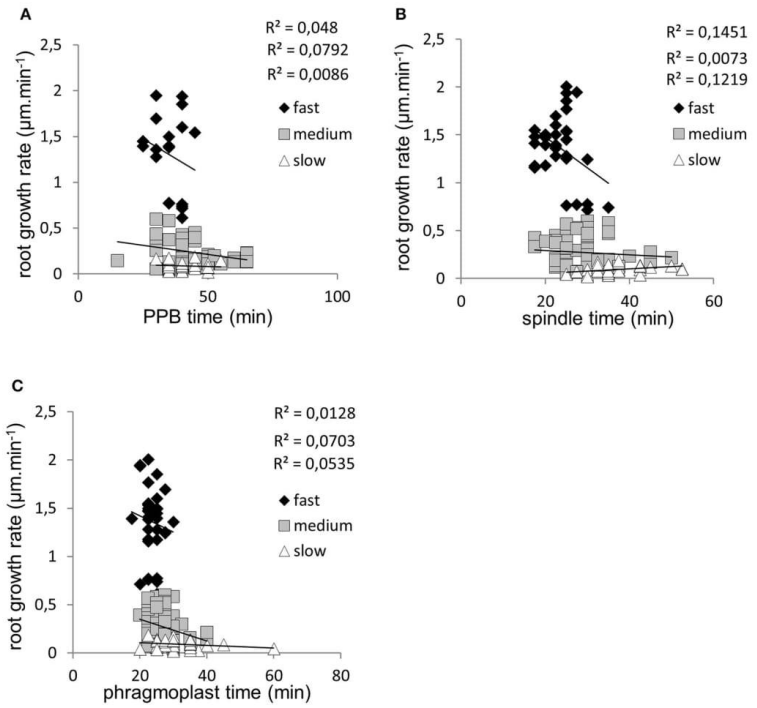

FIGURE 7 | Correlations between root growth rate and duration time of the PPB stage, mitotic spindle stage and phragmoplast stage of dividing cells. **(A)** Distribution of clusters, correlation lines and correlation coefficients for duration time of the PPB stage in all recorded dividing cells of fast-growing (♦), medium-growing (□), and slow-growing (Δ) roots according to root growth rate. **(B)** Distribution of clusters, correlation lines and correlation coefficients for duration time of the mitotic spindle stage in all recorded dividing cells of fast-growing (♦), medium-growing (□) and slow-growing (Δ) roots according to root growth rate. **(C)** Distribution of clusters, correlation lines and correlation coefficients for duration time of the phragmoplast stage in all recorded dividing cells of fast-growing (♦), medium-growing (□), and slow-growing (Δ) roots according to root growth rate.

and variation in their cell cycle duration) should be principally distinguished (reviewed by Baskin, 2000), determination of root growth rate ideally combines the spatial profile of cell length, cell velocity, relative elongation rate and cell division rate (Beemster and Baskin, 1998; Baskin, 2000). Functional interconnections of these critical parameters are obvious under unfavorable and stress environmental conditions. Responses of *A. thaliana* roots to temperature changes lead to alterations in the meristem length, which was compensated by changes in the cell length within the elongation zone or by changes in division rate helping to maintain equilibrated cell flux within the root meristem (Yang et al., 2017). Although, it is generally assumed that durations of individual mitotic and cytokinetic stages correlate only indirectly with total cell cycle duration, statistically evaluated parameters in *M. sativa* confirmed *vice versa* correlation of root growth rate with speed of these mitotic and cytokinetic stages in the root meristem. In principle, reduction in root growth rate was reflected by the prolongation of mitotic and cytokinetic stages. Such data were not available in crop species *M. sativa* before.

Moreover, the present study is the first one to provide large-scale imaging and quantitative characterization of cell divisions in the growing robust root of *M. sativa* using developmental live cell imaging. This was achieved by advanced LSFM, providing suitable technological and physiological tool for developmental live cell imaging of dividing cells in plant material with high spatial and excellent temporal resolution. LSFM is mesoscopic imaging method, overcoming several critical problems regarding the proper preparation and long-term maintenance of living plant samples. Low phototoxicity allows monitoring of Arabidopsis root growth for long time under physiological conditions (Maizel et al., 2011; Ovečka et al., 2015). Potential of LSFM for developmental imaging of mitotic microtubule arrays during cell division is obvious,

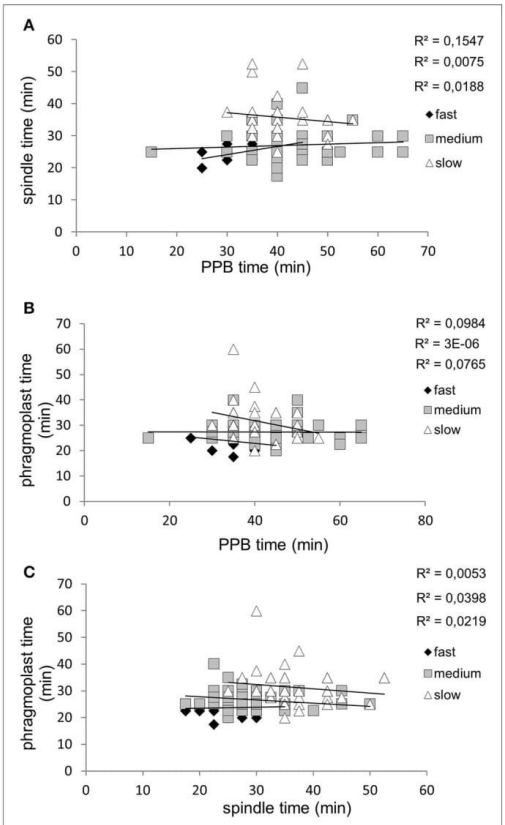

FIGURE 8 | Correlations between duration time of individual cell division stages in all measured dividing cells. **(A)** Correlations between duration time of the PPB stage and mitotic spindle stage in fast-growing (♦), medium-growing (□), and slow-growing (Δ) roots. **(B)** Correlations between duration time of the PPB stage and phragmoplast stage in fast-growing (♦), medium-growing (□) and slow-growing (Δ) roots. **(C)** Correlations between duration time of the mitotic spindle stage and phragmoplast stage in fast-growing (♦), medium-growing (□) and slow-growing (Δ) roots.

although it was so far utilized only in three studies on Arabidopsis. Previously, cell division in growing primary roots in long-term time-lapse experiments was observed in Arabidopsis plants carrying microtubule molecular markers GFP-MBD (Maizel et al., 2011) or GFP-TUA5 (Ovečka et al., 2015). LSFM was also used for characterization of tissue-specific and developmentally-regulated distribution of nuclear levels of GFP-tagged EB1c protein expressed under the control of native *EB1c* promoter. Quantitative correlation analysis revealed relationship between nuclear size and EB1c expression levels in diverse tissues like epidermis, cortex and endodermis, and in different developmental zones including meristematic, transition and elongation zone of *A. thaliana* roots (Novák et al., 2016). In this study we performed dynamic imaging of mitotic microtubule arrays in robust *M. sativa* growing roots using LSFM. For this purpose, we prepared stably transformed lines of *M. sativa* carrying molecular microtubule marker GFP-MBD and evaluated microtubule organization and dynamics during cell division of both epidermal and cortical root cells. Quantitative evaluation of cell division duration time was based on characterization of individual cell division stages, namely PPB, mitotic spindle and phragmoplast. The study clearly revealed an important link between duration of cell division in the root meristematic cells and root growth rates in *M. sativa*. These results suggest that spatio-temporal organization of microtubule-dependent cell divisions in the root meristem significantly contribute to the root growth rates. Importantly, LSFM is broadly applicable to any genetically modified and fluorescently labeled model legume species such as *M. truncatula* and *Lotus japonicus* as well as to agriculturally important legumes such as soybean, fava bean, pea or chickpea. Moreover, it is potentially interesting also for biotechnological applications such as bioimaging of *M. sativa* lines with RNAi-mediated genetic downregulation of stress-induced mitogen activated protein kinase kinase (SIMKK), an important component of signal transduction cascades in alfalfa (Bekešová et al., 2015), or crop transgenic lines with genetically manipulated cytoskeleton (Komis et al., 2015). Considering big potential of LSFM for deep imaging, it can be adapted and used to study interactions of legume roots expressing diverse subcellular markers (including microtubules) with beneficial microbes such as Rhizobia and mycorrhizal fungi.

Conclusively, previous achievements on Arabidopsis together with data presented in this study demonstrate a high potential of LSFM in developmental live cell imaging of mitotic cytoskeletal arrays in diverse plant species. High temporal and good spatial resolution combined with non-invasive and gentle live-cell imaging of cell divisions during growth and development of *M. sativa* roots favor light-sheet microscopy as the most promising imaging method for the future developmental bioimaging and characterization of robust crop species.

AUTHOR CONTRIBUTIONS

MO and PV conducted all live cell imaging. PV made all post acquisition analyses and quantitative evaluations with input from MO and JŠ. MO wrote first draft of the manuscript with input from all co-authors. JŠ conceived and supervised study, helped to interpret data, and finalized manuscript.

ACKNOWLEDGMENTS

We cordially acknowledge Katarína Takáčová for her help with alfalfa care and George Komis for critical reading of the manuscript. This work was funded by grant No. LO1204 (Sustainable development of research in the Center of the Region

Haná) from the National Program of Sustainability I, MEYS, Czech Republic.

SUPPLEMENTARY MATERIAL

The Supplementary Material for this article can be found online at: https://www.frontiersin.org/articles/10.3389/fpls.2017.01870/full#supplementary-material

Video S1 | Light-sheet imaging of fast-growing root of *M. sativa* stably expressing a GFP-MBD microtubule marker. Root was recorded for a time period of 3 h. Video was produced from time-lapse image acquisition of every 5 min and is presented in the speed of 10 fps.

Video S2 | Light-sheet imaging of medium-growing root of *M. sativa* stably expressing a GFP-MBD microtubule marker. Root was recorded for a time period of 3 h. Video was produced from time-lapse image acquisition of every 5 min and is presented in the speed of 10 fps.

Video S3 | Light-sheet imaging of slow-growing root of *M. sativa* stably expressing a GFP-MBD microtubule marker. Root was recorded for a time period of 3 h. Video was produced from time-lapse image acquisition of every 5 min and is presented in the speed of 10 fps.

REFERENCES

Ayaydin, F., Vissi, E., Mészáros, T., Miskolczi, P., Kovács, I., Fehér, A., et al. (2000). Inhibition of serine/threonine-specific protein phosphatases causes premature activation of cdc2MsF kinase at G2/M transition and early mitotic microtubule organisation in alfalfa. *Plant J.* 23, 85–96. doi: 10.1046/j.1365-313x.2000.00798.x

Azimzadeh, J., Nacry, P., Christodoulidou, A., Drevensek, S., Camilleri, C., Amiour, N., et al. (2008). Arabidopsis TONNEAU1 proteins are essential for preprophase band formation and interact with centrin. *Plant Cell* 20, 2146–2159. doi: 10.1105/tpc.107.056812

Baluška, F., Kubica, S., and Hauskrecht, M. (1990). Postmitotic 'isodiametric' cell growth in the maize root apex. *Planta* 181, 269–274. doi: 10.1007/BF00195876

Baskin, T. I. (2000). On the constancy of cell division rate in the root meristem. *Plant Mol. Biol.* 43, 545–554. doi: 10.1023/A:1006383921517

Baskin, T. I. (2013). Patterns of root growth acclimation: constant processes, changing boundaries. *WIREs Dev. Biol.* 2, 65–73. doi: 10.1002/wdev.94

Beck, M., Komis, G., Ziemann, A., Menzel, D., and Šamaj, J. (2011). Mitogen-activated protein kinase 4 is involved in the regulation of mitotic and cytokinetic microtubule transitions in *Arabidopsis thaliana*. *New Phytol.* 189, 1069–1083. doi: 10.1111/j.1469-8137.2010.03565.x

Beemster, G. T. S., and Baskin, T. I. (1998). Analysis of cell division and elongation underlying the developmental acceleration of root growth in *Arabidopsis thaliana*. *Plant Physiol.* 116, 1515–1526. doi: 10.1104/pp.116.4.1515

Beemster, G. T. S., De Vusser, K., De Tavernier, E., De Bock, K., and Inzé, D. (2002). Variation in growth rate between Arabidopsis ecotypes is correlated with cell division and A-type cyclin-dependent kinase activity. *Plant Physiol.* 129, 854–864. doi: 10.1104/pp.002923

Bekešová, S., Komis, G., Křenek, P., Vyplelová, P., Ovečka, M., Luptovčiak, I., et al. (2015). Monitoring protein phosphorylation by acrylamide pendant Phos-TagTM in various plants. *Front. Plant Sci.* 6:336. doi: 10.3389/fpls.2015.00336

Bingham, E. T. (1991). Registration of alfalfa hybrid Regen-SY germplasm for tissue culture and transformation research. *Crop Sci.* 31, 1098. doi: 10.2135/cropsci1991.0011183X003100040075x

Boruc, J., Weimer, A. K., Stoppin-Mellet, V., Mylle, E., Kosetsu, K., Cedeño, C., et al. (2017). Phosphorylation of MAP65-1 by Arabidopsis Aurora kinases is required for efficient cell cycle progression. *Plant Physiol.* 173, 582–599. doi: 10.1104/pp.16.01602

Calder, G., Hindle, C., Chan, J., and Shaw, P. (2015). An optical imaging chamber for viewing living plant cells and tissues at high resolution for extended periods. *Plant Methods* 11, 22. doi: 10.1186/s13007-015-0065-7

Campilho, A., Garcia, B., van den Toorn, H., van Wijk, H., Campilho, A., and Scheres, B. (2006). Time-lapse analysis of stem-cell divisions in the *Arabidopsis thaliana* root meristem. *Plant J.* 48, 619–627. doi: 10.1111/j.1365-313X.2006.02892.x

Chan, J., Calder, G. M., Doonan, J. H., and Lloyd, C. W. (2003). EB1 reveals mobile microtubule nucleation sites in *Arabidopsis*. *Nat. Cell Biol.* 5, 967–971. doi: 10.1038/ncb1057

Chan, J., Calder, G., Fox, S., and Lloyd, C. (2005). Localization of the microtubule end binding protein EB1 reveals alternative pathways of spindle development in Arabidopsis suspension cells. *Plant Cell* 17, 1737–1748. doi: 10.1105/tpc.105.032615

Chang, H.-Y., Smertenko, A. P., Igarashi, H., Dixon, D. P., and Hussey, P. J. (2005). Dynamic interaction of NtMAP65-1a with microtubules *in vivo*. *J. Cell. Sci.* 118, 3195–3201. doi: 10.1242/jcs.02433

Dhonukshe, P., and Gadella, T. W. Jr. (2003). Alteration of microtubule dynamic instability during preprophase band formation revealed by yellow fluorescent protein-CLIP170 microtubule plus-end labeling. *Plant Cell* 15, 597–611. doi: 10.1105/tpc.008961

Dhonukshe, P., Vischer, N., and Gadella, T. W. Jr. (2006). Contribution of microtubule growth polarity and flux to spindle assembly and functioning in plant cells. *J. Cell. Sci.* 119, 3193–3205. doi: 10.1242/jcs.03048

Gaillard, J., Neumann, E., Van Damme, D., Stoppin-Mellet, V., Ebel, C., Barbier, E., et al. (2008). Two microtubule-associated proteins of Arabidopsis MAP65s promote antiparallel microtubule bundling. *Mol. Biol. Cell* 19, 4534–4544. doi: 10.1091/mbc.E08-04-0341

Ho, C.-M. K., Hotta, T., Guo, F., Roberson, R. W., Lee, Y.-R. J., and Liu, B. (2011). Interaction of antiparallel microtubules in the phragmoplast is mediated by the microtubule-associated protein MAP65-3 in *Arabidopsis*. *Plant Cell* 23, 2909–2923. doi: 10.1105/tpc.110.078204

Ho, C.-M. K., Lee, Y.-R. J., Kiyma, L. D., Dinesh-Kumar, S. P., and Liu, B. (2012). *Arabidopsis* microtubule-associated protein MAP65-3 cross-links antiparallel microtubules toward their plus ends in the phragmoplast via its distinct C-terminal microtubule binding domain. *Plant Cell* 24, 2071–2085. doi: 10.1105/tpc.111.092569

Joubès, J., Chevalier, C., Dudits, D., Herberle-Bors, E., Inzé, D., Umeda, M., et al. (2000). CDK-related protein kinases in plants. *Plant Mol. Biol.* 43, 607–620. doi: 10.1023/A:1006470301554

Kimata, Y., Higaki, T., Kawashima, T., Kurihara, D., Sato, Y., Yamada, T., et al. (2016). Cytoskeleton dynamics control the first asymmetric cell division in *Arabidopsis* zygote. *Proc. Natl. Acad. Sci. U.S.A* 113, 14157–14162. doi: 10.1073/pnas.1613979113

Kirschner, G. K., Stahl, Y., Von Korff, M., and Simon, R. (2017). Unique and conserved features of the barley root meristem. *Front. Plant Sci.* 8:1240. doi: 10.3389/fpls.2017.01240

Komaki, S., Abe, T., Coutuer, S., Inzé, D., Russinova, E., and Hashimoto, T. (2009). Nuclear-localized subtype of end-binding 1 protein regulates spindle organization in *Arabidopsis*. *J. Cell. Sci.* 123, 451–459. doi: 10.1242/jcs.062703

Komis, G., Luptovčiak, I., Doskočilová, A., and Šamaj, J. (2015). Biotechnological aspects of cytoskeletal regulation in plants. *Biotech. Adv.* 33, 1043–1062. doi: 10.1016/j.biotechadv.2015.03.008

Komis, G., Luptovčiak, I., Ovečka, M., Samakovli, D., Šamajová, O., and Šamaj, J. (2017). Katanin effects on dynamics of cortical microtubules and mitotic arrays in *Arabidopsis thaliana* revealed by advanced live-cell imaging. *Front. Plant Sci.* 8:866. doi: 10.3389/fpls.2017.00866

Lavrekha, V. V., Pasternak, T., Ivanov, V. B., Palme, K., and Mironova, V. V. (2017). 3D analysis of mitosis distribution highlights the longitudinal zonation and diarch symmetry in proliferation activity of the *Arabidopsis thaliana* root meristem. *Plant J.* doi: 10.1111/tpj.13720. [Epub ahead of print].

Lee, Y.-R. J., and Liu, B. (2013). The rise and fall of the phragmoplast microtubule array. *Curr. Opin. Plant Biol.* 16, 757–763. doi: 10.1016/j.pbi.2013.10.008

Lucas, M., Kenobi, K., von Wangenheim, D., Voβ, U., Swarup, K., De Smet, I., et al. (2013). Lateral root morphogenesis is dependent on the mechanical

properties of the overlaying tissues. *Proc. Natl Acad. Sci. U.S.A.* 110, 5229–5234. doi: 10.1073/pnas.1210807110

Maizel, A., von Wangenheim, D., Federici, F., Haseloff, J., and Stelzer, E. H. K. (2011). High-resolution live imaging of plant growth in near physiological bright conditions using light sheet fluorescence microscopy. *Plant J.* 68, 377–385. doi: 10.1111/j.1365-313X.2011.04692.x

Mao, G., Chan, J., Calder, G., Doonan, J. H., and Lloyd, C. W. (2005). Modulated targeting of GFP-AtMAP65-1 to central spindle microtubules during division. *Plant J.* 43, 469–478. doi: 10.1111/j.1365-313X.2005.02464.x

Marc, J., Granger, C. L., Brincat, J., Fisher, D. D., Kao, T.-H., McCubbin, A. G., et al. (1998). A *GFP-MAP4* reporter gene for visualizing cortical microtubule rearrangements in living epidermal cells. *Plant Cell* 10, 1927–1939. doi: 10.2307/3870914

Marcus, A. I., Dixit, R., and Cyr, R. J. (2005). Narrowing of the preprophase microtubule band is not required for cell division plane determination in cultured plant cells. *Protoplasma* 226, 169–174. doi: 10.1007/s00709-005-0119-1

Mészáros, T., Miskolczi, P., Ayaydin, F., Pettkó-Szandtner, A., Peres, A., Magyar, Z., et al. (2000). Multiple cyclin-dependent kinase complexes and phosphatases control G2/M progression in alfalfa cells. *Plant Mol. Biol.* 43, 595–605. doi: 10.1023/A:1006412413671

Murata, T., Sano, T., Sasabe, M., Nonaka, S., Higashiyama, T., Hasezawa, S., et al. (2013). Mechanism of microtubule array expansion in the cytokinetic phragmoplast. *Nat. Commun.* 4, 1967. doi: 10.1038/ncomms2967

Nakamura, M., Ehrhardt, D. W., and Hashimoto, T. (2010). Microtubule and katanin-dependent dynamics of microtubule nucleation complexes in the acentrosomal *Arabidopsis* cortical array. *Nat. Cell Biol.* 12, 1064–1070. doi: 10.1038/ncb2110

Ni, J., Shen, Y., Zhang, Y., and Wu, P. (2014). Definition and stabilisation of the quiescent centre in rice roots. *Plant Biol.* 16, 1014–1019. doi: 10.1111/plb.12138

Novák, D., Kuchařová, A., Ovečka, M., Komis, G., and Šamaj, J. (2016). Develomental nuclear localization and quantification of GFP-tagged EB1c in *Arabidopsis* root using light-sheet microscopy. *Front. Plant Sci.* 6:1187. doi: 10.3389/fpls.2015.01187

Ovečka, M., Vaškebová, L., Komis, G., Luptovčiak, I., Smertenko, A., and Šamaj, J. (2015). Preparation of plants for developmental and cellular imaging by light-sheet microscopy. *Nat. Protoc.* 10, 1234–1247. doi: 10.1038/nprot.2015.081

Pasternak, T., Haser, T., Falk, T., Ronneberger, O., Palme, K., and Otten, L. (2017). A 3D digital atlas of the *Nicotiana tabacum* root tip and its use to investigate changes in the root apical meristem induced by the *Agrobacterium* 6b oncogene. *Plant J.* 92, 31–42. doi: 10.1111/tpj.13631

Pastuglia, M., Azimzadeh, J., Goussot, M., Camilleri, C., Belcram, K., Evrard, J.-L., et al. (2006). γ-Tubulin is essential for microtubule organization and development in *Arabidopsis*. *Plant Cell* 18, 1412–1425. doi: 10.1105/tpc.105.039644

Rasmussen, C. G., Humphries, J. A., and Smith, L. G. (2011). Determination of symmetric and asymmetric division planes in plant cells. *Ann. Rev. Plant Biol.* 62, 387–409. doi: 10.1146/annurev-arplant-042110-103802

Rebouillat, J., Dievart, A., Verdeil, J. L., Escoute, J., Giese, G., Breitler, J. C., et al. (2009). Molecular genetics of rice root development. *Rice* 2, 15–34. doi: 10.1007/s12284-008-9016-5

Rosero, A., Oulehlová, D., Stillerová, L., Schiebertová, P., Grunt, M., Žárský, V., et al. (2016). Arabidopsis FH1 formin affects cotyledon pavement cell shape by modulating cytoskeleton dynamics. *Plant Cell Physiol.* 57, 488–504. doi: 10.1093/pcp/pcv209

Rosquete, M. R., von Wangenheim, D., Marhavý, P., Barbez, E., Stelzer, E. H., Benková, E., et al. (2013). An auxin transport mechanism restricts positive orthogravitropism in lateral roots. *Curr. Biol.* 23, 817–822. doi: 10.1016/j.cub.2013.03.064

Sacks, M. M., Silk, W. K., and Burman, P. (1997). Effect of water stress on cortical cell division rates within the apical meristem of primary roots of maize. *Plant Physiol.* 114, 519–527. doi: 10.1104/pp.114.2.519

Samac, D. A., and Austin-Phillips, S. (2006). "Alfalfa (*Medicago sativa* L.)," in *Methods in Molecular Biology: Agrobacterium Protocols*, ed K. Wang (Tonowa: Springer), 301–311.

Schmidt, T., Pasternak, T., Liu, K., Blein, T., Aubry-Hivet, D., Dovzhenko, A., et al. (2014). The iRoCS Toolbox - 3D analysis of the plant root apical meristem at cellular resolution. *Plant J.* 77, 806–814. doi: 10.1111/tpj.12429

Shaw, S. L., and Lucas, J. (2011). Intrabundle microtubule dynamics in the *Arabidopsis* cortical array. *Cytoskeleton* 68, 56–67. doi: 10.1002/cm.20495

Sieberer, B. J., Timmers, A. C., and Emons, A. M. (2005). Nod factors alter the microtubule cytoskeleton in *Medicago truncatula* root hairs to allow root hair reorientation. *Mol. Plant Microbe. Interact.* 18, 1195–1204. doi: 10.1094/MPMI-18-1195

Sieberer, B. J., Timmers, A. C., Lhuissier, F. G., and Emons, A. M. (2002). Endoplasmic microtubules configure the subapical cytoplasm and are required for fast growth of *Medicago truncatula* root hairs. *Plant Physiol.* 130, 977–988. doi: 10.1104/pp.004267

Smertenko, A. P., Chang, H.-Y., Sonobe, S., Fenyk, S. I., Weingartner, M., Bögre, L., et al. (2006). Control of the MAP65-1 interaction with microtubules through the cell cycle. *J. Cell. Sci.* 119, 3227–3237. doi: 10.1242/jcs.03051

Smertenko, A., Assaad, F., Baluška, F., Bezanilla, M., Buschmann, H., Drakakaki, G., et al. (2017). Plant cytokinesis: terminology for structures and processes. *Trends Cell Biol.* doi: 10.1016/j.tcb.2017.08.008. [Epub ahead of print].

Stelzer, E. H. K. (2015). Light-sheet fluorescence microscopy for quantitative biology. *Nat. Methods* 12, 23–26. doi: 10.1038/nmeth.3219

Timmers, A. C. J., Valloton, P., Heym, C., and Menzel, D. (2007). Microtubule dynamics in root hairs of *Medicago truncatula*. *Eur. J. Cell Biol.* 86, 69–83. doi: 10.1016/j.ejcb.2006.11.001

Van Damme, D. (2009). Division plane determination during plant somatic cytokinesis. *Curr. Opin. Plant Biol.* 12, 745–751. doi: 10.1016/j.pbi.2009.09.014

Van Damme, D., Van Poucke, K., Boutant, E., Ritzenthaler, C., Inzé, D., and Geelen, D. (2004). *In vivo* dynamics and differential microtubule-binding activities of MAP65 proteins. *Plant Physiol.* 136, 3956–3967. doi: 10.1104/pp.104.051623

Van Damme, D., Vanstraelen, M., and Geelen, D. (2007). Cortical division zone establishment in plant cells. *Trends Plant Sci.* 12, 458–464. doi: 10.1016/j.tplants.2007.08.011

Vermeer, J. E. M., von Wangenheim, D., Barberon, M., Lee, Y., Stelzer, E. H. K., Maizel, A., et al. (2014). A spatial accommodation by neighboring cells is required for organ initiation in Arabidopsis. *Science* 343, 178–183. doi: 10.1126/science.1245871

Voigt, B., Timmers, A. C. J., Šamaj, J., Müller, J., Baluška, F., and Menzel, D. (2005). GFP–FABD2 fusion construct allows *in vivo* visualization of the dynamic actin cytoskeleton in all cells of Arabidopsis seedlings. *Eur. J. Cell Biol.* 84, 595–608. doi: 10.1016/j.ejcb.2004.11.011

von Wangenheim, D., Fangerau, J., Schmitz, A., Smith, R. S., Leitte, H., Stelzer, E. H. K., et al. (2016). Rules and self-organizing properties of post-embryonic plant organ cell division patterns. *Curr. Biol.* 26, 1–11. doi: 10.1016/j.cub.2015.12.047

Vos, J. W., Dogterom, M., and Emons, A. M. (2004). Microtubules become more dynamic but not shorter during preprophase band formation: a possible "search-and-capture" mechanism for microtubule translocation. *Cell Motil. Cytoskeleton* 57, 246–258. doi: 10.1002/cm.10169

Yang, X., Dong, G., Palaniappan, K., Mi, G., and Baskin, T. I. (2017). Temperature-compensated cell production rate and elongation zone length in the root of *Arabidopsis thaliana*. *Plant Cell Environ.* 40, 264–276. doi: 10.1111/pce.12855

Conflict of Interest Statement: The authors declare that the research was conducted in the absence of any commercial or financial relationships that could be construed as a potential conflict of interest.

Ph.D. Thesis summary

PALACKÝ UNIVERSITY OLOMOUC

Faculty of Science

Department of Biochemistry

New microscopic methods for studies of plant cytoskeleton

Ph.D. Thesis summary

P1406 Biochemistry

Mgr. Petra Illésová

Olomouc

2018

This Ph.D. thesis has been completed at the Department of Cell Biology, Centre of the Region Haná for Biotechnological and Agricultural Research, Faculty of Science, Palacký University Olomouc under the supervision of Prof. RNDr. Jozef Šamaj, DrSc.

Ph.D. Candidate: **Mgr. Petra Illésová**
Department of Cell Biology, Centre of the Region Haná
for Biotechnological and Agricultural Research
Faculty of Science, Palacký University Olomouc
Šlechtitelů 27, 779 00 Olomouc, Czech Republic

Supervisor: **Prof. RNDr. Jozef Šamaj, DrSc.**
Department of Cell Biology, Centre of the Region Haná
for Biotechnological and Agricultural Research
Faculty of Science, Palacký University Olomouc
Šlechtitelů 27, 779 00 Olomouc, Czech Republic

Reviewers: **Doc. RNDr. Jan Hejátko, Ph.D.**
Functional Genomics and Proteomics of Plants Central
European Institute of Technology
Masaryk University Brno
Kamenice 753/5, 625 00 Brno, Czech Republic

RNDr. Jan Petrášek, Ph.D.
Laboratory of Hormonal Regulations in Plants
Institute of Experimental Botany AS CR
Rozvojová 263, 165 02 Praha 6, Czech Republic

The evaluation of the Ph.D. thesis has been written by the Head of Department of Cell Biology CRH, Faculty of Science, Palacký University Olomouc.
The summary of the Ph.D. thesis has been sent out on …….
The oral defence will take place at the Faculty of Science, Šlechtitelů 27, Olomouc on ……
The Ph.D. thesis is available at the Library of the Biological Centre, Šlechtitelů 27, Olomouc

Prof. RNDr. Ivo Frébort, CSc., Ph.D.
Chairman of Doctoral Study Board in Biochemistry

CONTENT

1. ABSTRACT

This Ph.D. thesis is focused on the possibilities of studying the plant cytoskeleton using modern microscopic methods such as light-sheet fluorescence microscopy (LSFM), spinning disk confocal microscopy (SDCM) and Airyscan confocal laser scanning microscopy (CLSM). Microscopic analyses were performed on microtubules during cell divisions in the roots of the model species *Arabidopsis thaliana* and in the roots of the important legume crop *Medicago sativa*. The thesis is divided into three parts. The first part summarizes the current knowledge about plant cytoskeleton, its structure and function. This part contains chapters focused on the organization and the roles of microtubules (MTs) during the mitosis. In the same section, the chosen model plants are described while an account of the used microscopic methods is also given.

The second part is mainly focused on the preparation of plant material for subsequent microscopic analysis of mitotic MT arrays. Mitosis is a highly dynamic process, sensitive to many stress factors. For this reason, the selection of the suitable microscopic method is very important. Using genetically encoded fluorescent MT markers and modern microscopic methods (LSFM, SDCM and Airyscan CLSM) with high spatio-temporal capabilities, it was possible to track and document dynamic processes, such as mitosis, in real time.

The third part of thesis is more specified on the use of LSFM to study mitotic MTs in growing *M. sativa* roots expressing *35S::GFP:MBD* construct. Owing to the high optical resolution, efficient optical sectioning, high speed image acquisition, low phototoxicity and ability to scan the sample oriented in a vertical position, this microscopic method is suitable for the 4D long-term live-cell imaging of plant under nearly physiological conditions. In total, nine imaged *M. sativa* roots were divided into three groups according to their growth rates. In each group we recorded and quantitatively evaluated the duration of the mitotic cell division and specific mitotic MT arrays such as the preprophase band, the mitotic spindle and the phragmoplast in both, the epidermis and the first outer layer of cortex, respectively. Obtained data showed strong correlation between the root growth rate and the duration of cell division in the *M. sativa* roots.

Keywords	microtubule, *Medicago sativa*, light-sheet microscopy, spinning disk confocal microscopy, Airyscan, *Arabidopsis thaliana*, preprophase band, spindle, phragmoplast, mitosis
Number of pages	165
Number of appendices	3
Language	English

2. OBJECTIVES

1. Summary of knowledge about the plant cytoskeleton and advanced microscopic methods suitable for its study
2. Optimizing the preparation of plant material for the study of the *M. sativa* root using light-sheet microscopy
3. Study of mitotic microtubules during cell division in *M. sativa* using light-sheet microscopy
4. Measurement and statistical analysis of the duration of the individual mitotic stages
5. Preparation of plant material for the study of mitotic microtubules in dividing cells using spinning disk microscopy and Airyscan microscopy

3. GENERAL INTRODUCTION

3.1 Cytoskeleton

The cytoskeleton is a dynamic subcellular system that forms a three-dimensional network similar to a scaffolding. It has mainly the structural, transporting, signaling and motional functions. It determines the shape and orientation of cell growth and participates in the cellular movement and positioning of organelles and macromolecules. It also plays a key role in cell division, vesicle trafficking and programmed cell death (Goode *et al*., 2000; Smith, 2003; Smertenko and Franklin-Tong, 2011; Zhang and Dawe, 2011).

Generally, the cytoskeletal components of the actin and microtubule cytoskeleton are highly conserved. The origin of the cytoskeleton is most likely prokaryotic. Although the prokaryotic "ancestors" of actin and tubulin, such as MreB and FtsZ proteins respectively do not show a high homology with eukaryotic actin and tubulin (Erickson, 2007), these proteins have similar three dimentional structures and functions. For example, MreB in *Bacillus subtilis* has been shown to act as a cortical actin for the formation of lipid rafts and for the distribution of lipids and proteins in the plasma membrane (Chichili and Rodgers, 2009; Strahl *et al*., 2014). FtsZ, a bacterial homologue of tubulin, has the same tubulin GTPase activity and is indispensable for cell division (Bi and Lutkenhaus, 1991; Hong *et al*., 2013).

The cytoskeleton of green plants consists of microtubules and actin filaments (Wasteneys, 2002). Intermediate filaments have not been described, except some exceptions, in plants. Historically, actin filaments and microtubule arrays have been considered as separate cytoskeletal systems with different functions. However, the structural and functional cooperation of these two cytoskeletal components during cellular processes such as phragmoplast formation and cytokinesis was shown (Gavin, 1997; Bezanilla *et al*., 2015).

3.1.1 Mitotic MTs

In somatic cells, chromosomes and cytoplasm containing individual cell organelles and subcellular compartments are divided into two daughter cells during mitotic (M) phase of cell cycle. This M phase can be subdivided into two tightly interconnected parts – mitosis and cytokinesis. Chromosomes are segregated in mitosis, while the cytoplasm is partitioned during cytokinesis. The mitotic part itself is divided into five basic steps, namely prophase, prometaphase, metaphase, anaphase and telophase (Fig. 1).

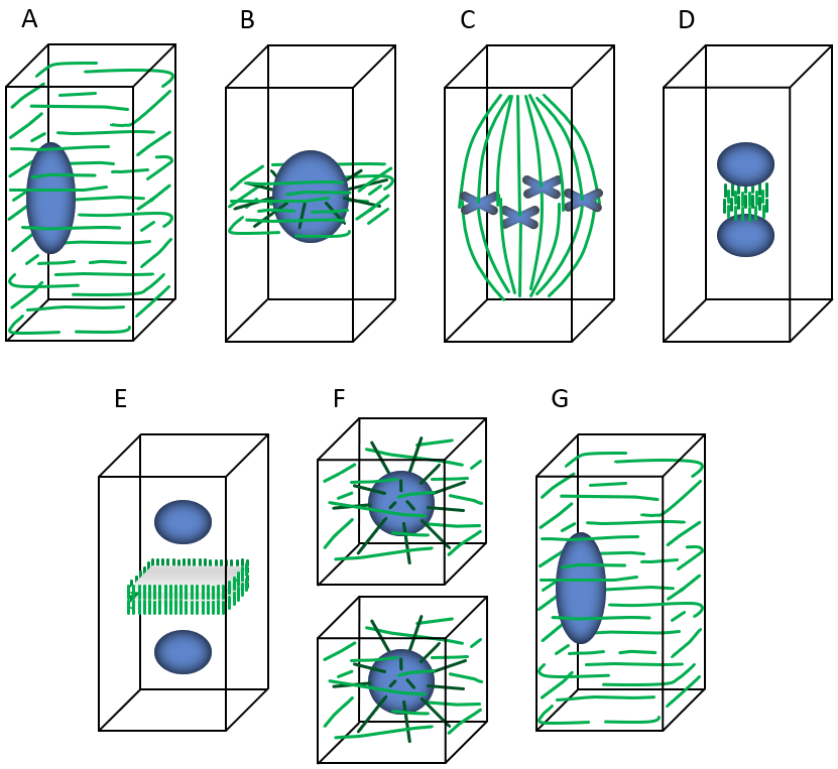

Figure 1. Scheme of MTs arrangement during the plant cell division. (A) Parallel arrangement of cortical MTs during interphase in mature plant cell. (B) Temporary rearrangement of MTs into PPB, which marks the future cell division plane. (C) MTs are formed into mitotic spindle during prometaphase. The chromosomes are localized in equatorial region. (D) The early phragmoplast is formed in place of the future cell plate. (E) The late phragmoplast is formed as temporary MTs ring between two daughter nuclei. (F) The cytokinesis is complete and two daughter cells are created. MTs extend from the nucleus toward the cell cortex and plasma membrane-associated MTs appear. (G) The cortical MTs are again formed in post-mitotic plant cell. Adapted from Wasteneys, 2002.

Preparation of cells for mitotic entry in plants is characterized by a dramatic reorganization of cortical MTs. These progressively coalesce to the so-called preprophase band (PPB). After maturation and disassembly, the PPB is rearranged to the mitotic spindle and eventually the cytokinetic phragmoplast during progression of mitosis and cytokinesis (Fig. 1; Yuan *et al*., 1994; Wasteneys, 2002; Hashimoto, 2015).

During prophase, the microtubular PPB disappears and the mitotic spindle begins to develop (Fig. 1B, C). In plants, however, minus ends of mitotic spindle MTs do not originate from centrosomes as in animals and yeasts but they are likely associated with MTOCs located close to the nuclear envelope (Dibbayawan *et al*., 2001; Binarova *et al*., 2006; Wiese and Zheng, 2006).

The prometaphase is determined by nuclear envelope breakdown. Chromosomes become attached to MTs of the mitotic spindle at kinetochores and progressively align to the equatorial plane of the dividing cell (Fig. 1C). Spindle is completed and three groups of spindle MTs are

apparent. Kinetochore MTs attach the chromosomes to the spindle pole, interpolar MTs which extend in a pole-to-pole fashion and astral MTs which project from the spindle pole towards the cell membrane in a radial fashion.

During anaphase, each chromosome separates to sister chromatids which move to opposite poles of the cell. Meanwhile, changes in MT length provide the mechanism for chromatid movements. Upon separation, chromatids mature to independent chromosomes.

During telophase, equivalent sister chromatid groups converge to the cell poles, and MTs gradually form the phragmoplast (Fig. 1D, E). Progressively a new nuclear envelope is formed around each group of chromosomes.

At the same time, the centrifugally expanding phragmoplast directs the deposition of the daughter cell wall – the cell plate – which physically partitions the two nuclei into two daughter cells (Fig. 1F; Alberts *et al*., 2008).

3.2 Plant models for studies of cytoskeleton during mitosis

Medicago sativa as a legume species represents a new and attractive plant organism in cell biology due to its biotechnology potencial. Our research is focused on the study of cytoskeleton during developmental processes. *M. sativa* is challenging organism for long-term live-cell imaging due to its robust size. *Arabidopsis thaliana* as an established model plant species is routinely used for microscopic analyses. It represents a crucial model in the studies devoted to dynamic cytoskeletal rearrangements in living plant cells.

In the first case, we prepared and regenerated *M. sativa* plants carrying cytoskeletal markers from transgenic somatic embryos while in the second case transgenic *A. thaliana* plants carrying MT marker were germinated from available seeds.

4. RESULTS

4.1 Advanced microscopy methods for bioimaging of mitotic microtubules in plants

4.1.1 Introduction

Cellular preparations for mitotic entry in plants are marked by a dramatic reorganization of the cortical MT array to an annular cortical assembly, the PPB (Rasmussen *et al*., 2011) which is considered as a marker of the cortical division zone (CDZ) and a predictor of cell plate fusion at the parent walls (Smertenko *et al*., 2017). In this way, PPB acts as a determinant of symmetric and asymmetric cell divisions (Rasmussen *et al*., 2011). Initially, the PPB is loosely organized but progressively narrows until the perinuclear prophase spindle assembles (e.g., Vos *et al*., 2004). Thereon the PPB disassembles and the mitotic chromosome segregation starts.

Principally, the PPB is a MT array and therefore primarily consists of MTs and a wide array of microtubule-associated proteins (MAPs) with bundling (e.g., members of the MAP65 family; Li *et al*., 2017), motor (members of the kinesin superfamily) and regulatory (e.g., End Binding 1 proteins; EB1; Chan *et al*., 2003; 2005, and the HEAT repeat protein MOR1/GEM; Twell *et al*., 2002) activities. Apart from MTs and MAPs, the PPB also contains actin microfilaments which facilitate the coalescence of cortical MTs (Kojo *et al*., 2013) and several other molecules recruited on site and persisting long after the disappearance of the PPB in a continuous or discontinuous manner. Such molecules, which serve as markers of the CDZ include TANGLED (TAN; Walker *et al*., 2007), PHRAGMOPLAST ORIENTING KINESIN 1 (POK1) and POK2 (Müller *et al*., 2006), FASS/TONNEAU2 (Camilleri *et al*., 2002), AUXIN-INDUCED IN ROOT cultures (AIR9; Buschmann *et al*., 2006), Ran GTPase ACTIVATING PROTEIN 1 (RanGAP1; Xu *et al*., 2008) and KINESIN-LIKE CALMODULIN-BINDING PROTEIN (KCBP; Buschmann *et al*., 2015). Characteristically, some mutants in corresponding genes exhibit marked CDP related phenotypes.

Segregation of duplicated genetic material between two daughter cells in the process of mitosis is a conserved feature among eukaryotes and requires the assembly of the mitotic spindle (Prosser and Pelletier, 2017). In animals and fungi, the assembly of the MT-based mitotic spindle is dominated by the occurrence of structurally defined MTOCs with MT nucleating capacity such as the centrosome (Vertii *et al*., 2016) and the spindle pole body (Kilmartin, 2014). In higher plants, however, mitotic spindle assembly is acentrosomal and its form undergoes significant changes during mitotic progression (Yamada and Goshima, 2017). The plant mitotic spindle is bipolar and it largely comprises of kinetochore MT bundles but it lacks astral MTs, possibly due to the absence of MTOCs at the spindle poles. As in the case of

the PPB, several MAPs involved in MT nucleation, regulation of plus-end dynamics, MT bundling and MT-dependent motor activities as well as other proteins with regulatory functions such as protein kinases were found to be enriched in the mitotic spindle (reviewed in Yamada and Goshima, 2017).

At the end of mitosis, the mitotic spindle is replaced by the plant specific cytokinetic apparatus, the phragmoplast. The phragmoplast directs the translocation of cell wall material containing vesicles to the equatorial plane, where they fuse and form the nascent daughter plasma membrane and the cell plate. The phragmoplast expands from the cell center towards the cell periphery in a well-defined plane, which is called the cell division plane (CDP; Smertenko *et al*., 2017). Finally, the expanding cell plate fuses to a well-defined cortical site which is called the cell plate fusion site. This site is adjusted to a predetermined CDZ (Smertenko *et al*., 2017) which is in turn defined by the PPB (Smertenko *et al*., 2017 and references therein). Phragmoplast expansion requires the gradual disappearance of MTs from its central area and their confinement to the cell periphery through a concerted function of γ-tubulin dependent MT nucleation and MAP65 dependent MT bundling. During the process, phragmoplast positioning may be subject to corrective motions (e.g., Komis *et al*., 2017) through a navigation process probably mediated by acto-myosin cytoskeleton (e.g., Wu and Bezanilla, 2014).

Significant studies on the progressive development of the PPB, the assembly and the positioning of the mitotic spindle as well as on the centrifugal expansion of the cytokinetic phragmoplast, and the deposition of the cell plate were done in non-model plants. Most such studies were carried out by means of transmission electron microscopy or immunofluorescence imaging (e.g., Gunning *et al*., 1978; Wick and Duniec, 1983; Samuels *et al*., 1995; Kojo *et al*., 2013) combined with the use of cytoskeletal (e.g., Panteris *et al*., 1995) or other inhibitors (e.g., Binarová *et al*., 1998) that broadly or selectively affected the above processes. The establishment of *A. thaliana* as a genetically tractable model of plant growth and development, the design of robust protocols for the generation of transgenic plants bearing appropriate fluorescent markers, and the establishment of confocal laser scanning microscopy (CLSM) as a routine method of imaging, allowed *in vivo* visualization of mitosis and cytokinesis in a dynamic manner. Other studies used suspension culture cells of tobacco bright yellow-2 (BY-2), a material that can be easily transformed, maintained and synchronized to provide thousands of cells in diverse mitotic stages for visualization (e.g., Granger and Cyr, 2000; Yoneda *et al*., 2005; Buschmann *et al*., 2011). However, such suspension-cultured cells lack the spatial constraints of mitotic progression found in intact tissues and they are not allowing

deductions on spindle orientation and the regulation of CDP orientation necessary for pattern formation, morphogenesis and organ development in plants.

The dynamic imaging of mitosis and cytokinesis in living plant cells can convey very useful information regarding the rates of PPB narrowing (e.g., Vos *et al*., 2004; Komis *et al*., 2017) and disturbances of its formation after pharmacological (e.g., Kojo *et al*., 2014) or genetic (Komis *et al*., 2017) interference. Moreover, this approach can provide data on the duration of mitosis and the subsequent phragmoplast expansion (e.g., Beck *et al*., 2011; Komis *et al*., 2017) and it can reveal mechanisms behind mitotic and cytokinetic aberrations of appropriate mutants. Keys to successful imaging of the above processes in plants include the sufficient depth of the selected microscopy method and adequate speed of acquisition to avoid motion artefacts arising by intracellular motions of the mitotic MTs. Most importantly, the selected method should ensure the minimal exposure of the dividing cell to phototoxic excitation illumination which may delay, abort or disturb the progress of mitosis and cytokinesis or compromise the viability of the sample during imaging (see Laissue *et al*., 2017 for a critical assessment of phototoxicity during live fluorescence imaging).

The present chapter aims to summarize the bioimaging possibilities in the studies of mitotic progression *in planta* by advanced methods that were developed and commercialized over the past few years. These methods have expanded the possibilities of dissecting mitosis and cytokinesis in living plants and provided a considerable improvement of spatial and temporal resolution. High speed and mass visualization of the mitoses can be done in whole organs such as roots or leaves with light-sheet fluorescence microscopy (LSFM) allowing imaging of subcellular details at a moderate spatial resolution. Mitosis can be followed in better spatial resolution with fast imaging modalities such as spinning disk confocal microscopy (SDCM), while high-resolution methods such as Airyscan CLSM can be used to decipher fine structural details in the assembly of the PPB, the mitotic spindle and the cytokinetic phragmoplast. We are providing imaging possibilities of two different plants, the plant model *A. thaliana* and the legume crop *M. sativa* which pose different challenges for sample preparation and image acquisition.

4.1.2 Materials and Methods

4.1.2.1 Preparation of plant material for light-sheet imaging of root cell mitotic progress

In general, mitotic cell divisions in plants are mostly concentrated in specialized multicellular domains, plant meristems. Cell proliferation in the root takes place within the root apical

meristem, where radial root zonation consists of several cell layers important for development of various tissues (Dolan *et al*., 1993; Baum *et al*., 2002; Scheres *et al*., 2002). Our understanding of how cell divisions in the root apical meristem are organized and regulated during plant growth and development thus requires microscopic imaging of dividing cells in the whole root apex with sufficient spatial and temporal resolution. Ideally, intact plants should be adapted in the microscope for long-term imaging under minimalized phototoxicity, photobleaching and proper environmental physiological conditions. A cutting edge technology fulfilling all requirements for developmental imaging under physiological conditions is represented by LSFM in animal developmental biology. LSFM has been introduced also into plant developmental biology, although the number of applications is not so high due to the more complicated preparation of living plants for long-term microscopy observations. However, substantial benefit of a vertically oriented plant (consistently with the gravity vector) prefers LSFM as an advanced microscopy technique for long-term plant developmental imaging. This method offers fast optical sectioning of the sample, restriction of the fluorophore excitation only to the thin light-sheet volume, and free rotation of the sample allowing multi-angular image acquisition. Live-cell imaging of dividing cells using LSFM is sufficient for resolving MT arrays during mitosis and cytokinesis, including deep imaging of dividing cells inside of living multicellular plant organs. Good spatial and high temporal resolution of LSFM ensures recording of cell division in growing and developing plant tissues in real time. Nevertheless, there are only very few LSFM studies on cytoskeletal proteins during plant cell division so far (Maizel *et al.,* 2011; Ovečka *et al.,* 2015; Novák *et al.,* 2016; Vyplelová *et al.,* 2017).

1. Plant root is the preferred organ for LSFM studies due to the high frequency of cell divisions and to the fact that it grows fully embedded in the culture medium. Solidified Phytagel-based culture medium containing all macro- and micro-nutrients and carbon source serves as an optimal cultivation environment for plant roots. In addition, being transparent it provides excellent optical properties (Maizel *et al.,* 2011; Ovečka *et al.,* 2015), and serves as an optimal imaging medium for LSFM. In our experiments we used a half-strength Murashige and Skoog (MS) basal salt mixture supplemented with 1% (w/v) sucrose and pH adjusted to 5.7, solidified with Phytagel at a concentration 0.6% (w/v). An alternative approach for embedding and imaging of plant samples is the use of a low-gelling-temperature agarose at appropriate concentrations (usually between 0.6% - 1.0% w/v) dissolved in water or liquid half-strength MS culture medium.

2. We prepared samples of whole intact plants in the "open system" developed for long-term live-cell imaging of *A. thaliana* seedlings (Ovečka *et al.*, 2015). Plants growing in the Phytagel–solidified culture medium were transferred to the microscope in fluorinated ethylene propylene tubes (FEP tubes). Roots grow in the culture medium inside of the FEP tube. Green parts of the plants are located in open space of the FEP tube providing access to air and light in the microscope during experiment. Alternative methods suitable for mounting *A. thaliana* plants to the light-sheet microscope supporting their growth during the imaging were also published (von Wangenheim *et al*., 2014).

3. Nourishing plants with nutrients from fresh culture medium is required, especially for long-term experiments. We use controlled perfusion of the imaging chamber with liquid half-strength MS medium without vitamins, supplemented with 1% (w/v) sucrose and pH adjusted to 5.7. Plant growth medium is filter-sterilized using a sterile syringe filter with a pore size of 0.2 μm before loading to the imaging chamber in order to prevent fungal and/or bacterial contamination.

4. Practical approaches on how to prepare plants for LSFM imaging described below are based on a published protocol optimized for *A. thaliana* (Ovečka *et al.*, 2015) and can be easily adapted for either single-cell system (e.g. cell suspension culture), or significantly thicker samples such as somatic embryos and developing plants of the legume crop plant *M. sativa*. It is applicable for both commercial and custom-built LSFM platforms.

Arabidopsis thaliana seedlings

1. Seeds of *A. thaliana* transgenic lines must be sterilized in 70% (v/v) ethanol for 2 min and subsequently in 1% (v/v) sodium hypochlorite containing 0.05% (v/v) Tween 20 for 8 min. The next step is thorough washing of the seeds (five times) with sterile MilliQ water. Sterile seeds are placed on a Petri dish filled with Phytagel-solidified half-strength MS medium. All steps of seed sterilization and plating must be done in aseptic conditions in the laminar flow box. Plates with seeds are then stored at 4°C for 2-3 days to break seed dormancy and synchronize germination. After it, plates are placed into the culture chamber at 22°C, 50% humidity and 16/8 h (light/darkness) photoperiod.

2. After germination (within 24-48 h after seed transfer to the culture chamber) seeds with ruptured testa and emerging root are transferred to round 90 × 25 mm Petri dishes filled with

80 ml of Phytagel-solidified half-strength MS medium. The thickness of culture medium should be approximately 15 mm, which is optimal for root growth and further sample preparation.

3. Two days later germinating plants with growing roots are picked up by gentle insertion of the FEP tube with an inner diameter of 2.8 mm to the culture medium enclosing the selected plant inside. The FEP tube with the plant and the culture medium inside is installed into the microscope observation chamber.

Medicago sativa roots

1. Small plantlets of *M. sativa* expressing fluorescent MT marker GFP-MBD are produced *in vitro* from somatic embryos (Vyplelová *et al*., 2017). Well-developed somatic embryos with proliferating root pole are first selected and transferred to a new plate containing Phytagel-solidified full-strength MS medium that is at least 15 mm thick. Somatic embryos are carefully inserted vertically into the solid culture medium to ensure that the root pole will grow vertically inside the medium and the upper green part of the plant will develop in the air above the culture medium.

2. Similarly as in the case of *A. thaliana* preparation, somatic embryos are surrounded by the FEP tube, but in this case with larger inner diameter of 4.2 mm. Insertion of the FEP tube into the culture medium must be careful enough to enclose individual somatic embryo, but not to damage the root pole. Moreover, it should provide enough surrounding culture medium inside the tube for further plant development during imaging.

3. After 1 to 2 days of somatic embryo stabilization and visual inspection of the root pole which should start elongation, such FEP tube with a germinating somatic embryo is carefully removed from the culture medium and prepared for LSFM.

Light-sheet fluorescence imaging

1. After removing from the culture plate the FEP tube with the sample is moved to the LSFM. To fix it in the sample holder, the FEP tube with *A. thaliana* plant (with inner diameter of 2.8 mm) is inserted to the glass capillary with an appropriate diameter while the FEP tube with *M. sativa* plant (with inner diameter of 4.2 mm) is inserted to the sterile plastic syringe of the 1 ml volume which was cut-open at the tip. Glass capillary or plastic syringe serve as a sample holder for fixing the sample in the microscope.

2. Imaging of plant roots described here is done with the light-sheet fluorescence microscope Z.1 (Carl Zeiss, Germany). The system is equipped with W Plan-Apochromat 20×/1.0 NA water immersion detection objective and two 10x/0.2 NA illumination objectives for left and right sample illumination. It is used for synchronized dual-side illumination and both left and right light-sheet illumination beams are modulated into a pivot scan mode.

3. Fluorescent MT markers GFP-TUA6 in *A. thaliana* and GFP-MBD in *M. sativa* are visualized with laser excitation line 488 nm and with emission filter BP505-545. Excitation intensity of the laser is set up to 2-3% of the laser intensity range available in order to minimalize photobleaching and phototoxicity. Time-lapse imaging is done by whole root image acquisition in Z-stack mode every 5 min and experiment duration is designed for a period of several hours (3-15 h). Images are recorded with the sCMOS camera (PCO.Edge, PCO AG) with exposure time of 20-50 ms per optical section.

4. Root growth rate of experimental plants during imaging is stable and fast enough that roots grow out of the field of view in the microscope. For this reason images are recorded in two or three subsequent fields of view coordinated to follow each other at the y axis in order to continuously record growing root displacement during long-term imaging experiments.

5. Acquired series of data characterizing MT arrays during cell division in x-, y-, z- and t-coordinates (Fig. 2) are edited and analysed using Zeiss Zen 2014 software (Black Version).

4.1.2.2 Preparation of plant material for high speed spinning disk recording of the mitotic progress

SDCM technology is based on a rotating disk with multiple pinholes simultaneously covering multiple locations of the field of view by the excitation light. Thus the speed of imaging in this microscope is very fast, making it suitable for documentation of dynamic cellular processes, including MT dynamics in living plant cells. Several studies addressed the dynamics of cortical MT arrays in plant cells. SDCM imaging was used for characterization of MT dynamics on plus and minus ends (Shaw and Lucas, 2011), MT dynamic instability (Shaw *et al*., 2003) or MT nucleation and reorientation in *KATANIN1* mutants (Nakamura *et al*., 2010; Lindeboom *et al*., 2013). Moreover, dynamic changes of complex MT arrays during cell division were also

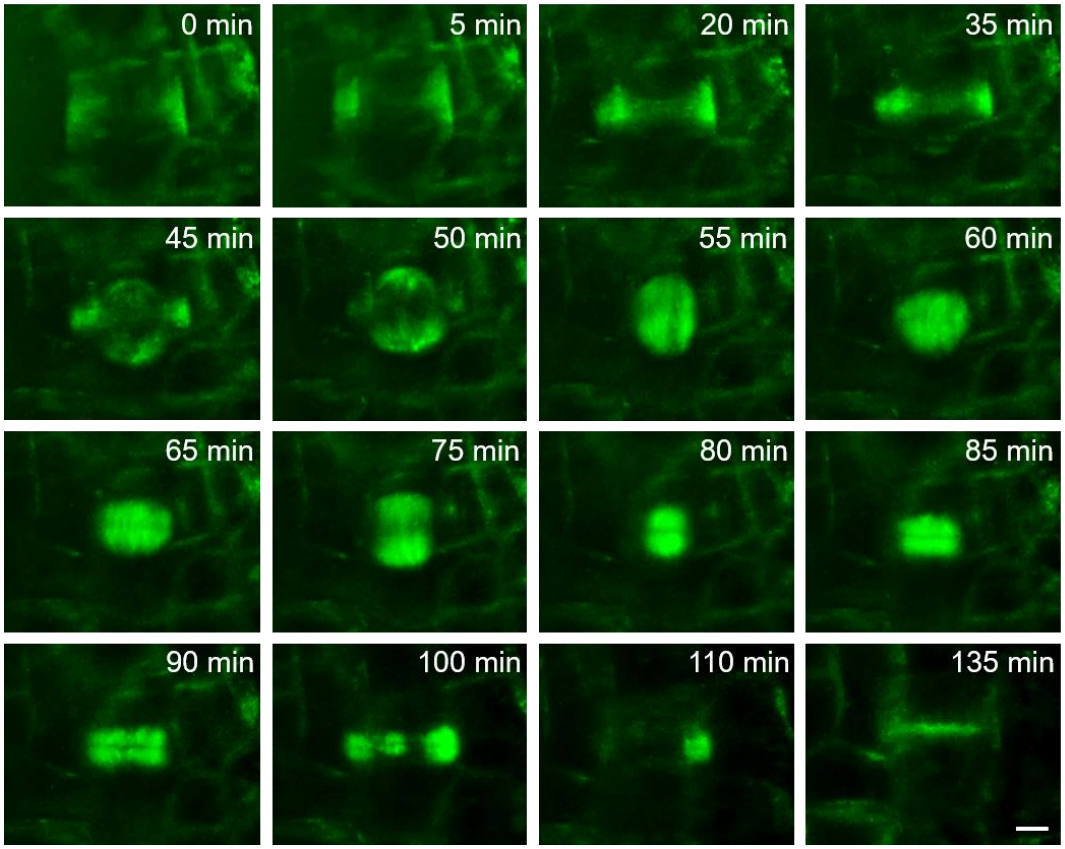

Figure 2. Time-lapse imaging of MT arrays during mitosis and cytokinesis in the root epidermal cell of *Medicago sativa* plant stably transformed with a *35S::GFP:MBD* construct using LSFM. Sequence of images showing progression of PPB narrowing and disappearance together with formation of the mitotic spindle, establishment of the phragmoplast, its centrifugal enlargement in lateral direction during the cytokinesis, final fusion of cell plate with parental cell wall and reappearance of cortical MT network in post-mitotic interphase cell. Time of the cell division progression is indicated in min. Scale bar: 5 μm. Adapted from Vyplelová *et al*., 2018.

described using SDCM quire recently (Murata *et al*., 2013; Komis *et al*., 2017). Time-lapse imaging of the entire process of mitosis brings temporal information on the duration of individual stages, including the formation of PPB, mitotic spindle and phragmoplast (Fig. 3).

1. Young seedlings of *A. thaliana* suitable for SDCM imaging are obtained from seeds 3-4 days after their germination. Before this, seeds of transgenic lines expressing an appropriate MT marker must be surface sterilized with 70% (v/v) ethanol for 2 min followed by 1% (v/v) sodium hypochlorite containing 0.05% (v/v) Tween 20 for 8 min. After plating sterile seeds on plates containing a half-strength MS medium without vitamins, with 1% (w/v) sucrose, pH adjusted to 5.7, and solidified with Phytagel at a concentration 0.6% (w/v), plates are stored for 2-4 days at 4^{o}C for stratification. Following this period plates with seeds are placed into the growth

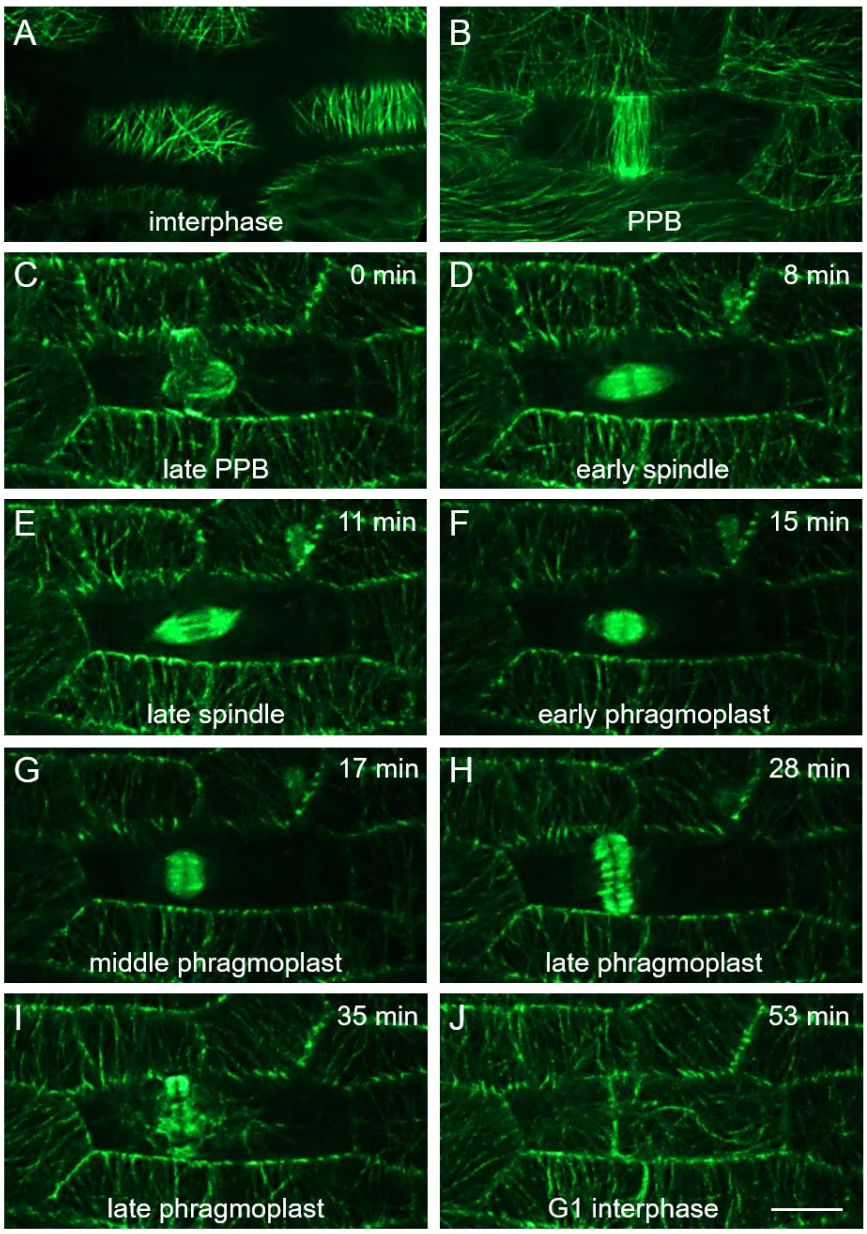

Figure 3. Time-lapse imaging of MT arrays during mitosis and cytokinesis in petiole epidermal cell of *Arabidopsis thaliana* plant stably transformed with a *35S::GFP:TUA6* construct using SDCM. Time-lapse recording of PPB narrowing from cells in interphase (A) to preprophase (B), PPB disappearance and mitotic spindle formation at prometaphase (C), mitotic spindle in metaphase and anaphase (D, E), early phragmoplast formation at telophase (F), progression of middle and late phragmoplast during cytokinesis (G, H), termination of the phragmoplast at the end of cytokinesis (I) and rearrangement of cortical MTs at the post-cytokinetic G1 phase (J). Time of the cell division progression is indicated in min. Scale bar: 100 μm. Adapted from Vyplelová *et al*., 2018.

chamber at 22°C, 50% humidity and 16/8 h (light/darkness) photoperiod for germination. Plates are positioned vertically to allow straight growth of roots at the surface of solidified medium.

2. Imaging of seedlings is performed using microscopy slides prepared in the form of microchambers consisting of microscopy slide, spacers on the side of the slide made from

double sided tape or parafilm, and a coverslip. Sample is thus sandwiched between slide and coverslip with a stable distance ensuring enough space for young *A. thaliana* plant. A drop of liquid half-strength MS medium is placed in the middle of the slide and one selected seedling is transferred to the drop. After closing the seedling with a coverslip the microchamber is sealed on the sides and edges by parafilm strips to prevent evaporation of liquid half-strength MS medium during time-lapsed imaging, which may last more than 1 h. Transfer of selected plants from the sterile culture medium to the microscopy slide should be done under sterile conditions in the laminar flow box.

3. A convenient part of young seedling possessing a high number of cells in different stages of mitotic cell division is the root tip. Young seedling plants (3-4 days after germination) are most suitable for such observations. Dividing cells in the green aerial part of *A. thaliana* plants can be found in the petiole of the young first true leaf (Fig. 3). This tissue is flat, well organized and easily accessible, but is available only later in the plant development, e.g. in 7 days old seedlings.

4. In our laboratory we operate a Cell Observer Z1 spinning disk confocal microscope (Carl Zeiss, Germany), equipped with high-resolution Evolve 512 back-thinned EM-CCD camera (Photometrics). Observation of cell division is regularly performed with an EC Plan-Neofluar 40×/1.3 NA oil immersion objective and Plan-Apochromat 63×/1.4 NA oil immersion objective. Plant samples with the MT marker GFP-TUA6 are imaged with excitation laser line 488 nm and emission filter BP525/50. For convenience, reduction of the dataset size and minimization of sample photodamage, entire z-stacks are acquired every 30 seconds, covering a period of ca. 1 h, which sufficiently covers the entire mitosis and cytokinesis. Data sets are analysed with Zeiss Zen 2014 software (Blue Version).

4.1.2.3 Imaging of plant mitotic MT arrays with the point-scanning confocal Airyscan system with improved resolution

CLSM equipped with Airyscan system represents a new application of a point-scanning imaging approach with improved resolution. The system is equipped with a 32 GaAsP detector providing high sensitivity and superior light collecting capacity. Samples can be scanned with the fast mode allowing sufficient temporal resolution during 3D spatial and temporal acquisition. Alternatively, a high-resolution mode could be used allowing improved 3D

resolution for acquiring single Z-stacks. Taking into account these technical improvements, we utilized the LSM880 Airyscan microscopy platform (Zeiss Microscopy, Oberkochen, Germany) for the documentation of the mitotic progress in cells of the *ktn1-2* mutant stably expressing the MT marker GFP-TUA6 (Komis *et al*., 2017). Defects in the organization of mitotic MT arrays in dividing cells caused by mutation in the *KATANIN1* gene were clearly documented by comparison to the corresponding control (Fig. 4).

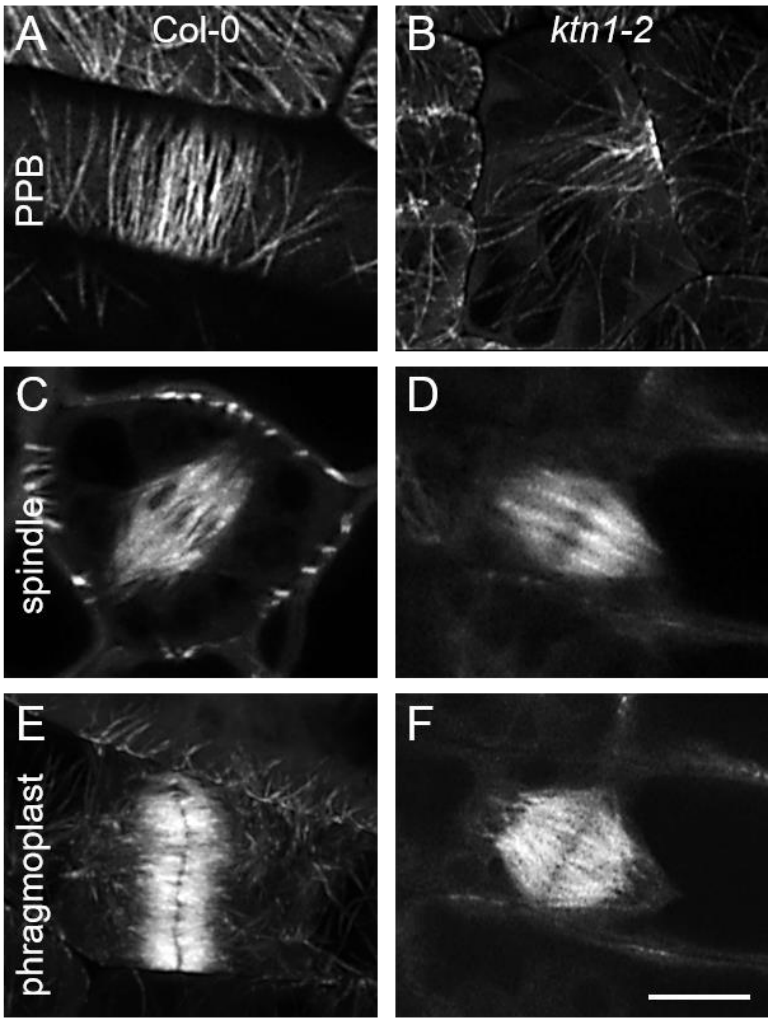

Figure 4. Comparative analysis of MT arrays during mitosis and cytokinesis of leaf petiole epidermal cells in *Arabidopsis thaliana* plants stably transformed with a *35S::GFP:TUA6* construct between wild type plants and a knock-out mutant *ktn1-2*, deficient in MT severing protein KATANIN 1 using CLSM equipped with the Airyscan system. Organization of MT arrays typical for particular cell division stages in cells of the wild type plant (A, C, E) and the *ktn1-2* mutant (B, D, F). (A, B) Narrowing of the PPB in late G2 phase of the cell cycle (preprophase stage). Note unipolar and disorganized arrangement of PPB MTs in the *ktn1-2* mutant (B). (C, D) Mitotic spindle organization, showing no structural changes between control and *ktn1-2* mutant cells. (E, F) Organization of phragmoplast MTs during cytokinesis. In comparison to control (E), phragmoplast in the *ktn1-2* mutant is abnormally shaped (F). Scale bar: 5 μm. Adapted from Vyplelová *et al*., 2018.

1. Seeds of transgenic lines expressing an appropriate MT marker (GFP-TUA6) are surface sterilized using 70% (v/v) ethanol for 2 min followed by 1% (v/v) sodium hypochlorite containing 0.05% (v/v) Tween 20 for 8 min. After washing sterile seeds are plated on the surface of half-strength MS medium without vitamins and with 1% (w/v) sucrose, pH adjusted to 5.7, solidified with Phytagel at a concentration 0.6% (w/v). Following seed stratification at 4°C for 2-4 days, they are cultivated in growth chamber at 22°C, 50% humidity and 16/8 h (light/darkness) photoperiod at a vertical position to allow straight growth of roots on the surface of the solidified medium.

2. First, it is necessary to build the observation chamber using a glass slide and coverslip spaced with parafilm or double sticky tape strips. A drop of liquid half-strength MS medium is placed in the middle of the slide and one selected seedling is transferred to the drop. The sample is sandwiched between slide and coverslip with a stable distance ensuring enough space for young *A. thaliana* plant. The microchamber is sealed on the sides and edges by parafilm strips to prevent evaporation of liquid half-strength MS medium during time-lapse imaging for more than 1 h.
Note: The transfer of selected plants from the culture medium to the microscopy slide should be done under sterile conditions in the laminar flow box.

3. Epidermal petiole cells of young first true leaf are suitable for observation of cell division in the green part of *A. thaliana* plants. The most preferable plants are 6-7 days old for preparation of such sample. The plant must be entirely covered by the coverslip and young first true leaf must be positioned by abaxial (lower) leaf side parallel to the coverslip.

4. The example given here (Fig. 4) was obtained using LSM880 with Airyscan (Zeiss Microscopy, Oberkochen, Germany). We used single photon excitation with the 488 nm laser line and a 32 GaAsP detector for fluorescence detection. The superior light collecting capacity of the Airyscan and the sensitivity of the GaAsP detector allowed setting laser power to a level not exceeding 2% of the range available. Observation of dividing cells was done with Plan-Apochromat 63×/1.4 NA oil immersion objective and data sets were analysed with Zeiss Zen 2014 software (Blue Version).

4.1.3 Conclusions

Sample preparation is of paramount importance for the adequate visualization of mitosis and cytokinesis in plants. The procedures described above aim to describe preparations for high resolution time lapse imaging of mitotic dynamics by Airyscan CLSM. Additionally we provide easy to follow procedures for mounting Arabidopsis seedlings for tracking and documenting mitotic cells in the multicellular context of entire organs such as roots and leaf petioles. High resolution studies with Airyscan may be used to reveal mechanisms of spindle and phragmoplast assembly progression in living cells, while light-sheet imaging can be used to obtain information on the coordination of the mitotic process in populations of hundreds of cells, e.g. within root apical meristem.

4.2 Alfalfa root growth rate correlates with progression of microtubules during mitosis and cytokinesis as revealed by environmental light-sheet microscopy

4.2.1 Introduction

Environmental and long-term imaging are compromised in such conventional microscopic methods as CLSM and SDCM because living model plants are exposed to several stresses (artificial horizontal position, tight microscopic chamber with limited nutrients and pressure between microscopic slides) and suffer from high energy illumination causing undesirable phototoxicity and photodamage. In comparison to Arabidopsis, crop species including alfalfa typically have more robust habitus and their roots are thicker because they consist from more tissue layers. Consequently, mounting of the whole alfalfa seedlings to classical horizontally-positioned microscopy stage is more challenging and affects fitness of such samples during long-term experiments. Obviously, microscopic techniques like CLSM and SDCM also suffer from serious limitations in imaging depth. Finally, all commercial CLSM and SDCM platforms are based on horizontal stages, not allowing for living plants to be observed normally oriented with respect to the gravity vector. All these disadvantages can be avoided by using LSFM. Optical sectioning of the sample with excitation sheet of light is very fast. Importantly, excitation of fluorophores is restricted within the light-sheet volume, which effectively eliminates out-of-focus fluorescence and bleaching. Emitted fluorescence light is detected by independent orthogonally-positioned detection objective. Focal plane of the light-sheet is harmonized with the focal plane of the detection objective and thus, very thin layer of the sample is detected by spherical aberration-free imaging. Sample can be freely rotated with respect to the light-sheet plane illumination allowing multi-angular image acquisition. Fast

imaging mode of LSFM ensures that imaged cells are illuminated with very low level of excitation energy (Stelzer, 2015). Finally, in some custom-made and commercial LSFM platforms, sample loading can be done vertically allowing typical gravitropic growth of plants during the course of imaging. All these technical benefits bring LSFM to the forefront of current standards for proper spatial, temporal and physiological imaging of developmental processes. So far the applications of LSFM in plants have been preferentially restricted to the developmental imaging of primary or lateral roots in Arabidopsis (Maizel *et al.,* 2011; Lucas *et al.,* 2013; Rosquete *et al.,* 2013; Vermeer *et al.,* 2014; Ovečka *et al.,* 2015; von Wangenheim *et al.,* 2016). Subcellular localizations of cytoskeletal components by LSFM in Arabidopsis are very few, and include structure and dynamics of both MT and actin cytoskeleton in different organs (Ovečka *et al.,* 2015), cell division in root epidermis (Maizel *et al.,* 2011) and developmental imaging of EB1c in cells of different tissues and developmental zones of the root tip (Novák *et al.,* 2016).

Generally, studies on cellular distributions of fluorescently-labelled proteins in *M. sativa* are more difficult due to the limited availability of established molecular tools and efficient transformation techniques. In contrast to Arabidopsis and tobacco, there are only scarce reports on cytoskeletal dynamics during cell division in *M. sativa*. It is known that transitions between G1/S and G2/M phases are controlled by cyclin-dependent Ser/Thr kinases, among others also by *M. sativa* kinase CDKB2;1 (Joubès *et al.,* 2000). This kinase is activated in mitotic cells and it is localized in PPB, perinuclear ring in early prophase, mitotic spindle and phragmoplast (Mészáros *et al.,* 2000). Activity of CDKB2;1 is controlled by protein phosphatase 2A (PP2A) which affects MT organization during the mitosis (Ayaydin *et al.,* 2000). However, both organization and dynamics of MTs was characterized only in developing and Nod factor-treated root hairs of *M. truncatula* (Sieberer *et al.,* 2002; 2005; Timmers *et al.,* 2007). In addition, actin cytoskeleton was visualized in interface and post-mitotic root cells and in root hairs using Plastin-GFP and GFP-mTalin in *M. truncatula* (Voigt *et al.,* 2005). Here we employed for the first time LSFM for long-term live-cell imaging of GFP-tagged MTs in thicker roots of a legume crop plant. We performed quantitative study of root growth rate and duration of individual mitotic stages in diverse tissues of robust roots of transgenic *M. sativa* plants originating from somatic embryogenesis that carried GFP-MBD MT marker. We show positive correlation between root growth rate and dynamic patterns of MT arrays in dividing cells during continuous root development.

4.2.2 Materials and Methods

4.2.2.1 Stable transformation of *Medicago sativa*

M. sativa stable transformation has been performed with *Agrobacterium tumefaciens* strain GV3101 containing construct carrying microtubule-binding domain (MBD) of the mammalian MICROTUBULE-ASSOCIATED PROTEIN 4 (MAP4) fused to green fluorescent protein (GFP) driven by constitutive 35S promoter. N-terminal GFP fusion with rifampicin and kanamycin resistance was prepared by classical cloning method in pCB302 vector with herbicide phosphinothricin as the selection marker *in planta*. Phosphinothricin has been added to each subculture medium to control successful transformation. The transformation procedure was performed according to protocol for efficient transformation of alfalfa described by Samac and Austin-Phillips (2006). Highly responsive cultivar Regen SY (RSY; Bingham, 1991) of *M. sativa* has been selected. Well-developed leaves at the third node from the shoot apex were used as a source plant material. Leaves explanted from plants were surface sterilized, cut in half and wounded on the surface with sterile scalpel blade. They were incubated with overnight grown *A. tumefaciens* culture with cell density between 0.6 and 0.8 at A_{600} nm for 30 min. Formation of calli and somatic embryos as well as induction and development of shoots and roots were achieved by transferring culture on the appropriate media (Schenk and Hildebrant medium for *A. tumefaciens* inoculation, Gamborg medium for cocultivation, callus initiation and embryo formation and Murashige and Skoog media for plant rooting, development and maintenance) for appropriate time in the culture chamber at 22°C, 50% humidity and 16/8 h light/dark photoperiod (Samac and Austin-Phillips, 2006). Regenerated plants were maintained on media with selective phosphinothricin marker and tested for the presence of GFP fusion proteins using fluorescence microscope. Transgenic *M. sativa* plants were further clonally propagated *in vitro* via somatic embryogenesis from leaf explants. Received somatic embryos stably expressing *35S::GFP:MBD* construct were used in further experiments.

4.2.2.2 Plant material and sample preparation for LSFM imaging

Transgenic somatic embryos carrying *35S::GFP:MBD* construct with well-developed root poles were separated, individually transferred and inserted vertically into solidified Murashige and Skoog-based root and plant development medium (MMS) or into Murashige and Skoog plant maintaining medium (MS). Embryos were enclosed from the upper part by FEP tube with an inner diameter of 4.2 mm and wall thickness of 0.2 mm (Wolf-Technik, Germany). FEP tubes were inserted into the culture medium carefully to enclose individual somatic embryo and

surrounding medium inside of the tube. After 1 to 2 days of somatic embryo stabilization and after visual inspection of the root pole which was starting elongation, such FEP tube with somatic embryo was carefully removed from culture medium and prepared for LSFM. Sample was prepared according to the "open system" protocol for long-term live-cell imaging of *A. thaliana* seedlings described by Ovečka *et al*. (2015), with a modification in the respect that *M. sativa* roots are thicker than *A. thaliana* roots. The block of the culture medium inside of the FEP tube serves as holder of the sample and simultaneously also as root growing medium. Upper green part of the somatic embryo and later on developing plantlet was in open space of the FEP tube with the access to air. Thus, the root was able to grow inside of the microscope chamber without stress during long-term experiments. After removing from the culture plate FEP tube with the sample was inserted into sterile plastic syringe (with 1 ml volume and an inner diameter of app. 5 mm), which was cut-open at the tip before use. Plastic syringe was used for fixing the sample in sample holder of the microscope. Sample holder with the sample was placed into observation chamber of the microscope tempered to 22°C using Peltier heating/cooling system. Before insertion of the sample to the microscope somatic embryo in the solidified culture medium was ejected slightly out of the FEP tube to the extent that root in the block of solidified culture medium was directly loaded into appropriate liquid medium (MMS or MS) in the microscope chamber. FEP tube was still holding the sample, but was no more surrounding the root part of the plant, which enhanced considerably quality of root deep imaging. To prevent contamination during long-term imaging, liquid medium filling the observation chamber was filter-sterilized using a sterile syringe filter. FEP tube was sterilized using 70% ethanol and dried out before use. After insertion of the sample to the observation chamber of the light-sheet microscope and 30 min stabilization, it was prepared for imaging.

4.2.2.3 LSFM

Long-term fluorescence live-cell imaging was done with the light-sheet Z.1 system (Carl Zeiss, Germany), equipped with W Plan-Apochromat 20×/1.0 NA water immersion detection objective (Carl Zeiss, Germany) and two LSFM 10x/0.2 NA illumination objectives (Carl Zeiss, Germany). Samples were imaged using dual-side illumination by a light-sheet modulated with a pivot scan mode. GFP-MBD was visualized with excitation line 488 nm and with emission filter BP505-545. Laser excitation intensity did not exceed 3% of the laser intensity range available. Image acquisition was done every 5 min in Z-stack mode for a period of 3-12 h. Scaling of images in x, y and z dimensions was 0.152 x 0.152 x 0.469 µm. Images were scanned

in two or three views coordinated to follow each other in y axis to record root growth in long-term imaging and to prevent the movement of the growing root out of the field of only one field of view. Images were recorded with the PCO.Edge camera (PCO AG, Germany) with the exposure time 20 ms or 50 ms per optical section.

4.2.2.4 Measurements and statistical analyses

Time-lapsed images of growing roots in x-, y-, z- and t-dimensions were acquired using Zen 2014 software, black edition (Carl Zeiss, Germany). Images in the .czi format were transformed to 2D images using Maximum intensity projection function. Subsets of data containing individual dividing cells were created either with defined x- and y- dimensions from maximum intensity projection images or from original data with defined x-, y- and z- dimensions. Root growth rate and displacement of individual cells in growing roots (representing a displacement distance of dividing cell in growing root in respect to the growth medium, Baskin, 2013) were recorded from the stage of mitotic spindle formation till the phragmoplast disappearance as well as width of PPB were measured using Line function of the Zen 2014 software. Duration of individual mitotic stages in min (stages of PPB, spindle and phragmoplast) in dividing cells was measured using Coordinate function of the Zen 2014 software. The initial stage of the measurement started at a progressive PPB narrowing which was defined by PPB width when it was in the range of 2 – 4 μm.

For measurement of duration of mitotic and cytokinetic stages only transverse cell divisions were selected. All parameters were measured and evaluated separately for epidermis and the first outer layer of cortex. Data from 9 individual roots were collected. After quantitative evaluation, measured roots were divided into three groups according to the root growth rate.

Final statistical data evaluation and plotting were done with Microsoft Excel software. Statistical significance was carried out using program STATISTICA 12 (StatSoft) according to one-way ANOVA and subsequent Fisher´s LSD test at the level of significance of $p < 0.05$.

4.2.3 Results

4.2.3.1 Root growth rate

Whole plantlets growing in a cylinder of solidified culture medium inside of FEP tubes were placed to the light-sheet microscope. However, due to the bulkiness of the samples, only the apical part of the root was selected for time-lapse imaging. Root growth inside of the light-sheet microscope was recorded in 5 min intervals. Due to the displacement of the continuously

growing root tip out of the selected field of view, images were recorded in two or three axially overlapping fields of view. Each field of view was 292.46 x 292.46 μm and thus, recording of root growth in two successive fields of view provided a frame 580 μm long within which we were able to measure root elongation. Based on the variability among characterized roots, their elongation speed was measured over time periods ranging from 3 to 12 h. Most likely due to the somaclonal variability during somatic embryogenesis, nine individual root tips which were taken into account elongated at different extents and so they were classified into three different groups (Fig. 5A-D) according to their root growth rate. Roots showing root growth rate in the range between 0.7 – 1.4 $\mu m.min^{-1}$ were characterized as fast-growing roots (Fig. 5A, D, E), roots with growth rate in the range of 0.2 – 0.5 $\mu m.min^{-1}$ were characterized as medium-growing roots (Fig. 5B, D, E) and roots with growth rate less than 0.2 $\mu m.min^{-1}$ were characterized as fast-growing roots (Fig. 5C, D, E). Measurement of the growth distance of representative roots from each group over a period of 3 h during LSFM imaging yielded values ranging between 145.1 μm for a fast-growing root (Fig. 5A) to 67.1 μm for a medium-growing root (Fig. 5B) and 32.6 μm for a slow-growing root (Fig. 5C). Selection of individual roots according to their root growth rate (Fig. 5D) was taken into consideration in all further quantitative analyses. Analysis of correlation between increase in length of growing roots and a given recording time during time-lapse light-sheet imaging clearly revealed different root growth rate of fast-growing, medium-growing and slow-growing roots (Fig. 5E), giving proof for distribution of analysed roots into three different groups for further quantitative analyses.

4.2.3.2 Duration time of individual cell division stages

Time-lapse LSFM imaging of growing roots of transgenic alfalfa plants in 5 min intervals over a period of several hours allowed recording of cells in the meristematic zone and at different stages of cell division. In particular, cells with established PPB (at late G2 phase) were monitored and their entrance to the cell division was documented in time. Preprophase and prophase stage of the cell division was identified from the stage of progressive PPB narrowing when PPB width was in the range of 2-4 μm. This time point has been set up as time 0 min. Recording of preprophase and prophase stage finished by PPB disappearance in cells entering mitosis with starting of mitotic spindle formation in prometaphase. Time-lapse recording of this stage in 5 min intervals revealed its duration for 35-40 min. Interestingly, in roots with different

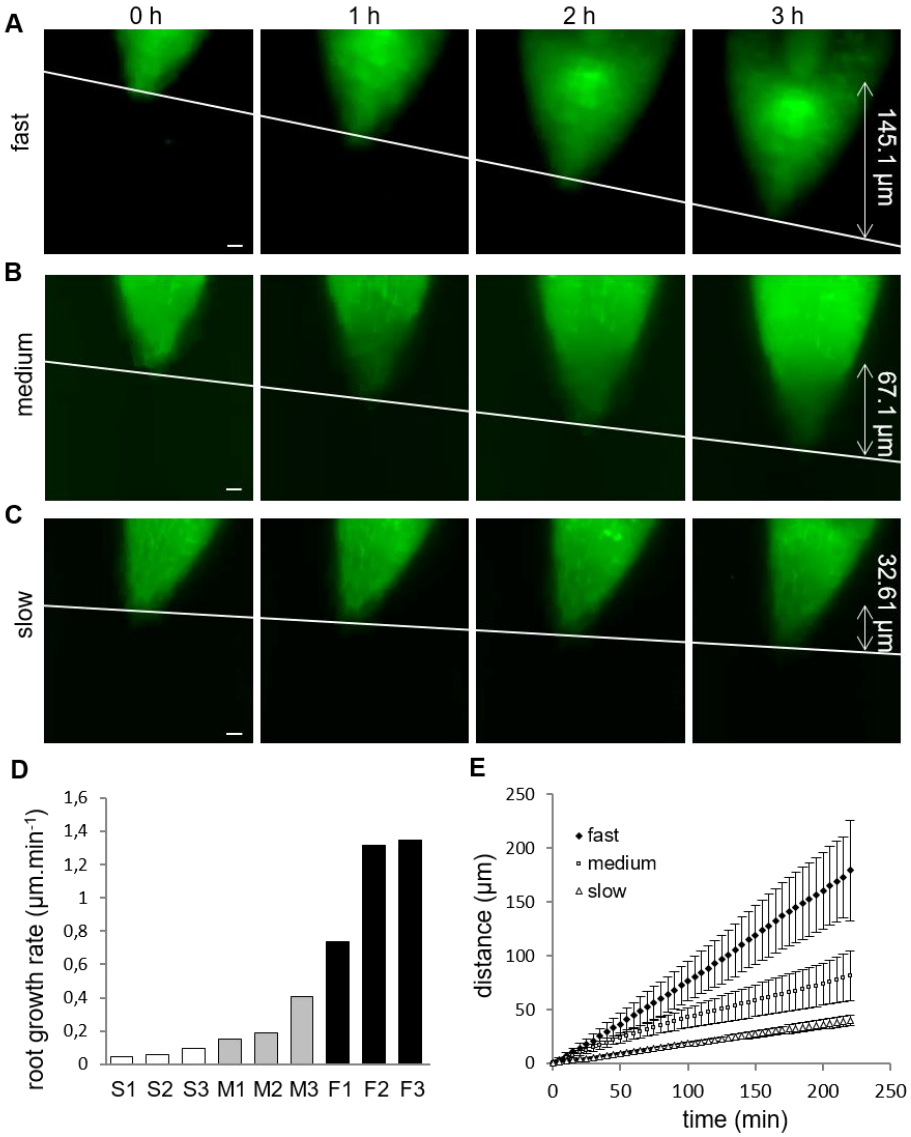

Figure 5. Root growth rate of *M. sativa* somatic embryo-derived plantlets, expressing *35S::GFP:MBD* construct. (A-C) LSFM imaging of root growth over the period of 3 h. Based on the root growth rate, roots were sub-divided into three different groups. Representative examples of a fast-growing root, grown in a distance of 145.1 µm in 3 h (A), a medium-growing root, grown in a distance of 67.1 µm in 3 h (B) and a slow-growing root, grown in a distance of 32.6 µm in 3 h (C). Double-pointed arrows with appropriate values on the right side of images show recorded distance in µm. White line indicates displacement of the root tip in individual time points of the measurement. (D) Bar chart illustrating distribution of measured individual roots according to their root growth rate. White bars represent slow-growing roots (S1, S2, S3), grey bars represent medium-growing roots (M1, M2, M3) and black bars represent fast-growing roots (F1, F2, F3). (E) Time course of primary root growth showing a correlation between average length increase of fast-growing (♦), medium-growing (□) and slow-growing (Δ) roots and recording time from time-lapse light-sheet imaging at 5 min intervals. Adapted from Vyplelová *et al*., 2017.

root growth rate this duration was different (Fig. 6A-C). In average, preprophase and prophase stage of cell division was fastest in fast-growing roots, while duration of this stage did not differ between medium-growing and slow-growing roots (Fig. 6D). Bars = 20 µm (A-C).

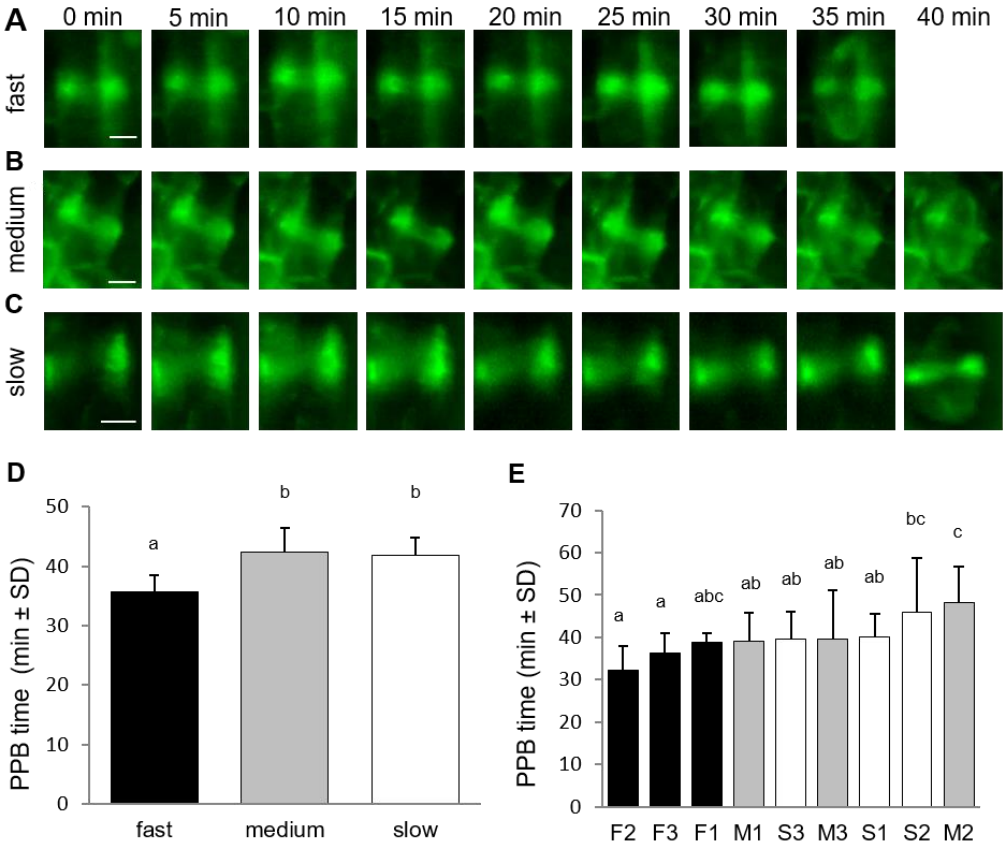

Figure 6. Duration of the preprophase and prophase stage of the cell division. (A-C) Series of stills from time-lapse light-sheet imaging of dividing cells in root epidermis and cortex of *M. sativa* plants expressing *35S::GFP:MBD* construct. Sequence of preprophase and prophase stage starting from PPB narrowing and finishing by last stage of PPB presence and early mitotic spindle formation. Progress of the preprophase and prophase stage is shown for fast-growing roots (A), medium-growing roots (B) and slow-growing roots (C). Series of images were recorded in 5 min intervals from the stage of cell division when progressive PPB narrowing was defined by PPB width in the range of 2-4 μm (time 0 min). (D) Average duration time of preprophase and prophase stage of cell division in all roots of fast-growing, medium-growing and slow-growing group of roots. (E) Average duration time of preprophase and prophase stage in all dividing cells of individual roots. Roots are arranged from shortest to longest average duration time of preprophase and prophase stage. Black bars represent fast-growing roots (F1, F2, F3), grey bars represent medium-growing roots (M1, M2, M3) and white bars represent slow-growing roots (S1, S2, S3). Different letters above the bars represent statistical significance according to one-way ANOVA test at $P < 0.05$. Bars = 5 μm (A-C). Adapted from Vyplelová *et al*., 2017.

Basically the same results were obtained after comparison of preprophase and prophase stage duration in individual roots (Fig. 6E).

Stage of mitotic spindle was measured from disappearance of the PPB with simultaneous mitotic spindle formation through metaphase and anaphase to mitotic spindle disappearance at late anaphase. Measurement revealed that termination of the mitotic spindle stage–at late anaphase was different among three groups of roots differing in their growth rate (Fig. 7A-C). The average duration time of this stage revealed that it was shortest in fast-growing roots,

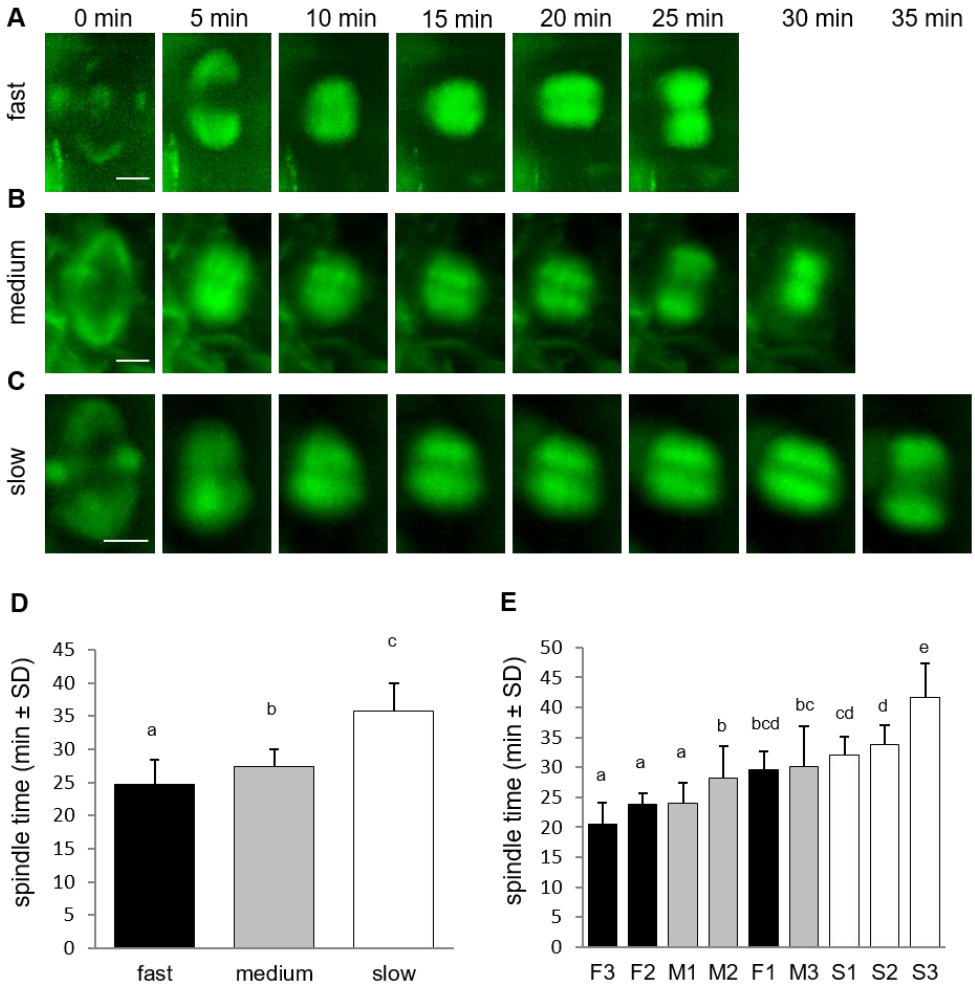

Figure 7. Duration of the mitotic spindle stage from prometaphase to telophase during the cell division. (A-C) Series of stills from time-lapse light-sheet imaging of dividing cells in root epidermis and cortex of *M. sativa* plants expressing *35S::GFP:MBD* construct. Sequence of prometaphase, metaphase, anaphase and telophase stages starting from PPB disappearance and mitotic spindle formation at prometaphase and finishing by last stage of mitotic spindle presence at telophase. Progress of the mitotic spindle stages is shown for fast-growing roots (A), medium-growing roots (B) and slow-growing roots (C). Series of images were recorded in 5 min intervals from the PPB disappearance and mitotic spindle formation at prometaphase (time 0 min). (D) Average duration time of mitotic spindle (prometaphase, metaphase, anaphase and telophase) stages of cell division in all roots of fast-growing, medium-growing and slow-growing group of roots. (E) Average duration time of mitotic spindle (prometaphase, metaphase, anaphase and telophase) stages in all dividing cells of individual roots. Roots are arranged from shortest to longest average duration time of mitotic spindle. Black bars represent fast-growing roots (F1, F2, F3), grey bars represent medium-growing roots (M1, M2, M3) and white bars represent slow-growing roots (S1, S2, S3). Different letters above the bars represent statistical significance according to one-way ANOVA test at $P < 0.05$. Bars = 5 μm (A-C). Adapted from Vyplelová *et al*., 2017.

significantly longer in medium-growing roots and the longest in slow-growing roots (Fig. 7D). Comparison of mitotic spindle duration in individual roots confirmed this observation, showing shortest duration of this stage in fast-growing roots and longest duration in slow-growing roots

(Fig. 7E). Duration of the phragmoplast stage was determined from mitotic spindle disappearance at late anaphase with the formation of early (disk) phragmoplast to disappearance of late (ring and discontinuous) phragmoplast at the end of cytokinesis. Consistent with the duration of previous cell division stages the termination of phragmoplast expansion also occurred at different time among the three groups of roots differing in their growth rate (Fig. 8A-C).

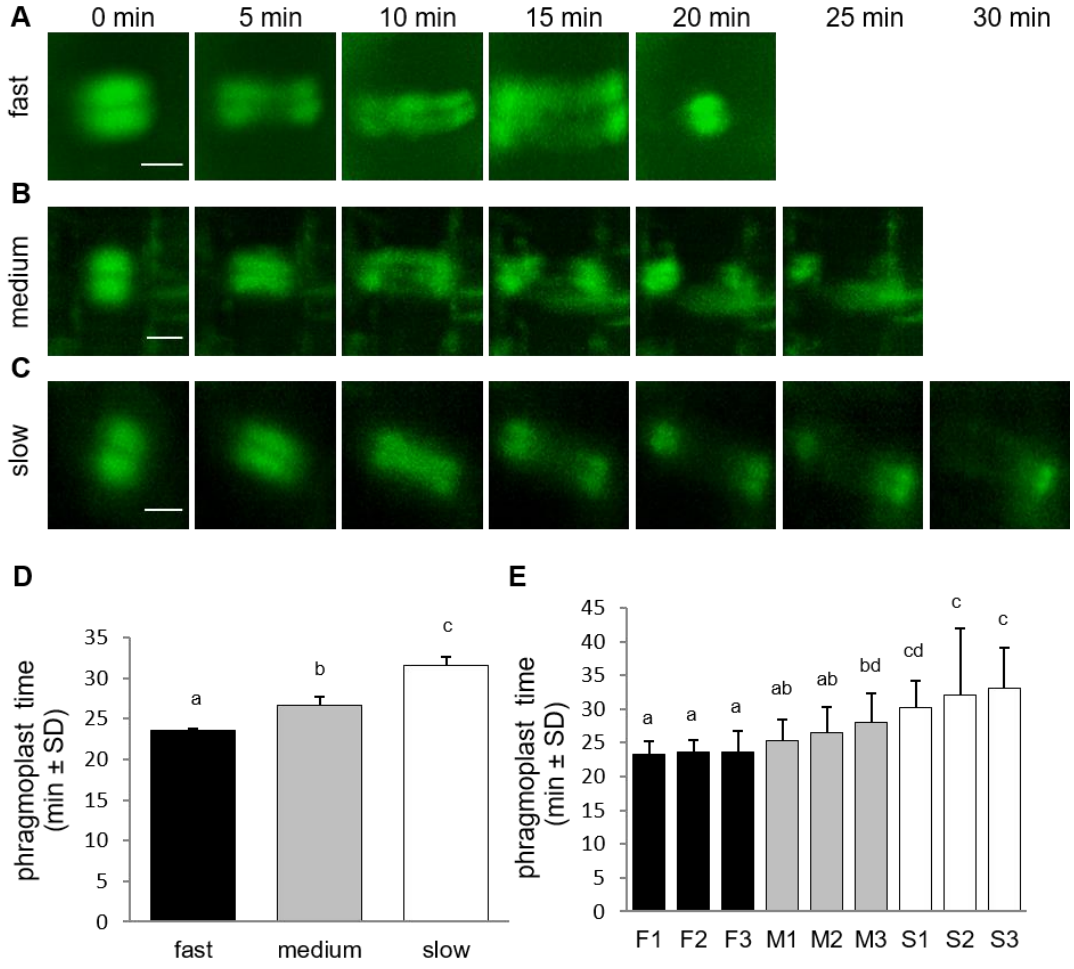

Figure 8. Duration of the phragmoplast stage of the cell division. (A-C) Series of stills from time-lapse light-sheet imaging of dividing cells in root epidermis and cortex of *M. sativa* plants expressing *35S::GFP:MBD* construct. Sequence of phragmoplast stages is shown for fast-growing roots (A), medium-growing roots (B) and slow-growing roots (C). Series of images were recorded in 5 min intervals from the stage of early phragmoplast formation (time 0 min). (D) Average duration time of phragmoplast stage of cell division in all roots of fast-growing, medium-growing and slow-growing group of roots. (E) Average duration time of phragmoplast stage in all dividing cells of individual roots. Roots are arranged from shortest to longest average duration time of phragmoplast. Black bars represent fast-growing roots (F1, F2, F3), grey bars represent medium-growing roots (M1, M2, M3) and white bars represent slow-growing roots (S1, S2, S3). Different letters above the bars represent statistical significance according to one-way ANOVA test at $P < 0.05$. Bars = 5 μm (A-C). Adapted from Vyplelová *et al*., 2017.

The average duration time of phragmoplast stage was shortest in fast-growing roots, significantly longer in medium-growing roots and the longest in slow-growing roots (Fig. 8D). Comparison of phragmoplast stage duration in individual roots confirmed this observation (Fig. 8E).

4.2.3.3 Correlation between duration of cell division stages and root growth rate

To reveal possible relationship between speed of root growth and duration of cell division in root apical meristem we analysed correlations between duration of individual cell division stages and root growth rates. Three groups of roots with different root growth rates were analysed separately. Cross-comparison of average root growth rate with average duration of PPB (Fig. 9A), mitotic spindle (Fig. 9B) and phragmoplast (Fig. 9C) stages revealed different tendency. Recorded data were arranged in clusters, distinctly separating groups of fast-growing, medium-growing and slow-growing roots (Fig. 9A-C). Overall data from all individual dividing cells showing duration time of the PPB (Fig. 9D), mitotic spindle (Fig. 9E) and phragmoplast (Fig. 9F) stages correlated very well with the root growth rates, and confirmed clear separation of fast-growing roots from the rest. Particularly values for roots F2 and F3 (Fig. 5D) segregated separately in the upper part of the graphs (Fig. 9D-F).

In general, the extend of correlation between root growth rate and duration time of the PPB (Fig. 9D), mitotic spindle (Fig. 9E) and phragmoplast (Fig. 9F) stages in all dividing cells of fast-, medium- and slow-growing roots is rather low, as documented by trends of correlation lines and values of correlation coefficients (Fig. 10). Negative slope of correlation lines (Fig. 10) indicates a tendency to prolong cell division stages with reducing root growth rates. Thus, clustering of data recorded from individual cell division stages (Fig. 9A-F) and clear separation of these clusters in fast-, medium- and slow-growing roots according to cross-correlation between average duration time of the PPB, mitotic spindle and phragmoplast stages (Fig. 9G) represents crucial aspect of our quantitative evaluation. Collectively, these results suggest correlative regulation of cell division duration depending on the speed of root growth.

4.2.4 Discussion and conclusions

Cell division is key regulatory component of plant morphogenesis and development and one of the most frequently studied biological processes in the plant biology. Monitoring cell divisions in living multicellular plant organs require real time microscopy approach for long-term observation of intact plants that are adapted to proper physiological conditions. Live-cell LSFM

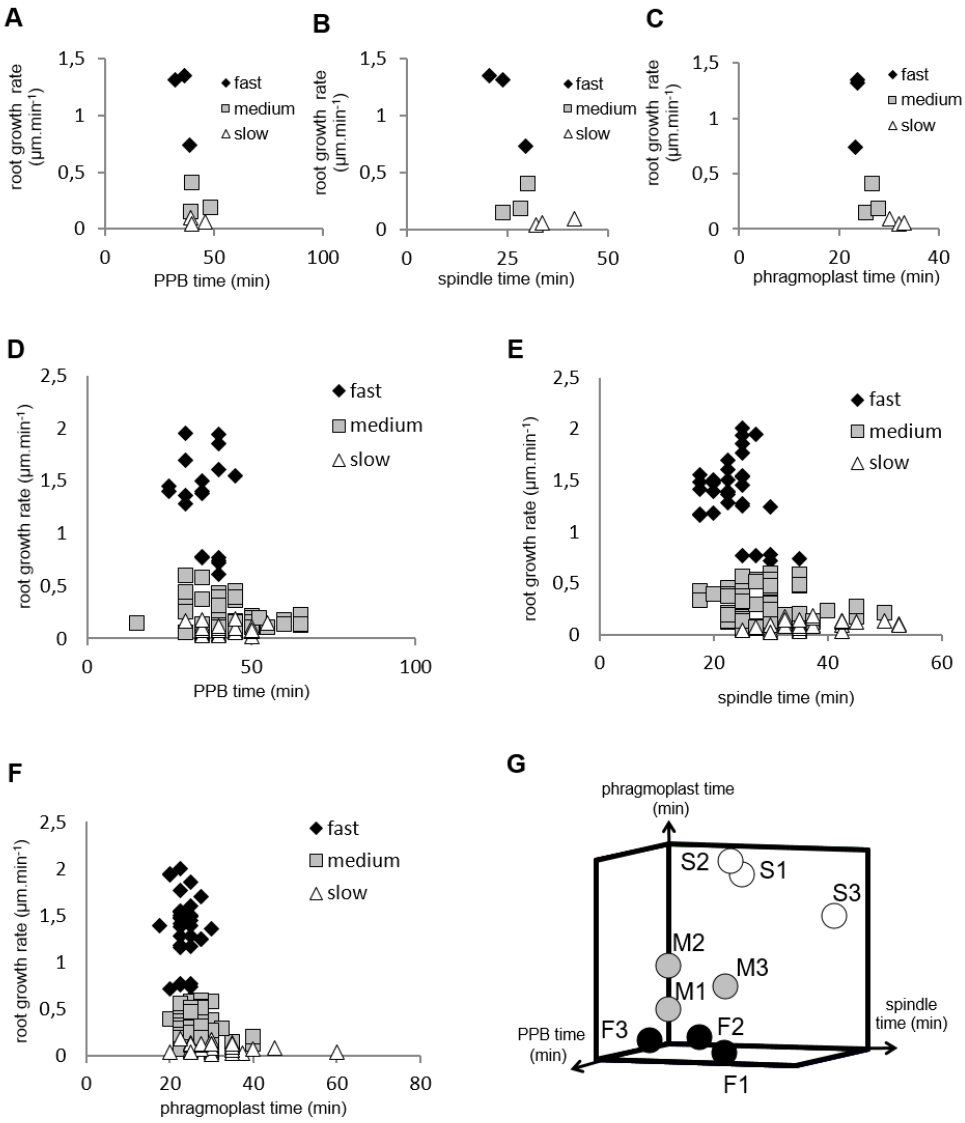

Figure 9. Two- and three-dimensional visualization of data clusters for duration time of individual cell division stages in fast-growing, medium-growing and slow-growing roots according to root growth rate. (A-C) Distribution of clusters for average duration time of the PPB stage (A), mitotic spindle stage (B) and phragmoplast stage (C) according to root growth rate in three fast-growing (♦), three medium-growing (□) and three slow-growing (Δ) roots. (D-F) Distribution of clusters for duration time of the PPB stage (D), mitotic spindle stage (E) and phragmoplast stage (F) according to root growth rate in all individual dividing cells of the fast-growing (♦), medium-growing (□) and slow-growing (Δ) roots. (G) Visualization of data clustering for three fast-growing (F1, F2, F3), three medium-growing (M1, M2, M3) and three slow-growing (S1, S2, S3) roots according to cross-correlation between average duration time of the PPB stage, mitotic spindle stage and phragmoplast stage. Adapted from Vyplelová *et al*., 2017.

imaging of dividing cells could ideally resolve details of cytoskeletal division machinery with high temporal resolution. Moreover, four dimensional monitoring of cell division in organ-,

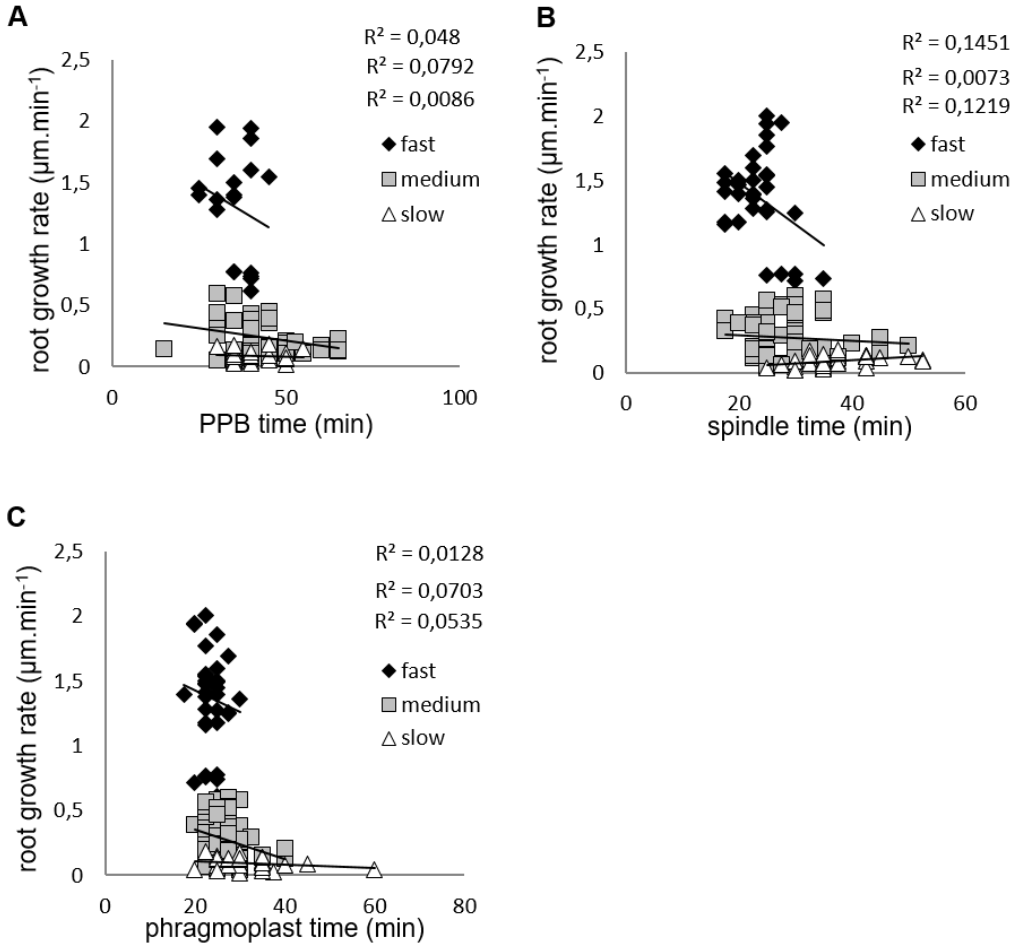

Figure 10. Correlations between root growth rate and duration time of the PPB stage, mitotic spindle stage and phragmoplast stage of dividing cells. (A) Distribution of clusters, correlation lines and correlation coefficients for duration time of the PPB stage in all recorded dividing cells of fast-growing (♦), medium-growing (□) and slow-growing (Δ) roots according to root growth rate. (B) Distribution of clusters, correlation lines and correlation coefficients for duration time of the mitotic spindle stage in all recorded dividing cells of fast-growing (♦), medium-growing (□) and slow-growing (Δ) roots according to root growth rate. (C) Distribution of clusters, correlation lines and correlation coefficients for duration time of the phragmoplast stage in all recorded dividing cells of fast-growing (♦), medium-growing (□) and slow-growing (Δ) roots according to root growth rate. Adapted from Vyplelová *et al*., 2017.

tissue- and cell type-specific context is required for fundamental understanding of cell division regulation during plant growth and development. Nowadays, different microscopy methods are used to study cell division in genetically, developmentally and microscopically-tractable plant model species. Critically important, however, is the adaptation of currently available microscopy techniques for routine live-cell developmental imaging of living robust plant samples, such as crop species. Together with application of efficient protocols for stable transformation of crop species, it should be based on implementation of new approaches, tools and concepts enabling scientific progress in plant cell imaging.

Progression of cell division in plant cells is regulated by particular MT structures, such as PPB, mitotic spindle and phragmoplast. These MT arrays are involved in CDP orientation, symmetry of cell division, segregation of nuclear material into two new cell nuclei and partitioning of cytoplasmic space of dividing cell into two daughter cells. Organization and dynamics of MTs during individual mitotic and cytokinetic stages control the progression of cell division. MT-dependent functions during cell division are mediated by modulators of MT organization and dynamics, such as MAPs, EB1 proteins and MT severing proteins. Study of MAPs from the MAP65 protein family (van Damme *et al.,* 2004; Chang *et al.,* 2005; Mao *et al.,* 2005; Smertenko *et al.,* 2006; Ho *et al.,* 2011; 2012) and EB1 proteins (Chan *et al.,* 2003; 2005; Komaki *et al.,* 2010) in their interactions with spindle and phragmoplast MTs promoted considerably our understanding how MTs are organized and how their dynamic properties regulate cell division progress and duration.

Roles of MT-severing proteins were traditionally connected to dynamic reorganization of cortical MT arrays. Recent study on knock-out mutant *ktn1-2* revealed that KATANIN 1 contributes to PPB formation and maturation, and is involved in the positioning of the mitotic spindle and the phragmoplast (Komis *et al.,* 2017). An important scientific question will be how complex MT network well described in models operates in legume crop species. Starting to address this question in *M. sativa*, we characterized MT arrays during the progress of mitotic cell division and sustained root growth. Main motivation of our study was to collect relevant data at near environmental condition, ensuring stress- and artefact-free imaging of living legume plant that is not interfering with normal plant growth and development. This was possible by implementation of LSFM and proper sample preparation protocols into live developmental imaging of alfalfa plants.

Progress of mitotic cell division, distribution of mitoses within the root meristematic zone and cessation of mitotic activity in the root transition zone are tissue-specifically regulated. It has been shown that cells of the cortex and epidermis quit cell division earlier than cells of the endodermis and central cylinder tissues (Baluška *et al.,* 1990; Schmidt *et al.,* 2014). Duration of the PPB stage can be considerably long, as compared to the duration of other subsequent cell division stages during mitosis (Dhonukshe and Gadella, 2003; Vos *et al.,* 2004; Komis *et al.,* 2017). Alterations in the duration of the phragmoplast expansion have been observed in the Arabidopsis *mpk4* mutant, which is devoid of the mitogen activated protein kinase 4 (MPK4). This stage of the cell division was considerably delayed in comparison to control plants (Beck *et al.,* 2011). Herein, we recorded and quantitatively evaluated duration time of PPB, mitotic

spindle and phragmoplast during cell division of epidermal and cortex cells in root meristem of transgenic *M. sativa*. Results suggested that duration time of cell division stages was different in roots with different growth rates. PPB stage was shortest in fast-growing roots, characterized by root growth rate of 0.7 – 1.4 $\mu m.min^{-1}$, similarly as duration time of mitotic spindle and phragmoplast. Stages of mitosis and cytokinesis lasted significantly longer time in medium-growing roots with root growth rate of 0.2 – 0.5 $\mu m.min^{-1}$ and duration of these stages was the longest in slow-growing roots with growth rate less than 0.2 $\mu m.min^{-1}$.

Quantitative kinematic study of primary root growth among 18 different ecotypes of *A. thaliana* revealed considerable variations, functionally linking root growth rate with cell cycle regulation. Along with variation in mature cortical cell length and number of dividing cells, also cell cycle duration contributed considerably to the observed variations in root growth rate (Beemster *et al.,* 2002). Because the rate of cell division and the rate of cell production (defined as number of dividing cells and variation in their cell cycle duration) should be principally distinguished (reviewed by Baskin, 2000), determination of root growth rate ideally combines the spatial profile of cell length, cell velocity, relative elongation rate and cell division rate (Beemster and Baskin, 1998; Baskin, 2000). Functional interconnections of these critical parameters are obvious under unfavourable and stress environmental conditions. Responses of *A. thaliana* roots to temperature changes lead to alterations in the meristem length, which was compensated by changes in the cell length within the elongation zone or by changes in division rate helping to maintain equilibrated cell flux within the root meristem (Yang *et al*., 2017). Although it is generally assumed that durations of individual mitotic and cytokinetic stages correlate only indirectly with total cell cycle duration, statistically evaluated parameters in *M. sativa* confirmed *vice versa* correlation of root growth rate with speed of these mitotic and cytokinetic stages in the root meristem. In principle, reduction in root growth rate was reflected by the prolongation of mitotic and cytokinetic stages. Such data were not available in crop species *M. sativa* before.

Moreover, the present study is the first one to provide large-scale imaging and quantitative characterization of cell divisions in the growing robust root of *M. sativa* using developmental live-cell imaging. This was achieved by advanced LSFM, providing suitable technological and physiological tool for developmental live-cell imaging of dividing cells in plant material with high spatial and excellent temporal resolution. LSFM is mesoscopic imaging method, overcoming several critical problems regarding the proper preparation and long-term maintenance of living plant samples. Low phototoxicity allows monitoring of Arabidopsis root growth for long time under physiological conditions (Maizel *et al.*, 2011; Ovečka *et al.*, 2015).

Potential of LSFM for developmental imaging of mitotic MT arrays during cell division is obvious, although it was so far utilized only in three studies on Arabidopsis. Previously, cell division in growing primary roots in long-term time-lapse experiments was observed in Arabidopsis plants carrying MT molecular markers GFP-MBD (Maizel *et al.*, 2011) or GFP-TUA5 (Ovečka *et al.*, 2015). LSFM was also used for characterization of tissue-specific and developmentally-regulated distribution of nuclear levels of GFP-tagged EB1c protein expressed under the control of native *EB1c* promoter. Quantitative correlation analysis revealed relationship between nuclear size and EB1c expression levels in diverse tissues like epidermis, cortex and endodermis, and in different developmental zones including meristematic, transition and elongation zone of *A. thaliana* roots (Novák *et al.*, 2016). In this study we performed dynamic imaging of mitotic MT arrays in robust *M. sativa* growing roots using LSFM. For this purpose, we prepared stably transformed lines of *M. sativa* carrying molecular MT marker GFP-MBD and evaluated MT organization and dynamics during cell division of both epidermal and cortical root cells. Quantitative evaluation of cell division duration time was based on characterization of individual cell division stages, namely PPB, mitotic spindle and phragmoplast. The study clearly revealed an important link between duration of cell division in the root meristematic cells and root growth rates in *M. sativa*. These results suggest that spatio-temporal organization of MT-dependent cell divisions in the root meristem significantly contribute to the root growth rates. Importantly, LSFM is broadly applicable to any genetically modified and fluorescently labelled model legume species such as *M. truncatula* and *Lotus japonicus* as well as to agriculturally important legumes such as soybean, fava bean, pea or chickpea. Moreover, it is potentially interesting also for biotechnological applications such as *M. sativa* lines with RNAi-mediated genetic downregulation of stress-induced mitogen activated protein kinase kinase (SIMKK), an important component of signal transduction cascades in alfalfa (Bekešová *et al.*, 2015), or crop transgenic lines with genetically manipulated cytoskeleton (Komis *et al*., 2015). Considering big potential of LSFM for deep imaging, it can be adapted and used to study interactions of legume roots expressing diverse subcellular markers (including MTs) with beneficial microbes such as Rhizobia and mycorrhizal fungi.

Conclusively, previous achievements on Arabidopsis together with data presented in this study demonstrate a high potential of LSFM in developmental live-cell imaging of mitotic cytoskeletal arrays in diverse plant species. High temporal and good spatial resolution combined with non-invasive and gentle live-cell imaging of cell divisions during growth and development of *M. sativa* roots favour light-sheet microscopy as the most promising imaging method for the future developmental bioimaging and characterization of robust crop species.

5. GENERAL CONCLUSIONS

The present Ph.D. thesis addresses aspects of the plant cytoskeleton, giving special emphasis on the role of MTs during the mitosis. The main aim of the work was the application of novel microscopic approaches and visualization methods in the study of mitotic microtubular structures such as PPB, mitotic spindle and phragmoplast. The thesis consists of three parts. The first part summarizes the existing basic knowledge on the plant cytoskeleton, with special attention being payed to the organization and dynamics of MTs. This section also includes important information on the large number of MAPs identified mainly in the model plant organism *A. thaliana* and their crucial role in the particular stages of cell division. Overall, mitosis is a highly dynamic process in which extensive reorganization of MTs occurs. Therefore, the selection of suitable method for preparation of plant material and application of appropriate visualization method is a key point in the successful study of microtubular system during the mitosis.

In the second part, the procedure of sample preparation was methodically described for three modern microscopic methods such as LSFM, SDCM and Airyscan CLSM. Due to the high speed imaging of SDCM and high resolution and sensitivity of Airyscan CLSM in combination with the additional Airyscan detector, significantly improving signal-to-noise ratio, both methods are suitable for the fast live-cell imaging during the short-term experiments. In addition, LSFM represents a potent tool for long-term plant imaging in real time due to the physiological vertical orientation of sample and low phototoxicity during imaging.

Last part of the thesis was devoted the use of LSFM for 4D long-term live deep-imaging of *M. sativa* roots expressing *35S::GFP:MBD* construct as genetically encoded MT marker. Optimization of sample preparation was important for obtaining of good quality resolution during the visualization of mitotic MT arrays in two different cell layers, the epidermis and the first outer layer of cortex. Based on the growth parameters, in total nine *M. sativa* roots were divided into three groups designed as fast-, medium- and slow-growing roots. Growth rates of individual roots, growth rates of elongating cells and duration of particular mitotic stages were measured and analyzed. It was observed that the durations of PPB, mitotic spindle and phragmoplast stages were shortest in the fast-growing roots, while in slow-growing roots all mitotic stages persisted for the longest period of time. Duration of PPB stage in medium- and slow-growing was approximately the same. Importantly, a positive correlation between the root growth rate and the duration of cell division in the *M. sativa* roots was found. Thus, LSFM

proved to be an efficient method for imaging of robust roots of legume species such as *M. sativa*.

6. REFERENCES

Alberts B, Johnson A, Lewis J, Raff M, Roberts K, Walter P. The cell cycle. In Molecular biology of the cell, 5th edition. Editors Anderson M, Granum S, Garland Science, NY, 2008, 1053 – 1114.

Ayaydin F, Vissi E, Mészáros T, Miskolczi P, Kovács I, Fehér A, Dombrádi V, Erdödi F, Gergely P, Dudits D. Inhibition of serine/threonine-specific protein phosphatases causes premature activation of cdc2MsF kinase at G2/M transition and early mitotic microtubule organisation in alfalfa. *Plant J* 2000; 23: 85 – 96.

Baluška F, Kubica S, Hauskrecht M. Postmitotic 'isodiametric' cell growth in the maize root apex. *Planta* 1990; 181: 269 – 274.

Baskin TI. On the constancy of cell division rate in the root meristem. *Plant Mol Biol* 2000; 43: 545 – 554.

Baskin TI. Patterns of root growth acclimation: constant processes, changing boundaries. *Wiley Interdiscip Rev Dev Biol* 2013; 2: 65 – 73.

Baum SF, Dubrovsky JG, Rost TL. Apical organization and maturation of the cortex and vascular cylinder in *Arabidopsis thaliana* (Brassicaceae) roots. *Am J Bot* 2002; 89: 908 – 920.

Beck M, Komis G, Ziemann A, Menzel D, Samaj J. Mitogen-activated protein kinase 4 is involved in the regulation of mitotic and cytokinetic microtubule transitions in *Arabidopsis thaliana*. *New Phytol* 2011; 189: 1069 – 1083.

Beemster GT, Baskin TI. Analysis of cell division and elongation underlying the developmental acceleration of root growth in *Arabidopsis thaliana*. *Plant Physiol* 1998; 116: 1515 – 1526.

Beemster GT, De Vusser K, De Tavernier E, De Bock K, Inzé D. Variation in growth rate between Arabidopsis ecotypes is correlated with cell division and A-type cyclin-dependent kinase activity. *Plant Physiol* 2002; 129: 854 – 864.

Bekešová S, Komis G, Křenek P, Vyplelová P, Ovečka M, Luptovčiak I, Illés P, Kuchařová A, Šamaj J. Monitoring protein phosphorylation by acrylamide pendant Phos-Tag™ in various plants. *Front Plant Sci* 2015; 6: 336. doi: 10.3389/fpls.2015.00336.

Bezanilla M, Gladfelter AS, Kovar DR, Lee WL. Cytoskeletal dynamics: a view from the membrane. *J Cell Biol* 2015; 209: 329 – 337.

Bi EF, Lutkenhaus J. FtsZ ring structure associated with division in *Escherichia coli*. *Nature* 1991; 354: 161 – 164.

Binarová P, Cenklová V, Procházková J, Doskočilová A, Volc J, Vrlík M, Bögre L. γ -tubulin is essential for acentrosomal microtubule nucleation and coordination of late mitotic events in *Arabidopsis*. *Plant Cell* 2006; 18: 1199 – 1212.

Binarová P, Dolezel J, Draber P, Heberle-Bors E, Strnad M, Bögre L. Treatment of *Vicia faba* root tip cells with specific inhibitors to cyclin-dependent kinases leads to abnormal spindle formation. *Plant J* 1998; 16: 697 – 707.

Bingham ET. Registration of alfalfa hybrid Regen-SY germplasm for tissue culture and transformation research. *Crop Sci* 1991; 31: 1098 doi:10.2135/cropsci1991.0011183X003100040075x.

Buschmann H, Dols J, Kopischke S, Peña EJ, Andrade-Navarro MA, Heinlein M, Szymanski DB, Zachgo S, Doonan JH, Lloyd CW. Arabidopsis KCBP interacts with AIR9 but stays in the cortical

division zone throughout mitosis via its MyTH4-FERM domain. *J Cell Sci* 2015; 128: 2033 – 2046.

Buschmann H, Green P, Sambade A, Doonan JH, Lloyd CW. Cytoskeletal dynamics in interphase, mitosis and cytokinesis analysed through *Agrobacterium*-mediated transient transformation of tobacco BY-2 cells. *New Phytol* 2011; 190: 258 – 267.

Buschmann H, Chan J, Sanchez-Pulido L, Andrade-Navarro MA, Doonan JH, Lloyd CW. Microtubule-associated AIR9 recognizes the cortical division site at preprophase and cell-plate insertion. *Curr Biol* 2006; 16: 1938 – 1943.

Camilleri C, Azimzadeh J, Pastuglia M, Bellini C, Grandjean O, Bouchez D. The Arabidopsis *TONNEAU2* gene encodes a putative novel protein phosphatase 2A regulatory subunit essential for the control of the cortical cytoskeleton. *Plant Cell* 2002; 14: 833 – 845.

Dhonukshe P, Gadella TW Jr. Alteration of microtubule dynamic instability during preprophase band formation revealed by yellow fluorescent protein-CLIP170 microtubule plus-end labeling. *Plant Cell* 2003; 15: 597 – 611.

Dibbayawan TP, Harper JD, Marc J. A γ-tubulin antibody against a plant peptide sequence localises to cell division-specific microtubule arrays and organelles in plants. *Micron* 2001; 32: 671 – 678.

Dolan L, Janmaat K, Willemsen V, Linstead P, Poethig S, Roberts K, Scheres B. Cellular organisation of the *Arabidopsis thaliana* root. *Development* 1993; 119: 71 – 84.

Erickson HP. Evolution of the cytoskeleton. *BioEssays* 2007; 29: 668 – 677.

Gavin RH. Microtubule-microfilament synergy in the cytoskeleton. *Int Rev Cytol* 1997; 173: 207 – 242.

Goode BL, Drubin DG, Barnes G. Functional cooperation between the mikrotubule and actin cytockeletons. *Curr Opin Cell Biol* 2000; 12: 63 – 71.

Granger CL, Cyr RJ. Microtubule reorganization in tobacco BY-2 cells stably expressing GFP-MBD. *Planta* 2000; 210: 502 – 509.

Gunning BE, Hardham AR, Hughes JE. Pre-prophase bands of microtubules in all categories of formative and proliferative cell division in *Azolla* roots. *Planta* 1978; 143: 145 – 160.

Hashimoto T. Microtubules in plants. *Arabidopsis Book* 2015; 13: e0179.

Ho CM, Hotta T, Guo F, Roberson RW, Lee YR, Liu B. Interaction of antiparallel microtubules in the phragmoplast is mediated by the microtubule-associated protein MAP65-3 in Arabidopsis. *Plant Cell* 2011; 23: 2909 – 2923.

Ho CM, Lee YR, Kiyama LD, Dinesh-Kumar SP, Liu B. *Arabidopsis* microtubule-associated protein MAP65-3 cross-links antiparallel microtubules toward their plus ends in the phragmoplast via its distinct C-terminal microtubule binding domain. *Plant Cell* 2012; 24: 2071 – 2085.

Hong W, Deng W, Xie J. The structure, function, and regulation of *Mycobacterium* FtsZ. *Cell Biochem Biophys* 2013; 65: 97 – 105.

Chan J, Calder G, Fox S, Lloyd C. Localization of the microtubule end binding protein EB1 reveals alternative pathways of spindle development in Arabidopsis suspension cells. *Plant Cell* 2005; 17: 1737 – 1748.

Chan J, Calder GM, Doonan JH, Lloyd CW. EB1 reveals mobile microtubule nucleation sites in *Arabidopsis*. *Nat Cell Biol* 2003; 5: 967 – 971.

Chang HY, Smertenko AP, Igarashi H, Dixon DP, Hussey PJ. Dynamic interaction of NtMAP65-1a with microtubules *in vivo*. *J Cell Sci* 2005; 118: 3195 – 3201.

Chichili GR, Rodgers W. Cytoskeleton-membrane interactions in membrane raft structure. *Cell Mol Life Sci* 2009; 66: 2319 – 2328.

Joubès J, Chevalier C, Dudits D, Heberle-Bors E, Inzé D, Umeda M, Renaudin JP. CDK-related protein kinases in plants. *Plant Mol Biol* 2000; 43: 607 – 620.

Kilmartin JV (2014). Lessons from yeast: the spindle pole body and the centrosome. *Philos Trans R Soc Lond B Biol Sci* 2014; 369: 20130456.

Kojo KH, Higaki T, Kutsuna N, Yoshida Y, Yasuhara H, Hasezawa S. Roles of cortical actin microfilament patterning in division plane orientation in plants. *Plant Cell Physiol* 2013; 54: 1491 – 1503.

Kojo KH, Yasuhara H, Hasezawa S. Time-sequential observation of spindle and phragmoplast orientation in BY-2 cells with altered cortical actin microfilament patterning. *Plant Signal Behav* 2014; 9: e29579.

Komaki S, Abe T, Coutuer S, Inzé D, Russinova E, Hashimoto T. Nuclear-localized subtype of end-binding 1 protein regulates spindle organization in Arabidopsis. *J Cell Sci* 2010; 123: 451 – 459.

Komis G, Luptovciak I, Doskocilova A, Samaj J. Biotechnological aspects of cytoskeletal regulation in plants. *Biotechnol Adv* 2015; 33: 1043 – 1062.

Komis G, Luptovčiak I, Ovečka M, Samakovli D, Šamajová O, Šamaj J. Katanin effects on dynamics of cortical microtubules and mitotic arrays in *Arabidopsis thaliana* revealed by advanced live-cell imaging. *Front Plant Sci* 2017; 8: 866.

Laissue PP, Alghamdi RA, Tomancak P, Reynaud EG, Shroff H. Assessing phototoxicity in live fluorescence imaging. *Nat Methods* 2017; 14: 657 – 661.

Li H, Sun B, Sasabe M, Deng X, Machida Y, Lin H, Julie Lee YR, Liu B. Arabidopsis MAP65-4 plays a role in phragmoplast microtubule organization and marks the cortical cell division site. *New Phytol* 2017; 215: 187 – 201.

Lindeboom JJ, Nakamura M, Hibbel A, Shundyak K, Gutierrez R, Ketelaar T, Emons AM, Mulder BM, Kirik V, Ehrhardt DW. A mechanism for reorientation of cortical microtubule arrays driven by microtubule severing. *Science* 2013; 342: 1245533. doi: 10.1126/science.1245533.

Lucas M, Kenobi K, von Wangenheim D, Voβ U, Swarup K, De Smet I, Van Damme D, Lawrence T, Péret B, Moscardi E, Barbeau D, Godin C, Salt D, Guyomarc'h S, Stelzer EH, Maizel A, Laplaze L, Bennett MJ. Lateral root morphogenesis is dependent on the mechanical properties of the overlaying tissues. *Proc Natl Acad Sci USA* 2013; 110: 5229 – 5234.

Maizel A, von Wangenheim D, Federici F, Haseloff J, Stelzer EH. High-resolution live imaging of plant growth in near physiological bright conditions using light sheet fluorescence microscopy. *Plant J* 2011; 68: 377 – 385.

Mao G, Chan J, Calder G, Doonan JH, Lloyd CW. Modulated targeting of GFP-AtMAP65-1 to central spindle microtubules during division. *Plant J* 2005; 43: 469 – 478.

Mészáros T, Miskolczi P, Ayaydin F, Pettkó-Szandtner A, Peres A, Magyar Z, Horváth GV, Bakó L, Fehér A, Dudits D. Multiple cyclin-dependent kinase complexes and phosphatases control G2/M progression in alfalfa cells. *Plant Mol Biol* 2000; 43: 595 – 605.

Müller S, Han S, Smith LG. Two kinesins are involved in the spatial control of cytokinesis in *Arabidopsis thaliana*. *Curr Biol* 2006; 16: 888 – 894.

Murata T, Sano T, Sasabe M, Nonaka S, Higashiyama T, Hasezawa S, Machida Y, Hasebe M. Mechanism of microtubule array expansion in the cytokinetic phragmoplast. *Nat Commun* 2013; 4: 1967.

Nakamura M, Ehrhardt DW, Hashimoto T. Microtubule and katanin-dependent dynamics of microtubule nucleation complexes in the acentrosomal Arabidopsis cortical array. *Nat Cell Biol* 2010; 12: 1064 – 1070.

Novák D, Kuchařová A, Ovečka M, Komis G, Šamaj J. Developmental nuclear localization and quantification of GFP-tagged EB1c in Arabidopsis root using light-sheet microscopy. *Front Plant Sci* 2016; 6: 1187. doi: 10.3389/fpls.2015.01187.

Ovečka M, Vaškebová L, Komis G, Luptovčiak I, Smertenko A, Šamaj J. Preparation of plants for developmental and cellular imaging by light-sheet microscopy. *Nat Protoc* 2015; 10: 1234 – 1247.

Panteris E, Apostolakos P, Galatis B. The effect of taxol on Triticum preprophase root cells: preprophase microtubule band organization seems to depend on new microtubule assembly. *Protoplasma* 1995; 186: 72 – 78.

Prosser SL, Pelletier L. Mitotic spindle assembly in animal cells: a fine balancing act. *Nat Rev Mol Cell Biol* 2017; 18: 187 – 201.

Rasmussen CG, Humphries JA, Smith LG. Determination of symmetric and asymmetric division planes in plant cells. *Annu Rev Plant Biol* 2011; 62: 387 – 409.

Rosquete MR, von Wangenheim D, Marhavý P, Barbez E, Stelzer EH, Benková E, Maizel A, Kleine-Vehn J. An auxin transport mechanism restricts positive orthogravitropism in lateral roots. *Curr Biol* 2013; 23: 817 – 822.

Samac DA, Austin-Phillips S. Alfalfa (*Medicago sativa L.*). *Methods Mol Biol* 2006; 343: 301 – 311.

Samuels AL, Giddings TH Jr, Staehelin LA. Cytokinesis in tobacco BY-2 and root tip cells: a new model of cell plate formation in higher plants. *J Cell Biol* 1995; 130: 1345 – 1357.

Shaw SL, Kamyar R, Ehrhardt DW. Sustained microtubule treadmilling in Arabidopsis cortical arrays. *Science* 2003; 300: 1715 – 1718.

Shaw SL, Lucas J. Intrabundle microtubule dynamics in the Arabidopsis cortical array. *Cytoskeleton* 2011; 68: 56 – 67.

Scheres B, Benfey P, Dolan L. Root development. *Arabidopsis Book* 2002; 1: e0101.

Schmidt T, Pasternak T, Liu K, Blein T, Aubry-Hivet D, Dovzhenko A, Duerr J, Teale W, Ditengou FA, Burkhardt H, Ronneberger O, Palme K. The iRoCS Toolbox--3D analysis of the plant root apical meristem at cellular resolution. *Plant J* 2014; 77: 806 – 814.

Sieberer BJ, Timmers AC, Emons AM. Nod factors alter the microtubule cytoskeleton in *Medicago truncatula* root hairs to allow root hair reorientation. *Mol Plant Microbe Interact* 2005; 18: 1195 – 1204.

Sieberer BJ, Timmers AC, Lhuissier FG, Emons AM. Endoplasmic microtubules configure the subapical cytoplasm and are required for fast growth of *Medicago truncatula* root hairs. *Plant Physiol* 2002; 130: 977 – 988.

Smertenko A, Assaad F, Baluška F, Bezanilla M, Buschmann H, Drakakaki G, Hauser MT, Janson M, Mineyuki Y, Moore I, Müller S, Murata T, Otegui MS, Panteris E, Rasmussen C, Schmit AC, Šamaj J, Samuels L, Staehelin LA, Van Damme D, Wasteneys G, Žárský V. Plant Cytokinesis: Terminology for structures and processes. *Trends Cell Biol* 2017; 27: 885 – 894.

Smertenko A, Franklin-Tong VE. Organisation and regulation of the cytoskeleton in plant programmed cell death. *Cell Death Differ* 2011; 18: 1263 – 1270.

Smertenko AP, Chang HY, Sonobe S, Fenyk SI, Weingartner M, Bögre L, Hussey PJ. Control of the AtMAP65-1 interaction with microtubules through the cell cycle. *J Cell Sci* 2006; 119: 3227 – 3237.

Smith LG. Cytoskeletal control of plant cell shape: getting the fine points. *Curr Opin Cell Biol* 2003; 6: 63 – 73.

Stelzer EH. Light-sheet fluorescence microscopy for quantitative biology. *Nat Methods* 2015; 12: 23 – 26.

Strahl H, Burmann F, Hamoen LW. The actin homologue MreB organizes the bacterial cell membrane. *Nat Commun* 2014; 5: 3442.

Timmers AC, Vallotton P, Heym C, Menzel D. Microtubule dynamics in root hairs of *Medicago truncatula*. *Eur J Cell Biol* 2007; 86: 69 – 83.

Twell D, Park SK, Hawkins TJ, Schubert D, Schmidt R, Smertenko A, Hussey PJ. MOR1/GEM1 has an essential role in the plant-specific cytokinetic phragmoplast. *Nat Cell Biol* 2002; 4: 711 – 714.

Van Damme D, Van Poucke K, Boutant E, Ritzenthaler C, Inzé D, Geelen D. In vivo dynamics and differential microtubule-binding activities of MAP65 proteins. *Plant Physiol* 2004; 136: 3956 – 3967.

Vermeer JEM, von Wangenheim D, Barberon M, Lee Y, Stelzer EHK, Maizel A, Geldner N. A spatial accommodation by neighboring cells is required for organ initiation in Arabidopsis. *Science* 2014; 343: 178 – 183.

Vertii A, Hehnly H, Doxsey S. The centrosome, a multitalented renaissance organelle. *Cold Spring Harb Perspect Biol* 2016; 8. pii: a025049.

Voigt B, Timmers ACJ, Šamaj J, Müller J, Baluška F, Menzel D. GFP-FABD2 fusion construct allows in vivo visualization of the dynamic actin cytoskeleton in all cells of Arabidopsis seedlings. *Eur J Cell Biol* 2005; 84: 595 – 608.

von Wangenheim D, Daum G, Lohmann JU, Stelzer EK, Maizel A. Live imaging of Arabidopsis development. *Methods Mol Biol* 2014; 1062: 539 – 550.

von Wangenheim D, Fangerau J, Schmitz A, Smith RS, Leitte H, Stelzer EH, Maizel A. Rules and self-organizing properties of post-embryonic plant organ cell division patterns. *Curr Biol* 2016; 26: 439 – 449.

Vos JW, Dogterom M, Emons AM. Microtubules become more dynamic but not shorter during preprophase band formation: a possible "search-and-capture" mechanism for microtubule translocation. *Cell Motil Cytoskeleton* 2004; 57: 246 – 258.

Vyplelová P, Ovečka M, Šamaj J. Alfalfa root growth rate correlates with progression of microtubules during mitosis and cytokinesis as revealed by environmental light-sheet microscopy. *Front Plant Sci* 2017; 8: 1870. doi: 10.3389/fpls.2017.01870.

Walker KL, Müller S, Moss D, Ehrhardt DW, Smith LG. Arabidopsis TANGLED identifies the division plane throughout mitosis and cytokinesis. *Curr Biol* 2007; 17: 1827 – 1836.

Wasteneys GO. Microtubule organization in the green kingdom: chaos or selforder?. *J Cell Sci* 2002; 115: 1345 – 1354.

Wick SM, Duniec J. Immunofluorescence microscopy of tubulin and microtubule arrays in plant cells. I. Preprophase band development and concomitant appearance of nuclear envelope-associated tubulin. *J Cell Biol* 1983; 97: 235 – 243.

Wiese C, Zheng Y. Microtubule nucleation: γ-tubulin and beyond. *J Cell Sci* 2006; 119: 4143 – 4153.

Wu SZ, Bezanilla M. Myosin VIII associates with microtubule ends and together with actin plays a role in guiding plant cell division. *Elife* 2014; 3: doi: 10.7554/eLife.03498.

Xu XM, Zhao Q, Rodrigo-Peiris T, Brkljacic J, He CS, Müller S, Meier I. RanGAP1 is a continuous marker of the Arabidopsis cell division plane. *Proc Natl Acad Sci USA* 2008; 105: 18637 – 18642.

Yamada M, Goshima G. Mitotic spindle assembly in land plants: Molecules and mechanisms. *Biology (Basel)* 2017; 6: 6.

Yang X, Dong G, Palaniappan K, Mi G, Baskin TI. Temperature-compensated cell production rate and elongation zone length in the root of *Arabidopsis thaliana*. *Plant Cell Environ* 2017; 40: 264 – 276.

Yoneda A, Akatsuka M, Hoshino H, Kumagai F, Hasezawa S. Decision of spindle poles and division plane by double preprophase bands in a BY-2 cell line expressing GFP-tubulin. *Plant Cell Physiol* 2005; 46: 531 – 538.

Yuan M, Shaw PJ, Warn RM, Lloyd CW. Dynamic reorientation of cortical microtubules, from transverse to longitudinal, in living plant cells. *Proc Natl Acad Sci USA* 1994; 91: 6050 – 6053.

Zhang H, Dawe RK. Mechanisms of plant spindle formation. *Chromosome Res* 2011; 19: 335 – 344.

7. LIST OF PUBLICATIONS

1. Vyplelová P, Ovečka M, Komis G, Šamaj J. Advanced microscopy methods for bioimaging of mitotic microtubules in plants. *Methods in Cell Biology* 2018; in press. https://doi.org/10.1016/bs.mcb.2018.03.019.

2. Vyplelová P*, Ovečka M*, Šamaj J. Alfalfa root growth rate correlates with progression of microtubules during mitosis and cytokinesis as revealed by environmental light-sheet microscopy. *Frontiers in Plant Science* 2017; 8: 1870. * joined first authors.

3. Bekešová S, Komis G, Křenek P, Vyplelová P, Ovečka M, Luptovčiak I, Illés P, Kuchařová A, Šamaj J. Monitoring protein phosphorylation by acrylamide pendant Phos-Tag™ in various plants. *Frontiers in Plant Science* 2015; 6: 336.

4. Křenek P, Niks RE, Vels A, Vyplelová P, Šamaj J. Genome-wide analysis of the barley MAPK gene family and its expression patterns in relation to *Puccinia hordei* infection. *Acta Physiologia Plantarum* 2015; 37: 1 – 16.

8. SUPPLEMENT

8.3 Abstrakt v českém jazyce

Předkládaná disertační práce je zaměřena na možnosti studia rostlinného cytoskeletu pomocí moderních mikroskopických metod jako jsou „light-sheet“ fluorescenční mikroskopie (LSFM), konfokální mikroskopie s rotujícím diskem (SDCM) a Airyscan konfokální laserová skenovací mikroskopie (CLSM). Mikroskopické analýzy byly provedeny na mikrotubulech v průběhu buněčného dělení v kořenech modelové rostliny *Arabidopsis thaliana* a v kořenech hospodářsky významné luštěniny *Medicago sativa*. Práce je rozdělena na tři části, z nichž první část shrnuje ověřené poznatky o rostlinném cytoskeletu, jeho složení a funkci. Tato část také obsahuje kapitoly pojednávající o uspořádání a úloze mikrotubulů (MT) v průběhu mitózy. Dále jsou zde charakterizovány jednotlivé modelové rostliny a základní principy použitých mikroskopických metod.

Druhá část práce je zaměřena zejména na přípravu rostlinného materiálu pro následnou mikroskopickou analýzu mitotických MT. Mitóza je velmi dynamický proces, který je citlivý na jakékoliv vnější stresové faktory. Z tohoto důvodu je výběr mikroskopické metody velice důležitý. Využitím fluorescenčně značených MT a moderních mikroskopických metod (LSFM, SDCM a Airyscan CLSM), které jsou dostatečně rychlé, mají vysoké rozlišení a zároveň jsou v průběhu snímání šetrnější k rostlinnému preparátu díky nižší fototoxicitě, jsme schopni studovat tyto dynamické procesy v reálném čase.

Třetí část této práce se zaměřuje na využití LSFM při studiu mitotických MT v rostoucích kořenech *M. sativa* exprimujících *35S::GFP:MBD* konstrukt. Zejména díky vysokému optickému rozlišení, možnosti vytváření efektivních optických řezů, vysoké rychlosti snímání, nízké fototoxicitě a možnosti snímání preparátu umístěného ve vertikální poloze je tato mikroskopická metoda vhodná pro dlouhodobé 4D snímání živých rostlinných preparátů při téměř fyziologických podmínkách růstu. Celkem devět snímaných kořenů *M. sativa* bylo rozděleno do tří skupin podle rychlosti jejich růstu. V každé skupině kořenů jsme zaznamenali a kvantitativně vyhodnotili trvání mitotického buněčného dělení, zejména trvání přítomnosti jednotlivých mitotických mikrotubulárních struktur jako je preprofázní svazek, mitotické vřeténko a fragmoplast a to jak v epidermis, tak v první vrstvě kortexu. Získaná data ukázala průkaznou korelaci mezi rychlostí růstu kořenů a trváním buněčného dělení v kořenech *M. sativa*.

Klíčová slova	mikrotubuly, *Medicago sativa*, „light-sheet“ mikroskopie, konfokální mikroskopie s rotujícím diskem, Airyscan, *Arabidopsis thaliana*, preprofázní svazek, dělicí vřeténko, fragmoplast, mitóza
Počet stran	165
Počet příloh	3
Jazyk	Anglický